22 May 2009 | $10

Science

AAAS

Affymetrix

Revolutionize life

With a limited view, you're simply left guessing.

With GeneChip® Exon and Gene 1.0 ST Arrays, you don't have to guess. Whole-transcript expression arrays allow you to measure the entire transcript, enabling you to detect gene-level expression, exon-level expression, and alternative splicing in a single experiment. Why settle for incomplete results when you can look beyond the 3' end of a gene? Extrapolation can only take you so far—Affymetrix will take you the rest of the way.

See the real biology at www.affymetrix.com/genechip/wtexpression

What makes you happy?
How about Western blots in 55 minutes without equipment?

Put a smile on your face and your research with the chemiluminescent Thermo Scientific Pierce Fast Western Blot Kit 55-minute Western blot procedure.

- Fast – all the sensitivity you need in a fraction of the time; save 3-4 hours per blot over traditional blotting methods
- Convenient – no expensive hardware or extra bench space needed; eliminates membrane clogging issues
- Economical – costs about the same as a classical Western blot
- Easy – optimized kit includes all reagents except primary antibody
- Versatile – kits work with both rabbit and mouse primary antibodies

Visit *www.thermo.com/fastwest*

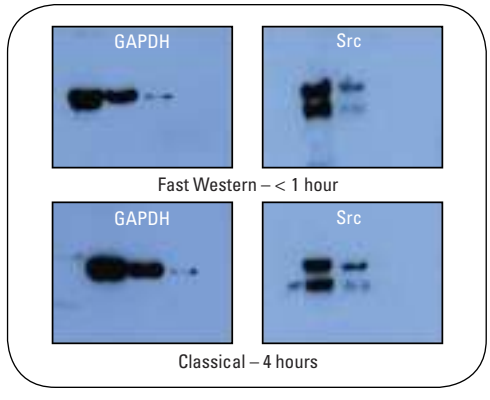

The sensitivity you need in less time with no expensive hardware.
Target proteins were probed using a classical Western blot procedure (3-4 hours) and the Fast Western Blot Kit procedure (55 minutes).

Moving science forward

Thermo SCIENTIFIC
Part of Thermo Fisher Scientific

GE Healthcare

Coordinate your application focus. Achieve greater operational efficiency.

GE Healthcare is focused on helping you develop efficient biopharmaceutical process flows and eliminating wasteful practices, taking your value stream to new frontiers. Through our wide range of technology platforms and services, upstream and downstream from process development to final manufacturing scale, GE Healthcare can connect you to the power of operational excellence.

Learn more about operational excellence at: www.gelifesciences.com/opex

imagination at work

GE Healthcare Bio-Sciences AB, a General Electric Company
Björkgatan 30, 751 84 Uppsala, Sweden

GE04-09. First printetd 09/2008.

EDITORIAL

NEWS OF THE WEEK

NEWS FOCUS

LETTERS

BOOKS *ET AL.*

POLICY FORUM

PERSPECTIVES

CONTENTS continued >>

page 1004

page 1017

COVER

Africa is the source of all modern humans. A genetic study of 121 populations from across the continent traces them back to 14 ancestral groups and documents the extent of diversity within and among African populations. See page 1035.

Image: Kaadaa/Corbis

DEPARTMENTS

Published by AAAS

Gene expression and function analysis sample and assay technologies by QIAGEN

Enjoy first-time success

Rely on QIAGEN's manual and automated workflow solutions for:

- **Sample collection and disruption**
- **RNA stabilization and purification**
- **Real-time PCR and RT-PCR and gene expression assays**
- **RNAi and gene silencing**
- **miRNA purification and assays**
- **Methylation analysis in epigenetics research**
- **Protein sample preparation and assays**

Making improvements in life possible — www.qiagen.com

QIAGEN®

Sample & Assay Technologies

GEFPorff0309S1WW

REVIEW

BREVIA

RESEARCH ARTICLE

REPORTS

CONTENTS continued **>>**

page 1058

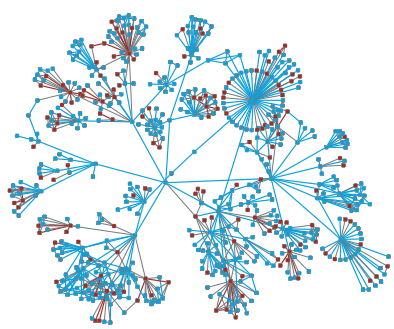

pages 1023 and 1071

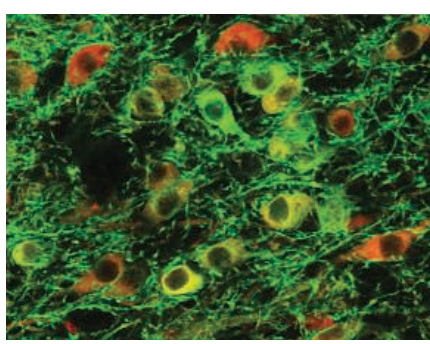

page 1080

Trusted!

SIGMA® Life Science

Insist on Sigma's FLAG® System…
Original and Proven Performance

FLAG is the established system for recombinant protein expression, purification, and detection. Don't settle for inferior systems.

- **Proven**: Cited in more than 2,000 publications
- **Ultrasensitive**: Antibodies detect as little as 100 femtomoles of protein
- **Comprehensive**: Complete systems in multiple formats

View the full range of FLAG products at ***sigma.com/flagtag***

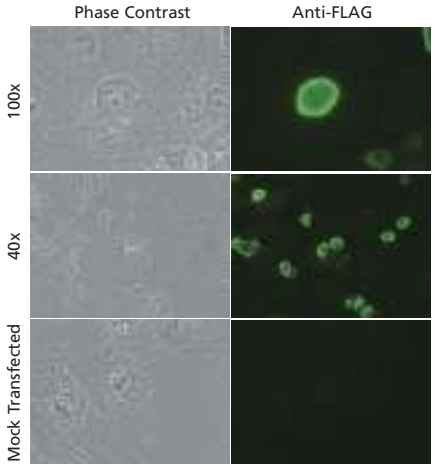

FLAG-p53 and mock transfected COS-7 cells were permeabilized, fixed, blocked, and incubated with anti-FLAG M2 antibody

Our Innovation, Your Research — Shaping the Future of Life Science

SCIENCEONLINE

SCIENCEXPRESS
www.sciencexpress.org

Germline P Granules Are Liquid Droplets That Localize by Controlled Dissolution/Condensation
C. P. Brangwynne et al.

Localization of RNA and protein-rich germ-cell granules occurs by controlled dissolution and condensation.
10.1126/science.1172046

Inhibition of Hedgehog Signaling Enhances Delivery of Chemotherapy in a Mouse Model of Pancreatic Cancer
K. P. Olive et al.

Pancreatic tumors are unresponsive to chemotherapy because their limited vasculature precludes efficient drug delivery.
10.1126/science.1171362

MicroRNA-92a Controls Angiogenesis and Functional Recovery of Ischemic Tissues in Mice
A. Bonauer et al.

Inhibition of a microRNA that represses blood vessel growth enhances the recovery of tissue damaged by an inadequate blood supply.
10.1126/science.1174381
>> Science *Podcast*

A Radio Pulsar/X-ray Binary Link
A. M. Archibald et al.

Radio observations reveal a system undergoing the transition from a low-mass x-ray binary star to a millisecond radio pulsar.
10.1126/science.1172740
>> Science *Podcast*

Beryllium Dimer—Caught in the Act of Bonding
J. M. Merritt et al.

High-resolution spectroscopy maps out the unusual ground state electronic potential of the beryllium dimer.
10.1126/science.1174326

TECHNICALCOMMENTS

Comment on "Functional Traits and Niche-Based Tree Community Assembly in an Amazonian Forest"
J. K. Lake and A. Ostling

full text at www.sciencemag.org/cgi/content/full/324/5930/1015-c

Response to Comment on "Functional Traits and Niche-Based Tree Community Assembly in an Amazonian Forest"
N. J. B. Kraft and D. D. Ackerly

full text at www.sciencemag.org/cgi/content/full/324/5930/1015-d

SCIENCENOW
www.sciencenow.org
Highlights From Our Daily News Coverage

How Plants Survived Chernobyl
Research sheds light on how soybeans and other vegetation respond to nuclear fallout.

Designer Antibodies Derail Monkey AIDS Virus
New "vaccine" approach could show promise for humans.

That Bird Knows Who You Are
Mockingbirds can pick a threatening person out of a crowd.

SCIENCESIGNALING
www.sciencesignaling.org
The Signal Transduction Knowledge Environment

RESEARCH ARTICLE: Deciphering Signaling Outcomes from a System of Complex Networks
R. C. Hsueh et al.

Despite exposure to multiple ligands, a macrophage cell line exhibits a surprisingly limited number of responses.

RESEARCH ARTICLE: TRPM2 Functions as a Lysosomal Ca^{2+}-Release Channel in β Cells
I. Lange et al.

TRPM2-mediated Ca^{2+} release from lysosomal stores contributes to pancreatic β cell death in response to oxidative stress.

PERSPECTIVE: Limb Development Takes a Measured Step Toward Systems Analysis
S. Mackem and M. Lewandoski

Gremlin links slow and fast signaling feedback loops, which contribute to robust regulation of mouse limb patterning.

PODCAST
E. Oancea and A. M. VanHook

TRPM1 is a cation channel found on vesicular membranes and associated with melanin content in melanocytes.

FORUM: Poster Award Winners from "Visualizing Immune System Complexity"
N. R. Gough

Three students are recognized for their work at an EMBO workshop held at the Centre d'Immunologie de Marseille-Luminy in France in January 2009.

E-LETTER: ACC Award
Science Signaling Editors

Naoki Sawada wins a Young Investigator Award from the American Academy of Cardiology for his *Science Signaling* Research Article.

SCIENCECAREERS
www.sciencecareers.org/career_magazine
Free Career Resources for Scientists

Academia or Industry? Finding the Right Fit
E. Pain

Despite some limitations, there are still advantages for scientists in industry.

Building a Science Career in the Defense Industry
A. Saini

The defense industry offers opportunities that go beyond designing weapons and aircraft.

Pharma Offers Bench-to-Bedside Opportunities
K. Hede

Scientists in pharma say working in their industry is one way to improve human health.

SCIENCENOW
Soy survivor.

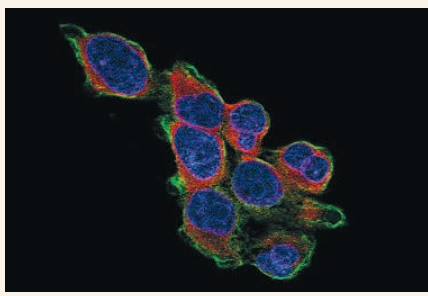

SCIENCESIGNALING
TRPM2 in pancreatic β cells.

SCIENCEPODCAST
www.sciencemag.org/multimedia/podcast
Free Weekly Show

Download the 22 May *Science* Podcast to hear about a microRNA that controls blood vessel growth, a neutron star transitioning to a radio pulsar, detecting scientific plagiarism, and more.

ORIGINSBLOG
blogs.sciencemag.org/origins
A History of Beginnings

SCIENCEINSIDER
blogs.sciencemag.org/scienceinsider
Science Policy News and Analysis

SCIENCE (ISSN 0036-8075) is published weekly on Friday, except the last week in December, by the American Association for the Advancement of Science, 1200 New York Avenue, NW, Washington, DC 20005. Periodicals Mail postage (publication No. 484460) paid at Washington, DC, and additional mailing offices. Domestic individual membership and subscription (51 issues): $146 ($74 allocated to subscription). Domestic institutional subscription (51 issues): $835; Foreign postage extra: Mexico, Caribbean (surface mail) $55; other countries (air assist delivery) $85. First class, airmail, student, and emeritus rates on request. Canadian rates with GST available upon request, GST #1254 88122. Publications Mail Agreement Number 1069624. **Printed in the U.S.A.**

Change of address: Allow 4 weeks, giving old and new addresses and 8-digit account number. **Postmaster:** Send change of address to AAAS, P.O. Box 96178, Washington, DC 20090–6178. **Single-copy sales:** $10.00 current issue, $15.00 back issue prepaid includes surface postage; bulk rates on request. **Authorization to photocopy** material for internal or personal use under circumstances not falling within the fair use provisions of the Copyright Act is granted by AAAS to libraries and other users registered with the Copyright Clearance Center (CCC) Transactional Reporting Service, provided that $20.00 per article is paid directly to CCC, 222 Rosewood Drive, Danvers, MA 01923. The identification code for *Science* is 0036-8075. *Science* is indexed in the *Reader's Guide to Periodical Literature* and in several specialized indexes.

AAAS
ADVANCING SCIENCE, SERVING SOCIETY

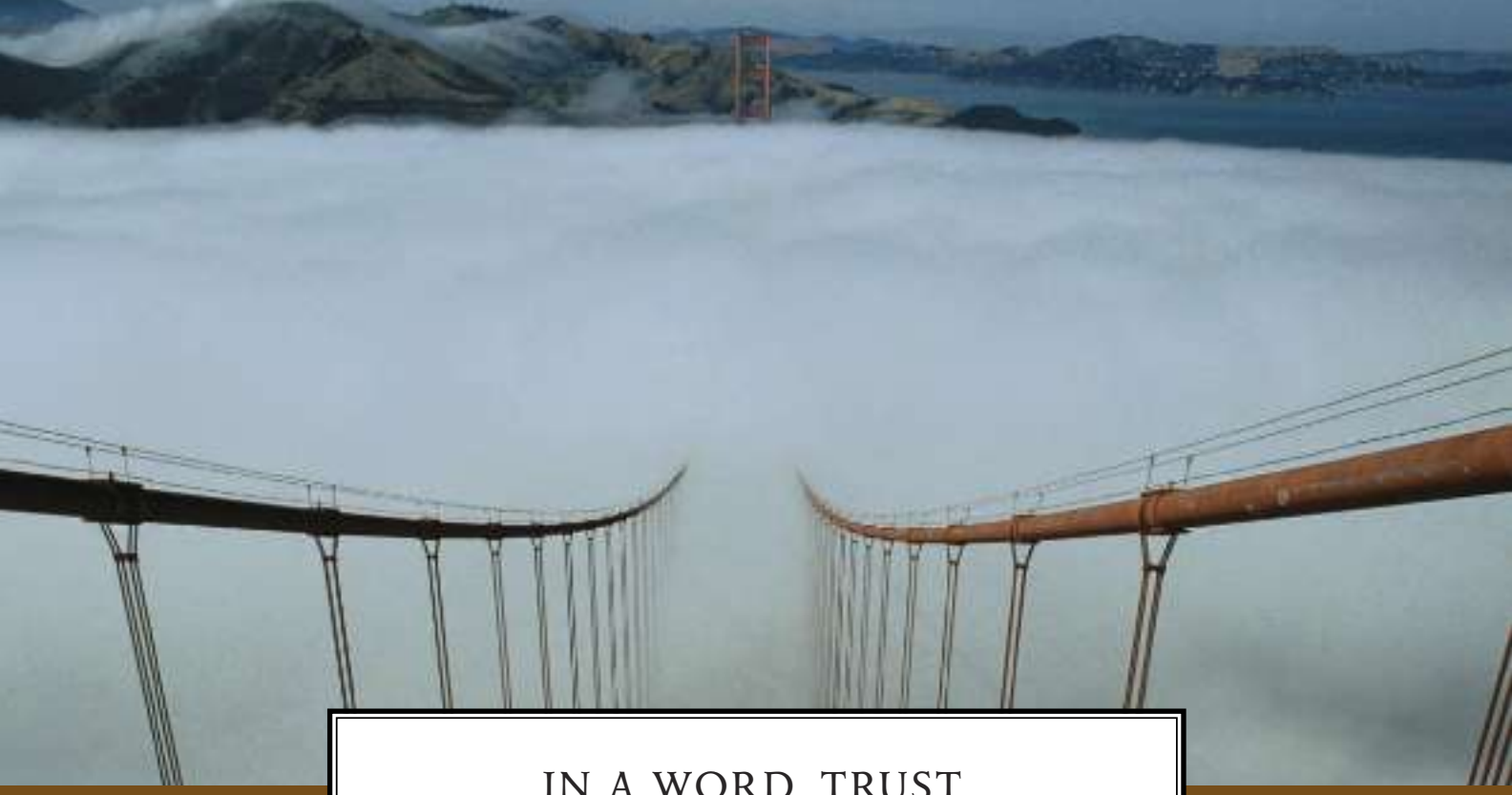

IN A WORD, TRUST.

T4 DNA Ligase

New England Biolabs is dedicated to providing our customers with guaranteed enzyme performance. Our recombinant T4 DNA Ligase is the most extensively used ligase for cloning experiments and other applications, including sample preparation and next generation sequencing. It is available at exceptional value, and an even greater value when purchased in large quantities for high throughput technologies. For cohesive, blunt, simple or complex reactions, make T4 DNA Ligase from NEB your first choice.

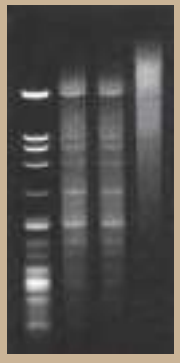

0 0.1 0.2 1.0
T4 DNA Ligase (µl)

Ligation of blunt-ended HaeIII fragments of Lambda DNA using various amounts of T4 DNA Ligase (400,000 cohesive end units/ml) in a 20 µl reaction volume. Reactions were incubated for 30 minutes at 16°C.

0 10 20 30 60
Time (min)

Ligation of HindIII fragments (4-base overhang) of Lambda DNA using 1 cohesive end unit (1µl of 1:400 dilution) of T4 DNA Ligase. Reactions were incubated at 25°C.

Advantages:

Quality - Highly pure enzyme with no lot-to-lot variation

Convenience - Choose original T4 DNA Ligase or the Quick Ligation Kit to meet the demands of a variety of reaction conditions

Flexibility - Active at room temperature or 16°C; reaction times run from 5 minutes to overnight

Robustness - Active in a variety of reaction buffers

T4 DNA Ligase* RR
Regular Concentration **M0202S/L**
For standard cloning reactions

High Concentration **M0202T/M**
For large or difficult constructs

Quick Ligation™ Kit* RR **M2200S/L**
For ligation of cohesive or blunt-end DNA fragments in 5 minutes at room temperature

RR = Recombinant
*NEB ligase products are BSA-free

For more information regarding customization and OEM opportunities, please contact **oem@neb.com**

New England Biolabs, Inc. is an ISO 9001 certified company

NEW ENGLAND BioLabs® Inc.
enabling technologies in the life sciences

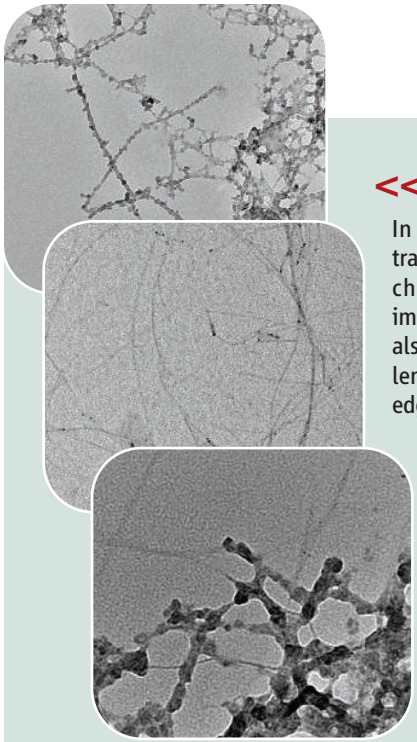

<< Viral Battery

In developing materials for batteries, there is a trade-off between charge capacity, conductivity, and chemical stability. Nanostructured materials improve the conductivity for some resistive materials, but fabricating stable materials at nanometer-length scales is difficult. Harnessing their knowledge of viruses as toolkits for materials fabrication, **Lee *et al.*** (p. 1051; published online 2 April) modified two genes in the filamentous bacteriophage M13 to produce a virus with an affinity for nucleating amorphous iron phosphate along its length and for attaching carbon nanotubes at one of the ends. In nanostructured form, the amorphous iron phosphate produced a useful cathode material, while the carbon nanotubes formed a percolating network that significantly enhanced conductivity.

Fuel Economy for Growing Cells

Sophisticated 21st-century analyses of the signaling pathways that control cell growth have led researchers back to the seminal work of Otto Warburg, who discovered in the 1920s that tumor cells generate their energy in an unusual way—by switching from mitochondrial respiration to glycolysis. The advantage conferred by this metabolic switch is puzzling because mitochondrial respiration is a more efficient way to produce ATP. **Vander Heiden *et al.*** (p. 1029) review arguments that rapidly growing cells have critical metabolic requirements that extend beyond ATP and that a better understanding of these requirements may shed new light on the "Warburg effect" and ultimately lead to new therapies for cancer.

African Origins

The modern human originated in Africa and subsequently spread across the globe. However, the genetic relationships among the diverse populations on the African continent have been unclear. **Tishkoff *et al.*** (p. 1035; see the cover, published online 30 April) provide a detailed genetic analysis of most major groups of African populations. The findings suggest that Africans represent 14 ancestral populations. Populations tend to be of mixed ancestry which documents historical migrations. The data mainly support but sometimes challenge proposed relationships between groups of self-identified ethnicity previously hypothesized on the basis of linguistic studies. The authors also examined populations of African Americans and individuals of mixed ancestry from Cape Town, documenting the variation and origins of admixture within these groups.

Future Fuels

In the scramble to develop more environmentally friendly transportation methods, a wide range of questions must be answered, including how automobiles may best be powered. Biomass might be an important source for that power, either to generate electricity for electric vehicles, or to make ethanol for combustion vehicles. **Campbell *et al.*** (p. 1055; published online 7 May; see the Policy Forum by **Ohlrogge *et al.***) examined each approach's demands on land-use, using a life-cycle assessment model, for a range of energy feedstocks, conversion methods, and vehicle types. In nearly all cases, bioelectricity would have a significantly higher net transportation efficiency per area of land used than bioethanol, owing to the greater efficiency of electric engines. Furthermore, bioelectricity would result in a smaller CO_2 burden. Thus, bioelectricity could represent an important bridge to more advanced transportation technologies with less environmental impact.

"Lake" Victoria?

After having explored the Eagle and Endurance craters, which are separated by only 800 meters, the Mars Exploration Rover Opportunity spent 2 years at Victoria, a much larger impact crater located 6 kilometers south across Meridiani Planum. Sedimentary rocks previously analyzed at Eagle and Endurance point to local environmental conditions that included abundant liquid water in the ancient past. Now, an analysis of rocks in the walls of Victoria by **Squyres *et al.*** (p. 1058) reveals that the aqueous alteration processes that operated at Eagle and Endurance also acted at Victoria. In addition, sedimentary layering in the crater walls preserves evidence of ancient wind-blown dunes.

Getting Below the Surface

Two-dimensional electron systems have proved to be a productive area for the study of low-dimensional transport. Despite decades of intense effort, the actual dispersion of the electronic excitations—how their energy behaves as a function of momentum as the they move through their two-dimensional space—have eluded experiments. This elusiveness is due to the samples being thin and buried. **Kukushkin *et al.*** (p. 1044; published online 30 April; see the Perspective by **Simon**) now introduce a technique based on launching surface acoustic waves through the sample. The excitations "ride" these waves, with their energy and momentum mapped out using pulses of laser light. The technique should also be applicable to other hard-to-get-at electronic systems.

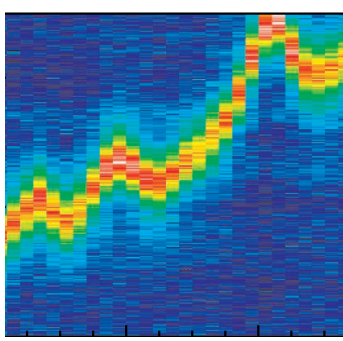

Death Mirrors Life

The accuracy with which fossil assemblages represent the actual composition of ancient ecological communities is very often uncertain. One way to assess the degree of fidelity between living and dead assemblages is to patiently compare modern living communities and the records they leave behind them in real time. **Western and Behrensmeyer** (p. 1061) recorded the composition of vertebrate herbivore communities in the Amboseli reserve in Kenya over four decades and compared this to the assemblages of bones left behind as the animals died. The results suggest a high level of fidelity of life-to-death assemblages, both in the composition and the relative abundance of species. Thus, older fossil assemblages might indeed give a reliable picture of past and extinct communities.

Continued on page 985

CREDITS (TOP TO BOTTOM): LEE *ET AL.*; KUKUSHKIN *ET AL.*

Tools for Gene Expression Analysis

Accurately, Sensitively Quantify RNA Levels in Any Species

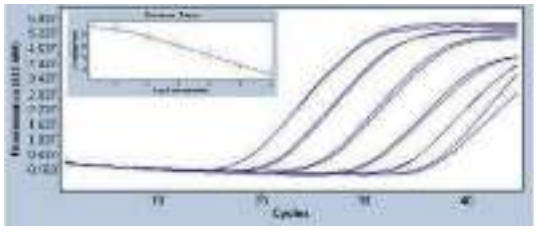

Figure 1. Quantification of β-actin on the LightCycler® 480 System, following sample preparation with the High Pure RNA Isolation Kit and reverse transcription with the Transcriptor First Strand cDNA Synthesis Kit. Total RNA of K-562 cells was purified using the High Pure RNA Isolation Kit; 1 pg to 1 µg aliquots were reverse transcribed with the Transcriptor First Strand cDNA Synthesis Kit. Subsequently, PCR was performed on the LightCycler® 480 System in duplicate with the LightCycler® 480 Probes Master and a Universal ProbeLibrary probe for β-actin.

Generate more accurate and sensitive gene expression results by using Roche Applied Science reagents and instruments. Choose from our comprehensive portfolio of technologies – from purifying RNA or miRNA, to identifying genes of interest through microarray analysis, to quantifying RNA by real-time PCR.

Select Roche for gene expression analysis that is

- **Accurate:** Rely on unbiased reverse transcription and the LightCycler® 480 Instrument's unmatched temperature homogeneity and powerful analysis software.
- **Sensitive:** Combine the Transcriptor First Strand cDNA Synthesis Kit with optimized qPCR Master Mixes (Figure 1).
- **Species independent:** Analyze expression in any species with the Universal ProbeLibrary and NimbleGen Microarrays.

Play our New Gene Expression Rave game. View Application Notes, promotions, and more, or challenge yourself on our new game at ***www.gene-expression-analysis.com***

RNA Isolation | **cDNA Synthesis** | **Real-Time PCR Instruments** | **qPCR Master Mixes** | **Probes for qPCR** | **Expression Assays**

Roche Diagnostics
Roche Applied Science
Indianapolis, Indiana

Roche

Continued from page 983

A Jump on Catalyst Kinetics

A common method for interrogating fast reaction kinetics is to create an abrupt initiation point, and, for reactions catalyzed by metals on oxide supports, one option is to induce a rapid temperature jump, provided that the part of the catalyst undergoing heating can be probed locally. **Thibault-Starzyk *et al.*** (p. 1048) used femtosecond laser pulses to heat catalysts for nitrogen oxide removal and followed the reaction with Fourier-transform infrared spectroscopy. These catalysts are designed to remove NO in fuel-efficient lean-burn engines through reaction with CO, rather than with hydrocarbons. A cyanide reaction intermediate was identified that moves from the silver nanoparticle to the alumina surface.

Viruses and Mobile Phones

While traditional cellphones have been relatively immune to viruses, smartphones (like Palm, Blackberry, iPhone, and many Nokia brands) that can share programs and data with each other could potentially be vulnerable to virus epidemics. Why then haven't we experienced any major mobile virus outbreak so far? **Wang *et al.*** (p. 1071; published online 2 April; see the Perspective by **Havlin**) believe that the answer is related to the spreading patterns possible in the current mobile phone systems. They studied the anonymized billing record of a mobile phone company, representing the calling patterns and the coordinates of the closest mobile phone tower each time a group of 6.2 million mobile phone subscribers used their phone. While a Bluetooth virus could reach all susceptible users given sufficient time, its spread, limited by human mobility, was relatively slow. In contrast, MMS viruses would have an explosive spreading pattern, but could only reach the group of individuals that know each other and carry the same phone. Thus, no major virus outbreak is likely until one operating system encompasses a larger fraction of the total smartphone market.

Chromatin Modifier Modulates Gene Expression

Modification of chromatin structure is usually thought of as a global, relatively nonspecific way of modulating gene expression. However, **Wellen *et al.*** (p. 1076; see the Perspective by **Rathmell and Newgard**) demonstrate that such regulation helps link growth factor–stimulated increases in metabolism to appropriate changes in gene expression. Adenosine triphosphate (ATP)–citrate lyase (ACL), which converts citrate to acetyl–coenzyme A (CoA) in the mitochondria of mammalian cells during metabolism of glucose, was also found to be present in the nucleus, where it might regulate activity of histone acetyl transferases (HATs) by controlling the availability of acetyl-CoA. Indeed, depletion of ACL from cultured human colon carcinoma cells specifically decreased histone acetylation in the nucleus, but appeared not to affect the overall amount of acetylation of proteins in the cells. Loss of ACL in cultured mouse 3T3-L1 cells diminished the increase in histone acetylation normally associated with hormone-stimulated differentiation of these cells and inhibited the increase in expression of specific genes, such as that encoding the Glut4 glucose transporter. Thus, ACL may help cells link metabolic activity to changes in gene expression.

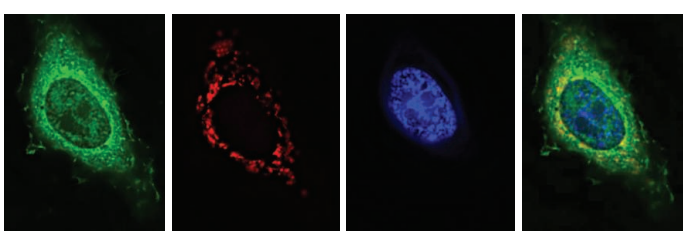

CREDIT: WELLEN *ET AL.*

Down But Not Out

The K-complex, a defining characteristic of slow wave sleep, is the largest spontaneously occurring component of the healthy human electroencephalogram (EEG) but little is known about its physiological characteristics in the human cortex. **Cash *et al.*** (p. 1084) investigated the intracortical origin of K-complexes in humans undergoing surgery for epileptic seizures. In simultaneous subdural EEG and intracortical multisite microelectrode recordings, K complexes represented cortical down-states reflecting a decrease in neural firing. These down-states are a fundamental mode of cortical operation that have been well studied in animals and may contribute to sleep preservation and memory consolidation.

Eppendorf Consumables – it's your sample

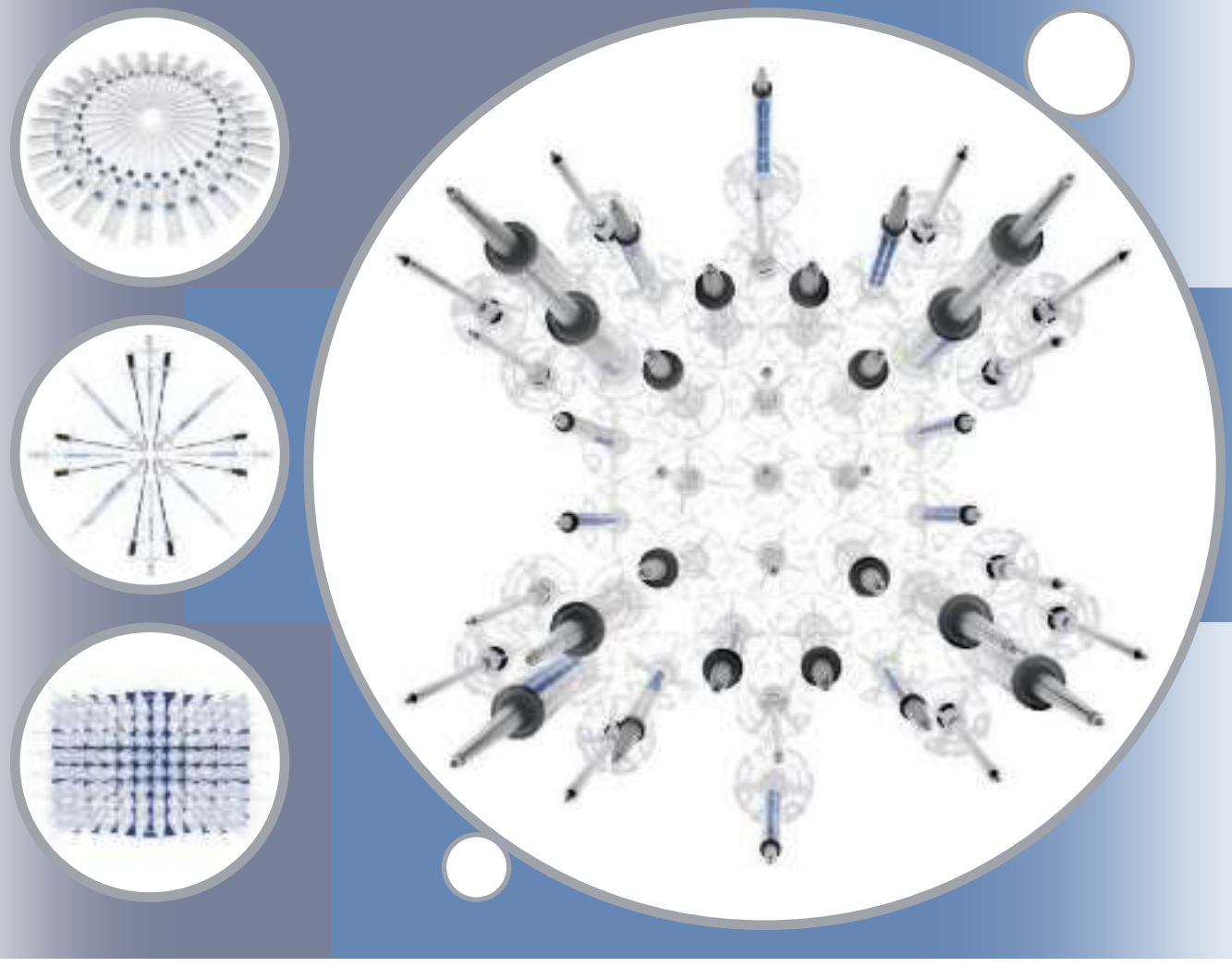

Make the best of it!

Top quality for your sample

Each of your valuable samples deserves the best treatment. See for yourself how the Eppendorf tips will save time and reduce costs.

With respect to material, fit, design and operating forces our tips set new standards. The close environment of each sample should be adapted to its specific quality and purity needs. This can involve a specific purity level or the absence of certain substances, but also stability, reliability, or geometry. The Eppendorf tips are designed to cover all of the specific needs of your samples!

Dispensing at its best! Eppendorf Combitips® plus

- Precise dispensing of liquids with high vapor pressure or higher viscosity
- Contamination-free dispensing due to positive-displacement principle
- Dispensing from 1 µl to 50 ml through 9 different sizes
- Automatic Combitip recognition with Multipette®* plus and Multipette* stream/Xstream®

Learn more about Eppendorf Combitips plus:
www.eppendorf.com/CBT

*Repeater in the U.S.

eppendorf

In touch with life

Your local distributor www.eppendorf.com/worldwide · **Application Support** E-Mail: support@eppendorf.com
Eppendorf AG · Hamburg · Germany · Tel: +49 40 538 01-0 · Eppendorf North America, Inc. · USA · Tel.: +1 800 645 3050

Harvey V. Fineberg is president of the Institute of Medicine.

Mary Elizabeth Wilson is associate professor of Global Health and Population at the Harvard School of Public Health and associate clinical professor at Harvard Medical School, Boston, MA.

Epidemic Science in Real Time

FEW SITUATIONS MORE DRAMATICALLY ILLUSTRATE THE SALIENCE OF SCIENCE TO POLICY THAN AN epidemic. The relevant science takes place rapidly and continually, in the laboratory, clinic, and community. In facing the current swine flu (H1N1 influenza) outbreak, the world has benefited from research investment over many years, as well as from preparedness exercises and planning in many countries. The global public health enterprise has been tempered by the outbreak of severe acute respiratory syndrome (SARS) in 2002–2003, the ongoing threat of highly pathogenic avian flu, and concerns over bioterrorism. Researchers and other experts are now able to make vital contributions in real time. By conducting the right science and communicating expert judgment, scientists can enable policies to be adjusted appropriately as an epidemic scenario unfolds.

In the past, scientists and policy-makers have often failed to take advantage of the opportunity to learn and adjust policy in real time. In 1976, for example, in response to a swine flu outbreak at Fort Dix, New Jersey, a decision was made to mount a nationwide immunization program against this virus because it was deemed similar to that responsible for the 1918–1919 flu pandemic. Immunizations were initiated months later despite the fact that not a single related case of infection had appeared by that time elsewhere in the United States or the world (www.iom.edu/swinefluaffair). Decision-makers failed to take seriously a key question: What additional information could lead to a different course of action? The answer is precisely what should drive a research agenda in real time today.

In the face of a threatened pandemic, policy-makers will want real-time answers in at least five areas where science can help: pandemic risk, vulnerable populations, available interventions, implementation possibilities and pitfalls, and public understanding. Pandemic risk, for example, entails both spread and severity. In the current H1N1 influenza outbreak, the causative virus and its genetic sequence were identified in a matter of days. Within a couple of weeks, an international consortium of investigators developed preliminary assessments of cases and mortality based on epidemic modeling.*

Specific genetic markers on flu viruses have been associated with more severe outbreaks. But virulence is an incompletely understood function of host-pathogen interaction, and the absence of a known marker in the current H1N1 virus does not mean it will remain relatively benign. It may mutate or acquire new genetic material. Thus, ongoing, refined estimates of its pandemic potential will benefit from tracking epidemiological patterns in the field and viral mutations in the laboratory. If epidemic models suggest that more precise estimates on specific elements such as attack rate, case fatality rate, or duration of viral shedding will be pivotal for projecting pandemic potential, then these measurements deserve special attention. Even when more is learned, a degree of uncertainty will persist, and scientists have the responsibility to accurately convey the extent of and change in scientific uncertainty as new information emerges.

A range of laboratory, epidemiologic, and social science research will similarly be required to provide answers about vulnerable populations; interventions to prevent, treat, and mitigate disease and other consequences of a pandemic; and ways of achieving public understanding that avoid both over- and underreaction. Also, we know from past experience that planning for the implementation of such projects has often been inadequate. For example, if the United States decides to immunize twice the number of people in half the usual time, are the existing channels of vaccine distribution and administration up to the task? On a global scale, making the rapid availability and administration of vaccine possible is an order of magnitude more daunting.

Scientists and other flu experts in the United States and around the world have much to occupy their attention. Time and resources are limited, however, and leaders in government agencies will need to ensure that the most consequential scientific questions are answered. In the meantime, scientists can discourage irrational policies, such as the banning of pork imports, and in the face of a threatened pandemic, energetically pursue science in real time.

– Harvey V. Fineberg and Mary Elizabeth Wilson

10.1126/science.1176297

*C. Fraser *et al.*, *Science* 11 May 2009 (10.1126/science.1176062).

www.roche-applied-science.com

LightCycler® 1536 Real-Time PCR System

High Throughput – Redefined

NEW

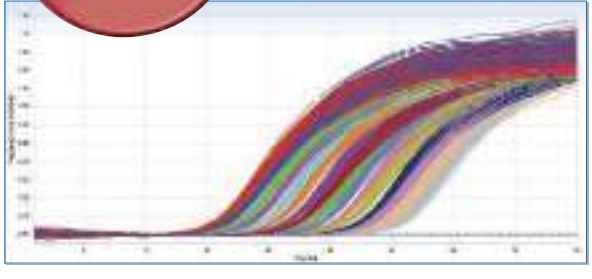

Figure 1: Sensitivity and reproducibility of the LightCycler® 1536 System. Use a fraction of the reaction volumes typical for lower throughput plate-based approaches (96- or 384-well format). Data quality is maintained even with low-volume reactions (0.5–2 µl). The real-time PCR plot shows sixteen concentration steps of a serial one-to-two dilution from 10^6 to 3×10^1 copies/sample (96 replicates each).

They said 1536 couldn't be done, but now it's here...

Introducing the **LightCycler® 1536 Real-Time PCR System** – an unprecedented breakthrough in qPCR technology.

- **Increase single-run throughput four-fold**
  Generate 1,536 data points in a single run in less than 50 minutes.
- **Cut your cost per data point in half**
  Benefit from advanced miniaturization that allows lower volumes of reagents and sample.
- **Forge ahead with data quality you can trust**
  Maintain continuity and comparability with your legacy results, even at extremely low reaction volumes.

Don't let the limitations of your current real-time PCR platform slow you down or hold you back any longer.

Learn more at *www.lightcycler1536.com*

For life science research only.

Roche Diagnostics
Roche Applied Science
Indianapolis, Indiana

Roche

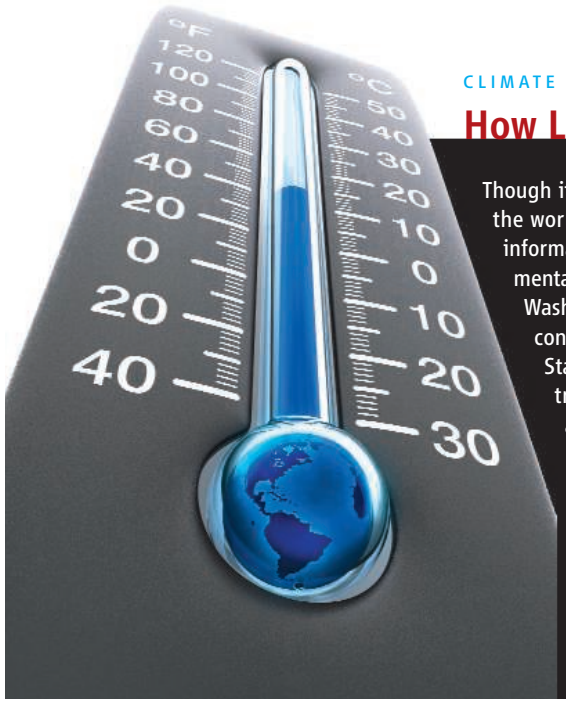

CLIMATE SCIENCE

How Low Can We Go?

Though it is well established that greenhouse gas emissions are causing the world to warm, policy-makers would benefit from further specific information in order to produce legislation that balances the environmental and economic effects of a given emissions reduction strategy. Washington *et al.* use a global coupled climate model to evaluate the consequences of a low-emission scenario developed by the United States Climate Change Science Program (CCSP), and thereby illustrate how aggressive mitigation can limit the rise of the global average tropospheric temperature to 1°C above current value by the year 2100. This temperature target is used because it is thought to represent the maximum at which the consequences of climate warming will remain manageable, before becoming dangerous. The authors also discuss ancillary climate consequences of this mitigation route, in an attempt to provide information relevant for the assessment of a wide range of policy options. — HJS

Geophys. Res. Lett. **36**, L08703 (2009).

HUMAN GENETICS

Expedited Pharmacogenomics

Drug-induced liver injury is one of the most common reasons that approved drugs are recalled from the market and that clinical trials of experimental drugs are terminated early. Susceptibility to liver damage and other adverse drug reactions are in part genetically determined, and a major goal of pharmacogenomics research is to find genetic markers that can be used to identify at-risk individuals in advance of drug treatment. The search for such biomarkers in human populations has proven to be labor-intensive, but a new study suggests that the hunt can be streamlined by using data derived from genetically diverse mouse populations to guide the human studies.

Harrill *et al*. studied 36 inbred strains of mice given large doses of acetaminophen and found that there were large strain-dependent variations in drug-induced liver injury, as assessed by histology and by elevated serum levels of the liver enzyme alanine aminotransferase (ALT). Candidate genes likely to be responsible for the inter-strain differences were identified by whole-genome association analysis, and the human versions of these genes were then sequenced in two small groups of humans. Sequence variants in several of these candidate genes—which, interestingly, encode proteins related to immune function rather than to xenobiotic metabolism—were indeed found to correlate with the presence of acetaminophen-induced elevation of serum ALT levels in the humans. — PAK

Genome Res. **19**, 10.1101/gr.090241.108 (2009).

CELL BIOLOGY

Warming Up to Its Host

The fungal pathogen *Candida albicans* responds to increases in temperature by initiating a transition from growing as a single-celled yeast to a multicellular filamentous form, the latter associated with greater virulence. Shapiro *et al.* report that inhibition of heat shock protein 90 (Hsp90) was necessary to promote filamentous growth in response to environmental conditions and was sufficient to promote filamentous growth in cells that would normally grow as the budding yeast form. Filament formation in cells with reduced expression of Hsp90 was more sensitive to increased temperature, and lower doses of a pharmacological inhibitor were required to promote filamentous growth at 37°C than at 30°C. Cells with mutations in the Ras1-PKA pathway [from the GTPase Ras1 to the cAMP-dependent protein kinase A (PKA)] failed to respond to inhibition of Hsp90. Genetic experiments also supported a role of Hsp90 in restraining filamentous differentiation by repressing signaling through the Ras1-PKA pathway, and in a mouse model, genetic depletion of Hsp90 completely cleared the kidney of *C. albicans*. — LBR

Curr. Biol. **19**, 621 (2009).

MICROBIOLOGY

Aeolian Microbes

In their day, Darwin and Pasteur both commented on microbe-bearing dust plumes from Africa. Climate change is exacerbating this phenomenon, and Hervàs *et al.* have investigated the potential for oligotrophic alpine lakes as sentinels for long-distance bacterial dispersal. Using 16*S* rRNA sequences, they compared the bacterial genera found in Mauritanian soil samples with those in dust plume

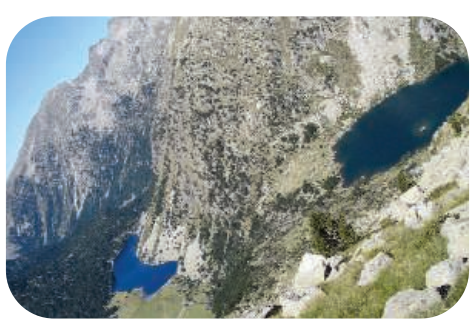

samples deposited in the Spanish Pyrenees and also examined the growth of the microbes in alpine lake water. Although the findings revealed the immigration capacity of certain taxa, many of the bacteria that survive passage to the Pyrenees are not spore-forming species. Some of the African soil samples contain organisms that do not survive air transport,

Continued on page 991

CREDITS (TOP TO BOTTOM): ISTOCK PHOTO; EMILIO CASAMAYOR

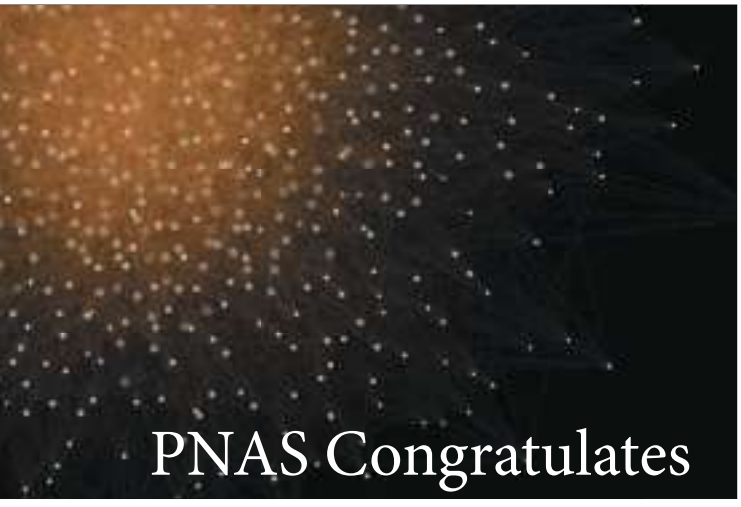

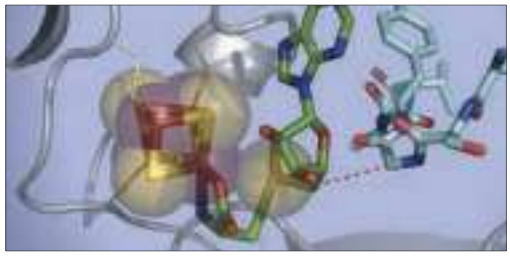

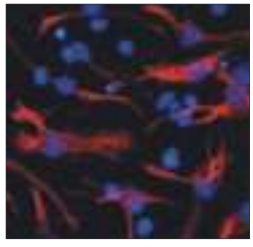

2008 Cozzarelli Prize Recipients

The *Proceedings of the National Academy of Sciences* (PNAS) has selected 6 outstanding articles for the 2008 Cozzarelli Prize, in recognition of their scientific excellence and originality. Winners were selected from the 3,500 research articles published online in PNAS in 2008 and represent exceptional contributions to the 6 broadly defined classes under which the National Academy of Sciences is organized.

2008 COZZARELLI PRIZE RECIPIENTS

Class I: Physical And Mathematical Sciences
Fluid helium at conditions of giant planetary interiors
Lars Stixrude and Raymond Jeanloz
(2008) PNAS 105:11071–11075

Class II: Biological Sciences
MicroRNA-directed transcriptional gene silencing in mammalian cells
Daniel H. Kim, Pål Sætrom, Ola Snøve, Jr., and John J. Rossi
(2008) PNAS 105:16230–16235

Class III: Engineering and Applied Sciences
The implications of human metabolic network topology for disease comorbidity
D.-S. Lee, J. Park, K. A. Kay, N. A. Christakis, Z. N. Oltvai, and A.-L. Barabási
(2008) PNAS 105:9880–9885

Class IV: Biomedical Sciences
Neurons derived from reprogrammed fibroblasts functionally integrate into the fetal brain and improve symptoms of rats with Parkinson's disease
Marius Wernig, Jian-Ping Zhao, Jan Pruszak, Eva Hedlund, Dongdong Fu, Frank Soldner, Vania Broccoli, Martha Constantine-Paton, Ole Isacson, and Rudolf Jaenisch
(2008) PNAS 105:5856–5861

Class V: Behavioral and Social Sciences
Cross-modal individual recognition in domestic horses (*Equus caballus*)
Leanne Proops, Karen McComb, and David Reby
(2009) PNAS 106:947–951

Class VI: Applied Biological, Agricultural, and Environmental Sciences
Decreases in dengue transmission may act to increase the incidence of dengue hemorrhagic fever
Yoshiro Nagao and Katia Koelle
(2008) PNAS 105:2238–2243

Podcast interviews with the authors will be available at www.pnas.org/site/misc/podcasts.shtml

PNAS
www.pnas.org

Continued from page 989

such as the cosmopolitan *Duganella zoogloeoides*, and pathogens, such as *Sphingomonas,* that have been implicated in coral disease in the Caribbean. — CA

Environ. Microbiol. **11**, 10.1111/j.1462-2920.2009.01926.x (2009).

CHEMISTRY

A Simple Twist

The topologically fascinating Möbius strip exhibits a single face and a single edge; it has no distinguishable back or front. At the molecular scale, Möbius strips intrigue chemists for the additional reason that they change the rules of aromaticity. Ring structures such as benzene and naphthalene have particular electronic stability on account of the atoms along the periphery sharing a certain number of pi-bonded electrons—specifically, even non-multiples of 4. If a twist is introduced into the ring framework, p orbitals overlap in an orientation opposite to that in a flat ring, and aromatic stabilization occurs instead when the pi electrons sum to multiples of 4. A few molecules exhibiting such Möbius aromaticity have been prepared, but the routes were complex. Tokuji *et al.* found that simple treatment of a hexaphyrin precursor with acetic acid yields an aromatic Möbius compound directly. The twist, confirmed crystallographically, ensues from the introduction of an oxygen atom that links a pendant perfluorophenyl group to the pyrrole backbone. — JSY

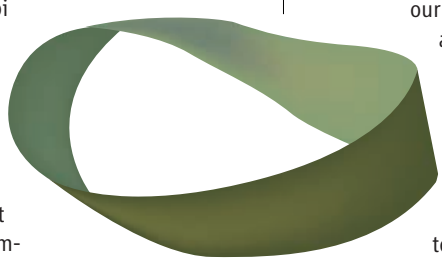

J. Am. Chem. Soc. **131**, 10.1021/ja902836x (2009).

GEOCHEMISTRY

Nanoparticle Coastlines

Mineral nanoparticles are naturally abundant in a wide range of environments, from the oceans to the atmosphere. Despite observations that particle size influences the reactivity of a mineral surface in a number of geochemical reactions, it is still largely unknown why nanoparticles behave differently than larger particles with the same composition. Spagnoli *et al*. show that in aqueous solutions, the size and shape of mineral particles influence the structure of the first few layers of water on their surfaces—an important determinant of reactivity. Using molecular dynamics simulations of the common iron-oxide mineral hematite, they found that water order and layering around the particle decreased for hematite particles of decreasing size. The residence time of water molecules near the surface was shorter for smaller, less-crystalline nanoparticles than for larger nanoparticles or a bulk hematite surface. Particles with facets or low curvature, however, tended to preferentially stabilize the water network and in some cases caused faceting within the water layer itself. The dynamic nature of the water solvation shell surrounding environmental nanoparticles probably influences the energetics of crystal growth and may help explain why some surface processes—including heterogenous catalysis, bacterial metal respiration, and ion adsorption—show trends that vary with particle size. — NW

Geochim. Cosmochim. Acta **73**, 10.1016/j.gca.2009.04.005 (2009).

HUMAN GENETICS

From AA to ZZ

Not only who we are, but also what diseases we suffer from is probably written somewhere in our DNA. Some genetic diseases are associated with the aggregation of misfolded mutant proteins that are toxic to cells. Quality-control mechanisms ensure that incorrectly folded proteins are usually degraded. For example, secretory proteins are folded in the endoplasmic reticulum (ER), and defective proteins are sorted and targeted for degradation, which is mediated in part by the enzyme ER mannosidase I (ERManI). A mutated version of the gene encoding alpha-1 antitrypsin (AAT) is associated with the accumulation of the misfolded Z variant of AAT in the ER and is a risk factor for the development of end-stage liver disease. However, the age of onset of this disease is variable, and other factors may be involved.

Pan *et al.* have discovered that a single-nucleotide polymorphism (A instead of G) in the 3′ untranslated region of the ERManI gene is associated with earlier onset. Individuals carrying two A alleles experience reduced synthesis of ERManI under stress, rendering them more vulnerable to deleterious effects if they should also be homozygous for the Z-variant anti-trypsin. These data provide a molecular mechanism for how a genetic locus can modify the severity of a protein-folding disease by moderating a quality-control checkpoint protein. — HP*

Hepatology **49**, 10.1002/hep.22974 (2009).

*Helen Pickersgill is a locum editor in *Science*'s editorial department.

www.sciencemag.org

Science

1200 New York Avenue, NW
Washington, DC 20005
Editorial: 202-326-6550, FAX 202-289-7562
News: 202-326-6581, FAX 202-371-9227
Bateman House, 82-88 Hills Road
Cambridge, UK CB2 1LQ
+44 (0) 1223 326500, FAX +44 (0) 1223 326501

Subscription Services For change of address, missing issues, new orders and renewals, and payment questions: 866-434-AAAS (2227) or 202-326-6417, FAX 202-842-1065. Mailing addresses: AAAS, P.O. Box 96178, Washington, DC 20090-6178 or AAAS Member Services, 1200 New York Avenue, NW, Washington, DC 20005

Institutional Site Licenses please call 202-326-6755 for any questions or information

Reprints: Author Inquiries 800-635-7181
Commercial Inquiries 803-359-4578

Permissions 202-326-7074, FAX 202-682-0816

Member Benefits AAAS/Barnes&Noble.com bookstore www.aaas.org/bn; AAAS Online Store www.apisource.com/aaas/ code MKB6; AAAS Travels: Betchart Expeditions 800-252-4910; Apple Store www.apple/eppstore/aaas; Bank of America MasterCard 1-800-833-6262 priority code FAA3YU; Cold Spring Harbor Laboratory Press Publications www.cshlpress.com/affiliates/aaas.htm; GEICO Auto Insurance www.geico.com/landingpage/go51.htm?logo=17624; Hertz 800-654-2200 CDP#343457; Office Depot https://bsd.officedepot.com/portalLogin.do; Seabury & Smith Life Insurance 800-424-9883; Subaru VIP Program 202-326-6417; VIP Moving Services www.vipmayflower.com/domestic/index.html; Other Benefits: AAAS Member Services 202-326-6417 or www.aaasmember.org.

science_editors@aaas.org	(for general editorial queries)
science_letters@aaas.org	(for queries about letters)
science_reviews@aaas.org	(for returning manuscript reviews)
science_bookrevs@aaas.org	(for book review queries)

Published by the American Association for the Advancement of Science (AAAS), *Science* serves its readers as a forum for the presentation and discussion of important issues related to the advancement of science, including the presentation of minority or conflicting points of view, rather than by publishing only material on which a consensus has been reached. Accordingly, all articles published in *Science*—including editorials, news and comment, and book reviews—are signed and reflect the individual views of the authors and not official points of view adopted by AAAS or the institutions with which the authors are affiliated.

AAAS was founded in 1848 and incorporated in 1874. Its mission is to advance science, engineering, and innovation throughout the world for the benefit of all people. The goals of the association are to: enhance communication among scientists, engineers, and the public; promote and defend the integrity of science and its use; strengthen support for the science and technology enterprise; provide a voice for science on societal issues; promote the responsible use of science in public policy; strengthen and diversify the science and technology workforce; foster education in science and technology for everyone; increase public engagement with science and technology; and advance international cooperation in science.

Information for Authors
See pages 807 and 808 of the 6 February 2009 issue or access www.sciencemag.org/about/authors

EDITOR-IN-CHIEF **Bruce Alberts**
EXECUTIVE EDITOR **Monica M. Bradford**
NEWS EDITOR **Colin Norman**
MANAGING EDITOR, RESEARCH JOURNALS **Katrina L. Kelner**
DEPUTY EDITORS **R. Brooks Hanson, Barbara R. Jasny, Andrew M. Sugden**

Editorial senior editor/perspectives Lisa D. Chong; **senior editors** Gilbert J. Chin, Pamela J. Hines, Paula A. Kiberstis (Boston), Marc S. Lavine (Toronto), Beverly A. Purnell, L. Bryan Ray, Guy Riddihough, H. Jesse Smith, Phillip D. Szuromi (Tennessee), Valda Vinson; **associate editors** Kristen L. Mueller, Nicholas S. Wigginton, Jake S. Yeston, Laura M. Zahn; **online editor** Stewart Wills; **associate online editors** Robert Frederick, Tara S. Marathe; **web content developer** Martyn Green; **book review editor** Sherman J. Suter; **associate letters editor** Jennifer Sills; **editorial manager** Cara Tate; **senior copy editors** Jeffrey E. Cook, Cynthia Howe, Harry Jach, Barbara P. Ordway, Trista Wagoner; **copy editors** Chris Filiatreau, Lauren Kmec; **editorial coordinators** Carolyn Kyle, Beverly Shields; **publications assistants** Ramatoulaye Diop, Carlos L. Durham, Joi S. Granger, Jeffrey Hearn, Lisa Johnson, Scott Miller, Jerry Richardson, Jennifer A. Seibert, Brian White, Anita Wynn; **editorial assistants** Emily Guise, Michael Hicks, Patricia M. Moore; **executive assistant** Sylvia S. Kihara; **administrative support** Maryrose Madrid

News deputy news editors Robert Coontz, Eliot Marshall, Jeffrey Mervis, Leslie Roberts; **contributing editors** Elizabeth Culotta, Polly Shulman; **news writers** Yudhijit Bhattacharjee, Adrian Cho, Jennifer Couzin, David Grimm, Constance Holden, Jocelyn Kaiser, Richard A. Kerr, Eli Kintisch, Andrew Lawler (New England), Greg Miller, Elizabeth Pennisi, Robert F. Service (Pacific NW), Erik Stokstad; **intern** Jackie D. Grom; **contributing correspondents** Dan Charles, Jon Cohen (San Diego, CA), Daniel Ferber, Ann Gibbons, Robert Koenig, Mitch Leslie, Charles C. Mann, Virginia Morell, Evelyn Strauss, Gary Taubes; **copy editors** Linda B. Felaco, Melvin Gatling, Melissa Raimondi; **administrative support** Scherraine Mack, Fannie Groom; **bureaus** New England: 207-549-7755, San Diego, CA: 760-942-3252, FAX 760-942-4979, Pacific Northwest: 503-963-1940

Production director James Landry; **senior manager** Wendy K. Shank; **assistant manager** Rebecca Doshi; **senior specialists** Steve Forrester, Chris Redwood; **specialist** Anthony Rosen; **Preflight director** David M. Tompkins; **manager** Marcus Spiegler; **specialist** Jason Hillman

Art director Yael Kats; **associate art director** Laura Creveling; **illustrators** Chris Bickel, Katharine Sutliff; **senior art associates** Holly Bishop, Preston Huey, Nayomi Kevitiyagala; **art associate** Jessica Newfield; **photo editor** Leslie Blizard

***Science* International**

Europe (science@science-int.co.uk) **editorial: international managing editor** Andrew M. Sugden; **senior editor/perspectives** Julia Fahrenkamp-Uppenbrink; **senior editors** Caroline Ash, Stella M. Hurtley, Ian S. Osborne, Peter Stern; **associate editor** Maria Cruz; **locum editor** Helen Pickersgill; **editorial support** Deborah Dennison, Rachel Roberts, Alice Whaley; **administrative support** John Cannell, Janet Clements, Louise Moore; **news: europe news editor** John Travis; **deputy news editor** Daniel Clery; **contributing correspondents** Michael Balter (Paris), John Bohannon (Vienna), Martin Enserink (Amsterdam and Paris), Gretchen Vogel (Berlin); **intern** Claire Thomas

Asia Japan Office: Asca Corporation, Eiko Ishioka, Fusako Tamura, 1-8-13, Hirano-cho, Chuo-ku, Osaka-shi, Osaka, 541-0046 Japan; +81 (0) 6 6202 6272, FAX +81 (0) 6 6202 6271; asca@os.gulf.or.jp; **asia news editor** Richard Stone (Beijing: rstone@aaas.org); **contributing correspondents** Dennis Normile (Japan: +81 (0) 3 3391 0630, FAX +81 (0) 3 5936 3531; dnormile@gol.com); Hao Xin (China: +86 (0) 10 6307 4439 or 6307 3676, FAX +86 (0) 10 6307 4358; cindyhao@gmail.com); Pallava Bagla (South Asia: +91 (0) 11 2271 2896; pbagla@vsnl.com)

EXECUTIVE PUBLISHER **Alan I. Leshner**
PUBLISHER **Beth Rosner**

Fulfillment Systems and Operations (membership@aaas.org); **director** Waylon Butler; **senior systems analyst** Jonny Blaker; **customer service supervisor** Pat Butler; **specialists** Latoya Casteel, LaVonda Crawford, Vicki Linton, April Marshall; **data entry supervisor** Cynthia Johnson; **specialists** Eintou Bowden, Tarrika Hill, William Jones

Business Operations and Administration director Deborah Rivera-Wienhold; **assistant director, business operations** Randy Yi; **manager, business analysis** Michael LoBue; **manager, business operations** Jessica Tierney; **financial analysts** Priti Pamnani, Celeste Troxler; **rights and permissions: administrator** Emilie David; **associate** Elizabeth Sandler; **marketing director** Ian King; **marketing manager** Allison Pritchard; **marketing associates** Aimee Aponte, Alison Chandler, Mary Ellen Crowley, Julianne Wielga, Wendy Wise; **marketing executive** Jennifer Reeves; **marketing/member services executive** Linda Rusk; **director, site licensing** Tom Ryan; **director, corporate relations** Eileen Bernadette Moran; **publisher relations, eresources specialist** Kiki Forsythe; **senior publisher relations specialist** Catherine Holland; **publisher relations, east coast** Phillip Smith; **publisher relations, west coast** Philip Tsolakidis; **fulfillment supervisor** Iquo Edim; **fulfillment coordinator** Laura Clemens; **electronic media: manager** Lizabeth Harman; **project manager** Trista Snyder; **assistant manager** Lisa Stanford; **senior production specialists** Christopher Coleman, Walter Jones; **production specialists** Nichele Johnston, Kimberly Oster

Advertising director, worldwide ad sales Bill Moran

Product (science_advertising@aaas.org); **midwest/west coast/w. canada** Rick Bongiovanni: 330-405-7080, FAX 330-405-7081; **east coast/e. canada** Laurie Faraday: 508-747-9395, FAX 617-507-8189; **uk/europe/asia** Roger Goncalves: TEL/FAX +41 43 243 1358; **japan** Mashy Yoshikawa: +81 (0) 3 3235 5961, FAX +81 (0) 3 3235 5852; **senior traffic associate** Deiandra Simms

Commercial Editor Sean Sanders: 202-326-6430

Project Director, Outreach Brianna Blaser

Classified (advertise@sciencecareers.org); **u.s.: sales manager** Daryl Anderson: 202-326-6543; **inside sales representative** Tina Burks: 202-326-6577; **key account manager/midwest** Joribah Able; **east coast** Alexis Fleming: 202-326-6578; **west/south central** Nicholas Hintibidze: 202-326-6533; **sales coordinators** Rohan Edmonson, Shirley Young; **international: sales manager** Tracy Holmes: +44 (0) 1223 326525, FAX +44 (0) 1223 326532; **sales** Susanne Kharraz, Dan Pennington, Alex Palmer; **japan** Mashy Yoshikawa: +81 (0) 3 3235 5961, FAX +81 (0) 3 3235 5852; **advertising support manager** Karen Foote: 202-326-6740; **advertising production operations manager** Deborah Tompkins; **senior production specialist/graphic designer** Amy Hardcastle; **senior production specialist** Robert Buck; **senior traffic associate** Christine Hall; **publications assistant** Mary Lagnaoui

AAAS Board of Directors retiring president, chair James J. McCarthy; **president** Peter C. Agre; **president-elect** Alice Huang; **treasurer** David E. Shaw; **chief executive officer** Alan I. Leshner; **board** Alice Gast, Linda P. B. Katehi, Nancy Knowlton, Cherry A. Murray, Julia M. Phillips, Thomas D. Pollard, David S. Sabatini, Thomas A. Woolsey

AAAS
ADVANCING SCIENCE, SERVING SOCIETY

SOLiD 3

YOUR TRANSCRIPTOME ANALYSIS

£MPOWERED

The SOLiD™ 3 System empowers you to discover new insights into gene regulation. With a hypothesis-generating, highly-sensitive assay that preserves the strand information of the original RNA molecule, the SOLiD 3 System enables you to detect novel transcripts, including non-coding RNA and distinguish strand-specific expression patterns. The combination of 400 million sequence tags and sample multiplexing capabilities allows for cost effective analysis of multiple samples in a single run while maintaining the sensitivity to detect low abundance transcripts. Combined with the SOLiD Small RNA Expression Kits, Whole Transcriptome Analysis Kits and application specific data analysis tools, the SOLiD 3 System provides a comprehensive solution that takes you from RNA to results.

For more SOLID PROOF, visit solid.appliedbiosystems.com

Applied Biosystems

Submission deadline August 1

Rewarding brilliance since 1995.

The GE & Science Prize for Young Life Scientists. Because brilliant ideas build better realities.

Imagine standing on the podium at the Grand Hotel in Stockholm, making your acceptance speech. Imagine joining the ranks of those published in Science magazine and having your essay on your work in molecular biology read by your peers around the world. Imagine taking part in a seminar with the other Prize winners and Nobel Prize laureates and discussing your work with leaders in the field. Imagine what you could do with the $25,000 prize money. Imagine what a brilliant start to your career, and where it could lead. Now stop imagining. If you were awarded your Ph.D in 2008, submit your 1000-word essay by August 1 and make it reality.

Want to build a better reality? Go to www.gelifesciences.com/science

GE & Science Prize for Young Life Scientists

imagination at work

Science AAAS

* For the purpose of this prize, molecular biology is defined as "that part of biology which attempts to interpret biological events in terms of the physico-chemical properties of molecules in a cell".

(McGraw-Hill Dictionary of Scientific and Technical Terms, 4th Edition).

Tale of Two Fishes

Two different populations of Mexican molly fish that share a habitat with a fish-eating water bug are showing how predators can shape evolution.

Sharp-eyed Atlantic molly fish swim in open streams right next door to small-eyed, dark-dwelling cave mollies, but the two populations won't mix. To find out whether the bug is keeping them apart, evolutionary ecologist Michael Tobler of Texas A&M University in College Station collected 94 fish from each habitat, paired one from each habitat in bottles, and threw in a water bug. He placed half of the bottles in the cave and the rest in the open stream.

When Tobler checked 24 hours later, he found that the water bug could be keeping the fish in their place. The mollies outside their natural environments were more likely to be attacked, he reported online 14 May in the journal *Biology Letters*. The study adds an "important contribution" to evidence that predation can play a major role in the speciation process, says R. Brian Langerhans of the University of Oklahoma Biological Station in Kingston. Tobler says the cave fish have enhanced nonvisual ways of sensing predators that don't help them in the light, whereas the surface fish, which rely on their eyesight, are at a loss in the dark.

Undersea Metropolis

The ancient Greek town of Pavlopetri has lain under the sea, just 50 meters off the southeastern tip of the Peloponnese, for more than 3000 years. After a brief flurry of research when the town was discovered in 1967, Pavlopetri has been ignored by science. Now, however, a team led by archaeologist Jon Henderson of the University of Nottingham in the United Kingdom plans to use new sonar technology to map the ruins and study the site.

The former town, probably submerged by earthquakes in about 1000 B.C.E., is near the present-day port of Neapolis. It lies under 3 to 4 meters of water, where the sandy seabed gives way to 500 square meters of stone remains of buildings, streets, and graves from the Mycenaean civilization (about 1680 to 1180 B.C.E.). "The power of the Mycenaeans largely came from their dominance of the eastern Mediterranean, but we know almost nothing about their harbor towns," says Henderson. Unearthing Pavlopetri could "give detailed insights" into Mycenaean sea trade, says archaeologist Geoff Bailey of the University of York, U.K.

SPREADING THE FLU

Even a pandemic can have a silver lining. A flood of visitors to an Irish exhibition about epidemics has become a mother lode of data on the spread of disease.

On 17 April, the Science Gallery at Trinity College Dublin launched an exhibit called INFECTIOUS. To give visitors a firsthand feel for "epidemic processes," everyone gets a radio-frequency identification tag. Tags are initially "uninfected" but can get "infected" by proximity to "infected" staff or visitors. A computer tracks everyone, mapping the spread of the infection.

The timing turned out to be propitious. Soon after the opening, swine flu panic hit. "We've had an amazing response," with more than 13,000 visitors so far, says gallery director Michael John Gorman. The data are flowing to computers in Italy, where epidemiologists at the Institute for Scientific Interchange Foundation in Turin are modeling epidemics. The experiment "does seem to address human-to-human contact at the most local level, which is the least well understood of organizational scales," says Oliver Pybus, an epidemiologist at the University of Oxford in the United Kingdom.

Ancestral Imprint

Just as the prospect of hanging concentrates the mind, information related to survival sticks in it. To test that proposition, cognitive psychologist James Nairne of Purdue University in West Lafayette, Indiana, and colleagues divided 250 students into four groups. Two groups were told to imagine themselves hunting or gathering for subsistence. The others were told to think about collecting food as part of a contest.

The researchers then gave each student the same 30 random nouns, such as chair, snow, and orange, and told them to associate the words with their scenario. A paper published online 5 May in *Psychological Science* reports that students in the survival scenario later remembered more of the words than those in the game-playing scenario, suggesting that connection with a life-or-death situation improved their memory.

The human mind "continues to bear the footprint of ancestral selection factors" that shaped cognition, Nairne says. Evolutionary psychologist Rick O'Gorman of Sheffield Hallam University in the United Kingdom calls the research "another link in the chain toward demonstrating the value of considering an evolutionary perspective on all areas of psychology."

CREDITS (TOP TO BOTTOM): MICHAEL TOBLER; JON HENDERSON; PATRICK BOLGER/SCIENCE GALLERY

Time to turn off Mars rovers?
998

Issues facing CDC's new head
1003

SWINE FLU OUTBREAK

Past Pandemics Provide Mixed Clues to H1N1's Next Moves

Ask influenza researchers where they think the swine flu outbreak is heading, and the stock reply is a flat-out refusal to speculate. But ask them whether their research into other influenza viruses and the course of past pandemics hold any clues, and they have insights aplenty. And many lessons from the past, they say, upend cherished dogma.

Like hurricane watchers, public health officials must try to predict the velocity and course of the influenza A virus causing this outbreak, a novel H1N1, because they have to make complicated and expensive decisions about how aggressively they should pursue vaccines, antivirals, and mitigation strategies like school closings. Given the fuzziness of the data about this new virus's behavior, researchers are looking to the past for clues about the seasonality and geography of pandemic flu, the relationship between the new viruses and existing ones, and the behavior of this new H1N1's parent viruses in swine.

Many would-be influenza seers expect that this H1N1 will soon leave the Northern Hemisphere for cooler, southern climes, infect millions there, become stronger, and then return north as temperatures drop, causing a second wave of infections in the north that are more devastating than the first. "It happens, but everybody is hedging their bets with this virus," says epidemiologist and historian Donald Olson, research director for the International Society for Disease Surveillance. Although abundant evidence confirms the seasonality of flu, a careful study of a different human influenza virus, H3N2, published in *Science* last year (18 April 2008, p. 340), showed that it typically starts in east and Southeast Asia, and then indeed moves from north to south—but rarely returns to the north. Virologist Robert Webster of St. Jude Children's Research Hospital in Memphis, Tennessee, adds that the new H1N1 has already shown that it doesn't give a whit about the ending of winter in the Northern Hemisphere. "It's too late in the season to be in humans at the moment, but it is," says Webster. "You can't lay down rules for flu viruses—they'll break them every time. It's almost as though the virus reads them and says, 'I'll do the damn opposite.'"

Researchers have relatively good data about four pandemics that have occurred since 1890, and they all followed different seasonal patterns (see graphic). The second wave of the first pandemic walloped London between April and June 1891. The infamous 1918 Spanish flu had its first wave in Copenhagen in July. The first wave of the 1957 Asian flu hit the United States in September. "Pandemic influenza viruses do not respect normal seasonality," concludes epidemiologist Lone Simonsen of George Washington University in Washington, D.C., who has closely studied each historical pandemic. She questions whether the new H1N1 will even leave the Northern Hemisphere in the next few weeks. "There could be a summer wave," she says. "I'd make a case for not putting our guards down now."

Epidemiologist Arnold Monto of the University of Michigan School of Public Health in Ann Arbor says when the 1957 flu surfaced in the United States, many researchers suspected the same north-south-north pattern would come into play. "People at that time were worried that they might be seeing a 1918," says Monto, who notes that air travel was not prevalent then. "So they sent people to the Southern Hemisphere … to study the outbreak as it took off, and in most countries, it didn't."

If the nightmare scenario of 1918 returns, the novel H1N1 could become more destructive during a second wave. In that pandemic, Simonsen and others suspect that the virus went through genetic drift, a process in which the human immune response leads the virus to mutate. "We would expect to see quite rapid drift of this virus once it generates a large-scale epidemic in one hemisphere," says Neil Ferguson, a mathematical epidemiologist at Imperial College London.

Virologist Peter Palese of

PANDEMIC WAVES

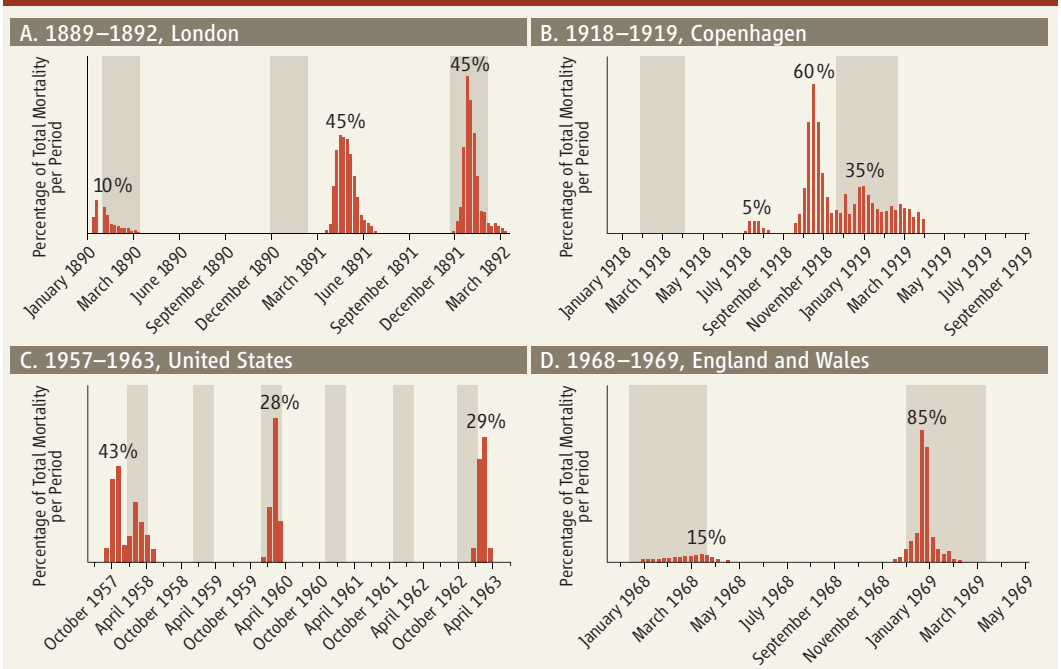

*Red bars ( ) indicate mortality. Shaded columns ( ) show normal seasonal influenza period.

CREDIT: ADAPTED FROM MARK MILLER *ET AL., N. ENGL. J. MED.* (2009)

Duplication in scientific papers
1004

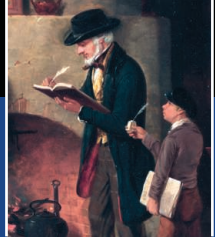

No consensus on census undercount
1008

Mount Sinai School of Medicine in New York City says that when gauging the threat posed by the new H1N1, scientists should keep in mind that it does not have a version of the protein called PB1-F2 that research has linked to the virulence of other pandemic strains. "That's one reason I don't believe this virus will cause a lot of problems," says Palese. The new H1N1 could also die out entirely. "There's a 50–50 chance it will continue to circulate," he predicts.

One worry is that the new virus could pick up genes from other influenzas, a process called reassortment, and develop more resistance to drugs or other dangerous features. Although there is no index to gauge a strain's likelihood to reassort, virologist Richard Webby, who works with Webster at St. Jude, says the well-studied parental viruses of this H1N1 suggest that it comes from a promiscuous family. The new virus is a so-called triple reassortant—a mix of swine, human, and avian genes—that researchers first found in North American pigs in 1998. Since then, Webby says researchers have discovered three different instances of human genes reassorting with these pig viruses.

But the good news, says Webby, is that no previously detected pig triple reassortants have caused severe disease in swine. The same is true of the other presumed parent of the novel H1N1, a Eurasian swine virus. "We know enough about the parents of this particular virus, which have been evolving in a mammalian host for extended periods, that I'm far from convinced that we'll see any exacerbation of disease," says Webby. "I'm not a big believer that this virus will come back with a punch in a second wave."

Yet at the end of the day, making predictions about this new H1N1's next move is a mug's game. "There's nothing more predictable about flu than its unpredictability," cautions epidemiologist Monto. "Who would have thunk something would have come out of North America and taken off first in Mexico and then gone to the United States and Canada?" **–JON COHEN**

For continuing coverage of the epidemic, go to blogs.sciencemag.org/scienceinsider.

CHINA

Appearances Can Deceive, Even With Standard Reagents

Culturing immortalized human cell lines for microRNA studies had been a routine procedure in Xi Jianzhong's lab at Peking University. Then last June, something went wrong. Time after time, black spots appeared in the flasks and the cells died within a week. Xi, a biomedical engineer, spent the rest of 2008 trying to figure out why his team's experiments were failing. He finally got a tip that a cell growth medium his lab was using—Dulbecco's Modified Eagle Medium (DMEM)—might be bogus. "DMEM is so basic that we never suspected it could have problems," says Xi. Sure enough, after obtaining a fresh batch from a well-known distributor, the cell lines grew without a hitch.

China is infamous for cheap knockoffs of brand-name consumer goods. Now many scientists are discovering to their dismay that a cottage industry of faux biochemical reagents has sprung up to take advantage of China's hefty increases in R&D funding. Scientists who until recently worked overseas are especially vulnerable because they may not know which dealers to trust, Xi says. "More and more researchers are returning to China. We don't want them to waste time and money like we did," says Huang Yanyi, who like Xi is a returnee in Peking University's biomedical engineering department.

After Xi learned that many colleagues had also been victimized but kept quiet about their experiences, he contacted ScienceNet.cn, a Web site for China's scientific community. In an online survey conducted with the biweekly magazine *Science News*, more than half of the nearly 500 respondents reported run-ins with fake reagents, according to results posted on ScienceNet.cn on 29 April.

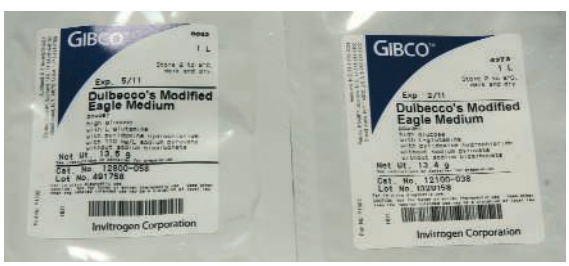

Spitting image. Authentic (*left*) and fake (*right*) packages of Dulbecco's Modified Eagle Medium.

Exposing scams may not prevent them. Currently, no Chinese agency regulates research reagents, except those used for medical tests. A database kept by Lab-on-web (www.bioon.com.cn) lists more than 500 reagent dealers in China; many are small operations claiming to be distributors of foreign products. The Web site has also published the names of unscrupulous dealers.

Legitimate companies say there is little they can do about the bad apples. "It is a widespread concern throughout the life science and other industries in China," says Johnson Ho, president for Greater China at Life Technologies, based in Foster City, California. Invitrogen, a division of Life Technologies, discovered that some of its products had been counterfeited. It has created a list of authorized distributors (www.invitrogen.com/site/us/en/home/Global/Contact-Us/RegionalContactUs/China.html). Ho suggests customers buy only from distributors on the list.

Earlier this year, Xi confronted the Beijing-based distributor who sold his lab the false DMEM. The dealer challenged Xi to prove his case. Xi called Invitrogen's office in Shanghai, which on 20 March dispatched representative Ju Jun to Xi's lab to examine the DMEM. At first glance, the packages looked genuine, but a search in Invitrogen's database by lot number, which anyone can do on the company's Web site, revealed that one lot number did not exist, and a second had an expiration date that was different from that stated on the fake DMEM's package.

Counterfeits are not limited to Invitrogen products. In recent years, others have reported fake enzyme-linked immunosorbent assay kits and ovalbumin products. More than time or money may be at stake, says Huang. If Chinese researchers were to publish spurious results because of fake reagents, he says, "we could lose our credibility as scientists." **–HAO XIN**

With reporting by Xu Zhiguo of *Science News* in Beijing.

CREDIT: COURTESY OF XI JIANZHONG

PLANETARY SCIENCE

Mars Rover Trapped in Sand, But What Can End a Mission?

Times are tough for the Spirit rover. Last week, in its 5th year of exploration, Spirit became mired in a dry martian version of quicksand. Mission engineers are studying how it might extricate itself, but the crisis raises a perennial question: When, if ever, should a mission in its declining years be put out of its misery? When does the diminishing science output no longer justify the millions of dollars it costs?

"NASA always has a hard time cutting off any operating mission," says planetary geologist Harry McSween of the University of Tennessee, Knoxville, who is on the Spirit science team. "If it turns out that Spirit can't move anymore, perhaps that decision will be easier."

No one has yet suggested ending Spirit's mission, but a permanently immobilized rover would certainly force the issue. NASA already conducts annual evaluations, which balance the cost of operating Spirit and its sister rover, Opportunity—currently $20 million per year—against the potential science payoff of continued operation. The two rovers have already run up initial costs of $400 million each, so their relatively modest annual costs have presented no obstacle to passing their annual reviews, despite the inevitable decline in major discoveries with time.

"The new findings [from the rovers] are dwindling to a trickle," says Michael Carr of the U.S. Geological Survey in Menlo Park, California, a nearly 40-year veteran of Mars exploration. That's partly because the rovers have thoroughly explored their immediate surroundings. Spirit is now nearly immobilized at what is likely an ancient steam vent, bogged down in deposits from the volcanic outlet—some of the very stuff that was one of its major discoveries.

On the other side of the planet, Opportunity is 3 kilometers into a 16-kilometer trek away from Victoria crater, which it explored for 2 years. On page 1058, Opportunity science team members report that the salty sediments exposed in Victoria's walls looked just like those in the two smaller craters Opportunity has also explored. At its present pace, Opportunity will take two more years to cross flat, familiar terrain before reaching its next target, the even larger Endeavour crater.

The discoveries also come more slowly because the rovers are getting long in the tooth. They are in surprisingly good shape for being years past their 90-day "warranties," but Spirit is dragging one of its six wheels, which has become inoperable. That is making uphill travel difficult or impossible. Opportunity has a wheel showing early signs of the same problem. Among other signs of advanced age: The two bits of radioactive cobalt-57 vital to each rover's Mössbauer mineral analyzer are so depleted that it "takes weeks to do what we were able to do in hours," says McSween.

Near, yet far. The Mars Spirit rover (*inset*) has bogged down in fluffy soil until its wheels are nearly buried (*left*). It had been on its way to another likely volcanic vent 200 meters away (*right*).

Long-running NASA missions like these rovers most often end in one of two ways. Controllers can lose them to a technical problem, perhaps through their own error. That often happens late in a mission when cost saving has shrunk the mission's operations staff, says Carr. He recalls how in the early 1980s, the skeleton crew running the two Viking landers on Mars ended up losing a lander after misorienting its communications antenna.

Or missions can run out of energy. After the Galileo orbiter ran low on thruster fuel in 2003, controllers flew it into Jupiter, making valuable observations in close-in regions. The two Voyager spacecraft, on the other hand, are on an "interstellar" mission beyond Pluto after their 1977 launches. Their waning radiogenic power sources still allow them to return a dribble of observations from the edge of the solar system, where no spacecraft has gone before.

Spirit and Opportunity rover team members half-expected that a predictable dearth of energy would end their mission, as martian dust accumulated on the rovers' solar panels and blocked sunlight. But wind gusts came to the rescue. Just a few weeks ago, several gusts—presumably swirling martian dust devils—cleaned Spirit's panels and returned its power to two-thirds its level on landing.

The rovers enjoy considerable political support in Congress, and the public finds the intrepid explorers adorable. But to Mars researchers, it's the new science the rovers might return that justifies their operating cost. "There's more that can be done," says John Mustard of Brown University, chair of NASA's Mars Exploration Program Analysis Group. "You don't turn off an operating rover. You can't predict what's around the next corner. You're moving, you're doing science, you go for it."

"Moving" will be key. "It's very easy to make a case if you get to a new place," says Torrence Johnson of NASA's Jet Propulsion Laboratory in Pasadena, California. Even if Spirit extricates itself, sand traps in its path ahead might still confine it to an already-explored patch of Mars. And if Opportunity's misbehaving wheel finally breaks, that rover could wind up hobbling across a relatively boring plain far from Endeavour. Either way, says rover science principal investigator Steven Squyres of Cornell University, mission scientists and engineers would "have to look case by case with NASA headquarters" to balance the newly limited science potential against the inevitable cost. Then someone at NASA—probably the administrator—would decide whether to pull the plug.

–RICHARD A. KERR

CREDITS: NASA/JPL-CALTECH; (INSET) NASA/JPL/CORNELL UNIVERSITY

Published by AAAS

NEWSMAKER INTERVIEW

NASA Asks Augustine to Point the Way

This month, Norman Augustine, former CEO of Lockheed Martin, agreed to lead a 90-day review of NASA's human space flight program. The 73-year-old aeronautics engineer has a sterling reputation for providing impartial and useful advice on science policy: In 2005, he chaired a similarly rapid examination of the federal research investment that produced the National Academies' wildly influential *Rising Above the Gathering Storm* (*RAGS*) report, and in 1990, he directed a review of the U.S. space program.

This time around, presidential science adviser John Holdren and acting NASA Administrator Christopher Scolese want Augustine to review the space "vision" laid out by President George W. Bush in January 2004. NASA has translated that vision into building a new rocket and space capsule that would replace the shuttle and service the international space station. The next step would be returning astronauts to the moon and, eventually, visiting Mars. Augustine says the panel will also be looking at "balancing" human exploration and science.

Augustine emphasized that he didn't want to speak for the commission, whose members are expected to be named shortly. But he did share his thoughts on a number of issues that the panel is likely to tackle. **–JEFFREY MERVIS**

Q: Do you expect this commission to break new ground?
N.A.: Sometimes it's a matter of putting the pieces together. When the *RAGS* report recommended increased support for basic research and fixing K–12 education, we weren't entering new territory. And I suspect the same will be true for this commission. It's not likely that we'll be finding a new planet. But sometimes restating the obvious is helpful.

Q: How much will you be constrained by NASA's tight budget?
N.A.: We've been asked to recommend what makes sense within that [budget] profile. But we will not be shy about saying that NASA doesn't have enough resources to do the job right, if that's what we believe is the case.

Q: You told appropriators in the House of Representatives recently that you think NASA's budget should be on the same doubling path as the National Science Foundation and the Department of Energy's science programs.
N.A.: It's my personal view that any agency performing basic research should be on that path, and that includes NASA.

Q: Will the panel also review NASA's space science program?
N.A.: The focus of our effort is on the human space program. But we will also be looking at the science programs that are associated with human flight. That includes aspects that might better be done without human involvement. … For example, we might look at the idea of a precursor mission, with a robotic probe, before you get humans involved. That would tell you if it even makes sense to go where you want to go.

Q: Would that be a new approach for NASA?
N.A.: Yes, I don't know that they have done that in the past. And I'm not saying that we would [suggest it]. But I think we'd at least want to look at that possibility. The previous [1990] study made the point that there are certain things that humans can do that robotics cannot, and vice versa. And I think it's important to keep that in mind as we go forward.

Q: What's your goal for the commission?
N.A.: Hopefully, we'll be able to recommend a way forward, but in a fiscally responsible manner.

CREDITS (TOP TO BOTTOM): MALCOLM LINTON; NORMAN AUGUSTINE/NSF

ScienceNOW.org

From *Science*'s Online Daily News Site

Surviving Chernobyl. You might expect the scene of the world's worst nuclear disaster to be a barren wasteland. But trees, bushes, and vines overtake abandoned streets surrounding the Chernobyl nuclear power facility in Ukraine. Now, researchers say they've discovered changes in the proteins of soybeans grown near Chernobyl that could explain how plants survive despite chronic radiation exposure. The findings, reported in the *Journal of Proteome Research*, could one day help researchers engineer radiation-resistant crops. http://tinyurl.com/ptgv56

Designer Antibodies and AIDS. A new antiviral strategy powerfully protects monkeys from SIV, the simian cousin of HIV. The approach, reported in *Nature Medicine*, combines elements of vaccines and gene therapy. Experts say the development could eventually lead to a vaccinelike weapon against AIDS—a goal that has thus far proved elusive. http://tinyurl.com/ph753f

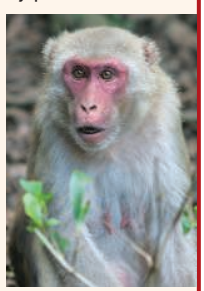

Putting Photons to Work. Researchers have built a nanoscale device that vibrates when struck by incoming laser light. The contraption, reported in *Nature*, is sensitive to the energy of a single photon. The advance could speed the development of new optical communications systems; it could also help scientists probe some of the fundamental properties of matter with greater precision. http://tinyurl.com/r45lzt

Sparrows Change Their Tune. The year was 1970. Simon and Garfunkel topped the charts, floppy disks were brand-new, and California white-crowned sparrows sang fast, machine-gun trills. Just a few decades later, the sparrows sing noticeably slower songs, and a new study reveals the reason. The birds' habitat has gotten scrubbier, and their melodies have evolved to better penetrate the thickets, researchers report in *The American Naturalist*. http://tinyurl.com/phd53h

Read the full postings, comments, and more on **sciencenow.sciencemag.org**.

Published by AAAS

BIOTECHNOLOGY

Lawsuit Challenges Legal Basis For Patenting Human Genes

Patents have been awarded on human genes for decades, but until last week, no one had directly challenged the underlying idea that genes can be owned in a U.S. court. Now, a challenge has begun.

With donated legal help, a group of patients, doctors, and research professionals sued in New York City on 12 May to invalidate perhaps the most famous gene patents: those on *BRCA1* and *BRCA2*, genes associated with risk for breast and ovarian cancer. The main argument in last week's legal filing in Manhattan's federal court is that *BRCA1* and *-2* are "products of nature" and should never have been patented. The suit names 12 defendants, including the U.S. Patent and Trademark Office (PTO), for allowing the patents, and Myriad Genetics Inc. of Salt Lake City for running a patent-protected gene testing monopoly.

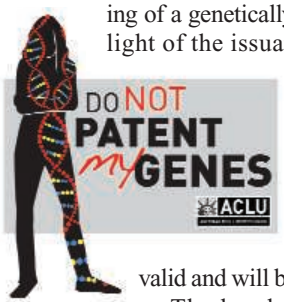

Test case. ACLU claims that gene patents were used to suppress free speech.

Myriad and others who hold *BRCA* patents—including the U.S. government—had not filed a response with the court at press time. Myriad spokesperson Richard Marsh said the company is still evaluating the case but added that a Supreme Court ruling in 1980 (*Diamond* v. *Chakrabarty*) upheld the patenting of a genetically engineered organism. "In light of the issuance of thousands of gene patents over 30 years, … we believe our patents are valid and will be upheld by the courts."

The legal muscle in the complaint against *BRCA* patents is provided by two groups in New York City, the American Civil Liberties Union (ACLU) and the Public Patent Foundation, a smaller advocacy group associated with the Benjamin N. Cardozo School of Law. According to an ACLU spokesperson, the civil rights champion has never before taken the lead in a science-laden case like this. The complaint goes beyond the "natural products" challenge and makes a second, more incendiary charge. It claims that Myriad violated defendants' freedom of speech, which is guaranteed by the U.S. Constitution, by using its monopoly to impede rival research, restrict clinical practice, and deny people access to medical information.

For example, the complaint says, Myriad issued a "cease and desist" letter to genetics researcher Haig Kazazian Jr. at the University of Pennsylvania—one of 20 plaintiffs in this case—ordering him in 1998 to stop *BRCA* screening in his clinic without Myriad's permission. Myriad issued eight other such orders, the complaint says, including one to Yale University, which subsequently stopped *BRCA* testing. Several patients who joined the suit also claim that they were blocked from getting independent, second medical opinions because Myriad did not allow other labs to conduct or interpret *BRCA* tests.

Although these charges may stir emotions, says Q. Todd Dickinson, former head of PTO

DATA SHARING

Group Calls for Rapid Release of More Genomics Data

In 1996, at a meeting in Bermuda, researchers participating in the Human Genome Project opened the floodgates of DNA data by agreeing to release sequence information daily into a public database. "It was a game-changing situation," recalls Eric Green of the National Human Genome Research Institute in Bethesda, Maryland. Until then, sequence data generally became available only upon publication. In 2003, the genome-sequencing community reiterated this pledge at a follow-up meeting in Fort Lauderdale, Florida, and came up with guidelines on how prepublication data should be used.

Now pressure is mounting to extend the Bermuda Principles to a broad range of publicly funded projects that go beyond sequencing. They include whole-genome association studies, microarray surveys, epigenomics scans, protein structures, large-scale screening of small molecules for biological activity, and functional genomics data, only some of which are now covered by prepublication data-release policies. "Life in genomics has gotten far more complicated than what we had to deal with in Bermuda and Fort Lauderdale," says Green. Last week, at the International Data Release Workshop held in Toronto, about 100 researchers, ethicists, and funding agency representatives began to hammer out guidelines for such efforts.

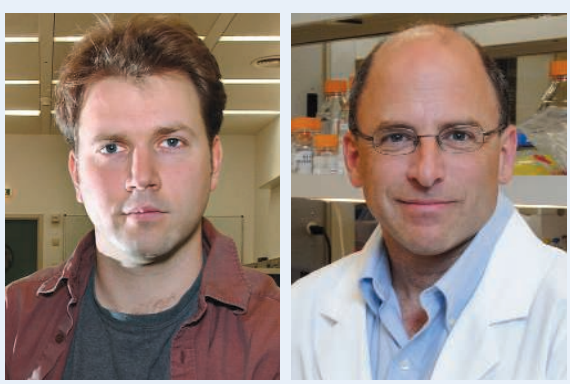

Wordsmiths. Co-chairs Ewan Birney (*left*) and Tom Hudson (*right*) are choosing their words carefully to convey their meeting's consensus about data-release policies.

In 1996, researchers were grappling with DNA sequence from just a few centers and with issues such as how to make data available quickly while preserving some rights to publish first on a whole data set. Now, 13 years later, data sets are proliferating and have become more diverse. Today, the point at which data should be released is less clear. For example, next-generation sequencing churns out huge quantities of data quickly, but the sequence needs some processing and has more errors than the raw sequence generated by the Human Genome Project.

And researchers want information about the traits and diseases of the people whose DNA has been sequenced. "The infusion of human subjects research is adding great complexity," says Green. Because of patient-protection concerns, these data are not in open databases; how to regulate access to the information is still being worked out.

Five years ago, high-throughput genome centers did the lion's share of the sequencing

CREDITS: (TOP) ACLU; (BOTTOM, LEFT TO RIGHT) MAJ. BRITT HANSEN, EMBL-PHOTOLAB; ONTARIO INSTITUTE FOR CANCER RESEARCH

Published by AAAS

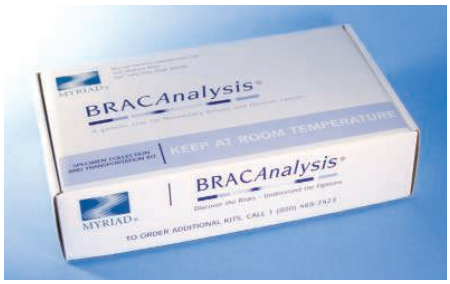

Embattled. Myriad Genetics's monopoly on *BRCA* gene testing is under fire.

and current director of the American Intellectual Property Law Association, judges are likely to be more interested in the primary legal issue: whether PTO made a fundamental mistake in granting gene patents. That argument may have some legal traction, several patent experts said, as U.S. courts have been moving to restrict the scope of patents.

Myriad, which won a broad U.S. patent on *BRCA1* in 1997 and has since acquired and licensed other *BRCA* patents, has faced similar challenges in Europe, where it has been embroiled in continuous legal skirmishes. There, too, Myriad was accused of interfering with *BRCA* research and trying to impede clinical work. In particular, Myriad was faulted by researchers for being slow to acknowledge the importance of European data showing that some deletion mutations in *BRCA* genes could increase risk, says Michael Watson, executive director of the American College of Medical Genetics, which has opposed gene patenting for a decade and is a plaintiff in the ACLU case. These mutations were not part of the company's original test procedure, Watson notes, and the firm later added them (*Science*, 31 March 2006, p. 1847). The European Patent Office, meanwhile, has sharply narrowed Myriad's patent claims (*Science*, 24 June 2005, p. 1851).

Hans Sauer, associate general counsel for the Biotechnology Industry Organization in Washington, D.C., says that gene patents are needed to secure investments in risky new projects, particularly for work on new therapies. In his view, there's essentially "no evidence" that patents have impeded research or medicine. Nonetheless, the ACLU suit is an interesting "test case," he says, because it raises important questions about how to pay for the development of genetic medicine.

–ELIOT MARSHALL

as part of so-called community resource projects. Whole genomes were deemed community resources and released prepublication in one form or another. But in the next 5 years, faster, cheaper sequencing technologies should allow individual labs to tackle large genomes. How willing or able will those labs be to release data before publication? These smaller groups "don't have the expertise to develop the tools or set up their data in a way that others can use it," says meeting co-organizer Tom Hudson of the Ontario Institute for Cancer Research in Toronto, Canada. And some may not want to for fear of being scooped.

At the meeting, participants debated how to ensure that researchers who release data early get credit for the work and a chance to publish their analyses first. "That tension was a very old tension," says Ewan Birney of the European Bioinformatics Institute in Hinxton, U.K., a co-organizer of the meeting. There was general agreement that the community needs to come up with a standardized way of citing prepublication databases so credit goes to the data producers. Participants also called for granting agencies and journals to encourage prepublication release. "It's the responsibility of the users and the funding agencies to try to make that happen," says Hudson.

The proliferation of controlled-access databases, many of which contain human genotype and trait information, poses more difficult problems. At issue is how to permit access to the data while protecting privacy—a task complicated by the fact that some databases contain information from multiple countries that vary in their patient-protection rules. "We need to do this in a context that doesn't make progress impossible," says David Haussler of the University of California, Santa Cruz. He advocates one centralized authorization board. Hudson agrees. Eventually, "every scientist in the world will need passwords," he says. "The question is whether they will need to have hundreds or one."

In the next several months, a final report—and, it is hoped, a publication on the topic—should help spell out how to extend prepublication data release beyond the sequencing community and further the discussion on controlled-access databases. As Tim Hubbard of the Wellcome Trust Sanger Institute sums up, "What came out was the need for clarity" about the proper etiquette for releasing, using, and accessing these data.

–ELIZABETH PENNISI

CREDIT: COURTESY OF MYRIAD GENETICS INC.

*Science*Insider

From the *Science* Policy Blog

*Science*Insider continues to provide up-to-the-minute coverage of the H1N1 outbreak as public health officials and scientists around the world take steps to stop the virus. As of 18 May, WHO reported **8480 confirmed cases** in 39 countries, with the number of H1N1 cases in Japan rising from four to 129 in 2 days.

Austria's chancellor has overturned a decision by his science minister and decided that the country will **remain a member of CERN**, the European particle physics laboratory near Geneva.

The National Science Foundation has decided to begin building **a research ship, a solar telescope, and a network of ocean observatories** with an investment of $400 million from the agency's $3 billion pot of stimulus money. Officials hope the allocation of $148 million will be enough to build the ice-enabled Alaska Region Research Vessel. Another $106 million will kick off the Ocean Observatories Initiative, and $146 million will build 60% of the Advanced Technology Solar Telescope in Hawaii.

A Japanese plan to build **the world's fastest supercomputer** hit a roadblock last week when NEC and Hitachi announced they are withdrawing from the $1 billion project for fiscal reasons. Their departure may require officials to reconfigure the computer, which is supposed to be completed by 2012.

The U.S. Transportation Security Administration is planning to institute new security requirements for **the shipping of pathogens**. The move could lead some courier companies to stop accepting shipments of pathogen samples for delivery. That step, in turn, could hurt collaborations between research labs and impede responses to public health emergencies. The proposed measures include requiring packages to be tracked at all times and mandating background checks for all employees of the courier company who might have access to the packages.

For updates and other news, visit **blogs.sciencemag.org/scienceinsider**.

Published by AAAS

Eppendorf & Science Prize for

Neurobiology

$25,000 Prize

Get recognized!

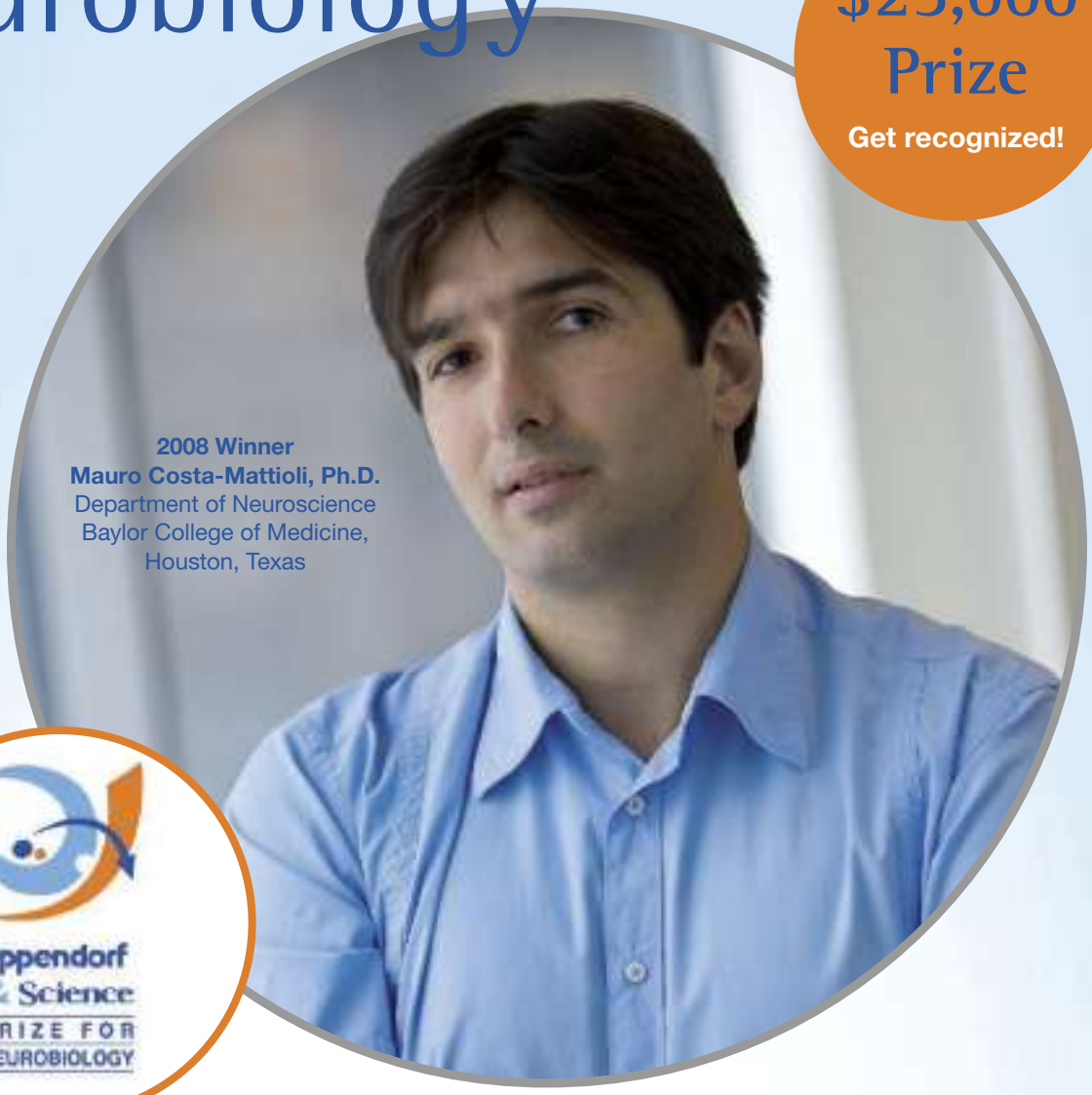

2008 Winner
Mauro Costa-Mattioli, Ph.D.
Department of Neuroscience
Baylor College of Medicine,
Houston, Texas

eppendorf & Science PRIZE FOR NEUROBIOLOGY

Deadline for entries
June 15, 2009

For more information
www.eppendorf.com/prize

This annual international research prize recognizes accomplishments in neurobiology research based on methods of molecular and cell biology. The winner and finalists are selected by a committee of independent scientists, chaired by the Editor-in-Chief of *Science*. Past winners include postdoctoral scholars and assistant professors.

To be eligible, you must be 35 years of age or younger. If you´re selected as this year´s winner, you will receive $25,000, have your work published in the prestigious journal *Science* and be invited to visit Eppendorf in Hamburg, Germany.

eppendorf
In touch with life

Science
AAAS

Kurstin Roe Photography

PUBLIC HEALTH

Scourge of Tobacco and Trans Fats Chosen for CDC

As a young epidemic intelligence officer assigned to New York City by the Centers for Disease Control and Prevention (CDC) nearly 2 decades ago, Thomas R. Frieden documented a serious outbreak of drug-resistant tuberculosis. Within 2 years, he was directing the city's successful efforts to contain the fast-growing outbreak, developing a program that became a model for TB control.

Now Frieden, who has been New York City's health commissioner since 2002, is returning to CDC as its director. In a sense, he will be both an insider and an outsider, for despite his dozen years as a CDC employee working in New York City and later in India on TB control, he was never assigned to the agency's sprawling headquarters in Atlanta, Georgia.

"He knows the CDC well, but he also has a valuable outside perspective from the front lines of public health," says former CDC deputy director David Fleming, now public health director of King County, Washington. Adds former CDC chief Jeffrey P. Koplan, now vice president for global health at the Woodruff Health Sciences Center at Emory University in Atlanta: "He's innovative and smart, with the breadth and depth of experience in public health that's needed to lead the CDC."

That won't be easy. The nation's premier public health agency, with 15,000 employees and a $9 billion annual budget, was racked by allegations of political influence during President George W. Bush's Administration and divided by a reorganization advocated by former director Julie Gerberding, who left in January (*Science*, 16 January, p. 324). The acting director, Richard Besser, who has been widely praised for his response to the H1N1 influenza epidemic, has tried to improve morale by asking for a reassessment of some controversial changes made in recent years.

Frieden's first weeks after he starts at CDC in early June are likely to be dominated by decisions related to the ongoing influenza epidemic, but he will also need to restore confidence in the agency. CDC staffers got a sense of his leadership style when Frieden, shortly after President Barack Obama appointed him, sent an all-agency e-mail saying that he will be "renewing and strengthening" the agency's commitment to science in public health. "Rigorous surveillance and epidemiology are not only our most powerful tools, they also are our ethos and the foundation of our authority," Frieden wrote.

Colleagues say Frieden, who has an M.D. from Columbia University's medical school and an MPH from the university's School of Public Health, has always focused on getting the science right. "He analyzes scientific data, applies it, and makes changes to improve public health," says Roy Gulick, chief of the infectious disease division at Cornell University's Weill Medical College in New York City, who was a medical resident with Frieden. Gerald Keusch, Boston University's associate provost for global health, says Frieden "has great credibility among the science and public health communities for being thoughtful but tough when public health is at risk. He can make hard decisions quickly, act on them, and defend them."

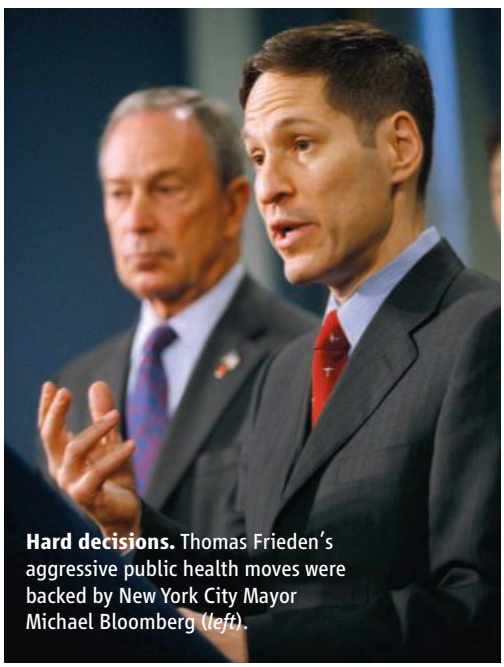

Hard decisions. Thomas Frieden's aggressive public health moves were backed by New York City Mayor Michael Bloomberg (*left*).

CREDIT: CHIP EAST/REUTERS/LANDOV

Tackling difficult public health challenges has been a hallmark of Frieden's 7 years as commissioner of New York City's Department of Health and Mental Hygiene, which has more than 6000 employees and a $1.7 billion annual budget. He waged a successful campaign to ban smoking in the city's restaurants and bars, required dining places to stop using trans fats and to post menu calorie counts, demanded that HIV tests be routine in medical exams, ordered electronic record keeping of diabetes blood-sugar tests, and advocated limiting salt content and imposing a tax on sugary drinks.

"His work on tobacco control and his efforts to address the obesity epidemic have made New York a model" for other cities, says William Schaffner, who chairs the preventive medicine department at Vanderbilt University School of Medicine in Nashville, Tennessee. "He'll be an innovator—not a caretaker—at the CDC." Frieden's activist style has, however, raised some concerns among those who fear he has an agenda. Scott Gottlieb, a physician and former U.S. Food and Drug Administration (FDA) deputy commissioner who is a resident fellow at the American Enterprise Institute for Public Policy Research in Washington, D.C., says Frieden is qualified but tends to be political in his approach. "To the extent that Frieden is, in my view, a political leader with a very clear policy agenda," says Gottlieb, "his leadership is better directed out of HHS [Health and Human Services] proper" rather than out of CDC.

Other concerns relate to whether some directives, such as the electronic reporting of diabetic patients' A1C blood-sugar test results, might intrude on privacy. David Rothman, president of the Institute on Medicine as a Profession at Columbia University, contends that Frieden's "confidence and certainty are so overwhelming that some worry that he's not concerned enough about the countervailing issues of personal liberty." Frieden has argued that a blood-test registry is essential for accurate diabetes surveillance and that his department has vowed to protect confidential data.

Frieden's success at CDC will depend partly on his political skills, says Arthur Reingold, head of epidemiology at the University of California, Berkeley. "The CDC director has to be an adept politician to deal with the 50 state health departments and myriad local health offices that play an important role in public health."

Frieden will also need to coordinate efforts, in areas such as investigating food-borne outbreaks and developing influenza vaccines, with FDA. CDC's relations with FDA have at times been rocky, but Frieden knows both the new FDA chief, former New York City health commissioner Margaret Hamburg, and her deputy, former Baltimore City health director Joshua Sharfstein.

"Having a CDC head and FDA head who have a close prior working relationship is going to be an advantage to both agencies," says Gottlieb. "This is an opportunity to reset that relationship."

–ROBERT KOENIG

Published by AAAS

Plagiarism Sleuths

A Texas group is trolling through publications worldwide hunting for signs of duplicated material. The thousands of articles they've flagged online raise questions about standards in publishing—and about the group's own tactics

HAROLD "SKIP" GARNER NEVER INTENDED to become an enforcer. The affable computational biologist set out 7 years ago with a modest enough goal: to access the scientific literature more efficiently. With colleagues, he crafted a computer program called eTBLAST that could detect similarities in published abstracts, making it relatively easy to sort through the 19 million papers in a database like MEDLINE and pick out those in a narrow slice of science.

But his group at the University of Texas (UT) Southwestern Medical Center in Dallas quickly realized that eTBLAST had another, tantalizing application. "We could do stuff like find plagiarisms," says Garner. That held definite appeal—but first, Garner wanted to sharpen the program's accuracy. Two years ago, with support from the Office of Research Integrity and the National Institutes of Health, he launched Déjà vu, an online database that bills itself as "a study of scientific publication ethics." It now lists 74,790 pairs of papers drawn from MEDLINE that eTBLAST has found with striking similarities in language or content. The authors include everyone from Nobel Prize winners to scientists toiling in obscure institutions in every corner of the world. When *Science* conducted random searches of illustrious names, between one-third and one-half showed up in Déjà vu as potential duplicators of their own or others' work. Garner and his crew have built a powerful tool for uncovering repetitious papers—and for raising authors' hackles.

Online
sciencemag.org
Podcast interview with author Jennifer Couzin-Frankel.

Over the past year or so, Déjà vu has rapidly gained prominence. It has prompted discussions with journal editors and at least 48 retractions of suspicious papers. In March, a rheumatologist resigned from Harvard Medical School after Déjà vu detected similarities between a review article he had published and an earlier article by a Texas researcher. Some journals now run accepted papers through eTBLAST software, which is freely available, to hunt for duplications prior to publication. Some senior faculty members contacted by *Science* say they would consider using Déjà vu to help guide hiring, promotion, and publication decisions.

But how reliable is Déjà vu, and what do its developers hope to accomplish? *Science* examined many papers listed there and found that Déjà vu casts a wide net, scooping up innocent papers (such as translations) along with suspicious ones. Its large haul raises questions about writing and publication standards for scientific papers; it is also leaving frustrated scientists in its wake. "It's inappropriate to flag these sorts of papers," says Lawrence Solin, a radiation oncologist at the Albert Einstein Healthcare Network in Philadelphia, Pennsylvania, who was angry to learn that he had three pairs of papers in Déjà vu, all written by him. "These people have a serious obligation to do this correctly or not do it at all. And in my view, they are simply not doing this correctly."

The vast majority of listings in Déjà vu, nearly 66,000, are from scientists who, like Solin, appear to be repeating their own previously published work. Repetitious reviews and incremental reports are part of an accepted tradition, and authors say they are less than thrilled to be fingered. Others say Déjà vu makes mistakes—for example, flagging similar studies on different populations.

CREDITS: PHOTOS.COM; J. NEWFIELD/*SCIENCE*

Published by AAAS

Carbon copy. Déjà vu detected this pair of suspect papers by different groups of authors; the one highlighted in yellow was published later and recently retracted.

But Déjà vu's masters at UT Southwestern are not just out to nail plagiarists. They are challenging accepted and gray-area practices, particularly the tendency by authors and journals to recast previously published work as novel. "We don't consider ourselves the publication police," says Garner. At the same time, he says, for Déjà vu's team, seeing what makes up the scientific literature has been one "of the most eye-opening experiences in our life."

Worst offenders

Garner and his team of four run an efficient shop. The first step is automated: eTBLAST picks up suspicious papers based on similar titles and abstracts, and Déjà vu slaps them online for anyone to see. But eTBLAST isn't perfect, Garner acknowledges, so these papers are labeled "unverified"—a classification that includes more than 90% of Déjà vu's listings.

Reviewing papers manually is a painstaking task, led primarily by Tara Long, a mathematics major who began working with Garner in 2006 while still in college. If a great deal of text, figures, and references matches that of another paper published earlier, it is classified as a "duplicate." On average, duplicates whose full text has been examined share 85% of their text, says Long. (Each entry consists of two papers, the earlier one and the later one.)

Scrutinizing papers, Long shifts them out of the unverified classification and into one of four main categories: Distinct, Sanctioned, Update, or Duplicate. The first two comprise only appropriate examples of repeated work, whereas in the latter two, suitability varies depending on the circumstance (for example, if a paper was reprinted with permission). Of the 5833 pairs of papers in these four groupings, 2124 are labeled duplicates. Another key question is whether papers have different authors. Déjà vu lists close to 66,000 pairs of papers with shared authors, whereas the rest, just over 9000, have different authors. Of the 2124 listings in the duplicate category, 258 have different authors on the earlier and later paper, suggesting that they may be examples of plagiarism.

These are the ones Garner's group has focused on most aggressively, systematically contacting authors and journals. They have followed up on 165 cases so far and prompted some acknowledgments of wrongdoing and retractions.

Many apparent instances of plagiarism picked up by Déjà vu reflect a strategy known as "patchwriting"—an underrecognized problem in scientific publishing, according to Garner. Patchwriters lift large portions of the introduction, scientific design, and other sections of a published paper, then plug in details from their own experiment. "They don't take the data, but they take the scientific design," says Beth Notzon, who has taught classes on publication ethics to young physicians at M. D. Anderson Cancer Center in Houston, Texas, and is administrative editor at the *International Journal of Radiation Oncology, Biology, Physics*. "They're able to repeat the whole thing but in a different population of patients."

Riding high. Skip Garner, with one of his horses, runs Déjà vu and receives dozens of tips—and complaints.

Notzon's journal was alerted to such a case by Déjà vu. A group in China had, by Déjà vu's estimate, copied more than 95% of a paper on breast cancer first published in 2003 in the *International Journal of Radiation Oncology, Biology, Physics*. The Chinese group changed the focus from breast cancer to nasopharyngeal cancer, which is much more common in those of Asian ancestry, and reported data from their own patients. The lead author of the original paper, Odilia Popanda of the German Cancer Research Center in Heidelberg, notes that she was rather miffed that the Chinese work, published in 2005, appeared in a higher profile journal, *Clinical Cancer Research*.

The first author of the *Clinical Cancer Research* paper, Wei-dong Wang, an oncologist at Xinqiao Hospital in Chongqing, China, wrote in an e-mail message to *Science* that "our English skill was not good enough to meet the language requirements" of *Clinical Cancer Research*. "To publish our findings as quickly as possible, the first author Dr. Wang organized our results in the similar pattern of Popanda's publication," Wei-dong Wang continued, referring to himself in the message. He stressed, however, that the type of cancer and the results were different.

Wang also wrote that "we have done foolish things" and "we should express our findings in our own words." Wang wrote in a later e-mail message to *Science* that he and his co-authors had decided to withdraw the paper, and it was retracted late last month.

Wang's account of patchwriting jibes with what Notzon has seen in her classes. She was startled to find that many foreign scholars at M. D. Anderson, particularly those from Asia, consider it perfectly appropriate. "We had a young woman visiting from China who taught writing and editing in China, and she said laughingly, 'Oh, we encourage this sort of thing because people don't have good idiomatic English.' " But, Notzon says, patchwriting is "wrong because it's really a kind of plagiarism—they're taking someone else's research idea."

Challenging standards

More discomforting questions raised by Déjà vu focus on the norms of scientific publishing. Take reviews, which make up about 20% of the listed papers, Long estimates. They often contain duplicated material, particularly from the author's own published articles. "You can't just copy your introduction [on an article]. But to what extent is that wrong? There's definitely a gray area," says Notzon.

When it comes to repetition of their own writing, few scientists see a problem. "When

CREDIT: KIM MENIER

Repetition Is Not Duplication

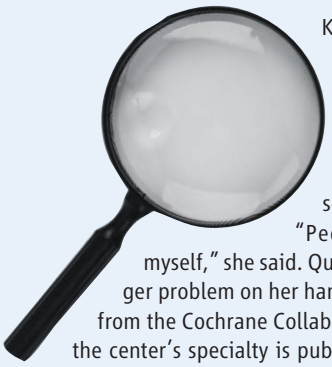

Kay Dickersin, an epidemiologist at Johns Hopkins University in Baltimore, Maryland, grew intrigued by Déjà vu after encountering a case of plagiarism in a class she taught. On a lark, she plugged her own name into the database and was shocked to see a pair of papers she'd authored come up. "People are going to think I'm plagiarizing myself," she said. Quickly, Dickersin realized she had an even bigger problem on her hands: Déjà vu was riddled with papers like hers from the Cochrane Collaboration, whose U.S. center she runs, because the center's specialty is publishing updated reviews of clinical research. They are repetitive by design.

The Cochrane database, containing about 3800 papers in all, has a whopping 2879 papers listed on Déjà vu. We "realized straight away that people would say, 'These guys in Cochrane are just ripping each other off,' " says Nick Royle, CEO of Cochrane, based in Oxford, U.K. He immediately wrote to Harold "Skip" Garner of the University of Texas Southwestern Medical Center in Dallas, who runs Déjà vu.

Garner responded by creating a new category for the Cochrane papers: All 2879 are now listed as "sanctioned," a class of legitimate duplications. "To his credit," says Royle, Garner grasped the problem. Still, Royle is uneasy with the outcome, concerned that the term "sanctioned" will be misconstrued as negative. Dickersin, who admits she might be "paranoid" about showing up in Déjà vu, would rather see the papers removed from the database altogether. But that's something Garner won't do.

Garner has become accustomed to fielding queries from panicked, nervous, or irate scientists. He has written personal notes to more than 100 people in an attempt to assuage concerns. But not once has a listing been pulled, he says, and he won't grant special exemptions, no matter how eminent the researcher.

Does Garner worry about posting inaccurate listings or insinuating that someone has plagiarized when they have not? "Hell, yeah," he says. "This is a touchy subject, and it can affect people's careers." With that in mind, Déjà vu's minders examine papers brought to their attention by the authors, and Garner then writes them to explain that the paper was reviewed and—in most cases—determined to be benign. It's then placed in an innocuous category. Pulling papers, Garner believes, would dilute Déjà vu's potency. "It's valuable to show other categories where things are highly similar," he says, "but also valuable to science." **–J.C.-F.**

you labor over a sentence, when you love that sentence, it's really hard to move too many commas around" if you use it again, says Douglas Mann, a cardiologist at Washington University in St. Louis, Missouri, who has five pairs of papers on Déjà vu, all 10 of them reviews authored or co-authored by him. Four sets are "unverified" and one is listed as a duplicate.

"There's going to be redundancy" in review articles, Mann continues, echoing similar comments by others, "but I don't think that's scientific misconduct." Some blame the system. Often when a topic is trendy, journals solicit many reviews from the same author, on the same subject, in a short period of time. Authors respond with repetitive articles. In original research papers, too, wording may overlap substantially. When it comes to writing introductions, "if you have a series of papers on the same topic, I can imagine some of the same narrative getting in there, consciously or unconsciously," says William Gelbart, a geneticist at Harvard University.

More clear-cut is the use of material published by other researchers without proper attribution. Rudolf Weiner, a bariatric surgeon at the hospital Krankenhaus Sachsenhausen in Frankfurt, Germany, was notified of a paper that Déjà vu declared a duplication of obesity research from another bariatric surgeon at Mount Sinai School of Medicine in New York City, Daniel Herron. "Between one-third and half of the article was essentially word for word taken from my article," a review, Herron says.

In an e-mail to *Science*, Weiner, the first author on the later paper, wrote that one of his co-authors "received the order to create an introduction for this article about morbid obesity" and "he made a copy (obviously) of an introduction from the previous article." Weiner emphasized that the article was an overview, not original research. He declined to answer any additional questions. The co-author in question died suddenly, he says. The article was not retracted, and the journal, *Surgical Technology International*, did not return calls seeking comment.

Falsely fingered? Patrick Bossuyt discovered 19 listings under his name and says all are ethical publications.

One duplication spotted by Déjà vu led to a resignation. Rheumatologist Lee Simon of Harvard Medical School in Boston stepped down in March after Déjà vu determined that a review published by him in August 2004 describing new treatments for rheumatoid arthritis was similar to a paper released 13 months earlier, by Roy Fleischmann of UT Southwestern. Simon could not be reached for comment. Harvard spokesperson David Cameron confirmed that Simon had resigned and that Harvard had investigated the case, but gave no details.

Guilt by association

Garner believes that there's no problem with quoting one's own or others' work as long as the later article cites the earlier one and makes clear what's being repeated. Translations are an obvious form of approved duplication. Indeed, a paper that Garner, Long, and their colleagues published earlier this year in *Science* about Déjà vu (*Science*, 6 March, p. 1293) will likely fall into Déjà vu's duplicate category if a translation appears in a Spanish journal, as one has requested. Garner says that because the Spanish version will note the publication in which the article was first published, he has no qualms about appearing in Déjà vu.

But many with whom *Science* spoke disagree: Surfacing in Déjà vu, they say, suggests wrongdoing. They also lament Déjà vu's decision to publicly post tens of thousands of unverified papers. "A list like this that's computer generated can cause much harm and then put the onus on a young scientist to explain away why their entirely appro-

CREDITS (TOP TO BOTTOM): PHOTOS.COM; AMC/UNIVERSITY OF AMSTERDAM

Published by AAAS

priate use of review material got them onto the list," says Jeffrey Macklis, a neuroscientist at Harvard whose own reviews appear on Déjà vu's unverified list because of their similarity. Macklis says all of these papers properly cited his previous reviews. If just showing up in Déjà vu suggests wrongdoing, as he worries it does, that's comparable to McCarthy-era blacklists from the 1950s that, he says, "were feared" in his house. "This is meant to be a shame-and-blame list," says Karl-Heinz Krause, a physician who studies stem cells at the University of Geneva in Switzerland. He appears in Déjà vu's duplicate category because, he says, a journal in which he published, *Swiss Medical Weekly*, republished a paper of his in a supplement without notifying him.

Patrick Bossuyt, a clinical epidemiologist at the University of Amsterdam in the Netherlands, anxiously searched Déjà vu after a colleague told him that several of his papers were listed there as "fraudulent." (In reality, Déjà vu has no such category.) At least 10 of his 19 listings appeared in one of the "safe" categories; the others were mostly unverified, with one labeled a duplicate. The unverified listings, he says, refer to a combination of translations, updates, and distinct papers, whereas the duplicate listing captures two identical introductory articles used to present a series in different issues of *Nature Reviews Microbiology*. Bossuyt calls them all examples of ethical publication but still worries that so many listings could sully his reputation.

Some also question Déjà vu's accuracy, pointing to papers it had flagged that they deem unique experiments. Nader Rifai, a clinical chemist at Harvard Medical School, appears in three listings in Déjà vu with articles that are "completely different," he says. One includes two papers that investigated two distinct drugs. Another, for which Rifai is only on the earlier paper and not the later one, examined hormone levels associated with diabetes, with one experiment in men and one in women, he says. Walter Willett, a prominent epidemiologist and nutrition expert at Harvard School of Public Health, had a similar experience: Two of the six unverified listings on which he appears in Déjà vu describe a similar study of high blood pressure performed in different populations, men and women. Willett's other listings are reviews, which have to "cover the waterfront," he says. "If you come back and review something in 2 years, it will probably be 80%" like the earlier article.

Shades of gray

Just 2 years after its launch, Déjà vu has become the place to go to for anyone who wants to report suspicions of plagiarism or inappropriate duplication. It receives dozens of tips, Garner says, from "people who reported their previous mentors, their department chairman." Garner's group spends hours contacting journals and authors to alert them of Déjà vu's findings.

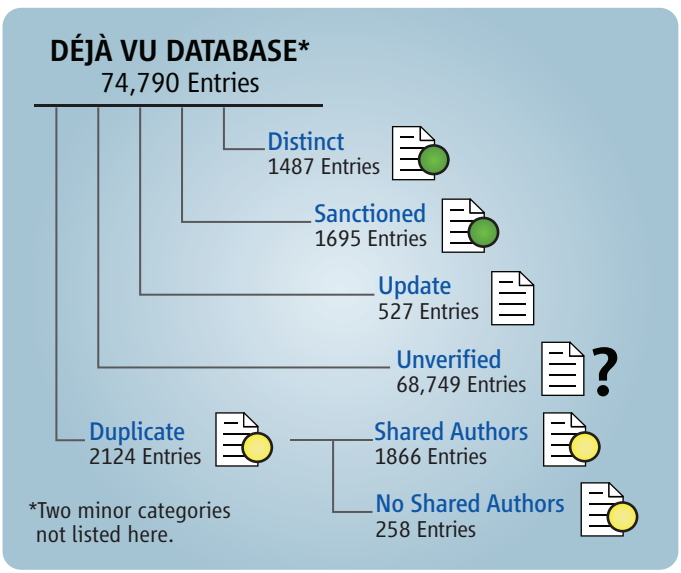

Yellow and green. Some of Déjà vu's categories, such as "duplicate," may reflect inappropriate publication, whereas others, such as "distinct," indicate no problem.

SOURCE: DÉJÀ VU

Garner says his aim is cleaning up the literature and coaxing scientists and journals to reconsider what's appropriate. Gelbart, himself a member of the booming club listed in Déjà vu, agrees that including many types of repetitious work is "useful as fodder for the scientific community to decide whether this falls within the norms of acceptable behavior or not." His pair of listings in Déjà vu were progress reports "written with a lot of boilerplate," he says, intended to get the word out about FlyBase, a database of fruit fly genes that began in the early 1990s.

Journals have responded to Déjà vu in different ways. Many have ignored inquiries about suspect papers. Journals in India and Egypt contacted by *Science* because the database listed them as having published more than a dozen duplicate papers did not respond.

Some journals have embraced Déjà vu or adjusted their standards because of it. Natalie Marty, managing editor of *Swiss Medical Weekly*—which Krause says republished his paper without prior notification—admitted that it had reprinted many papers in a supplement but cited the initial publication. PubMed, however, failed to pick up that the papers were reprinted, and Marty says the journal has notified PubMed to add a comment to this effect. The journals *Annals of Surgery* and *Anaesthesia and Intensive Care* both learned of duplication cases from Déjà vu and now screen accepted articles with eTBLAST, available for free online, before they're printed. "It gives us more confidence about what we publish," says Pamela Nevar, the managing editor of *Annals of Surgery*.

John Loadsman, an anesthesiologist in Sydney, Australia, and editor of *Anaesthesia and Intensive Care*, hopes to set up an automated system to check every paper submitted to the journal with eTBLAST. His journal had 21 cases listed in Déjà vu, three of which turned out to be "true cases of duplicate publication," he says. Loadsman doesn't believe false positives are a problem, as "it's very easy to work out" which are real.

Some researchers say they would willingly use Déjà vu to check papers when making hiring and promotion decisions. But others—particularly those who say they appear in Déjà vu wrongly—consider that a terrible idea. Witold Filipowicz, an RNA biologist at the Friedrich Miescher Institute in Basel, Switzerland, says it's useful for scientists to be "aware that there is a watchdog." He emigrated from Poland 25 years ago, where at the time, as in other Eastern European countries, promotions, funding, and other career decisions were primarily "based on number of publications," he says. Although that has changed, Filipowicz estimates that now worldwide, "50% or 70% of what is published is just of no value." Garner agrees that one issue underscored by Déjà vu is an excess of journals and of review articles in particular.

Still, Filipowicz thinks Déjà vu ought to highlight true plagiarism and lessen its emphasis on articles that are not original research. (One of his own papers, a symposium report based on an earlier publication, has been flagged by Déjà vu as an unverified case.) "If 90% [of listings] are benign," he says, "they will in a way muddy the real crimes," distracting attention from where he says it should lie.

–JENNIFER COUZIN-FRANKEL AND JACKIE GROM

Face to face. The U.S. census didn't use the mails until 1970.

CREDIT: © THE METROPOLITAN MUSEUM OF ART

THE 2010 CENSUS

America's Uncounted Millions

It is getting increasingly difficult to count a mobile population, but an "adjustment" based on postcensus sampling is politically unacceptable

Next April, the United States will embark on by far the most expensive decennial census the country has ever seen: It will cost about $15 billion—double the cost of the 2000 census—to count an estimated 309 million U.S. residents. Billed as the country's "largest peacetime mobilization," it will send out 1.2 million temporary workers in early May to knock on the doors of about one-third of the population: the people who haven't sent in their census forms. Despite the best efforts of these workers, who may go back to the same addresses as many as six times, many people will be missed.

How to deal with this undercount has occupied statisticians for decades. It's also of perennial interest to politicians because the census is used to reapportion seats in the House of Representatives. The Obama Administration has repeatedly said it has no plans to conduct an "adjustment" in the 2010 census count, as many statisticians have advocated. But that hasn't stopped several House Republicans from agitating about such a possibility, which they fear would benefit Democrats, and they have accused the Administration of attempting to politicize the census.

The flames have been fanned as President Barack Obama tries to get his Commerce team in place. In February, alarm calls went out when a White House spokesperson seemed to say that Obama planned to have the census director report directly to the White House, bypassing the commerce secretary. That fuss is one reason Commerce nominee Judd Gregg, a Republican senator from New Hampshire, withdrew his name. Former census director Kenneth Prewitt, the top choice to head the bureau, dropped out soon afterward as the political heat rose.

The new census nominee, sociologist Robert Groves of the University of Michigan, Ann Arbor, has an impeccable reputation in the statistical community. But he has been greeted with suspicion by Republicans who identify him with past attempts to adjust, or correct, the census. He spent a good deal of this month, as well as part of his confirmation hearing on 15 May, reassuring legislators that an adjustment is not on the table and that it would be too late to try in the 2010 census even if he wanted to. "Any major change would bring so much risk that the benefits would have to be clearly established," he said.

The adjustment in question is also referred to as "sampling," which Republican critics say violates the Constitution's call to count every citizen rather than just sample the population. Many statisticians argue that casting the debate this way distracts from real concerns about the future of the census in a high-tech and increasingly mobile and diverse society. In fact, the technique in question does not substitute sampling for counting. Rather, it's a methodology for assessing the accuracy of an inevitably incomplete count.

Missing millions

The undercount problem was first recognized after the 1940 census, when the Defense Department was registering men for the draft. "More young black males registered for the draft than the census bureau thought were in the country," says historian Margo Anderson of the University of Wisconsin, Milwaukee. It's more of a political issue in the United States than it is elsewhere, she adds, because here it is used to determine how states are represented in Congress. Furthermore, as census figures came to be used for more and more purposes, such as federal revenue-sharing, there was "huge pressure on getting census figures right," says former House staffer David McMillen, now at the National Archives and Records Administration.

By the late 1980s, Republicans were worrying that any adjustments to the undercount would benefit Democrats because the people who end up not being counted—the poor and minorities—tend to vote Democratic. In 1990, for example, according to a 2004 report from the National Academy of Sciences (NAS), there were 16.3 million erroneous or duplicate counts and 20.3 million people weren't counted at all. Blacks—young black males in particular—were missed at a rate

Published by AAAS

four times as high as that for whites that year, according to the U.S. Census Bureau. Affluent whites, on the other hand—such as people with multiple homes or students counted both by schools and by their parents—are disproportionately found in overcounts. In 2000, NAS says 15.9 million people were missed, whereas the overcount was 17.2 million.

By the time planning was under way for the 1990 census, adjustment had become a very contentious issue. The methodology in question is called dual system estimation (DSE). It uses a post-enumeration survey conducted independently from the census but very soon afterward. As former census director Prewitt explains, DSE is based on "capture-recapture" principles for counting wildlife. First you count as many as you can of a population and tag them (the census). Then in a separate operation (the post-enumeration survey), you capture a representative sample of the population and see how many have already been tagged (counted). From the ratio of tagged to newly captured, you can make a revised, and presumably more accurate, estimate of the total population.

In 1990, President George H. W. Bush's census director, Barbara Bryant, planned to use a post-enumeration survey of 300,000 households as the basis for an adjustment of the final census count. Census nominee Groves, who was associate director of statistical design from 1990 to 1992, favored the approach, as did most of the bureau's senior staff, according to McMillen. But Secretary of Commerce Robert Mosbacher Sr. quashed the plan.

The bureau again planned an adjustment for the 2000 census. This time it was challenged by a case that went to the Supreme Court in 1998. In the suit, *Department of Commerce* v. *U.S. House of Representatives*, Indiana Republican Representative Gary Hofmeister claimed that if the plan went forward, Indiana would lose a seat that would presumably go instead to a predominantly Democratic state. The court ruled that any adjustment of the final census count based on DSE could not be used for apportionment—that is, reallocation of the fixed number (435) of House seats among the states. It did not rule out DSE for other uses, including congressional redistricting (redrawing House district lines within states) and allocation of federal funds.

Using a post-enumeration survey as an accuracy check on the census is seen as an important way for the census bureau to evaluate its data, but to date it has not been used to adjust the final count. And it's not clear it ever will be. According to Hermann Habermann, deputy director of the U.S. Census Bureau from 2002 to 2006, statisticians inside and outside the bureau have said that there are too many possible flaws in the procedure to use it for that purpose. In 2003, the Census Bureau said there would be no adjustment for other purposes either, such as redistricting or the allocation of federal funds. Since then, officials have repeatedly stated that no adjustment is planned for the 2010 census. It's not even "technically feasible" at this late date, says Prewitt. The census "is a rocket that's on the launch pad, and they're about to ignite it. They can't redesign rocket fuel at this stage." Asked at his confirmation hearing about an adjustment in the future, Groves said, "I have no plans to do that for 2020." In his prepared material, he added, "I believe the Supreme Court ruling stands as the guidance on this issue."

None of this has stopped Republicans from fretting about the possibility that the procedure will be revived in 2010. As one House Republican staffer says, "If they wanted to, they could probably do it." In a statement last month, House Minority Leader John Boehner from Ohio accused Groves of having "advocated a scheme [in 1990] to … manipulate Census data, rather than simply conducting an accurate count of the American people." Warned Boehner: "We will have to watch closely to ensure the 2010 census is conducted without attempting similar statistical sleight of hand."

"Any major change would bring so much risk that the benefits would have to be clearly established."

—ROBERT GROVES, UNIVERSITY OF MICHIGAN, ANN ARBOR

CREDIT: AP PHOTO

A moving target

Aside from the adjustment issue, other improvements to the census process are sorely needed, say statisticians. There has been one major development: Next year, for the first time, citizens won't have to grapple with the Long Form, a lengthy questionnaire that used to go to one in six respondents; fewer and fewer people were bothering to fill it out. It's been replaced by the American Community Survey (ACS), a "rolling" survey that covers 300,000 people each month.

Although the ACS is generally hailed as an advance in obtaining thorough and timely information, it doesn't compensate for the fact that U.S. residents are getting ever harder to count. With traditional households few and far between, the census must count an increasingly mobile population; one where many people are suffering dislocation because of the economic recession or other factors; one with millions of illegal immigrants as well as others who prefer to avoid contact with the feds; one where even rich people can be hard to count because of the increase in hard-to-access gated communities.

With the long form out of the way, "it means you can think of doing the census in perhaps radically different ways," says statistician Stephen Fienberg of Carnegie Mellon University in Pittsburgh, Pennsylvania. The census is based on a system of physical addresses; its purpose is to locate an individual at "a particular geographic spot" at a particular time, says Anderson. But as the population becomes harder to track down, she says the postal system—used for the first time in the 1970 census—is already becoming "archaic" as a means to deliver the form. And modern modes of communication, the Internet and mobile phones, have the disconcerting feature of not being tied to any location. "The real question, I think, is, can you move to a person-based instead of a physical household census," says Fienberg.

As for reducing the undercount, the main strategy being explored is the use of "administrative records"—that is, tax data, Social Security numbers, driver's licenses, and even data from utilities to supplement census forms, an idea that's been around at least since a 1972 report, *America's Uncounted People*—the first of a long line of census reports from NAS. But heavy reliance on such a strategy is a long way off, not only because of privacy and security concerns but also because of the country's "decentralized statistical system," Anderson says.

Centralizing records such as driver's licenses would be in line with an even more radical step: a national registry. Prewitt is a proponent. In some other countries, particularly in northern Europe, traditional censuses have been eliminated, says Prewitt, as citizens are required to tell the government every time they move. "Without a national registry, we will seriously undercount," he says, pointing out that if we miss half the estimated 12 million immigrants now in the country illegally, that's 6 million right there.

Unfortunately, says Anderson, "unresolved debates" from past censuses "are obfuscating [and] drowning out other issues we should be talking about."

–CONSTANCE HOLDEN

Published by AAAS

DNA Target Enrichment Strategies

Bringing Efficiencies to Genome Sequencing

WEBINAR

Wednesday, June 10, 2009

12 noon ET, 9 a.m. PT, 4 p.m. GMT

You are invited to join the discussion of strategies for DNA target enrichment with our panel of distinguished thought leaders in a live video webinar. During the broadcast, the presenters will:

- provide a general introduction to the target enrichment methods they use.
- discuss how these technologies can be applied to the next-generation sequencing workflow.
- share data from studies that have benefited from their approach.
- answer your questions live!

Participating Experts:

Daniel Turner, Ph.D.
Wellcome Trust Sanger Institute,
Cambridge, UK

Kelly Frazer, Ph.D
Scripps Genomic Medicine
San Diego, CA

While next-generation technologies have revolutionized the way genomes are sequenced, this technology possesses a fundamental weakness—the inability to easily target specific regions of a genome. To address this inefficiency in the workflow, a variety of methodologies for performing DNA target enrichment are being developed and commercialized. All methods have a particular "sweet spot" for performance: some are more appropriate for smaller studies, where only a few samples are being examined, while others have the ability to scale and use automation for studies ranging from low to ultrahigh throughput. Costs, in terms of equipment and consumables, can also vary, depending on the technology used.

Join our panel of experts in a live discussion. Register to participate.

Questions can be submitted live to the panel during the webinar or in advance via e-mail provided with registration.
To register, visit:

www.sciencemag.org/webinar

Science
AAAS

Brought to you by the
AAAS/*Science* Business Office

Webinar sponsored by
Agilent Technologies

CHINA

An Unprecedented Dilemma: One University, Two Political Systems

The University of Macau's plans for a new campus in mainland China pose a challenge to preserving academic freedom in the former colony

MACAU—A hilly island crowned with wind turbines and little else beckons just off the western shore of this cramped city. Macau's land-hungry authorities ogle its barren real estate, a kind of Promised Land of ample space. But Hengqin Island is also a political minefield. Macau is planning to build a new campus for the University of Macau (UM) on Hengqin; the catch is that Hengqin is part of mainland China, so the new campus may no longer come under Macau's legal and administrative system. At stake are academic freedoms and an open social milieu that Macau residents enjoy and most Chinese do not: unfettered Internet access, for instance, and a legal system that excludes capital punishment.

The proposed Hengqin campus, expected to open as early as 2012, is "an unprecedented challenge to 'one country, two systems,' and for that reason it is extremely sensitive," says a UM professor who requested anonymity. He predicts an exodus from UM if it adopts mainland rules. Rector Wei Zhao has vowed to preserve UM's identity. Ultimately, however, that will be Beijing's call. "It is our understanding that the decision to grant our wishes lies with the highest level in the central government," university council chair Daniel Tse wrote in a 6 May open letter to the UM community.

Negotiators from the mainland China and Macau governments are now trying to craft a blueprint for a new campus that satisfies UM's concerns and those of officials in Zhuhai, the city in Guangdong Province to which Hengqin belongs. The pressure is intense. During a visit to Macau in January, Chinese Vice President Xi Jinping, heir apparent to President Hu Jintao, extolled development of Hengqin as a way to diversify Macau's economy, which now depends on tourism revenue from gambling. Then in February, China's powerful National Development and Reform Commission (NDRC) touted the Hengqin campus. "Xi's blessing and NDRC support make it a fait accompli," says the UM professor. "They have to find a way to make it happen."

When Portugal returned Europe's first and last Asian colony to China in December 1999, China brought Macau under its military and foreign affairs umbrella. A Beijing-approved chief executive now governs the Macau Special Administrative Region. But as it did for Hong Kong in 1997, China granted Macau considerable autonomy, including a pledge to leave Macau's European-style legal code intact until at least 2049.

Making a case for space. Rector Wei Zhao outlines Hengqin plans to students.

CREDIT: UNIVERSITY OF MACAU

For several years after its return to the motherland, Macau flourished as China's only haven for legal gambling. Last autumn, however, China imposed restrictions on mainlanders' travel to Macau, and casinos reported a 10% decline in revenue. This gave a fresh impetus to efforts to diversify Macau's economy. That will be no mean feat, as rapid growth has already left the tiny city—a mere 29 square kilometers comprised of Macau peninsula and two islands, Taipa and Coloane—bursting at the seams.

UM needs elbow room, Zhao says. Its present campus is hemmed into a sliver of Taipa, capping enrollment at about 6600. He notes that whereas Harvard University boasts 960 m^2 of campus per student and Tsinghua University in Beijing has 150 m^2, UM has precisely 8.7 m^2. The Hengqin campus, on a 1.4-km^2 plot across a narrow inlet from Taipa, would comfortably accommodate 10,000 students in a residential college system modeled after Yale University's, says Zhao.

In March, Zhao and other UM administrators held a series of 17 meetings with academic and local communities. Faculty and students credit UM's leaders for their openness; at the same time, many have argued that the university would change irrevocably if the new campus were under mainland jurisdiction. "I go to the University of Macau because it's not China," one mainland Chinese student flatly declared at a town hall meeting in March.

That's a sore point for the new host jurisdiction of Zhuhai. Local officials have questioned how Zhuhai would benefit if a piece of Hengqin, the largest of Zhuhai's 146 islands, were essentially handed over to Macau. "In the short term, there may appear to be no advantage to Zhuhai. But having a brand-name university right on their doorstep will help them tremendously," argues Zhao. For starters, he says, UM intends to adopt a preferential admissions policy for Guangdong applicants.

In a presentation last month, Zhao and fellow administrators portrayed the Hengqin campus as an island within an island. Macau's legal system and the university charter would prevail, they said, and Macau would oversee all services, including phone lines and Internet. UM leaders said "segregation measures"—such as forests and artificial lakes—surrounding the campus would "ensure security." They also proposed a dedicated bridge between the Hengqin campus and Taipa so that staff and students need not pass through immigration controls. (UM would retain its Taipa campus.) This month, the university commissioned a "first draft" of a campus plan that would serve as the basis for negotiations between Macau and Guangdong.

There are bound to be bumps along the way. Last month, Macau legislators questioned whether the city can afford UM's expansion; some worry that if the Hengqin campus were subject to Chinese law, UM would struggle to maintain, let alone boost, enrollment. In contrast, one Zhuhai power broker is worried about too much liberty: Running the Hengqin campus under Macau's legal system would be "seriously unlawful" and "damage Zhuhai's interests," petroleum magnate Li Jiankang, a representative of Zhuhai People's Congress, told the newspaper *Nanfang Dushi Bao* last month.

Still, with China's presumptive next president eyeing developments, few people doubt the Hengqin expansion will occur under the banner of one country, two systems. The only question is which system that will be.

–RICHARD STONE

Published by AAAS

PLANT BIOLOGY

Stressed Out Over a Stress Hormone

The hormone ABA lets plants handle rough times and holds promise for making drought-resistant crops, if only researchers could nail down its molecular partners

When stresses mount, plants can't simply walk away from their problems or head to the nearest bar. Instead of turning to a stiff drink, plants can count on a chemical called abscisic acid (ABA) to bail them out. Discovered in the 1960s by groups searching for substances that regulate bud dormancy and the shedding of leaves and fruits, ABA has turned out to be a vital hormone that plants use when conditions are rough. Concentrations of ABA in leaves shoot up when plants dry out or get too cold; and as the hormone spreads throughout the plant, it stimulates genes involved in a variety of responses. The hormone curtails water loss, helps seeds wait out bad conditions, and inhibits root and other vegetative growth.

Plant biologists have labored for decades to understand how plant cells sense and react to ABA. The payoffs could be substantial. "If, based on improved knowledge of how plants perceive and respond to ABA, we can improve crop yield in the face of drought and other stresses, this can have a major impact on food production and freshwater availability," says Sarah Assmann, a plant biologist at Pennsylvania State University, University Park.

But the hunt for an ABA receptor, a plant-cell protein that recognizes the hormone and conveys its gene-regulating orders to the nucleus, has been full of frustration and controversy. In 2006, plant biologists finally celebrated the first report of such a receptor. And within a year, two other putative ABA receptors were identified in high-profile papers. But the initial receptor discovery soon had to be retracted, and the other candidate receptors have also fallen under intense scrutiny. A fourth, reported just 5 months ago, is provoking debate, too. Those in and outside the field are shaking their heads. "The whole field of plant biology has been hurt," says Alan Jones, a cell biologist at the University of North Carolina, Chapel Hill.

Now, two more research teams are jumping into the fray. They have independently homed in on yet another ABA receptor, which they describe on pages 1064 and 1068. "They provide the first convincing report of a class of proteins that link ABA binding with downstream ABA responses," says Richard Macknight of the University of Otago in Dunedin, New Zealand. "They are landmark papers." Given the events of the past 3 years, however, some plant biologists reserve final judgment on whether the hunt for an ABA receptor is over. The two groups offer "the best data set" so far, Jones says, "but no single work is sufficient to reach such an important conclusion."

First but flawed

Several factors have stymied researchers on the ABA receptor trail. The hormone's influence is pervasive, affecting many genes and pathways. These pathways can sometimes overlap, making it difficult to find and characterize mutant plants with clear-cut defects in ABA responses. The hunt is also complicated by the fact that plants have evolved their own distinct receptors, so computer scans that look for plant genes similar to those that code for receptors in animals can miss likely candidates.

Breakaway growth. Seeds from plants with mutant receptors (right three) don't recognize ABA's signal to stay dormant and are at risk of sprouting in adverse conditions.

Test-tube studies offer their own problems. Plant cells contain packets of protein-destroying enzymes that are easily released when the cell is disturbed, so isolating intact proteins from plant cells is challenging. And proving that a protein and ABA bind specifically, and at realistic hormone concentrations, "is an easy thing to screw up," says Michael Sussman, a biochemist at the University of Wisconsin, Madison. Thirty years ago, Sussman notes, experiments he did "proved" that talcum powder was a receptor to the plant hormone cytokinin.

Nonetheless, a team led by Robert Hill of the University of Manitoba in Winnipeg, Canada, appeared to have overcome these hurdles in 2006, identifying a protein called FCA as a probable ABA receptor. FCA works in a plant cell's nucleus, where it binds to strands of messenger RNA, effectively curtailing the production of a protein called FLC that otherwise inhibits flowering. FCA requires a partner protein, FY, to do this job, and Hill's team reported in the 19 January 2006 issue of *Nature* that ABA bound FCA, interfering with its interactions with FY both in lab tests and in living plants. As a result, the amount of FLC messenger RNA (and presumably, the resulting protein) soars, delaying flowering. "A door to understanding ABA perception has been opened," declared Julian Schroeder and Josef Kuhn of the University of California (UC), San Diego, in an accompanying commentary.

It slammed shut fast, however. A group led by Macknight had trouble confirming the FCA results and notified Hill's team, which was having similar problems. Hill and his group spent 6 months in vain trying to replicate their own work. Ultimately, in the 11 December 2008 issue of *Nature*, Macknight's group published

CREDITS (TOP TO BOTTOM): PEDRO L. RODRIGUEZ EGEA/UNIVERSIDAD POLITECNICA, SPAIN; SANG PARK

Frugal water use. Plants with the most enhanced sensitivity to the hormone ABA (*far right*) do better than their wild counterparts (*far left*) in drought.

its negative findings on FCA, and Hill's team formally retracted the 2006 paper, citing "errors in the calculations" and "difficulties" with the original data.

Even as that episode was playing out, other putative ABA receptors emerged—and they would prove almost as controversial. Schroeder and Kuhn's commentary had pointed out that FCA wasn't involved in other plant properties, such as seed dormancy or root growth, that ABA was known to regulate. That meant more ABA receptors were waiting to be discovered, plant biologists surmised.

Da-Peng Zhang of China Agricultural University in Beijing claimed to find one late in 2006. It was part of an enzyme called magnesium chelatase, known to be involved in making chlorophyll. Zhang and his colleagues showed that it bound to ABA and that disabling the magnesium chelatase gene in *Arabidopsis* plants made them unresponsive to ABA. Their seeds germinated even after exposure to ABA, and the stomata didn't close down the way they should have when water was withheld, Zhang's team reported in the 19 October 2006 issue of *Nature*.

Doubts about this putative receptor have grown, too. Mats Hansson of the Carlsberg Laboratory in Copenhagen recently looked at barley plants in his lab that have mutations disabling the enzyme's gene. If the chelatase was an ABA receptor, those mutants should have little to no response to treatments with the hormone. But the mutant plants reacted like normal ones, he and his colleagues reported online on 28 January in *Plant Physiology Preview*. "We were very disappointed," Hansson recalls.

Magnesium chelatase, like FCA, resides inside a plant cell. Yet previous ABA studies had indicated that plants sense the hormone outside the cells as well. That's why Ligeng Ma of the National Institute of Biological Sciences in Beijing and his colleagues took a different tack as they hunted for the ABA receptor. They focused on a well-known family of membrane-spanning molecules called G protein–coupled receptors that often convey signals from the cell surface. In a computer search for similar gene sequences in the *Arabidopsis* genome, Ma's team found a gene for a new one, *GCR2*. Its protein bound to ABA, Ma and his colleagues discovered. And when the investigators disrupted the *GCR2* gene in *Arabidopsis*, its seeds sprouted prematurely and the mutant plant's stomata got stuck open, indications that ABA was not able to do its job (*Science*, 23 March 2007, p. 1712).

However, within months, this ABA receptor was challenged. Jones and colleagues argued that GCR2 was neither a G protein–coupled receptor nor a transmembrane protein (*Science*, 9 November 2007, p. 914). And several other papers have also questioned the idea of GCR2 as an ABA receptor, with Macknight offering data indicating it doesn't actually bind to the hormone.

Zhang and Ma maintain that the chelatase and GCR2 are ABA receptors, and each continues to study his respective discovery. In the meantime, a fresh ABA receptor controversy has been brewing. In the 9 January issue of *Cell*, Assmann linked a new subtype of G protein–coupled receptors called GTGs to ABA perception. The proteins bind ABA, and mutant plants lacking GTGs lose most of their ability to respond to the hormone, she and her colleagues reported.

But test-tube assays that measure how effectively the proteins latch onto ABA indicate that only 1% of the GTG present was locking up hormone, leaving open the question of just how good a "receptor" the GTG proteins are. Such studies are difficult to do with membrane proteins. In animals, the equivalent protein is an ion channel, so it's possible that's what GTGs do in plants, Erwin Grill and Alexander Christmann of the Technical University of Munich in Germany suggested in a *Cell* commentary. Until more evidence comes in, "we should just be cautious," says Jones.

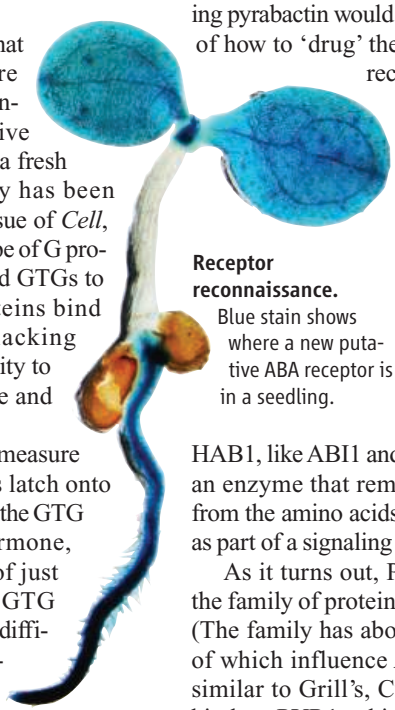

Receptor reconnaissance. Blue stain shows where a new putative ABA receptor is in a seedling.

CREDIT: YUE MA *ET AL.*, *SCIENCE*

The real McCoy?

Two groups have brought the newest candidate ABA receptor to light. Grill decided to work his way into the hormone's signaling mechanism by starting with two enzymes called ABI1 and ABI2. Mutations in the genes for these proteins produce plants that no longer respond well to ABA, so Grill went fishing for plant-cell proteins that bind with ABI1 or ABI2. The researchers eventually isolated two new proteins, dubbing each a "regulatory component of ABA receptor" (RCAR).

Their experiments showed that although either ABI1 or ABI2 alone bind weakly to ABA, complexes of one of the enzymes and an RCAR bind quickly and strongly to the hormone. The team concluded that the hormone starts its signaling cascade by binding to the RCAR-enzyme complexes and shutting down the enzyme's activity.

Unbeknownst to Grill until a year ago, Sean Cutler of the UC Riverside was homing in on the same ABA receptor complex using a very different approach. His team hunts down molecules that can control plant growth. They found one, which they called pyrabactin, that revved up ABA activity when it was applied to plants, delaying seed germination and improving drought tolerance. "I figured characterizing pyrabactin would lead to an understanding of how to 'drug' the ABA pathway," Cutler recalls. "I also hoped, very wishfully, that we might get a receptor out of our efforts."

It took 3 years, but Cutler's wish came true when experiments showed that a protein that pyrabactin binds to, which Cutler dubbed PYR1, links up with a molecule called HAB1. HAB1, like ABI1 and ABI2, is a phosphatase, an enzyme that removes phosphate groups from the amino acids on other proteins, often as part of a signaling cascade.

As it turns out, PYR1 was a member of the family of proteins that Grill calls RCAR. (The family has about 14 members, several of which influence ABA activity.) In work similar to Grill's, Cutler showed that ABA binds to PYR1, which then inhibits its phosphatase partner. In test-tube experiments, ABA doesn't inhibit phosphatase activity, except when PYR1 or some of its relatives is present as a gatekeeper. The test-tube studies "are some of the most important strengths of the two papers," says Sussman. "It fits in with the biology."

Others are more cautious. Assmann calls for more control experiments in the binding studies. And the data from the two groups differ in the degree to which the enzymes shut down by ABA are themselves required to promote the interactions between the hormone and RCAR/PYR1 molecules. Are the enzymes part of a true receptor complex, or are RCAR/PYR1 alone the hormone receptors, which then act upon the enzymes? "There are some discrepancies," says Jones.

Given all the skepticism about previous finds, adds Jones, any proposed ABA receptor won't be validated by a paper or two. "There have been a number of red herrings in this field," Assmann agrees, "so at this point there may be some reluctance to accept even bona fide ABA receptors." For a hormone that helps plants deal with stress, ABA is certainly stressing out the plant biology community.

–ELIZABETH PENNISI

LETTERS

edited by Jennifer Sills

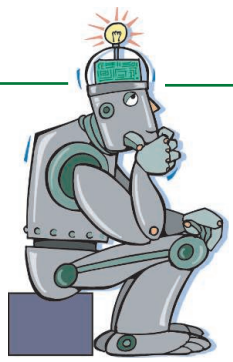

Robot Inventors: Patently Impossible?

AS TWO PATENT ATTORNEYS AND A TECHnical adviser at a long-established Philadelphia intellectual property law firm, we read R. D. King *et al.*'s Report about robotic inventors ("The automation of science," 3 April, p. 85) with interest. We wonder whether the products invented by robots will ultimately become free to the public without the possibility for patent protection.

American patent law (35 U.S.C. Section 102) says that a "*person* shall be entitled to a patent unless…" (emphasis added). That preamble to section 102 limits the ability to patent to a person; machines are presumably excluded. This conclusion is reinforced by section 101, which limits the invention to the discoverer: "Whoever invents…may obtain a patent…." Section 101 uses "whoever," not "whatever." Thus, a person using a robot that invents something may face some serious statutory impediments to patent protection.

The situation is compounded by Section 102(f), which states that one cannot obtain a patent if "he did not himself invent the subject matter sought to be patented." Thus, Section 102(f) prevents one from obtaining valid patent protection if he gets the idea in question—even in private—from another source.

Some existing U.S. patent practice offers hope. Existing DNA/amino acid sequencing machines provide inventors with information that inventors later patent, of course. Another case in point involves high-throughput compound screening to identify promising compounds for pharmaceutical, agricultural, and other purposes. However, there are differences: Such machines are automated and not capable of cognition, and humans provide and select the inputs and analyze the data. Unlike these examples, the robots discussed in King *et al.*'s article seem to have an independent ability to generate and verify hypotheses, perhaps leading in patent parlance to independent "invention" by the robot, not the human.

Europe may differ. Article 58 of the European Patent Convention states that a "European patent application may be filed by any natural or legal person, or any body equivalent to a legal person by virtue of the law governing it." This language seems to provide some wiggle room for the possibility of a robot being an inventor in Europe.

ROBERT W. STEVENSON,* JOSEPH F. MURPHY, THOMAS J. CLARE

Caesar, Rivise, Bernstein, Cohen, and Pokotilow, Ltd., 1635 Market Street, 11th Floor, Philadelphia, PA 19103, USA.

*To whom correspondence should be addressed. E-mail: rstevenson@crbcp.com

Painless Deprivation

IN THEIR PERSPECTIVE ("PAINS AND PLEASures of social life," 13 February, p. 890), M. D. Lieberman and N. I. Eisenberger argue that for every type of deprivation, there is an associated pain, and that the more deprived one is, the more pleasurable fulfilling the need will be. This harkens back to need-reduction theories of reinforcement, along the lines of Hull (*1*). However, there are numerous counterexamples [as Mazur (*2*) points out].

For example, rats need thiamine, but despite the fact that foods containing the nutrient would constitute "the salve that will take the pain away and satisfy the underlying need," rats cannot detect thiamine in food, and so do not seek it out. Similarly, humans need oxygen, but carbon monoxide poisoning does not generate a pain. People instead fall asleep and die.

It is unclear whether a distinction between wants and needs (as the argument is sometimes framed) has implications for the basic argument made by Lieberman and Eisenberger regarding the representation of pleasure and pain in the brain, but it is certainly a distinction that should not be ignored.

WILLIAM VAUGHAN JR.

Casco Courseware, LLC, 207 South Road, Chebeague Island, ME 04017, USA. E-mail: wvaughan@chebeague.net

References

1. C. L. Hull, *Principles of Behavior* (Appleton-Century-Crofts, New York, 1943).
2. J. E. Mazur, *Learning and Behavior* (Prentice Hall, Upper Saddle River, NJ, 1998).

Letters to the Editor

Letters (~300 words) discuss material published in *Science* in the previous 3 months or issues of general interest. They can be submitted through the Web (www.submit2science.org) or by regular mail (1200 New York Ave., NW, Washington, DC 20005, USA). Letters are not acknowledged upon receipt, nor are authors generally consulted before publication. Whether published in full or in part, letters are subject to editing for clarity and space.

Shared Ownership of Biological Resources

THE POLICY FORUM "COULD ACCESS REquirements stifle your research?" (S. Jinnah and S. Jungcurt, 23 January, p. 464) should be viewed in the wider context of the Convention on Biological Diversity (CBD), which recognizes the sovereign rights of the nation states over their biological resources and undermines the concept of biological resources as a common heritage of mankind. National legislation in many countries restricts access to biological resources. Such parochial restrictive measures are gradually becoming ubiqui-

Published by AAAS


Rubber in Southeast Asia
1024
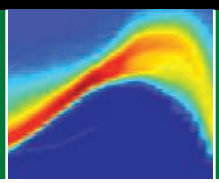
Making use of seismic noise
1026

tous, imperiling not only academic research but even global food security.

Cultivated plants have originated in different regions of the globe. The nations of the world are connected in a complex network of plant genetic interdependence. With extreme dependence on imported genetic materials, no country can afford to isolate itself, or to be isolated, from access to plant germplasm in other regions. Given that genetic resources are truly renewable, their use in a given system does not reduce options elsewhere. Thus, it is imperative that genetic resources be treated as a common heritage to serve the best interest of humanity. The International Treaty on Plant Genetic Resources for Food and Agriculture represents an appropriate step in this direction.

National legislations regulating access to biological resources often do not differentiate between academic and commercial research because their boundaries are vaguely defined. Even if the Ad Hoc Open-Ended Working Group on Access and Benefit-Sharing (ABSWG) resolves to exempt academic research from restrictions, the nation states would continue with the restrictive regimes. Current negotiations within the framework of the CBD on access and benefit sharing do not address the issues created by nationalization of genetic resources. Hence, a dialogue should be initiated in the next Conference of the Parties (COP) of the CBD to correct the historic aberration of nationalization and to treat biological diversity as a common heritage of mankind.

PRIYADARSANAN DHARMA RAJAN[1]* AND PRATHAPAN DIVAKARAN[2]

[1]Ashoka Trust for Research in Ecology and the Environment (ATREE), Jakkur Post, Bangalore 560 064, India. [2]Department of Entomology, Kerala Agricultural University, Trivandrum, Kerala 695 522, India.

*To whom correspondence should be addressed. E-mail: priyan@atree.org

Biological Invasions: Benefits versus Risks

A COMPREHENSIVE ASSESSMENT OF BIOLOGical invasions ("Will threat of biological invasions unite the European Union?" P. E. Hulme *et al*., Policy Forum, 3 April, p. 40) requires a quantification of the benefits provided to humans by the introduced species as well as their negative impacts. Potential benefits include aquaculture (*1*), sport fishing (*2*), forestry (*3*), horticulture (*3*), and game hunting (*4*). Human needs for food explain 51% of alien fish introductions worldwide (*2*). In 2006, European aquaculture production was reported to be $8.65 billion (*1*), and most invasive aquatic alien species introduced in Europe are currently part of European aquaculture's portfolio (*2*, *5*). The economic value of many exotic species provides a strong incentive to their further introduction, despite the potential ecological risks (*2*). Acknowledging this paradox is central to developing a unified approach to biological invasion (*2*).

Hulme *et al*. also fail to recognize that species blacklisted in one area may be Red Listed (*6*) (i.e., considered as conservation priorities) in another (*7*). Invasion of new territory by such species could constitute assisted species relocation, a positive outcome in conservation terms (*8*).

Considering all impacts of species introductions as negative is counterproductive and ignores their benefits to the European economy (*1*). Policy advisers should not ignore risks of biological invasions, but they should also examine their potential impacts on a wide range of ecosystem services. Neither should they seek to limit trade by citing the precautionary principle as a surrogate for our scientific ignorance.

RODOLPHE E. GOZLAN* AND ADRIAN C. NEWTON

School of Conservation Sciences, Bournemouth University, Talbot Campus, Fern Barrow, Poole, Dorset BH12 5BB, UK.

*To whom correspondence should be addressed. E-mail: rgozlan@bournemouth.ac.uk

References

1. FAO, The State of World Fisheries and Aquaculture, ISSN 1020-5489 (2008).
2. R. E. Gozlan, *Fish Fish*. **9**, 106 (2008).
3. H. L. Hyland, *Env. Rev*. **4**, 26 (1977).
4. M. J. Butler *et al*., *Wildl. Soc. Bull.* **33**, 381 (2005).
5. FAO, Fisheries and Aquaculture Department, Software (www.fao.org/fi/statist/statit.asp).
6. IUCN–The World Conservation Union, *IUCN Red List Categories and Criteria*, *Version 3.1* (IUCN, Gland, Switzerland and Cambridge, UK, 2001).
7. R. E. Gozlan *et al*., *Nature* **435**, 1046 (2005).
8. E. Maris, *Nat. Rep. Clim. Change* **2**, 112 (2008).

Response

OUR POLICY FORUM AIMED TO HIGHLIGHT several challenges to implementing a pan-European Invasive Species Strategy, one of which is how best to prioritize invasive species for blacklisting. Among many potential criteria used to blacklist species (*1*), we would argue against making an allowance for species conservation status in the native territory or the potential economic value in the introduced region. If a species is perceived as a pest where introduced, it will often be blacklisted, regardless of its conservation status in its native range. Two of our examples of native European species that are invasive elsewhere in Europe are either Red Listed (*2*) or classified as nationally threatened (*3*), but this has not stemmed eradication attempts in the places where they are considered invasive.

TECHNICAL COMMENT ABSTRACTS

Comment on "Functional Traits and Niche-Based Tree Community Assembly in an Amazonian Forest"

Jeffrey K. Lake and Annette Ostling

Kraft *et al*. (Reports, 24 October 2008, p. 580) used a variety of metrics describing the distribution of functional traits within a tropical forest community to demonstrate simultaneous environmental filtering and niche differentiation. We discuss how these results could have arisen from sampling design and statistical assumptions, suggesting alternative approaches that could better resolve these questions.

Full text at www.sciencemag.org/cgi/content/full/324/5930/1015c

Response to Comment on "Functional Traits and Niche-Based Tree Community Assembly in an Amazonian Forest"

Nathan J. B. Kraft and David D. Ackerly

Lake and Ostling address several issues that they suggest could influence our analyses of tropical forest community assembly. Some of the issues have already been considered, whereas others appear to arise from misunderstandings. We offer clarification of our analyses and additional discussion of our results.

Full text at www.sciencemag.org/cgi/content/full/324/5930/1015d

It is well known that many alien species have been introduced deliberately to Europe for economic benefit (*4*), and we have addressed elsewhere how policy-makers could address and manage these risks (*5*). In our assessment of the impacts of alien species on European ecosystems, we emphasize how difficult it is to balance the environmental costs and economic benefits of species introductions (*6*). Major aquaculture species such as the crayfish *Procambarus clarkii* and Pacific cupped oyster *Crassostrea gigas* threaten endemic species through predation, competition, and/or the spread of diseases, and these two specific examples are widely recognized as some of the worst invasive species in the region (*7*); however, assessing these impacts in terms of comparable monetary costs is difficult (*8*). Furthermore, economic benefits are often gained by one sector of society while the costs are borne by the wider public. The history of biological invasions in Europe has too many examples of shortsighted decisions targeting perceived economic gains that have resulted in much larger (and often irreversible) costs to society (*4*, *7*). Thus, such "balance sheet" decision-making promoted by Gozlan and Newton, rather than a precautionary approach, is not only naïve but potentially dangerous.

PHILIP E. HULME,[1]* WOLFGANG NENTWIG,[2] PETR PYŠEK,[3,4] MONTSERRAT VILÀ[5]

[1]The Bio-Protection Research Centre, Lincoln University, Post Office Box 84, Canterbury, New Zealand. [2]Institute of Ecology and Evolution, University of Bern, Baltzerstrasse 6, CH-3012 Bern, Switzerland. [3]Institute of Botany, Academy of Sciences of the Czech Republic, CZ-252 43 Průhonice, Czech Republic. [4]Department of Ecology, Charles University, CZ-128 01 Viničná 7, Prague, Czech Republic. [5]Estación Biológica de Doñana (EBD-CSIC), Avinguda Américo Vespucio, E-41092 Sevilla, Spain.

*To whom correspondence should be addressed. E-mail: philip.hulme@lincoln.ac.nz

References

1. P. E. Hulme, *J. Appl. Ecol.* **43**, 835 (2006).
2. IUCN–The World Conservation Union, *IUCN Red List Categories and Criteria, Version 3.1* (IUCN, Gland, Switzerland and Cambridge, UK, 2001).
3. A. Erfmeier, H. Bruelheide, *Flora* **199**, 120 (2004).
4. P. E. Hulme, *Issues Env. Sci. Technol.* **25**, 56 (2007).
5. P. E. Hulme *et al.*, *J. Appl. Ecol.* **45**, 403 (2008).
6. M. Vilà *et al.*, *Front. Ecol. Environ.*, 10.1890/080083 (2009).
7. DAISIE, *Handbook of Alien Species in Europe* (Springer, Dordrecht, Netherlands, 2009).
8. A. Balmford *et al.*, *Science* **297**, 950 (2002).

NASA Must Be Held to Account

THE NEWS FOCUS STORY BY A. LAWLER ("Trouble on the final frontier," 3 April, p. 34) describes the history of NASA's over-budget and behind-schedule projects over the years. Despite the protests of the various science teams that they are doing their best to develop sound budgets and schedules, the fact remains that they have not been able to make credible estimates, sometimes missing the mark by huge amounts. And yet, NASA management continues to accept the estimates. As long as there is no accountability for the science teams and NASA management—in the form of canceled programs and bars to future contracts and grants—and as long as Congress continues to view NASA as a jobs program instead of an investment of taxpayer dollars in the advancement of sound science, we should expect more of the same. Projects will be forecast as affordable, only to balloon out of control. Then more money will be poured in and no one will be held to account.

DAVID N. CLARK

Marysville, OH, USA. E-mail: clarkdn@imetweb.net

Comment on "Functional Traits and Niche-Based Tree Community Assembly in an Amazonian Forest"

Jeffrey K. Lake* and Annette Ostling

Kraft *et al*. (Reports, 24 October 2008, p. 580) used a variety of metrics describing the distribution of functional traits within a tropical forest community to demonstrate simultaneous environmental filtering and niche differentiation. We discuss how these results could have arisen from sampling design and statistical assumptions, suggesting alternative approaches that could better resolve these questions.

Kraft *et al*. (*1*) used the distribution of functional traits in a diverse tropical forest community to test hypotheses of community assembly. The study focused on six traits that drive diverse ecological functions. By comparing metrics of observed distributions of each trait with those expected under different null models, the authors showed evidence for both classical niche differentiation and environmental filtering at the scale of 20- by 20-m quadrats. Relative to null expectations, environmental filtering was indicated by shifting trait means, decreased trait range, and variance within quadrats, whereas differentiation was indicated by overdispersion, measured by standard deviation (SD) of nearest-neighbor distance in trait space, and kurtosis of the within-quadrat trait distribution. Combined, these tests were used to argue for the important role of stabilizing processes in the maintenance of biodiversity in a hyperdiverse tropical forest. This approach represents movement toward a more comprehensive use of functional traits in testing processes of community assembly. Nevertheless, there are some subtle problems in the Kraft *et al*. analysis that we expand upon here.

First, Kraft *et al*. (*1*) inappropriately tested for both environmental filtering and niche differentiation using null models that select randomly from the entire species pool. If environmental filtering limits the range of traits of species that can occur in a given quadrat, an accurate test of niche differentiation within quadrats must sample only from species that fall between the minimum and maximum traits present in a quadrat. The larger the available trait space, the larger the possible range of nearest-neighbor distances in trait space, and hence the bigger the SD of nearest-neighbor distances will be under a random draw from that available trait space. Thus, if limitations on the range of trait values in each quadrat due to habitat filtering are not accounted for in the null trait distribution used in the niche differentiation test, one might artificially conclude that the observed SD of nearest-neighbor distances is smaller than expected by chance and that niche differentiation is occurring. Similar problems might arise in the comparison of kurtosis values.

Second, Kraft *et al*. ignored intraspecific variation. Due to the obvious difficulty of collecting trait data for all individuals, the authors targeted outer canopy leaves of trees in the 1- to 5-cm diameter at breast height (dbh) size class growing under closed canopy that were readily accessed from the ground, leading to a collection of 2 to 5 leaves from 1 to 20 individuals for most of the 1089 species. Hence they had to generate observed quadrat-level trait distributions by assigning trait values to the occurrence of each species in each quadrat (known from the spatial tree data available for the plot), based on the limited information they have collected for the 1 to 20 individuals of that species across the plot. Based on three arguments—that a relatively low percentage of explained variance in traits is driven by individual and leaf sampled, that there is only limited correlation between traits and measured environmental gradients, and that species' rank order of trait values measured from canopy trees is relatively similar to their rank ordering based on juvenile measurements—Kraft *et al*. assigned the species' mean sapling trait values to all individuals of that species, regardless of individual size and light exposure.

Yet traits can vary 2- to 3-fold or more across ontogeny or light environment within a species, whereas the interspecific range within a community is similar or only moderately higher (*2*–*5*). This is not true for all traits (seed size varies intraspecifically, but not ontogenetically, and maximum size is a species-level trait), but for the traits related to leaf size, structure, and chemistry, intraspecific variation can be substantial. It is

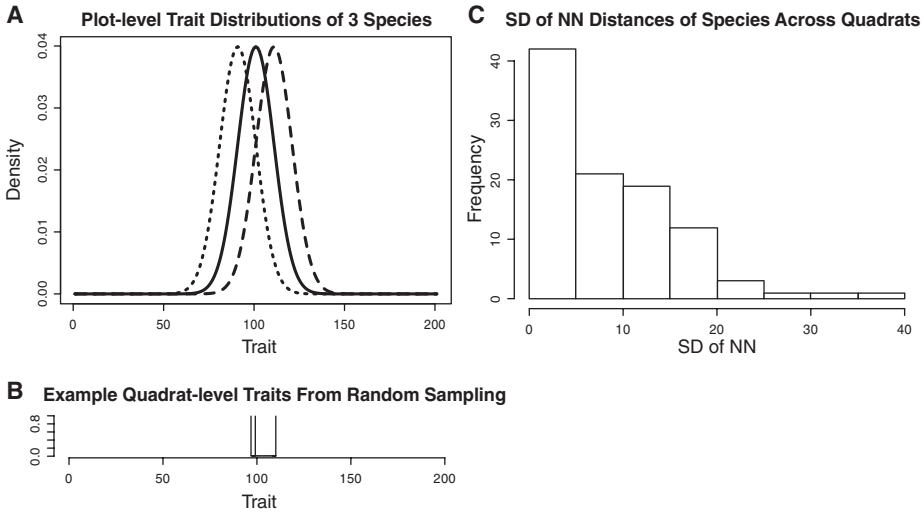

Fig. 1. Representation of the effect of sampling from intraspecific variability. (**A**) Hypothetical plot-level trait distributions of three species with a perfectly overdispersed, normally distributed trait, with means of 90, 100, and 110, respectively, and a SD of 10. (**B**) An example within-quadrat trait distribution that results when we sample one "real" individual from the distribution for each species instead of assuming that individual follows the species means, as Kraft *et al*. did. The height of the bars represents the number of occurrences, which is one for each species. (**C**) The resulting distribution of SD of nearest-neighbor distances (SD of NN) across 100 quadrats created in this way. The values of SD of NN if species means were used as Kraft *et al*. did is 0. Hence, intraspecific variation causes the SD of NN to go up on average. It will have this effect on both the observed and null model SD of NN. However the effect on the null model SD of NN will be extremely small because the species are so tightly packed in trait space at the plot level that traits sampled from species near one another in trait space become essentially interchangeable. The net result is that the observed SD of NN goes up, whereas the null SD of NN remains approximately the same, when intraspecific variation is accounted for, and the evidence for niche differentiation gets weaker.

Department of Ecology and Evolutionary Biology, University of Michigan, Kraus Natural Sciences Building, 830 North University, Ann Arbor, MI 48109, USA.

*To whom correspondence should be addressed. E-mail: lakejk@umich.edu

virtually certain that the individuals within a given quadrat are a mix of sizes (and light exposures) of different species. Hence, trait range and variance within quadrats, as well as the SD of nearest-neighbor distances and kurtosis of the trait distributions within quadrats, would all change dramatically if ontogenetic variation were included, and the impact on the observed trait distributions relative to the null predictions is highly unpredictable. The arguments of Kraft *et al*. for ignoring intraspecific variation do not alter this fact.

Furthermore, even the small amount of intraspecific variation among saplings could affect Kraft *et al*.'s more conservative test for niche differentiation, which uses only the spatial arrangement of individuals close in size to the size class for which trait data was actually collected (specifically 1- to 10-cm dbh individuals). A quadrat where species trait means are dispersed when occurrences are simply assumed to correspond to plot-level sapling means might really be randomly assembled based on the actual species' mean trait values for that quadrat. Consider, for example, the extreme case in which the traits of individuals of each species in a quadrat are a random draw from that species' plot-level trait distribution. The nearest-neighbor distances between species' quadrat mean trait values will then be more variable than the distances between the plot-level means of those species (Fig. 1). Here, there is much greater potential for shifts in the observed distribution than in the null, where the close packing of species should lead to little change after sampling from species trait distributions. Although it is impossible to know with certainty the impacts of ignoring intraspecific variation in traits without a good measure of that variability, it is certain that, at best, species means provide a first approximation of the trait distribution patterns resulting from the community assembly processes acting in this forest.

The unfortunate solution to this problem seems to be sampling traits from many more individuals to gain spatially resolved trait data. This is a logistical hurdle, especially given the difficulty of sampling sun-exposed leaves of adults. However, because size structure can play an important role in competition (*6*, *7*), overcoming these challenges seems necessary for understanding the assembly of a forest community where individuals vary so greatly in size. One alternative is to sample randomly from the known intraspecific distributions of traits for individuals within a given size class and light environment within each species when assigning trait values, that is, to consider the extreme case we described. Although this could mask the effects of niche differentiation driven by local competition—traits of individuals within a given quadrat may not be a random sample from that species' trait distribution—a rejection of the null even in this alternative analysis would provide clearer evidence for niche differentiation.

There are two final points we wish to make. First, as the authors note, the results they find for this forest are rather subtle. Although the statistical significance Kraft *et al*. found is high, effect size is often negligible or small. This is especially true for tests for overdispersion of traits at the quadrat level. Second, given how small this overdispersion is, ignoring intraspecific variation presents a problem more fundamental than the statistical issues we have raised. If intraspecific variation is high, species probably overlap a great deal in their trait distributions. If the strength of interspecific competition is proportional to this overlap, then interspecific competition may indeed be stronger than intraspecific competition, and the species may not be stably coexisting and hence not be truly niche differentiated even if there is a tendency for overdispersion (*8*). Hence, evaluating process on the basis of overdispersion patterns in the absence of information about overlap may lead us to an invalid conclusion about the nature of community assembly. However, establishing a detailed relationship between the strength of interspecific competition and the amount of trait overlap requires a mechanistic understanding of competition in this forest that is currently unavailable, so Kraft *et al*. have carried out the most thorough analysis currently possible in this regard.

We applaud this overall approach and the substantial effort involved in moving toward tests of niche and neutral processes. These types of studies, particularly if combined with demographic data on individual trees, can move us toward a better understanding of the forces governing community assembly. However, we suggest that further analysis is needed before the signature of community assembly (in particular of niche differentiation) can be clearly detected in the observed trait distributions in this forest.

References and Notes

1. N. J. B. Kraft, R. Valencia, D. D. Ackerly, *Science* **322**, 580 (2008).
2. L. Poorter, F. Bongers, *Ecology* **87**, 1733 (2006).
3. D. M. A. Rozendaal, V. H. Hurtado, L. Poorter, *Funct. Ecol.* **20**, 207 (2006).
4. L. Sack, P. J. Melcher, W. H. Liu, E. Middleton, T. Pardee, *Am. J. Bot.* **93**, 829 (2006).
5. P. B. Reich *et al*., *Funct. Ecol.* **12**, 327 (1998).
6. D. E. Goldberg, P. A. Werner, *Am. J. Bot.* **70**, 1098 (1983).
7. C. J. Peterson, E. R. Squiers, *J. Ecol.* **83**, 449 (1995).
8. R. MacArthur, R. Levins, *Am. Nat.* **101**, 377 (1967).
9. We benefited from discussions with D. Goldberg, S. Hubbell, N. Kraft, B. Sedio, Z. Brym and R. Warren II. We also thank two anonymous reviewers for many constructive suggestions.

12 December 2008; accepted 28 April 2009
10.1126/science.1169721

Response to Comment on "Functional Traits and Niche-Based Tree Community Assembly in an Amazonian Forest"

Nathan J. B. Kraft* and David D. Ackerly

Lake and Ostling address several issues that they suggest could influence our analyses of tropical forest community assembly. Some of the issues have already been considered, whereas others appear to arise from misunderstandings. We offer clarification of our analyses and additional discussion of our results.

Lake and Ostling (*1*) express several concerns that they suggest could influence our analyses of tropical forest community assembly (*2*). Here, we address each comment in turn.

Lake and Ostling point out, as others have previously (*3*, *4*), that an appropriate null model for detecting even spacing may need to incorporate the effects of habitat filtering. In some instances, habitat filtering, which reduces the range and possibly the variance of trait values among co-occurring species, may also produce nonrandom patterns in trait spacing, when compared to a null model including species from multiple habitats. In our analyses (*2*), we addressed the interaction between habitat filtering and niche differentiation by using habitat-restricted null models. Previous analyses of the Yasuní plot (*5*) identified two primary habitat types within the plot, ridgetops and valley bottoms, and our tests of trait averages strongly mirrored the distribution of these habitats [figures 1A and S1 in (*2*)]. We therefore expected that limiting the species pool to just species occurring within each habitat should reduce the habitat filtering signal for plots within the respective habitats, which it did in many cases. If Lake and Ostling were correct that our even spacing results were driven entirely by habitat filtering, using a habitat-restricted pool also should have reduced the signal of niche differentiation. In many cases, the niche differentiation signal was stronger under habitat-specific null models (*2*), which suggests that there are at least two distinct nonrandom processes occurring.

There are additional ways to address the interaction between habitat filtering and niche differentiation that we did not present. One way (*3*) is to standardize spacing metrics by the observed range of trait values within a quadrat. Thus, instead of the standard deviation of nearest-neighbor distances (SDNN), one can use SDNN divided by the range as the test metric. Using this metric to repeat the analyses shown in table 1 in (*2*), we detect even spacing in three traits (leaf nitrogen Wilcoxon $P = 0.011$; leaf size $P < 0.0001$; maximum diameter at breast high (dbh) $P = 0.0005$), although specific leaf area (SLA, leaf area divided by dry mass) is no longer significant (*6*). Alternatively, the null model can be restricted to include only species that occur within the range of values found within the quadrat (*4*). This approach, which treats each quadrat as if it is located at a distinct position along a continuous environmental gradient, seems biologically implausible given what we know about habitat associations at Yasuní and other tropical forests (*5*, *7*); however, it can be applied. Repeating the analyses summarized in table 1 in (*2*), modified to include a restricted range null model in quadrats where significant filtering was detected, our basic conclusions about the presence of even spacing hold (leaf nitrogen Wilcoxon $P = 0.01$; leaf size $P = 0.007$; maximum dbh $P < 0.0001$; other traits not significant). Both of these alternative analyses offer the same general result as our main analysis, with the exception of SLA, which was significant in our main analysis but had a very small effect size.

Next, Lake and Ostling suggest that intraspecific variation should be considered. We heartily agree that greater sampling and study of intraspecific variation in forests like Yasuní would be valuable, but we are doubtful that the effect of such variation in a properly specified null model analysis of Yasuní would be as dramatic as they envision.

First, there is an important general point about what individual trait variation represents. Variability in measurements between individuals can be due to plastic phenotypic responses to the environment, ontogenetic changes, genetic variation, sampling error, and other sources. Plastic phenotypic and ontogenetic responses are often correlated among species, and we contend that a proper null model that incorporates intraspecific variation should apply this type of variation in a correlated way across species. This would reduce the degree of intraspecific variability in analyses relative to the figures that Lake and Ostling cite. For example, they cite 2- to 3-fold variation in leaf traits across ontogeny in other studies, whereas we find an average of 1.7-fold variation in SLA within well-sampled species [table S6 in (*2*)] of similar stature and light exposure. This is in contrast to the 9-fold variation we find in mean SLA across species of similar stature and light exposure, 6-fold variation in species mean leaf nitrogen, >5000-fold variation in species mean leaf size (we measured minimum photosynthetic units), 6-fold variation in adult wood density, 180-fold

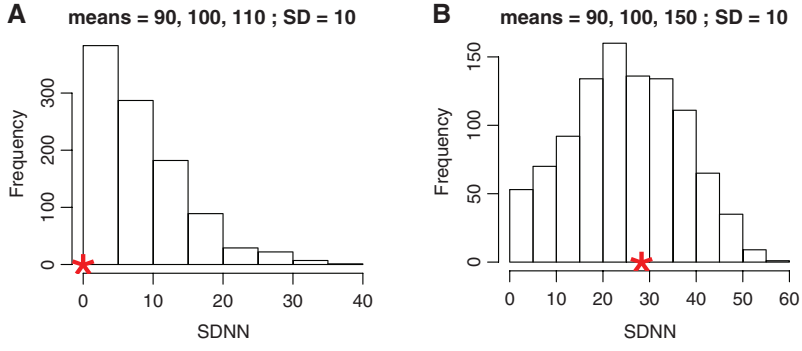

Fig. 1. Effect of including intraspecific trait variability in the estimation of SDNN in two cases, following Lake and Ostling's (*1*) example. (**A**) Same case as figure 1C in (*1*), where one individual of three species with trait means of 90, 100, and 110, and each with a trait SD of 10, is randomly sampled and the SDNN is calculated. Here the process is repeated 1000 times to generate a distribution of SDNN values. The asterisk (*) indicates the SDNN value calculated from the species mean alone (which is 0). In this case, stochastic sampling from intraspecific trait distributions can only increase SDNN relative to the value calculated from means, as the species means are perfectly spaced already (and because SD values are bounded at 0). However, in any instance where species mean values are less than perfectly spaced (and therefore SDNN calculated from species means is greater than 0) (**B**), as is the case in every trait in every quadrat of our study (*2*), adding stochastic sampling of intraspecific variation can result in either larger or smaller estimates of SDNN than would be produced by simply using species means. Therefore, in real communities, using species means should not systematically underestimate SDNN calculated from intraspecific data, as Lake and Ostling suggest.

Department of Integrative Biology, University of California, Berkeley, CA 94720, USA.

*To whom correspondence should be addressed. E-mail: nkraft@berkeley.edu

variation in maximum dbh, and >209,000-fold variation in seed size.

Second, we disagree with Lake and Ostling that measures of species spacing, such as SDNN, are the ideal metric for use with intraspecific variation. They suggest adding stochastic sampling variation to species means, which seems to bypass a history in ecology of using niche overlap indices (*8*) when considering intraspecific variation. Recent work (*3*), for example, uses spacing metrics similar to ours for species means and niche overlap metrics for analyses with intraspecific data, and we find this distinction useful.

Third, Lake and Ostling argue that incorporating intraspecific variation will dramatically alter the outcome of our tests of even spacing using SDNN. This is in part because they incorrectly assume that stochastically applied intraspecific variation will result in a distribution of SDNN values in which all values are equal to or greater than SDNN calculated from species means, indicating less even spacing [figure 1 in (*1*)]. This result arises from a biologically implausible parameter choice in their example (Fig. 1A). In all other cases, adding intraspecific variation can either increase or decrease estimates of SDNN, making communities appear either more or less randomly assembled (Fig. 1B). This is hard to construe as a systematic bias, particularly for abundant species within communities, where Lake and Ostling's approach would be no different from using species means. This issue aside, it should be noted that the magnitude or variability of SDNN values have little bearing in any absolute sense; the key is the value of the observed SDNN relative to the null expectation. As the variation should be added to both the null and the observed data, the effect on the test outcome, if any, will likely be small when intraspecific variation is small relative to interspecific differences.

Lake and Ostling's comments in this area raise an interesting question: Do the functional traits of leaves, seeds, and wood directly influence plant establishment and community assembly, or are the traits proxies or correlates of overall strategies that may be assembling nonrandomly within these communities? We would argue that it is the latter, whereas Lake and Ostling's concerns regarding intraspecific variation seem to presume the former, in which it is the actual trait value of the individuals in a plot that is responsible for the community assembly processes. This distinction is most apparent for some of the traits included in our analysis that Lake and Ostling did not focus on, such as seed size and maximum dbh. In both of these cases, actual values cannot be applied to the tens of thousands of immature individuals within the plot, so species averages serve as a proxy for associated ecological strategies.

Lake and Ostling state, as we did in (*2*), that the evidence for nonrandom assembly processes at Yasuní is subtle. They go on to suggest that nonrandom assembly processes are therefore unimportant or negligible. We contend that the difference between a fully neutral community and a largely equalized community with weak stabilizing forces (*9*), as both our habitat filtering and even spacing results suggest, lies at the heart of the argument over the importance of neutral theory. As Purves and Pacala (*10*) have shown, the patterns in relative abundance that have been used to support neutral theory arise from stochastic demographic processes, not from ecological equivalence of species (two distinct aspects of the neutral theory that are often conflated). A combination of gap dynamics, soil and topographically based habitat filtering, impacts of natural enemies, and strategy differentiation at local scales all may act in concert to produce the patterns that we reported. These nonrandom stabilizing processes, even if they are subtle, have important implications for the fate of rare species within communities, the turnover of communities in space and time, and the structure and function of ecosystems.

References and Notes

1. J. K. Lake, A. Ostling, *Science* **324**, 1015 (2009); www.sciencemag.org/cgi/content/full/324/5930/1015c.
2. N. J. B. Kraft, R. Valencia, D. Ackerly, *Science* **322**, 580 (2008).
3. W. J. Stubbs, J. B. Wilson, *J. Ecol.* **92**, 557 (2004).
4. W. K. Cornwell, D. Ackerly, *Ecol. Monogr.* **79**, 109 (2009).
5. R. Valencia *et al*., *J. Ecol.* **92**, 214 (2004).
6. N. J. B. Kraft, thesis, University of California, Berkeley (2008).
7. S. J. Wright, *Oecologia* **130**, 1 (2002).
8. M. L. Cody, in *Ecology and Evolution of Communities,* M. L. Cody, J. M. Diamond, Eds. (Harvard Univ. Press, Cambridge, 1975), pp. 214–257.
9. P. Chesson, *Annu. Rev. Ecol. Syst.* **31**, 343 (2000).
10. D. W. Purves, S. W. Pacala, in *Biotic Interactions in the Tropics,* D. Burslem, M. Pinard, S. Hartley, Eds. (Cambridge Univ. Press, Cambridge, 2005), pp. 107–138.

11. We have benefited from conversations with J. Lake, A. Ostling, W. Cornwell, and S. Kembel about these and related issues. Our response was improved by the comments of two anonymous reviewers.

9 January 2009; accepted 29 April 2009
10.1126/science.1169885

ECOLOGY AND EVOLUTION

Problems Well Worth Pondering

Hanna Kokko

Big Questions in Ecology and Evolution

by Thomas N. Sherratt and David M. Wilkinson

Oxford University Press, New York, 2009.
311 pp. $99, £55.
ISBN 9780199548606.
Paper, $45, £27.50.
ISBN 9780199548613.

Big Questions in Ecology and Evolution sounds like an ambitious title, particularly for a book of only 300 pages (tens of which are taken up by an extensive bibliography). It is also a brave choice for a book that has only two authors. I would have thought one needs more contributors for a volume that describes how Chinese officials in the T'ang dynasty began collecting annual reports on the abundance of migratory locusts and then lucidly moves on to cite astronomy sources on quasars when discussing a science fiction story of a planet in trouble. In the first few pages, the ecologists Thomas Sherratt and David Wilkinson thank their home institutions (Carleton University, Canada, and Liverpool John Moores University, UK, respectively) for granting them their first-ever sabbaticals. Reading the book truly made me wonder if I'll be able to put my own upcoming sabbatical to equally good use. Sherratt and Wilkinson have clearly spent considerable time in the library, and the stuff they found there ranges from the quirky to the really important and cutting edge.

So, what are the big questions? The authors' choices are somewhat eccentric, but a general theme emerges. Sherratt and Wilkinson explore topics that one could easily take for granted, and for which it takes a scientist—or a child—to ask the relevant "why?" To mention a few: Why do we age? Why is the land green (instead of having been overgrazed by expanding populations of herbivores)? Why is the sea blue (as opposed to being thick with plants, as most terrestrial habitats are)? Why does life not consist of just a single species? One could, of course, suggest additions to or alterations of the authors' particular list of topics. (For instance, the authors discuss possible ways in which life on Earth may be ended, whereas they do not cover what we know about life's beginnings on our planet.) However, that would be nitpicking. The book should simply be appreciated for presenting ten convincing examples of how stopping taking things for granted can lead to intellectual wonder and amazement.

The chapters on topics with which I was familiar I found well written, and those I knew nothing about beforehand were eye-opening. By now I am surprised (and mildly ashamed) that I had no clue about the possibility that Earth's biosphere might end long before the expanding Sun vaporizes the planet because feedback through the geological carbon cycle can make atmospheric carbon dioxide levels plummet while temperatures rise. That is truly counterintuitive given our current climate crisis. (The authors are quick to also point out that human activities that are presently increasing atmospheric CO_2 cannot be seen as a good deed in this long-term context either.) I can imagine similar "wow" moments for most readers. In particular, evolutionary biologists will learn a lot about ecology from the authors' considerations of potential answers to the questions, and ecologists will be reminded of the advantages of knowing more about evolution. In fact, one of the book's more serious messages is that ecology and evolution are so intertwined that neither can be understood without considering the other. I found myself wholeheartedly agreeing with the suggestion that G. Evelyn Hutchinson's famous phrase about the "ecological theatre and the evolutionary play" depicts a hierarchy that perhaps should be replaced with something more egalitarian.

Green land and blue sea. Along the scenic coast of Queensland, Australia (here, Cape Tribulation), lush rainforests abut the clear waters of the Coral Sea.

CREDIT: COURTESY TOURISM QUEENSLAND

The book left me a little jealous of the authors. They manage to convey the fun they clearly had writing it and to maintain a high standard of rigor. Lest you conclude that I have been carried away by my enthusiam, I must note a few quibbles. The authors mention that, because the answers to the questions they explore are highly controversial, they hope that their explanations will be read critically. Given that the book whets an appetite of childlike curiosity, it is perhaps telling that I frowned most often when reading about topics in which my naïveté peaks. For example, the authors' explanation for why large (multicellular) floating plants do not cover the oceans relies in part on currents that would so often convey the plants up onto beaches or off to wrong parts of the globe. This aspect prompted me to a comparison of the "green land" and the "blue sea." Although terrestrial plants are better rooted to the ground, their seeds and pollen certainly often lack precise means to end up in suitable places—so are the arguments really qualitatively different? Lots of populations exist as sources and sinks, after all. But being baffled with new thoughts hardly counts as a truly negative experience.

A few other shortcomings (to show that I tried to be a critical reader): The styles in the different chapters are not seamlessly united, a problem that is hard to avoid in any co-authored book. I very much enjoyed the metaphors and anecdotes sprinkled here and there, and gradually I came to expect such quips much more often in certain chapters than in others. I believe that popular culture references from sci-fi films to nursery rhymes help to make explanations fun as well as mem-

The reviewer is at the Laboratory of Ecological and Evolutionary Dynamics, Department of Biological and Environmental Sciences, University of Helsinki, 00014 Helsinki, Finland. E-mail: hanna.kokko@helsinki.fi

Published by AAAS

orable (teaching staff, take note). That is a matter of taste, but the differences between the chapters left me a little hungry for more of these sparks.

Such quibbles are indeed minor faults. The serious fun of *Big Questions in Ecology and Evolution* comes from considering the child-like "why?" Unlike the average responses to questions posed by children, here Sherratt and Wilkinson offer answers as good as science currently can deliver.

10.1126/science.1174574

BIOETHICS

Reflections from the Silver Screen

Jeremy Sugarman

One of the captivating aspects of bioethics is its stories. These include tales that span the life cycle during times of health or illness as well as those related to the pursuit of enhanced scientific understanding and medical technologies. They may involve patients and clinicians, scientists and society, individuals and families, politicians and clergy, nonhuman animals and the environment. Almost emblematically, they entail conflicts, especially conflicts of moral values. Through the lens of bioethics, these stories prompt ethical analysis and interpretation, while through the lens of the cinematographer they can be rich sources for plots. Therefore, not surprisingly, bioethical issues have appeared in many good movies.

Even those who eschew aspects of popular culture will likely recognize some of the many films that incorporate topics relevant to bioethics. Consider, for example, the films *Babe*, *The Cider House Rules*, *Dad*, *The Diving Bell and the Butterfly*, *Gattaca*, *Million Dollar Baby*, *Soylent Green*, *Star Trek: Nemesis*, and *Wit*. Collectively, they raise myriad ethical issues, such as those related to animal welfare, abortion, aging, spinal cord injury, genetic determinism, euthanasia, cloning, research ethics, and decision-making at the end of life.

Bioethics at the Movies

Sandra Shapshay, Ed.

Johns Hopkins University Press, Baltimore, MD, 2009. 400 pp. $55. ISBN 9780801890772. Paper, $25. ISBN 9780801890789.

Enter *Bioethics at the Movies*. Sandra Shapshay (a philosopher at Indiana University, Bloomington) has put together a series of contributed chapters that examine bioethical issues that have been portrayed in the cinema. She groups the essays into five sections, an organization that follows "the syllabi for many bioethics courses." The first explores contentious issues such as those related to abortion and personhood. The following three take up aspects of genetic technologies and human cloning, medical research and constituents of a good life, and "aging and the good death." The volume ends with essays examining films that challenge now somewhat standard bioethical approaches and explore ways that cultural context might influence bioethics.

The volume is best considered as a textbook. Many of the contributors "use popular, narrative films for the sake of bioethical reflection." Movies can offer compelling examples of bioethical issues. Cinematic treatments of these issues can increase the viewers' familiarity with the complexities associated with them. And films can provide "rich thought-experiments that tap into moral intuitions and advance ethical thinking." These pedagogical, interpretive, and experimental approaches are creative, yet not terribly controversial. In contrast, some of the authors argue that the films themselves are "doing philosophy."

Most chapters focus on a particular film, and only a few films receive attention from more than one author. Both *Gattaca* and *Million Dollar Baby* are examined in paired chapters. These contrasting readings are quite informative because they reveal the different ways in which film may be interpreted even through the lens of bioethics. For example, one of the chapters analyzing the ethical aspects of euthanasia as depicted in *Million Dollar Baby* privileges a perspective emanating from disability studies, while the other employs an approach from analytic philosophy.

As might be expected for an edited volume from multiple authors having different kinds of expertise, the essays are a bit uneven. For instance, some chapters assume a fairly sophisticated level of understanding of moral philosophy, whereas others are written at a very basic level. Such differences will make wholesale classroom use of the volume a bit challenging. Nevertheless, one could easily assign selected chapters. Alternatively, teachers could use the book to help them to select films and appropriate readings for their courses. Their decisions might be facilitated by reviewing the "questions for consideration" provided at the end of each chapter.

Not worth the risk. In *Gattaca*, companies use genetic discrimination to try to keep their workforce as healthy and productive as possible. "In-valids" are accepted only for the most menial jobs.

CREDIT: COLUMBIA PICTURES/THE KOBAL COLLECTION

Similarly, some authors assume that the reader is familiar with the film being discussed, while others provide helpful background. Although I had seen many of the films considered, some I had only viewed years earlier and others were unfamiliar—the book contributed several additions to my "must watch" list. Including a short synopsis for each of the focal films would improve future editions. Another addition to the volume that would contribute to the discourse about bioethics and film would be an annotated list of popular films (generally older) that are not treated in the text. This could include movies such as *Awakenings* (which depicts the implications of using experimental treatments), *The Doctor* (the clinician-patient relationship and facing life-threatening illness), *Lorenzo's Oil* (the struggles of parents to gain access to experimental therapies), *On Golden Pond* (struggles in families with aging and dementia), and *One Flew Over the Cuckoo's Nest* (treatment of the mentally ill).

Regardless, *Bioethics at the Movies* should serve as a resource not only for teachers of bioethics courses but also for those engaged in understanding the relationship of the humanities to medicine and to bioethics. In addition, the book may prompt serious discussion of popular films that address complex topics and stories that have bioethical implications.

10.1126/science.1172663

The reviewer is at the Berman Institute of Bioethics and the Department of Medicine, Johns Hopkins University, Baltimore, MD 21205, USA. E-mail: jsugarm1@jhmi.edu

ENERGY

Driving on Biomass

Burning biomass to produce electricity for battery-driven vehicles can power more travel and displace more petroleum than converting it to ethanol or other fermentation products.

John Ohlrogge,[1]* Doug Allen,[1] Bill Berguson,[2] Dean DellaPenna,[3] Yair Shachar-Hill,[1] Sten Stymne[4]

The development of the internal combustion engine (ICE) vehicle dramatically influenced American society during the 20th century by providing affordable, reliable transportation. However, the ICE vehicle is an inherently inefficient converter of chemical energy to mechanical power; less than 20% of the energy in gasoline is transformed into mechanical work, and the remainder is lost as heat. With seemingly unlimited supplies of low-cost petroleum in the last century, the poor efficiency of the ICE was initially less important than the power, convenience, and reliability it provided. However, two major factors make it likely that electric vehicles, rather than the ICE, will be the power source of choice for passenger vehicles in the 21st century. First, heightened world petroleum demand coupled with more expensive oil recovery will continue to increase gasoline costs. Second, concerns over the environmental impact of CO_2 production are leading toward carbon taxes, cap-and-trade limits, and other strategies that will impact the ICE.

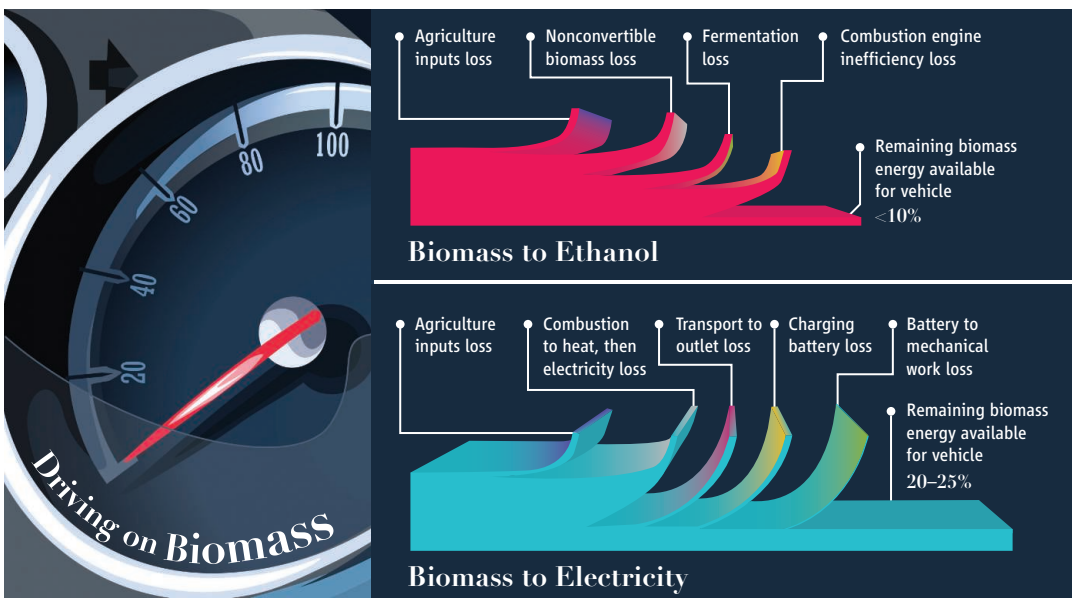

Driving on biomass. Energy losses in conversion of biomass to electricity or to ethanol for automobile propulsion.

In response to escalating monetary and political costs of imported petroleum and the existence of surplus U.S. agricultural capacity in the 20th century, the U.S. government instituted policies to support the conversion of the chemical energy stored in plant-derived starch to ethanol. This conversion now consumes almost 30% of U.S. corn production. Starch is a simple polymer of glucose that is easily converted to ethanol with existing technology, yet almost one-third of the chemical energy of starch is lost in producing ethanol (*1*). Concerns about fuel competing with food, fertilizer runoff, and potent greenhouse gases such as NO_2 released from microbial conversion of fertilizer in agricultural fields have brought into question the sustainability of corn-based ethanol production (*2*). Therefore, a major effort has begun to develop alternative feedstocks for ethanol (or other liquid fuels) by using crop residues, forest by-products, perennial grasses, and other forms of plant biomass that are collectively termed "lignocellulosics." The 2005 "billion-ton vision" (*3*) proposed by the U.S. Departments of Energy (DOE) and Agriculture (USDA) has set a goal of replacing 30% of U.S. petroleum consumption with lignocellulosic-derived liquid fuels—a goal that would require the production of ~60 billion gallons of ethanol annually by 2030. Several billion dollars have been invested for research and development toward this goal, and tax advantages and other subsidies for ethanol and biodiesel production have been estimated at $9 billion for 2008 and could increase to over $30 billion annually under current legislation (*4*).

Unlike starch, lignocellulose is one of the most complex natural heteropolymers, and its conversion to liquid fuels is not yet economically sustainable. Currently, the recovery of fermentable sugars from most lignocellulosics represents <70% of the chemical energy content. About 27% of this chemical energy is then lost during fermentation. Loss of energy as heat in an ICE results in less than 10% of the original energy of lignocellulose available for vehicle propulsion (see figure above). In addition, development of the capacity to produce 60 billion gallons of liquid fuel annually from lignocellulosics will require new and large infrastructures, including facilities for storage and processing of enormous volumes of biomass, as well as for the distribution of ethanol.

Since the introduction of the DOE billion-ton biomass vision, many alternatives have emerged. Among these, improved technologies for electric motor vehicles and diesel engines should provide some of the best strategies to offset petroleum consumption. Burning biomass in power plants to produce electricity for battery-driven vehicles captures more biomass energy and provides more vehicle miles than converting it to ethanol or other fermentation products for ICE vehicles [see report by Campbell *et al.*, (*5*)] (see figure, above).

Although producing electric power directly by burning carbon-based fuels is only 30 to 40% efficient in conventional power plants, comparatively small losses occur between electric generation and vehicle propulsion,

[1]Department of Plant Biology and Great Lakes Bioenergy Research Center, Michigan State University, East Lansing, MI 48824, USA. [2]Forestry Program, Natural Resources Research Institute, University of Minnesota, Duluth, MN 55811, USA. [3]Department of Biochemistry and Molecular Biology, Michigan State University, East Lansing, MI 48824, USA. [4]Department of Plant Breeding and Biotechnology, Swedish University of Agricultural Sciences, Alnarp, Sweden.

*Author for correspondence. E-mail: ohlrogge@msu.edu

Published by AAAS

resulting in conversion of 20 to 25% of the chemical energy of a biofuel stock to vehicle power. Therefore, roughly twice as much petroleum can be displaced by lignocellulosic biomass via electric vehicles as compared with ICE. Furthermore, rather than being lost to the environment as in an ICE, excess heat generated in burning biomass for electricity can be used for heating water and buildings. This allows the overall efficiency of chemical energy conversion to rise to 60% or higher (*6*). Such cogeneration (or combined heat and power plants) generate almost 50% of electric power in Denmark, but less than 10% in the United States.

If biomass is burned for electricity generation rather than conversion to liquid fuels, the "billion-ton vision" of replacing 30% of U.S. petroleum consumption by biomass could be met with a half or less of the land and less infrastructure. In fact, if the ~12 million hectares of farm land now devoted to biofuels are used to produce miscanthus biomass at 20 to 30 tons per hectare (*7*) for electricity generation, the mileage from electric cars would be roughly equivalent to the mileage obtained from a target of 60 billion gallons of renewable fuel by 2030. Thus, in principle, little additional farmland would be needed to meet the petroleum displacement targets of the billion-ton vision.

The widespread use of plug-in electric vehicles will increase electricity consumption. This increased demand can be met from a wide range of carbon-neutral sources, including solar, nuclear, wind, and hydroelectric, as well as biomass, or from coal and natural gas. In the near to midterm, electric vehicles will not require large changes in electrical infrastructure because up to 70 million vehicles can be charged overnight by the existing electrical grid (*8*). By contrast, the infrastructure for fueling this number of cars with 60 billion gallons of ethanol will be much greater.

The large subsidies and tax advantages now and projected for future liquid biofuels might be better directed to support electric vehicle production and to offset the initial high purchase price. In this regard, the Emergency Economic Stabilization Act of 2008 (H.R. 1424) includes up to a $7500 (€5600) tax offset for the purchase of plug-in electric vehicles (*9*).

A primary consumer advantage of electric power for vehicles is the greatly reduced cost of 1 to 3 cents per mile for fuel compared with gasoline cars at 8 to 12 cents per mile (*10*). This leads to savings of up to $10,000 (€7500) per 100,000 miles. Electric vehicles in the past have been substantially limited in range, but recent advances in battery technology and designs with range-extending small gas engines have overcome these limitations, and this technology will continue to improve. In fact, the consensus of the car industry is that electric vehicles will gain substantial market share in the coming years. Most major automotive manufacturers and a number of smaller companies plan to sell plug-in hybrid or all-electric vehicles beginning in 2010 or soon after (*11*). The success of hybrids (>50% average growth per year, 2001–07) (*12*) may be matched or exceeded by electric vehicles and/or plug-in hybrids. By 2030, it is forecast that about one-third of vehicle miles in the United States may be powered by electricity (*8*).

The Future for Diesel

Because of battery weight, electric motors offer the greatest advantage for smaller vehicles. For vans, large sport utility vehicles (SUVs), and light trucks (~50% of U.S. vehicle sales) a transition from gasoline to diesel engines can be expected. Diesel is a better fuel than ethanol or gasoline because of higher energy density and at least 30% higher mileage (*13*). Large trucks, buses, most trains, and other heavy vehicles will continue to use diesel (now 30% of U.S. transportation fuel use). Diesel cars are the major passenger vehicle in much of Europe, and new diesel engines are quiet, have very low emissions, and are nearly indistinguishable from gasoline engines in performance (*13*). The increased fuel efficiency of diesel engines could yield a further 10 to 20% reduction in U.S. petroleum consumption if much of the passenger car, light-truck, and SUV fleet switches from gas to diesel. The higher initial cost of a diesel engine can be offset with tax incentives and fuel cost recoveries.

Future Research

Increasing supplies of biodiesel is one priority for future biofuel research. However, production of biodiesel from temperate oilseed crops can provide only a small part of U.S. transportation needs (*14*). Therefore, non–seed-based production systems, perhaps including algae or thermochemical conversion of biomass, should be developed.

Public funding should support research alternatives that look beyond "lignocellulose fermentation" technology and focus both on increasing biomass yields and the energy density of biomass. Perennial grasses and trees are the most sustainable future sources of biomass. Additional resources devoted to breeding and agronomy for higher biomass per hectare are likely to pay the greatest immediate dividends. Other promising research targets include the following:

Reducing the loss of 20 to 50% of biomass that occurs during senescence or late-season storage in the field. Targets might include engineering crops to retain starch and other carbohydrates that usually break down for translocation to roots and seeds. Increasing the cellulose and/or hemicellulose content will capture carbon in forms that are not remobilized for seed or rhizome storage.

Increasing energy density of biomass. Lignin has 1.7-fold, and oils and isoprenoids have twofold, the energy of a kilogram of cellulose. Increasing these components would increase the energy density of biomass either for burning or for biodiesel production. Reducing leaf loss during senescence could contribute 10% or more to biomass yields and might be achieved by engineering reduced abscission. Reducing water content at harvest by accelerated drying in the field may be achievable owing to recent advances in understanding the control of stoma apertures.

In summary, although there are uncertainties in the pace of electric car development and market penetration, replacement of gasoline by bioelectricity in cars and with diesel engines in heavier vehicles may be the best route to the goal of reducing petroleum consumption and CO_2 emissions.

References

1. G. P. Towler, A. R. Oroskar, S. E. Smith, *Environ. Progr.* **23**, 334 (2004).
2. G. P. Robertson *et al.*, *Science* **322**, 49 (2008).
3. R. D. Perlack *et al.*, *Biomass as Feedstock for a Bioenergy and Bioproduction Industry: The Technical Feasibility of a Billion-Ton Annual Supply* (USDA and DOE, Washington, DC, 2005); www1.eere.energy.gov/biomass/pdfs/final_billionton_vision_report2.pdf
4. D. Koplow, *Biofuels—At What Cost? Government Support for Ethanol and Biodiesel in the United States: 2007 Update* (International Institute of Sustainable Development, Geneva, 2007); www.globalsubsidies.org/files/assets/Brochure_-_US_Update.pdf.
5. J. E. Campbell, D. B. Lobell, C. B. Field, *Science* **324**, 1055 (2009); published online 7 May 2009, 10.1126/science.1168885.
6. A. Franco, N. Giannini, *Int. J. Thermal Sci.* **44**, 163 (2005).
7. E. A. Heaton, F. G. Dohleman, S. P. Long, *Global Change Biol.* **14**, 2000(2008).
8. National Resources Defense Council and Electric Power Research Institute (EPRI), *Environmental Assessment of Plug-In Hybrid Electric Vehicles* (EPRI, Palo Alto, CA, vol. 1, 2007) http://mydocs.epri.com/docs/public/000000000001015325.pdf.
9. Emergency Economic Stabilization Act of 2008, http://thomas.loc.gov/cgi-bin/query/z?c110:H.R.1424.enr:.
10. Comparing vehicle energy costs per mile, http://avt.inl.gov/pdf/fsev/costs.pdf.
11. Hybrid cars, www.hybridcars.com/.
12. Vehicle Technologies Program, DOE, www1.eere.energy.gov/vehiclesandfuels/facts/2008_fotw514.html.
13. Diesel vehicles, DOE, www.fueleconomy.gov/feg/di_diesels.shtml
14. T. P. Durrett, C. Benning, J. Ohlrogge, *Plant J.* **54**, 593 (2008).

10.1126/science.1171740

BIOCHEMISTRY

A Glucose-to-Gene Link

A regulatory loop links glucose metabolism to chromatin alterations and the controlled expression of metabolic genes.

Jeffrey C. Rathmell[1,2,3] and Christopher B. Newgard[1,3]

Eukaryotic cell growth demands an increase in glucose uptake and metabolism to support energetic and biosynthetic needs, accompanied by changes in gene expression that control cell lineage or fate. These gene expression patterns are determined by lineage-specific or differentiation stage–specific transcription factors, as well as by modifications of chromatin (the complex of nucleic acids and proteins that constitute chromosomes) that regulate access of transcription factors to specific DNA loci. On page 1076 of this issue, Wellen *et al.* propose a new mechanism to link glucose metabolism to chromatin modification and global transcriptional control via the enzyme ATP-citrate lyase and production of acetyl–coenzyme A (acetyl-CoA) (*1*).

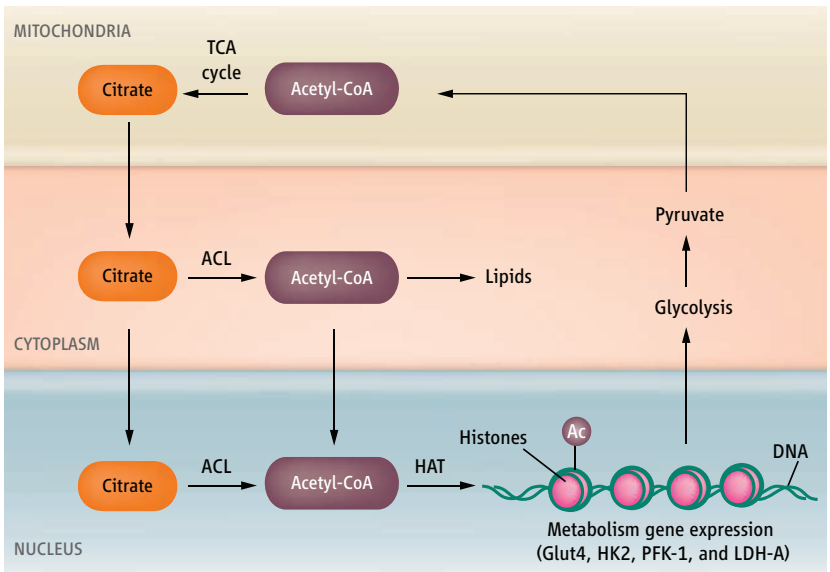

A mitochondria-nucleus circuit. Wellen *et al.* propose that in mammalian cells, adequate glucose leads to increased glycolysis and generation of mitochondrial citrate that is transported to the nucleus or the cytosol. ATP-citrate lyase (ACL) converts citrate to acetyl-CoA. In the nucleus, acetyl-CoA serves as a substrate for histone acetyltransferases (HATs) that modify histones with acetate (Ac) to affect the transcription of key metabolic genes. In the cytosol, acetyl-CoA supports lipid synthesis.

Acetyl-CoA is a key intermediate in three major metabolic pathways (see the figure). As a product of pyruvate dehydrogenase in the mitochondria, it serves as an initiating metabolite of the tricarboxylic acid (TCA) cycle in fed or anabolic states. It is also the end product of the mitochondrial fatty acid β-oxidation pathway, again serving as an important TCA cycle initiator, particularly in fasted or catabolic states. And under glucose-replete conditions, citrate exits the mitochondria to be converted by ATP-citrate lyase to acetyl-CoA for lipid synthesis.

In addition to these roles, acetyl-CoA is the substrate of protein acetylases, including histone acetyltransferases that modify histone proteins and consequently chromatin structure. In yeast, deletion of the gene encoding acetyl-CoA synthetase (Acs2p), which produces acetyl-CoA from acetate, results in defective histone acetylation and altered transcription (*2*). Although mammals express a homolog of Acs2p (AceCS1), it has not been implicated in histone modification. The pool of acetyl-CoA used for histone acetylation and lipid synthesis must originate in the cytoplasm and/or nucleus rather than the mitochondria. Both ATP-citrate lyase and AceCS1 are expressed in the cytoplasm, but only expression of the former is essential to support the synthesis of lipids required for new membrane formation upon growth factor stimulation (*3*–*5*). Indeed, pharmacologic inhibition of ATP-citrate lyase has been proposed to prevent tumor growth (*6*).

Although ATP-citrate lyase deficiency decreases the amount of cellular acetyl-CoA (*6*), the effect of such metabolic limitation on protein acetylation had not been described. Wellen *et al.* show that suppressing ATP-citrate lyase expression (via small interfering RNA) decreased global histone acetylation in several different mammalian cell types. The authors also studied two conditions that induce histone acetylation—serum starvation and re-feeding, which synchronizes cells for entry into the cell division cycle, and differentiation of fibroblast cells into adipocytes. Reducing ATP-citrate lyase expression reduced histone acetylation in both circumstances. Moreover, histone acetylation depended on glucose, with fatty acids unable to substitute, consistent with a requirement for a cytosolic or nuclear (not mitochondrial) pool of acetyl-CoA. The impairment of histone acetylation by reducing ATP-citrate lyase expression was not mimicked by a lack of the acetyl-CoA synthetase Acs2p, but could be rescued by acetate, indicating that Acs2p regulates histone acetylation only when acetate is present, and not when glucose is abundant.

These studies also uncovered an interesting connection between ATP-citrate lyase–mediated acetyl-CoA production and the expression of key genes involved in glucose metabolism (see the figure). Suppressing ATP-citrate lyase in differentiating adipocytes prevented the expression of a major adipocyte glucose transporter, Glut4, as well as glucose-metabolizing enzymes [hexokinase 2 (HK2), phosphofructokinase-1 (PFK-1), and lactate dehydrogenase–A (LDH-A)]. This effect was rescued by treating cells with acetate, thereby implicating acetyl-CoA in this regulatory loop. Moreover, acetylation of histones was reduced at the promoter of the Glut4-encoding gene in adipocytes that lack ATP-citrate lyase. However, these findings do not eliminate a possible role for transcription factors with global control effects on specific metabolic pathways. Indeed, one such factor, ChREBP, was suppressed by the absence of ATP-citrate lyase and restored by acetate, and others may have been similarly affected.

Surprisingly, reducing ATP-citrate lyase influenced acetylation of only a select set of substrates. The reason for this specificity is unclear, but several possibilities exist. Distinct histone acetyltransferases or histone deacetylases could interact with different substrates (*7*) and/or may have different affinities for acetyl-CoA, with those that regulate acetylation being most sensitive to acetyl-CoA limitation. In fact, Wellen *et al.* found that reducing the expression of either ATP-citrate lyase or a specific histone

[1]Department of Pharmacology and Cancer Biology, [2]Department of Immunology, [3]Sarah W. Stedman Nutrition and Metabolism Center, Duke University Medical Center, Durham, NC 27710, USA. E-mail: newga002@mc.duke.edu

Published by AAAS

acetyltransferase (GCN5) suppressed global histone acetylation but not acetylation of tubulin, a cytoskeletal protein that is acetylated by the Elongator histone acetyltransferase complex (*7*). The site of acetyl-CoA generation may also play a role in specificity. Wellen *et al.* show that ATP-citrate lyase is found throughout the cell, including diffuse localization in the cytosol and nucleus. Specific roles of these discrete enzyme pools on histone acetylation remain to be determined.

Wellen *et al.* provide strong evidence in cultured cells that acetyl-CoA derived from glucose and ATP-citrate lyase generates a substrate for chromatin modification and a signal for activating a glycolytic metabolic program. However, its importance for normal physiologic adaptations (such as fasting and refeeding cycles in mammals) is unknown. Fasted mammals spare glucose and rely heavily on fatty acid and amino acid oxidation for energy needs, whereas glucose becomes the predominant fuel metabolite in the fed condition. Does this imply that chromatin remodeling is driven by acetyl-CoA derived from glucose in the fed state, and that this is a key mechanism for initiating glycolytic and lipogenic programs under such conditions? Such questions remain to be answered.

References

1. K. E. Wellen *et al.*, *Science* **324**, 1076 (2009).
2. H. Takahashi, J. M. McCaffery, R. A. Irizarry, J. D. Boeke, *Mol. Cell* **23**, 207 (2006).
3. A. Szutowicz, J. Kwiatkowski, S. Angielski, *Br. J. Cancer* **39**, 681 (1979).
4. J. Turyn *et al.*, *Horm. Metab. Res.* **35**, 565 (2003).
5. D. E. Bauer, G. Hatzivassiliou, F. Zhao, C. Andreadis, C. B. Thompson, *Oncogene* **24**, 6314 (2005).
6. G. Hatzivassiliou *et al.*, *Cancer Cell* **8**, 311 (2005).
7. C. Creppe *et al.*, *Cell* **136**, 551 (2009).

10.1126/science.1174665

PHYSICS

A Sound (and Light) Way to Measure Confined Electrons

A technique that uses the wavelength of sound and the energy of light can probe the elusive properties of electrons in quantum Hall states.

Steven H. Simon

The conservation of momentum and energy underlies many powerful spectroscopic techniques. Absorption spectroscopy is based on the principle that a wave incident on an object can only be absorbed if both its momentum and energy match that of an excitation mode of the object. On page 1044 of this issue, Kukushkin *et al.* (*1*) describe a variant of this technique for measuring the energy and momentum dependence of the excitations of a two-dimensional (2D) electron system. In this technique, momentum is imparted with sound and, separately, energy is imparted with light. This approach allows the spectrum of "magnetorotons"—characteristic excitations of the states associated with the fractional quantum Hall effect—to be measured directly. The observed spectral features were predicted many years ago (*2*–*4*) but have eluded direct measurement until now.

The excitations of a state of matter define many of its most important properties. For example, the remarkable properties of superfluid helium-4 reflect the fact that this substance has only a single excitation mode with both low energy and low momentum—a sound wave. Landau was able to describe many of the superfluid's properties using only this sound mode and a roton mode (another low-energy excitation with higher momentum). The predicted roton was later observed in neutron-scattering experiments and explained in a detailed theory by Feynman (*5*).

Rudolf Peierls Centre for Theoretical Physics, University of Oxford, Oxford OX1 3NP, UK. E-mail: s.simon1@physics.ox.ac.uk

In high magnetic fields, 2D electron systems can condense at low temperatures into quantum Hall states of matter that share many properties with other superfluids, including being able to flow with no dissipation. In 1986, a generalization of the Feynman theory (*2*) showed that certain quantum Hall states should have an analogous low-energy mode, dubbed the "magnetoroton." Later, magnetorotons were explained as an orbiting motion of composite-fermion quasiparticles (*4*), which can be thought of roughly as an electron bound to quanta of magnetic flux. Such magnetorotons were predicted to be excitations of almost every known quantum Hall state.

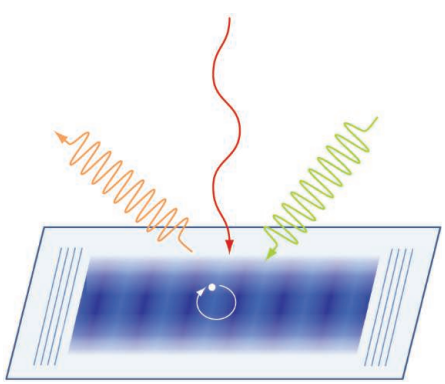

Sounding out excitations. Sound waves (blue) from transducers impart a grating on the surface of the sample. Microwaves (red) excite magnetorotons, shown as a composite fermion particle making orbits. A visible light signal (green) is imparted on the sample and the spectrum of emitted light (orange) is measured to determine how much energy has been absorbed.

Direct observation of these magnetorotons has, however, been quite a challenge. The sample size is small: The experiment must detect excitations of only 10^{11} electrons per square centimeter within the 2D layer, but filter out the 10^{23} atoms per cubic centimeter in the surrounding material. Furthermore, the active 2D electron layer is buried deep within a bulk semiconductor crystal, making it inaccessible to many probes. Neutrons, x-rays, alpha particles, and many other probes are essentially useless, leaving light and sound as the only feasible options. However, the use of light or sound still faces a major difficulty that arises from the relation between energy E and momentum p for these waves: $E = vp$, where v is the wave velocity. Because the speed of light is very high and that of sound is very low, neither provides a good match for both the energy and momentum of the magnetoroton. Although both light and sound scattering experiments have been quite informative in the past (*6*, *7*), experiments that vary energy and momentum independently have been limited to a small range of very low momenta (*8*).

The approach taken by Kukushkin *et al.* uses sound and light simultaneously to take a much more complete snapshot of the excitation spectrum, including the magnetoroton, over a broad range of energies and momenta. This scheme imposes a wavelength λ on the sample by setting up standing sound waves within a cavity, where in quantum mechanics wavelength is related to momentum via $p = h/\lambda$, where h is Planck's constant. Energy is then imparted with microwave photons. The idea is

that when the energy of the light and the wavelength of the sound match that of an excitation of the system, energy is absorbed. To detect this absorption, the authors monitor heating of the sample by looking at photoluminescence; they fire higher-energy photons at the sample and observe the spectrum of photons emitted.

One slight puzzle in the results of this technique relates to energy and momentum conservation. If the system absorbs the momentum of a sound wave, it should also absorb its energy. However, in the experiment, this does not seem to be happening. Nonetheless, cross-checks on the experiment make a compelling case that the experiment does indeed measure excitations with the momentum of the sound and the energy of only the microwave.

The technique of using both light and sound seems sufficiently powerful that it should be extremely useful for measuring low-energy excitations of a wide variety of 2D electron systems, and maybe even for 3D systems. At this point, Kukushkin *et al.* can declare victory that the magnetoroton spectrum has finally been measured; with luck, this is only the first of many such victories.

References

1. I. V. Kukushkin, J. H. Smet, V. W. Scarola, V. Umansky, K. von Klitzing, *Science* **324**, 1044 (2009); published online 30 April 2009 (10.1126/science.1171472).
2. S. M. Girvin *et al.*, *Phys. Rev. B* **33**, 2481 (1986).
3. R. E. Prange, S. M. Girvin, Eds., *The Quantum Hall Effect* (Springer-Verlag, New York, ed. 2, 1990).
4. O. Heinonen, Ed., *Composite Fermions: A Unified View of the Quantum Hall Regime* (World Scientific, Singapore, 1998).
5. P. Nozieres, D. Pines, *Theory of Quantum Liquids* (Addison-Wesley, New York, 1990), vol. 2.
6. J. G. Groshaus *et al.*, *Phys. Rev. Lett.* **100**, 046804 (2008).
7. R. L. Willett *et al.*, *Phys. Rev. B* **47**, 7344 (1993).
8. M. Eriksson *et al.*, *Phys. Rev. Lett.* **82**, 2163 (1999).

10.1126/science.1173828

EPIDEMIOLOGY

Phone Infections

Is a mobile phone virus epidemic on the horizon?

Shlomo Havlin

In 1854, John Snow identified a water pump as the source of the cholera outbreak affecting the Soho district of London. This transformed the British physician into a public health giant, whose story is still celebrated in medical and public health history books. The weapon in his fight against cholera was a map of London on which he marked the residence of the individuals that had been infected by the disease. This enabled him to identify the Broad Street pump as the outbreak's source, allowing him to stop cholera proliferation in London. Snow understood the spontaneous nature of epidemics and is regarded as a founder of modern epidemiology (*1*). Following in his footsteps, we understand today that the spread of infectious diseases follows reproducible patterns, whether they occur in the narrow streets of 19th-century London or along the digital highways of the 21st century. This is because diseases spread via networks of connections among individuals. On page 1071 of this issue, Wang *et al*. analyze the temporal and spatial spreading patterns of a new kind of virus—one that can spread through mobile phone networks (*2*).

Why, despite the more than 400 mobile phone viruses documented by cybersecurity organizations, is there no apparent serious concern about the prospect of viruses infecting mobile phones? By combining network science and percolation theory, Wang *et al*. examined mobility and communications data on the activity of more than 6 million individuals to study the speed and breadth of potential mobile phone virus outbreaks. Their conclusion is rather unexpected: Although mobile phone viruses do not pose a threat of spreading right now, the increasing market share of smartphones—mobile phones with computer-like operating systems and advanced features (such as electronic mail and Internet access)—will soon reach a phase transition point, beyond which mobile viruses could become far more damaging and widespread than current computer viruses (see the figure).

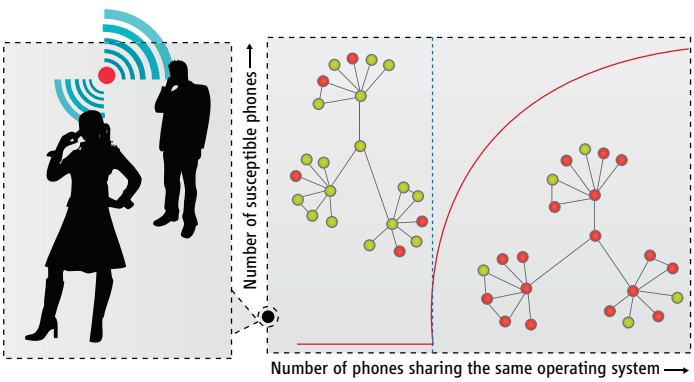

Epidemics to come. Currently, very few smartphones are susceptible to a virus (red circles; nonsusceptible phones, green circles), a number that is below the threshold of transition to an epidemic (vertical blue line). In future epidemics, as the number of smartphones increases, the market share of a single operating system will reach a critical threshold and facilitate virus spread, potentially leading to a pandemic.

Mobile viruses are of two main types, Bluetooth and Multimedia Messaging Service (MMS), based on the communication protocol they exploit. Bluetooth is a short-range communication protocol that can transmit data between mobile phones within a 10- to 30-m radius. Thus, Bluetooth viruses spread among individuals like influenza virus, infecting only nearby Bluetooth-enabled phones. In contrast, MMS is a messaging protocol that allows sharing of media and programs between mobile phones within minutes and across the world. Thus, an MMS virus can send a copy of itself in a short time frame to all the phone numbers found in a phone's address book, resulting in a long-range spreading pattern that previously was common only in computer viruses.

Wang *et al*. discovered major differences in the speed and in the spreading patterns between Bluetooth and MMS virus outbreaks. The spread of Bluetooth viruses is relatively slow, as it is driven by human mobility (*3*, *4*) and will take days or weeks to reach a large fraction of mobile phone users. During this time frame, "infected" phones can be easily filtered out of that part of the network provided by mobile phone services that support Bluetooth technology.

The real danger is posed by MMS viruses (*5*, *6*), whose spread is almost instantaneous. Wang *et al*. show that although MMS viruses can be transmitted quite rapidly, currently their spread is limited to small clusters of mobile phones due to the fragmentation of the underlying social networks (see the figure). This containment is due to different operating systems that various phones use.

Indeed, if all mobile phones had the same operating system, an MMS virus could instantaneously reach a large fraction of phone users. In reality, there are several competing operating systems in the mobile phone market, so the social network is separated into clusters of users with phones that use the same operating system, but who do not communicate with users in other

Physics Department, Bar-Ilan University, Ramat-Gan, 52900 Israel. E-mail: havlin@ophir.ph.biu.ac.il

CREDIT: N. KEVITYAGALA/*SCIENCE*

clusters whose phones have a different operating system. As more and more users start using similar phones and operating systems, the size of these clusters will increase. Percolation theory predicts that once the market share of any operating system reaches a critical threshold, the system undergoes a phase transition and most of the isolated clusters will merge into a single large cluster containing a substantial fraction of mobile phone users. At that point, an MMS virus will be able to instantaneously reach most mobile phone users, and consequently, we'll become seriously concerned about mobile phone viruses. Wang *et al*. also show that this transition point can be accurately predicted by percolation theory (*7*). This transition also explains the relative absence of MMS mobile phone virus outbreaks: Currently, we are below the critical threshold, as smartphones still have a small market share, which is further fragmented by the large number of different operating systems competing in the market.

Yet, consolidation of the mobile phone industry is unavoidable, which means that the phase-transition threshold will be inevitably reached in the near future. Exactly when that happens depends less on network science than on market forces, i.e., the rate at which individuals switch to smartphones. However, some estimates indicate that within 2 to 3 years, there will be more smartphones than desktop computers. Thus, now is the time to start preparing the theoretical knowledge and tools to deal with this expected major threat to mobile communications.

References

1. S. Hempel, *The Strange Case of the Broad Street Pump: John Snow and the Mystery of Cholera* (Univ. of California Press, Berkley, CA, 2007).
2. P. Wang, M. C. González, C. A. Hidalgo, A.-L. Barabási, *Science* **324**, 1071 (2009); published online 2 April 2009 (10.1126/science.1167053).
3. M. C. González, C. A. Hidalgo, A.-L. Barabási, *Nature* **453**, 779 (2008).
4. R. Lambiotte *et al*., *Physica* A **387**, 5317 (2008).
5. C. A. Hidalgo, C. Rodriguez-Sickert, *Physica* A **387**, 3017 (2008).
6. J.-P. Onnela *et al*., *Proc. Natl. Acad. Sci.* **104**, 7332 (2007).
7. R. Cohen, K. Erez, D. ben-Avraham, S. Havlin, *Phys. Rev. Lett*. **85**, 4626 (2000).

10.1126/science.1174658

AGRICULTURE

The Rubber Juggernaut

The demise of swidden cultivation in Southeast Asia may have devastating environmental consequences.

Alan D. Ziegler,[1] Jefferson M. Fox,[2] Jianchu Xu[3]

Rubber plantations are expanding rapidly throughout montane mainland Southeast Asia (*1*–*3*). More than 500,000 ha may have been converted already in the uplands of China, Laos, Thailand, Vietnam, Cambodia, and Myanmar (see the figure, panel A). By 2050, the area of land dedicated to rubber and other diversified farming systems could more than double or triple, largely by replacing lands now occupied by evergreen broadleaf trees and swidden-related secondary vegetation (*2*). What are the environmental consequences of this conversion of vast landscapes to rubber?

Swidden versus rubber. (**A**) Montane mainland Southeast Asia (green shaded areas) is defined here as the lands between 300 and 3000 m above sea level. (**B**) Most swidden fields and fallows on slopes near villages and roads in this area in Xishuangbanna have been converted to terraced rubber stands.

The conversion of both primary and secondary forests to rubber threatens biodiversity and may result in reduced total carbon biomass (*3*–*5*). Negative hydrological consequences are also of concern—for example, in the Xishuangbanna prefecture of Yunnan province, China—but current data are too sparse to quantify the extent of the impacts (*3*, *6*). The effect of conversion to rubber on catchment or regional hydrology depends, in part, on the water use of rubber versus that of the original displaced vegetation. Another factor is the degree to which rainwater infiltration is reduced when terraces are constructed on sloping lands (see the figure, panel B). Unfortunately, a recent investigation into this issue in Xishuangbanna was terminated by regional authorities before sufficient data were collected (*6*, *7*).

The rapid emergence of rubber is the hallmark of a larger land-cover transition that has been sweeping through montane mainland Southeast Asia in recent decades: the demise of swidden cultivation (also referred to as shifting or slash-and-burn cultivation) (*8*). Much of the upland areas that have been converted to rubber in the region are historically associated with swidden cultivation. Clinging to the perception that swidden cultivation is a destructive system that leads only to forest loss and degradation, governments in Southeast Asia have tried to control or terminate it through bans, declaration of forest reserves, forced resettlement, monetary incentives, and crop substitution programs (*9*, *10*). The uncontrolled expansion of rubber in China was encouraged in part because it was seen as a favorable alternative to swiddening. Policies such as the Sloping Land Conversion Program supported the planting of rubber, because it counts as reforestation. Yet such policies have not always improved environmental conditions. In the case of rubber, homogeneous monocultures with myriad negative environmental consequences have emerged. This situation is not new or isolated. The permanent loss of forest cover through agrarian conversion to oil palm in insular Southeast Asia provides a parallel (*11*, *12*).

[1]Department of Geography, National University of Singapore, Singapore 117570. [2]East-West Center, Honolulu, HI 96848, USA. [3]World Agroforestry Centre, Kunming Institute of Botany, China. E-mail: adz@nus.edu.sg

In retrospect, it has become clear that the environmental impacts of traditional swidden-ing were inconsequential until mountain populations increased, cropping periods lengthened, fallow periods became shorter, and the cultivation of opium as a cash crop proliferated after the Second World War. Recent intensification of permanent agriculture has had numerous negative environmental consequences: Erosion has accelerated and stream sediment loads have increased where repetitive cultivation is performed on steep slopes without appropriate conservation methods; permanent conversion of hill slopes and road building have increased the risk of landslides; irrigation of cash crops in the dry season has desiccated streams; and use of pesticides and fertilizers to sustain commercial agriculture has reduced water quality (*13*–*15*).

The unrestricted expansion of rubber in montane mainland Southeast Asia could have devastating environmental effects. A reliable assessment of the hydrological threat requires new data, but time is too short to wait for results from future catchment monitoring programs aimed at quantifying changes in streamflow variables caused by rapid land-cover conversion to rubber. Therefore, studies of rubber evapotranspiration and water use, such as those currently being conducted in Thailand, Cambodia, and Laos, are becoming increasingly important. A substantial increase in natural reserve areas could help to reduce the threats to biodiversity and carbon stocks. Another possible strategy involves paying upland farmers to preserve forest resources. A more realistic approach may be to promote diversified agroforestry systems in which cash crops such as rubber and oil palm play important roles, but are not planted as monocultures.

References and Notes

1. V. Manivong, R. A. Cramb, *Agroforest Syst.* **74**, 113 (2008).
2. J. M. Fox *et al.* (East-West Center, HI, 2009); see www.eastwestcenter.org/fileadmin/stored/pics/CLUEFinal.pdf.
3. J. Qiu, *Nature* **457**, 246 (2009).
4. H. M. Li *et al.*, *Biodivers. Conserv*. **16**, 1731 (2007).
5. H. M. Li *et al.*, *Forest Ecol. Manage*. **225**, 16 (2008).
6. M. T. Guardiola-Claramonte *et al.*, *Ecohydrology* **1**, 13 (2008).
7. D. Cryanoski, *Nature* **251**, 871 (2008).
8. C. Padoch *et al.*, *Geogr. Tidsskr. Dan. J. Geog.* **107**, 29 (2007).
9. J. Fox *et al.*, *BioScience* **50**, 521 (2000).
10. D. J. Schmidt-Vogt, *Trop. Forest Sci.* **13**, 748 (2001).
11. J. McMorrow, M. A. Talip. *Global Environ. Change* **11**, 217 (2001).
12. L. P. Koh, D. S. Wilcove, *Nature* **448**, 993 (2007).
13. R. C. Sidle *et al.*, *Forest Ecol. Manage*. **224**, 199 (2006).
14. T. Forsyth, A. Walker, *Forest Guardians*, *Forest Destroyers* (Univ. of Washington Press, Seattle, WA, 2008).
15. I. Douglas, *Geog. Res.* **44**, 123 (2006).
16. This work was supported by NASA grants NNG04GH59G and NNX08AL90G and by APN grant ARCP2006-0GNMY. We acknowledge the contributions of M. Guardiola-Claramonte, T. W. Giambelluca, J. B. Vogler, P. Troch, and J. Sturgeon.

10.1126/science.1173833

GEOPHYSICS

Deep Tremors and Slow Quakes

Detection and monitoring of slow earthquakes may provide a better understanding of ordinary earthquakes.

Gregory C. Beroza[1] and Satoshi Ide[2]

The past decade has witnessed the discovery of a family of unusual earthquakes in what might be termed the infrared part of the seismic spectrum. They are characterized by weak, if any, wave excitation at high frequencies because they happen more slowly than do ordinary, fast earthquakes. The expectation is that these slow earthquakes may provide a better understanding of regular earthquakes, but we are still in the early stages of understanding them.

Slow earthquakes go by a variety of names depending on their magnitude and duration: low-frequency earthquakes with durations of <1 s (*1*), very-low-frequency earthquakes lasting about 20 s (*2*), and slow-slip events that continue for days to months (*3*). Slow earthquakes are frequently accompanied by deep tremor (*4*), which itself appears to be a swarm of low-frequency earthquakes (*5*). To the extent that we have been able to discern their mechanism, slow earthquakes occur as shear slip events of tectonic plates, just like ordinary earthquakes (*2*, *3*, *6*). Although slow earthquakes are located on the same faults that host ordinary, fast earthquakes, they differ in several important respects. They grow steadily, rather than explosively, with time (*7*), and their stress drops are low (*8*).

We'd like to know what relation slow earthquakes have with ordinary earthquakes. Their location on the deep extension of major faults means that they will increase the shear stress on the dangerous shallower stretches of these faults (see the figure). It is therefore important to know whether slow earthquakes cause an increase in the likelihood of an adjacent large earthquake. Slow slip has triggered small nearby earthquakes in several instances (*9*, *10*). However, there have been many well-documented episodes of slow slip in Cascadia, Japan, Mexico, Alaska, and Costa Rica, none of which have been accompanied by a large earthquake. Strong triggering of tremor by lunar tides indicates that tremor can be sensitive to small variations in stress. It is reasonable, then, to speculate that tremor behavior might vary along with variations in stress during the seismic cycle between large earthquakes in subduction zones. Slow slip might even play a role in a slow nucleation process leading to a large earthquake, but that notion remains conjectural.

Tremor can be triggered by waves from distant earthquakes. Most areas that are known to experience tremor in California are of this type (*11*). One location south of Parkfield also has tremor that occurs spontaneously, without being set off by seismic waves, but what about the areas of triggered tremor? Triggered tremor appears to have much in common with spontaneous tremor, but the relation to slow slip is not clear. Does triggered tremor, like spontaneous tremor, occur by shear slip on the deep extension of faults, or is some other mechanism involved? Finding better locations for triggered tremor will be an important first step in addressing this question. Location of tremors near Cholame place them on the deep extension of the San Andreas Fault (*12*).

We would like to understand the distribution and characteristics of tremor and slow earthquakes more generally. In a few areas, such as Japan and western North America, monitoring can detect tremor and slow slip, but in most areas of the world, seismic stations are too widely separated to detect it. Does tremor occur only in tectonically active areas? Even where tremor and slow slip are known to occur, there are mysteries in its distribution. Slow slip is colocated with tremor in Cascadia (*13*) and Japan (*14*), but the overlap may only be partial in Mexico (*15*), and no tremor at all is observed during slow slip in New Zealand (*16*). Spontaneous tremor is seen under part of the San Andreas Fault but not in other subduction zones. Triggered

[1]Department of Geophysics, Stanford University, Stanford, CA 94305, USA. [2]Department of Earth and Planetary Science, University of Tokyo, Tokyo 113-0033, Japan. E-mail: beroza@stanford.edu

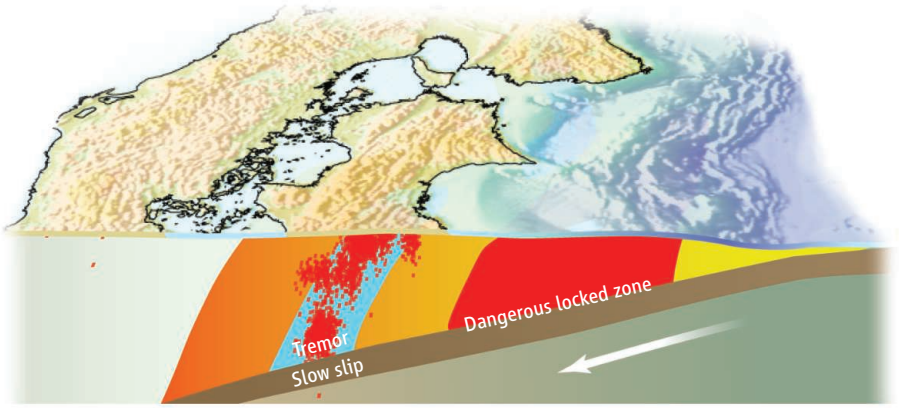

At fault. Perspective view of subduction of the Philippine Sea Plate under southwest Japan. Blue zone with red dots shows the location tremor and slow earthquakes under Shikoku; shallower orange area is the dangerous, locked zone that last ruptured in two large earthquakes in 1944 and 1946.

tremor in California occurs under some faults but not others.

Given the variable seismic network coverage in these areas, and the fact that tremor occurs near the detection threshold of seismic networks, we have to check carefully whether the absence of tremor in some areas is simply due to the inability of existing monitoring networks to detect it. The same is true for slow slip: Most slow-slip events in Cascadia and Mexico are large enough to be detectable by Global Positioning System, whereas in Japan the smaller observed slow-slip events are only visible on more sensitive tiltmeters and strainmeters, which suggests a detectability problem. Nevertheless, it seems clear that there are strong variations in the distribution of tremor and slow slip in areas of similar tectonics. What causes these variations?

Finally, there is the central question of why slow earthquakes are slow. Ordinary earthquakes grow at a large fraction of the medium velocity because stresses transmitted by seismic waves efficiently promote failure in the direction of propagation. This failure mechanism is common from the laboratory scale to the scale of the largest earthquakes. But slow earthquakes clearly have something else going on.

Tremor and slow slip occur on parts of faults where the behavior is transitional between fast, brittle rupture and slow, steady deformation. Depth-dependent friction laws can model repeated deep slow earthquakes to some extent (*17*). Moreover, tremor can migrate fairly rapidly, but not as fast as ordinary earthquakes. How can it be that so many small, slow earthquakes should be starting and stopping in quick succession?

Simple friction laws by themselves do not provide an explanation for this complex behavior. Petrology and seismic tomography both suggest a role for pore fluids in tremor, but exactly what that role is has yet to be worked out. Much remains unclear, but one thing is clear: A better understanding of slow earthquakes has the potential to fundamentally change our understanding of the earthquake process.

References and Notes

1. A. Katsumata, N. Kamaya, *Geophys. Res. Lett.* **30**, 1020 (2003).
2. Y. Ito, K. Obara, K. Shiomi, S. Sekine, H. Hirose, *Science* **315**, 503 (2007); published online 29 November 2006 (10.1126/science.1134454).
3. H. Dragert, K. Wang, T. S. James, *Science* **292**, 1525 (2001); published online 19 April 2001 (10.1126/science.1060152).
4. K. Obara, *Science* **296**, 1679 (2002).
5. D. R. Shelly, G. C. Beroza, S. Ide, *Nature* **446**, 305 (2007).
6. S. Ide, D. R. Shelly, G. C. Beroza, *Geophys. Res. Lett.* **34**, L03308 (2007).
7. S. Ide, G. C. Beroza, D. R. Shelly, T. Uchide, *Nature* **447**, 76 (2007).
8. E. E. Brodsky, J. Mori, *Geophys. Res. Lett.* **34**, L16309 (2007).
9. P. Segall, E. K. Desmarais, D. Shelly, A. Miklius, P. Cervelli, *Nature* **442**, 71 (2006).
10. Y. Liu, J. R. Rice, K. M. Larson, *Earth Planet. Sci. Lett.* **262**, 493 (2007).
11. J. Gomberg *et al.*, *Science* **319**, 173 (2008); published online 21 November 2007 (10.1126/science.1149164).
12. D. R. Shelly *et al.*, *Geophys. Res. Lett.* **36**, L01303 (2009).
13. G. Rogers, H. Dragert, *Science* **300**, 1942 (2003); published online 8 May 2003 (10.1126/science.1084783).
14. K. Obara, H. Hirose, F. Yamamizu, K. Kasahara, *Geophys. Res. Lett.* **31**, L23602 (2004).
15. J. S. Payero *et al.*, *Geophys. Res. Lett.* **35**, L07305 (2008).
16. R. McCaffrey, L. M. Wallace, J. Beavan, *Nat. Geosci.* **1**, 316 (2008).
17. B. Shibazaki, T. Shimamoto, *Geophys. J. Int.* **171**, 191 (2007).
18. Supported by NSF grant EAR-0409917 and a grant-in-aid for scientific research from the Ministry of Education, Sports, Science and Technology, Japan.

10.1126/science.1171231

GEOPHYSICS

Earth Vibrations

Seismic "noise" can be used to monitor climate change effects, locate storms, and elucidate the structure of Earth's crust.

Peter D. Bromirski

Scripps Institution of Oceanography, University of California, San Diego, La Jolla, CA 92093–0209. E-mail: pbromirski@ucsd.edu

Intense cyclonic storm systems generate strong ocean-surface winds that transfer atmospheric energy into ocean gravity waves. Some of the ocean wave energy couples to the solid earth, causing what seismologists have long considered as ambient "noise," because it interferes with the study of earthquake signals measured by seismometers. However, rising ambient noise levels imply increasing oceanic storminess (*1*), which is linked to climate change. In this context, the roles are reversed, with earthquakes being the noise that needs to be excluded from the climate-related signals. Studies of long-term seismic records suggest that wave-generated ambient noise is increasing globally (*2*).

Historic paper seismograms produced by classic drum recording systems have been archived at select locations since about 1930. Treasure troves of these archived seismograms are now being tapped for climate change information. The length of these seismic records and the stability of the recording platforms are advantages over many climate-related records, which often have large gaps and changes in measurement methodologies that make reliable long-term trend assessment difficult.

At periods shorter than 30 seconds, the ambient noise spectrum is dominated by microseism energy (see the figure). Microseisms are generated by two mechanisms. Single-frequency (SF) microseisms, observed at the period of the forcing waves, are generated only in shallow coastal waters by direct

pressure fluctuations on the ocean bottom from shoaling and/or breaking waves (*3*). The dominant double-frequency (DF) peak, observed at half the period of the ocean waves, results from the nonlinear interaction of waves traveling in nearly opposite directions (*4*). This "wave-wave" mechanism generates a pressure pulse that propagates nearly unattenuated to the sea floor, where it is transformed mainly into seismic Rayleigh waves that can propagate long distances.

High-amplitude DF microseisms observed by seismometers on the sea floor in the deep ocean are caused by wave activity under nearby storms (*5*); these microseism signals should be observable on land. However, even extreme storms approaching the coast generate microseisms that are detected on land only when their waves reach nearshore locations (*1*, *6*, *7*), where shore-reflected/scattered waves provide opposing wave components at swell periods (*6*). To date, there is no unambiguous evidence that deep-ocean-generated microseisms are observed on land.

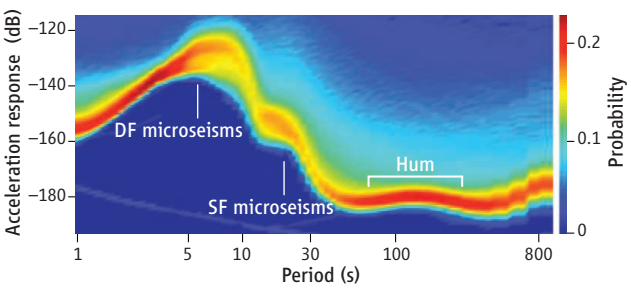

Distribution of seismic noise energy. The data, obtained at a "quiet" seismic station (TUC in Tucson, Arizona) between 6 November 1998 and 30 December 2008, show the observed range of variability over the 10-year record for the DF and SF microseisms and for the hum band (*21*). The highest probability obtained means that these levels were observed >20% of the time at this inland location, an indication of the persistence and ubiquitous nature of wave-generated signals.

The ubiquitous microseism vibrations are sensed at seismic stations globally, even deep in continental interiors (*1*, *8*). Their integrative quality allows assessment of trends in coastal wave activity at regional and global spatial scales using the global seismic network (GSN). The close relationship between near-coastal measurements of DF microseisms and the nearby wave climate allows an accurate estimate of historical near-coastal wave variability from archived seismograms (*9*), important for investigating changes in storm wave frequency, intensity, and duration associated with climate change. Upward trends in the number of strong microseism events indicate that coastal wave intensity is increasing globally (*2*).

Microseism measurements may also have other uses beyond climate studies. Because microseisms are generated continuously at multiple source areas along coastlines, compared with infrequent earthquake signals arriving along single azimuths, they provide useful signals for seismic array tomography (*10*) to probe the structure of Earth's crust. Storm tracking using microseism noise is also getting renewed interest. In addition to generating Rayleigh waves, a portion of the DF microseism pressure pulse produced under storms is converted at the ocean bottom to seismic *P* waves that can be observed by land-based seismic arrays, allowing the locations of storms to be determined (*11*).

Microseisms should not be confused with Earth's "hum," a term referring to bell-like ringing associated with the fundamental resonant spheroidal oscillations of Earth (*12*) at periods between 1 and 8 minutes (see the figure). Initially it was thought that hum was forced by direct coupling of atmospheric pressure fluctuations to the solid Earth (*12*), but recent studies favor hum excitation by ocean infragravity (IG) waves (*13*–*16*). A portion of ocean swell that reaches coastlines is transformed into much longer period (>50 second) IG waves (*17*), partly through the same wave-wave mechanism that produces DF microseisms. IG-wave amplitudes depend on swell amplitudes impacting coasts, which in turn depend on climate factors affecting storm track and storm intensity. Consequently, the locations of dominant hum excitation and hum levels, both seasonally and longer term, are climate-related.

Early analyses suggested that hum modes are excited by IG waves in the deep ocean (*13*). However, because IG-wave amplitudes are much higher over the shelf than the deep ocean, shallow continental shelf waters are more likely to be the dominant source regions (*15*, *16*). Hum modulation has been associated with changing source regions as storm waves arrive at different coastal locations (*18*), locally generating IG waves. Whether low-amplitude background hum levels are excited by IG waves over the deep ocean remains uncertain. Newly available USArray (*19*) data, which provide an unprecedentedly dense large-aperture network of broadband seismic stations, may help to identify the dominant hum source regions.

Recent analysis of horizontal motions recorded by seismometers suggests the existence of "toroidal" hum modes (*20*). The cause of these modes is unknown, but Kurrle and Widmer-Schnidrig (*20*) suggest that the horizontal forces needed to excite these modes may result from coupled wind energy along mountain range fronts or long period ocean waves impacting steep oceanic topographic features such as island chains or continental shelves. Alternatively, the toroidal modes may be a consequence of the wave-wave hum forcing mechanism. The USArray data may also advance our understanding of toroidal hum sources and their characteristics.

The direct association of storm-driven ocean waves with microseisms and hum shows that the solid Earth is not independent of the global "climate system." Microseisms and nonearthquake hum levels are regional and/or global integrators of storm intensity that complement near-coastal oceanographic observations. As rising sea levels allow more wave energy to reach farther shoreward, changes in microseism and hum levels could provide a useful proxy for wave energy reaching coasts.

References and Notes

1. P. D. Bromirski, *Geochem. Geophys. Geosys.* **2**, 2000GC000119 (2001).
2. D. McNamara, R. Aster, P. D. Bromirski, C. Hutt, L. Gee, *Eos Trans. AGU*, **88**(52), fall meet. suppl., abstract S11D-05 (2007).
3. K. Hasselmann, *Rev. Geophys.* **1**, 177 (1963).
4. M. S. Longuet-Higgins, *Phil. Trans. R. Soc. A* **243**, 1 (1950).
5. P. D. Bromirski, F. K. Duennebier, R. A. Stephen, *Geochem. Geophys. Geosyst.* **6**, Q04009, 10.1029/2004GC000768 (2005).
6. P. D. Bromirski, F. Duennebier, *J. Geophys. Res. B* **107**, 10.1029/2001JB000265 (2002).
7. P. Gerstoft, T. Tanimoto, *Geophys. Res. Lett.* **34**, L20304, 10.1029/2007GL031091 (2007).
8. R. Aster, D. McNamara, P. D. Bromirski, L. Gee, C. Hutt, *Seismol. Res. Lett.* **79**, 194 (2008).
9. P. D. Bromirski, R.E. Flick, N. Graham, *J. Geophys. Res. Oceans* **104**, 20753 (1999).
10. N. M. Shapiro, M. Campillo, L. Stehly, M. H. Ritzwoller, *Science* **307**, 1615 (2005).
11. P. Gerstoft, P. M. Shearer, N. Harmon, J. Zhang, *Geophys. Res. Lett.* **35**, L23306, 10.1029/2008GL036111 (2008).
12. K. Nishida, N. Kobayashi, Y. Fukao, *Science* **287**, 2244 (2000).
13. J. Rhie, B. Romanowicz, *Nature* **431**, 552 (2004).
14. T. Tanimoto, *Geophys. J. Int.* **160**, 276 (2005).
15. S. C. Webb, *Nature* **445**, 754 (2007).
16. S. Webb, *Geophys. J. Int.* **174**, 10.1111/j.1365-246X.2008.03801.x (2008).
17. T. H. C. Herbers, S. Elgar, R. T. Guza, *J. Geophys. Res. Oceans* **100** (C12), 24863 (1995).
18. J. Rhie, B. Romanowicz, *Geochem. Geophys. Geosyst.* **7**, 10:1029/2006GC001274 (2006).
19. USArray (www.iris.edu/USArray) is one of the components of the EarthScope (www.earthscope.org) initiative in the United States.
20. D. Kurrle, R. Widmer-Schnidrig, *Geophys. Res. Lett.* **35**, 10.1029/2007GL033125 (2008).
21. D. McNamara, R. Buland, *Bull. Seis. Soc. Am.* **94**, 1517 (2004).

10.1126/science.1171839

RETROSPECTIVE

John Maddox (1925–2009)

An unorthodox editor with a love of ideas enlivened science and single-handedly shook up the world of scientific publishing.

Nicholas Wade

Scientific ideas are exciting, yet the scientific literature is far from lively. John Maddox's achievement was to sidestep the drabness of scientific writing by emphasizing the ideas that thrived beneath the leaden prose. In doing so he made *Nature* a compellingly interesting journal whose success forced others in the staid world of scientific publishing to adopt many of his ideas.

Though trained as a physical chemist, Maddox was a journalist at heart, having spent his formative early career as a science writer for the *Manchester Guardian*. On becoming editor of *Nature* in 1966, he recognized that the dry format of the scientific article could not be greatly changed but that the excitement of scientific ideas could be conveyed by other kinds of articles. Maddox expanded the News and Views section of *Nature* into a lively commentary on the scientific issues of the day.

Long is the list of original ideas that have been rejected by *Nature* or *Science* but later proved correct. My guess is that far fewer of these mistaken rejections occurred while Maddox was editor. He loved new ideas and was always ready to take a chance on a bold paper.

His other great virtue as an editor was that he thought like a publisher. Instead of waiting for interesting papers to come in, he went around asking for them, and people responded to his enthusiasm. The more visible *Nature* became under its unorthodox new editor, the more its prestige and circulation grew, especially in the United States.

Maddox's many talents were alloyed with limitations that diminished what he might otherwise have achieved. Although he was a wonderful conversationalist, there was a certain coldness in his attitude toward others. He trusted only his stalwart secretary Mary Sheehan, a specialist at extricating him from scrapes of his own making. Without a team approach, he was limited to what could be achieved by a one-man band.

Maddox cleared up the vast backlog of papers left by his predecessor, but he was no devotee of management. He preferred chaos, the milieu that created the highest demand for his improvisational skills. He left in his wake a continuous train of irate phone calls from aggrieved authors, and smoldering correspondence of the sort that ran, "Dear Mr. Maddox, Much as I enjoy reviewing the manuscripts submitted to you for consideration, I draw the line at reviewing my own."

Another limitation was the vice he perversely made out of a quite remarkable journalistic talent, the ability to write acceptably readable prose at almost conversational speed. Because he could write so fast, and got bored so quickly, he was always dashing things off without careful preparation. If only his editorials in *Nature* had been appended with a footnote, "This was written in 20 minutes flat," readers could at least have admired his astonishing facility. The alternative approach, of spending 40 minutes on the editorial and making it really good, was less often to his taste.

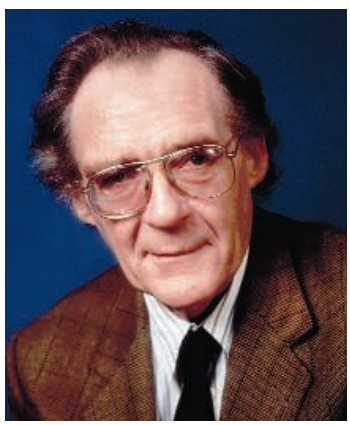

In one memorable editorial, he referred to a proposition he deemed too well known to check, that the Church of England drew a handsome income from the brothels on its many real estate holdings in London. A visit from the church's lawyers duly ensued, and *Nature* was obliged to run a groveling apology.

An unforgettable aspect of Maddox's thrill-seeking was his practice of writing his weekly editorials at literally the very last minute. Many weeks, when failing to get them done the day before press day, he would drive out to *Nature*'s printing plant in the outskirts of London. There he would ensconce himself in a small room with his secretary and, to the thunder of the presses next door, he would dictate his editorial thoughts. A printer's messenger would hover nervously at the door, waiting to snatch each page from Mary Sheehan's typewriter. Had Maddox faltered for an instant, the week's press run would have been delayed or even lost.

On one occasion I arrived by mistake at the printer's, thinking it was my turn to read the page proofs. Seeing that I had nothing to do, Maddox told me to write one of the editorials on his roster, a commentary on the first heart transplant that had taken place earlier in the week. "But I know nothing about heart transplants," I said. "That," he replied, "is the best possible qualification for writing an editorial on a subject." I was amazed to see the editorial quoted in *Scientific American* the following week with deferential attribution to the "distinguished scientific journal *Nature*."

I did not slavishly follow Maddox's dictum during the 10 years I spent writing editorials for the *New York Times*. But it was always a source of encouragement when plunging into some daunting new issue.

Working for Maddox was exhilarating, if one was young and had no preconceptions. You had only to be standing nearby when he got bored with his latest project, and suddenly it was all yours. I was put in charge of writing the daily column of science news that *Nature* then supplied to the London *Times*. This gave me the chance to absorb a lot of science in a hurry, although it also put all of my learning errors in full public view.

On another occasion he opened a Washington office for *Nature* and then directed me to succeed him in writing weekly news articles. I asked for some guidance on how to cover this strange and complex foreign capital. "Don't worry," he said, "I'll leave notes on everything you need to know in a drawer in the office." Eagerly opening the drawer, I found a single piece of paper that listed nothing but the phone number of the space agency's press officer—John's way of saying, "Don't bother me, figure it out for yourself."

By taking a chance on young people and giving them large responsibilities, he launched many into successful careers beyond *Nature*, such as Benjamin Lewin at *Cell*, Colin Norman, *Science*'s news editor, and many others. It was the cyclone of activity he generated that created all these opportunities. And the cyclone was powered by a mind passionately interested, to the exclusion of almost all else, in scientific ideas and their power to explain and to change the world.

Nicholas Wade, now at the *New York Times*, was at *Nature* from 1968 to 1971. E-mail: nwade@nytimes.com

10.1126/science.1175760

Understanding the Warburg Effect: The Metabolic Requirements of Cell Proliferation

Matthew G. Vander Heiden,[1,2] Lewis C. Cantley,[2*] Craig B. Thompson[3*]

In contrast to normal differentiated cells, which rely primarily on mitochondrial oxidative phosphorylation to generate the energy needed for cellular processes, most cancer cells instead rely on aerobic glycolysis, a phenomenon termed "the Warburg effect." Aerobic glycolysis is an inefficient way to generate adenosine 5′-triphosphate (ATP), however, and the advantage it confers to cancer cells has been unclear. Here we propose that the metabolism of cancer cells, and indeed all proliferating cells, is adapted to facilitate the uptake and incorporation of nutrients into the biomass (e.g., nucleotides, amino acids, and lipids) needed to produce a new cell. Supporting this idea are recent studies showing that (i) several signaling pathways implicated in cell proliferation also regulate metabolic pathways that incorporate nutrients into biomass; and that (ii) certain cancer-associated mutations enable cancer cells to acquire and metabolize nutrients in a manner conducive to proliferation rather than efficient ATP production. A better understanding of the mechanistic links between cellular metabolism and growth control may ultimately lead to better treatments for human cancer.

For unicellular organisms such as microbes, there is evolutionary pressure to reproduce as quickly as possible when nutrients are available. Their metabolic control systems have evolved to sense an adequate supply of nutrients and channel the requisite carbon, nitrogen, and free energy into generating the building blocks needed to produce a new cell. When nutrients are scarce, the cells cease biomass production and adapt metabolism to extract the maximum free energy from available resources to survive the starvation period (Fig. 1). Reflecting these fundamental differences in metabolic needs, distinct regulatory mechanisms have evolved to control cellular metabolism in proliferating versus nonproliferating cells.

In multicellular organisms, most cells are exposed to a constant supply of nutrients. Survival of the organism requires control systems that prevent aberrant individual cell proliferation when nutrient availability exceeds the levels needed to support cell division. Uncontrolled proliferation is prevented because mammalian cells do not normally take up nutrients from their environment unless stimulated to do so by growth factors. Cancer cells overcome this growth factor dependence by acquiring genetic mutations that functionally alter receptor-initiated signaling pathways. There is growing evidence that some of these pathways constitutively activate the uptake and metabolism of nutrients that both promote cell survival and fuel cell growth (*1*, *2*). Oncogenic mutations can result in the uptake of nutrients, particularly glucose, that meet or exceed the bioenergetic demands of cell growth and proliferation. This realization has brought renewed attention to Otto Warburg's observation in 1924 that cancer cells metabolize glucose in a manner that is distinct from that of cells in normal tissues (*3*, *4*). By examining how Louis Pasteur's observations regarding fermentation of glucose to ethanol might apply to mammalian tissues, Warburg found that unlike most normal tissues, cancer cells tend to "ferment" glucose into lactate even in the presence of sufficient oxygen to support mitochondrial oxidative phosphorylation. A definitive explanation for Warburg's observation has remained elusive, at least in part because the energy requirements of cell proliferation appear at first glance to be better met by complete catabolism of glucose using mitochondrial oxidative phosphorylation to maximize adenosine 5′-triphosphate (ATP) production.

In this review, we explore the metabolic requirements of cell proliferation in an attempt to understand why proliferating cells metabolize glucose by aerobic glycolysis. Knowledge of what proliferating cells need in terms of energy to generate biomass will help illuminate the connection between signaling pathways that drive cell growth and the regulation of cell metabolism.

Proliferating Mammalian Cells Exhibit Anabolic Metabolism

Our current understanding of metabolic pathways is based largely on studies of nonproliferating cells in differentiated tissues. In the presence of oxygen, most differentiated cells primarily metabolize glucose to carbon dioxide by oxidation of glycolytic pyruvate in the mitochondrial tricarboxylic acid (TCA) cycle. This reaction produces NADH [nicotinamide adenine dinucleotide (NAD^+), reduced], which then fuels oxidative phosphorylation to maximize ATP

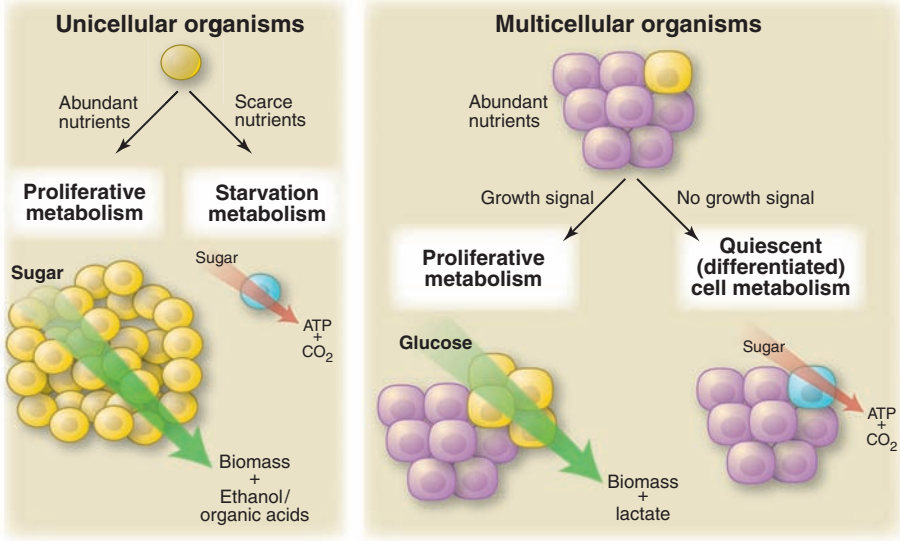

Fig. 1. Microbes and cells from multicellular organisms have similar metabolic phenotypes under similar environmental conditions. Unicellular organisms undergoing exponential growth often grow by fermentation of glucose into a small organic molecule such as ethanol. These organisms, and proliferating cells in a multicellular organism, both metabolize glucose primarily through glycolysis, excreting large amounts of carbon in the form of ethanol, lactate, or another organic acid such as acetate or butyrate. Unicellular organisms starved of nutrients rely primarily on oxidative metabolism, as do cells in a multicellular organism that are not stimulated to proliferate. This evolutionary conservation suggests that there is an advantage to oxidative metabolism during nutrient limitation and nonoxidative metabolism during cell proliferation.

[1]Department of Medical Oncology, Dana-Farber Cancer Institute, Boston, MA 02115, USA. [2]Beth-Israel Deaconess Cancer Center and Department of Systems Biology, Harvard Medical School, Boston, MA 02115, USA. [3]Department of Cancer Biology, Abramson Cancer Center, University of Pennsylvania, Philadelphia, PA 19104, USA.

*To whom correspondence should be addressed: E-mail: lewis_cantley@hms.harvard.edu; craig@mail.med.upenn.edu

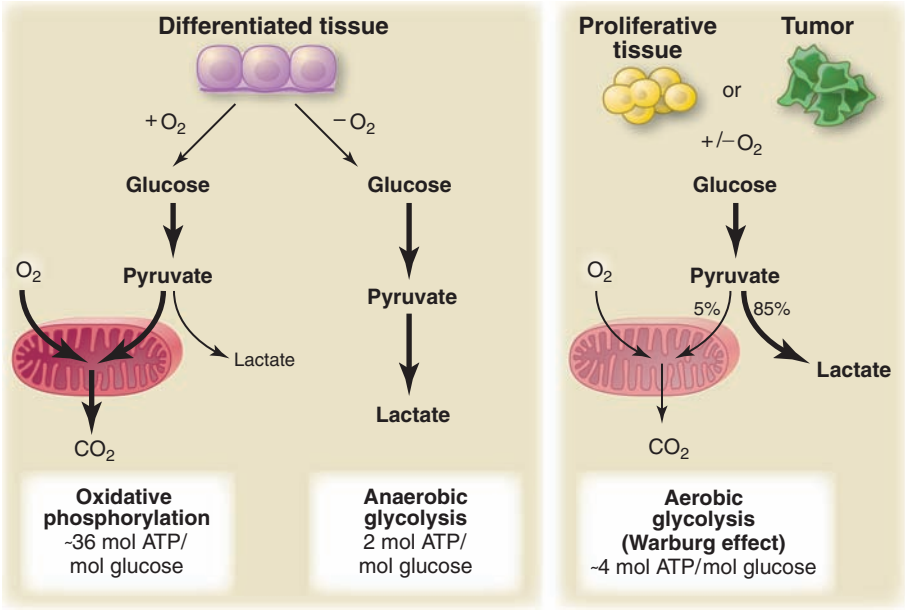

Fig. 2. Schematic representation of the differences between oxidative phosphorylation, anaerobic glycolysis, and aerobic glycolysis (Warburg effect). In the presence of oxygen, nonproliferating (differentiated) tissues first metabolize glucose to pyruvate via glycolysis and then completely oxidize most of that pyruvate in the mitochondria to CO_2 during the process of oxidative phosphorylation. Because oxygen is required as the final electron acceptor to completely oxidize the glucose, oxygen is essential for this process. When oxygen is limiting, cells can redirect the pyruvate generated by glycolysis away from mitochondrial oxidative phosphorylation by generating lactate (anaerobic glycolysis). This generation of lactate during anaerobic glycolysis allows glycolysis to continue (by cycling NADH back to NAD^+), but results in minimal ATP production when compared with oxidative phosphorylation. Warburg observed that cancer cells tend to convert most glucose to lactate regardless of whether oxygen is present (aerobic glycolysis). This property is shared by normal proliferative tissues. Mitochondria remain functional and some oxidative phosphorylation continues in both cancer cells and normal proliferating cells. Nevertheless, aerobic glycolysis is less efficient than oxidative phosphorylation for generating ATP. In proliferating cells, ~10% of the glucose is diverted into biosynthetic pathways upstream of pyruvate production.

production, with minimal production of lactate (Fig. 2). It is only under anaerobic conditions that differentiated cells produce large amounts of lactate. In contrast, most cancer cells produce large amounts of lactate regardless of the availability of oxygen and hence their metabolism is often referred to as "aerobic glycolysis." Warburg originally hypothesized that cancer cells develop a defect in mitochondria that leads to impaired aerobic respiration and a subsequent reliance on glycolytic metabolism (*4*). However, subsequent work showed that mitochondrial function is not impaired in most cancer cells (*5*–*7*), suggesting an alternative explanation for aerobic glycolysis in cancer cells.

Why Do Proliferating Cells Switch to a Less Efficient Metabolism?

As noted above, many unicellular organisms proliferate using fermentation, a microbial equivalent of aerobic glycolysis, and analogous to human cancer cells, preferentially ferment glucose even when oxygen is abundant (Fig. 1). This demonstrates that aerobic glycolytic metabolism can provide sufficient energy for cell proliferation. The metabolism of glucose to lactate generates only 2 ATPs per molecule of glucose, whereas oxidative phosphorylation generates up to 36 ATPs upon complete oxidation of one glucose molecule (*8*). This raises the question of why a less efficient metabolism, at least in terms of ATP production, would be selected for in proliferating cells.

One possible explanation is that inefficient ATP production is a problem only when resources are scarce. This is not the case for proliferating mammalian cells, which are exposed to a continual supply of glucose and other nutrients in circulating blood. Metabolic pathways and their regulation have only recently been studied in actively proliferating cells, and there is evidence that ATP may never be limiting in these cells. No matter how much they are stimulated to divide, cells using aerobic glycolysis also exhibit high ratios of ATP/ADP (adenosine 5′-diphosphate) and $NADH/NAD^+$ (*2*, *9*). Further, even minor perturbations in the ATP/ADP ratio can impair growth. Cells deficient in ATP often undergo apoptosis (*10*, *11*). Normal proliferating cells can also undergo cell cycle arrest and reactivate catabolic metabolism when their ability to produce ATP from glucose is compromised (*12*, *13*), and signaling pathways exist to sense energy status. The best characterized of these is initiated by the activity of adenylate kinases that buffer declining ATP production by converting two ADPs to one ATP and one AMP (adenosine 5′-monophosphate). This helps maintain a viable ATP/ADP ratio as ATP production declines, but the accumulation of AMP activates AMP-activated protein kinase (AMPK). This activation is dependent on the tumor suppressor protein LKB1 and leads to phosphorylation of several targets to improve energy charge in cells (*14*). LKB1 was initially identified as a tumor suppressor gene, suggesting that the ability to sense energy stress could be an important checkpoint to prevent malignant transformation in some cell types.

A second possible explanation for the switch to aerobic glycolysis, discussed in detail below, is that proliferating cells have important metabolic requirements that extend beyond ATP.

Crunching the Numbers—What Are the Metabolic Needs of Proliferating Cells?

To produce two viable daughter cells at mitosis, a proliferating cell must replicate all of its cellular contents. This imposes a large requirement for nucleotides, amino acids, and lipids. During growth, glucose is used to generate biomass as well as produce ATP. Although ATP hydrolysis provides free energy for some of the biochemical reactions responsible for replication of biomass, these reactions have additional requirements. For instance, synthesis of palmitate, a major constituent of cellular membranes, requires 7 molecules of ATP, 16 carbons from 8 molecules of acetyl-CoA (coenzyme A), and 28 electrons from 14 molecules of NADPH [nicotinamide adenine dinucleotide phosphate ($NADP^+$), reduced] (*8*). Likewise, synthesis of amino acids and nucleotides also consumes more equivalents of carbon and NADPH than of ATP. A glucose molecule can generate up to 36 ATPs, or 30 ATPs and 2 NADPHs [if diverted into the pentose phosphate shunt (*8*, *15*)], or provide 6 carbons for macromolecular synthesis. Thus, to make a 16-carbon fatty acyl chain, a single glucose molecule can provide five times the ATP required, whereas 7 glucose molecules are needed to generate the NADPH required. This 35-fold asymmetry is only partially compensated by the consumption of 3 glucose molecules in acetyl-CoA production to satisfy the carbon requirement of the acyl chain itself. It is clear that for a cell to proliferate, the bulk of the glucose cannot be committed to carbon catabolism for ATP production. In addition, if this were the case, the resulting rise in the ATP/ADP ratio would severely impair the flux through glycolytic intermediates, limiting the production of the acetyl-CoA and NADPH required for macromolecular synthesis.

For most mammalian cells in culture, the only two molecules catabolized in appreciable quantities are glucose and glutamine. This means that glucose and glutamine supply most of the carbon, nitrogen, free energy, and reducing equivalents necessary to support cell growth and division. From this perspective, it becomes clear that converting all of the glucose to CO_2 via oxidative phosphorylation in the mitochondria to maximize ATP production runs

counter to the needs of a proliferating cell. Some glucose must be diverted to macromolecular precursors such as acetyl-CoA for fatty acids, glycolytic intermediates for nonessential amino acids, and ribose for nucleotides. This may explain at least part of the selective advantage provided by the Warburg effect, a hypothesis supported by recent ^{13}C–nuclear magnetic resonance spectroscopy measurements showing that glioblastoma cells in culture convert as much as 90% of glucose and 60% of glutamine they acquire into lactate or alanine (*16*). Although most of this lactate and alanine is excreted from the cell as waste, one "byproduct" of their generation is a robust production of NADPH (Fig. 3). In addition to providing nitrogen for nonessential amino acids through transamination reactions, the catabolism of glutamine into lactate produces NADPH via the activity of $NADP^+$-specific malate dehydrogenase (malic enzyme). Growth factor signaling also regulates the activity of the glycolytic enzyme pyruvate kinase and modulates flux of carbon through the later steps of glycolysis (*9*, *17*). This modulation of pyruvate kinase may facilitate the redirection of glucose metabolites into the pentose phosphate shunt, as well as nucleotide and amino acid biosynthesis pathways. The conversion of both glucose and glutamine to lactate involves the enzyme lactate dehydrogenase (LDH). Inhibiting LDH activity impairs cell proliferation (*6*), possibly by interfering with the cell's ability to excrete excess carbon. Elimination of excess carbon might be required to generate sufficient NADPH to support cell proliferation.

Most of the carbon for fatty acid synthesis is derived from glucose. During this process, glucose is first converted to acetyl-CoA in the mitochondrial matrix and used to synthesize citrate in the TCA cycle. Under conditions of high ATP/ADP and $NADH/NAD^+$ exhibited by most proliferating cells, this citrate is excreted back into the cytosol where lipids are generated. In the cytosol, acetyl-CoA is recaptured from citrate and used as the carbon source for the growing acyl chains. Synthesis of acetyl-CoA from citrate requires the enzyme ATP citrate lyase (ACL), and disruption of ACL impairs tumor growth (*18*). Glutamine uptake also appears to be critical for lipid synthesis in that it supplies carbon in the form of mitochondrial oxaloacetate to maintain citrate production in the first step of the TCA cycle (*16*). Thus, metabolism of both glutamine and glucose is orchestrated to support the production of acetyl-CoA and NADPH needed for fatty acid synthesis. Flux of metabolites into

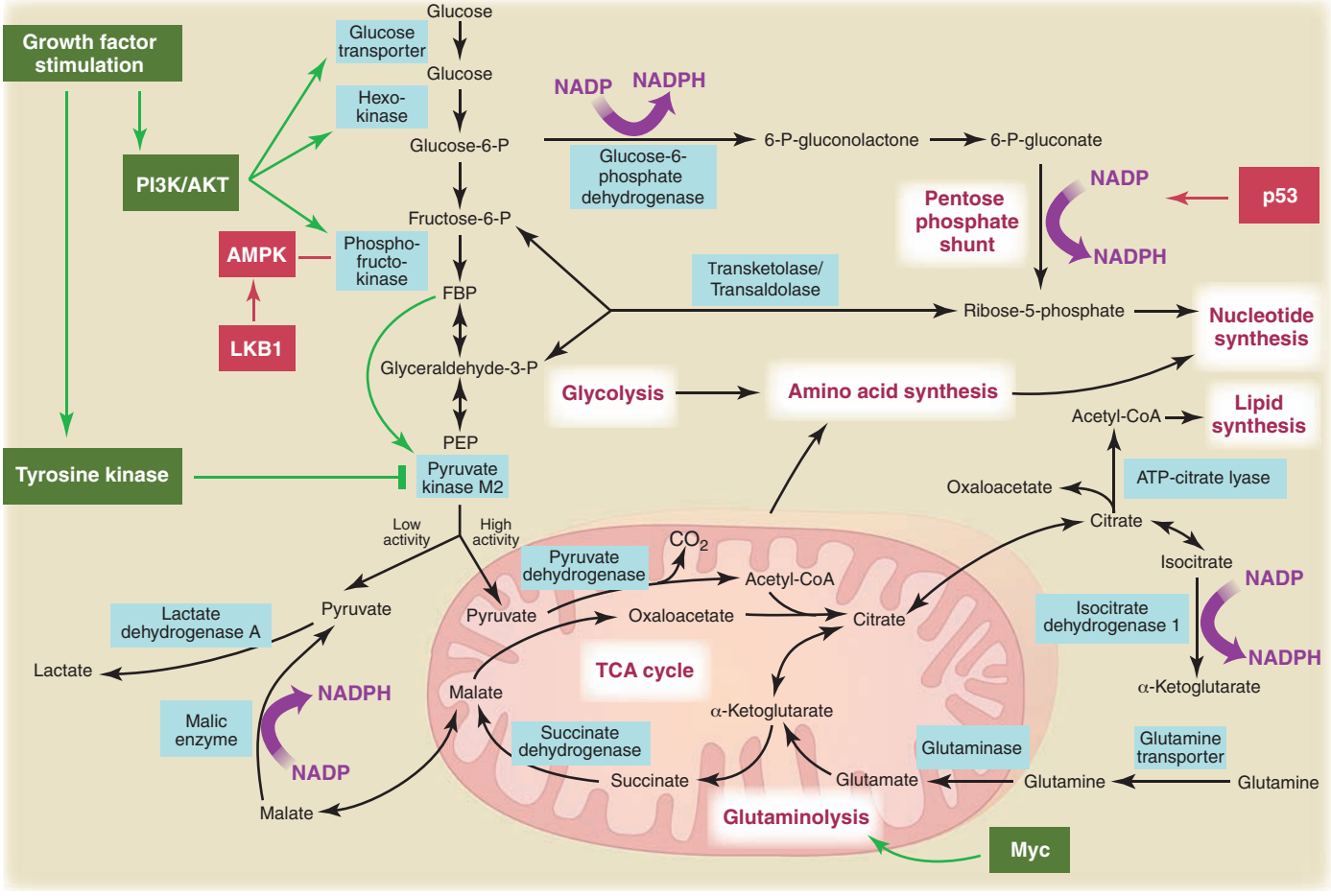

Fig. 3. Metabolic pathways active in proliferating cells are directly controlled by signaling pathways involving known oncogenes and tumor suppressor genes. This schematic shows our current understanding of how glycolysis, oxidative phosphorylation, the pentose phosphate pathway, and glutamine metabolism are interconnected in proliferating cells. This metabolic wiring allows for both NADPH production and acetyl-CoA flux to the cytosol for lipid synthesis. Key steps in these metabolic pathways can be influenced by signaling pathways known to be important for cell proliferation. Activation of growth factor receptors leads to both tyrosine kinase signaling and PI3K activation. Via AKT, PI3K activation stimulates glucose uptake and flux through the early part of glycolysis. Tyrosine kinase signaling negatively regulates flux through the late steps of glycolysis, making glycolytic intermediates available for macromolecular synthesis as well as supporting NADPH production. Myc drives glutamine metabolism, which also supports NADPH production. LKB1/AMPK signaling and p53 decrease metabolic flux through glycolysis in response to cell stress. Decreased glycolytic flux in response to LKB/AMPK or p53 may be an adaptive response to shut off proliferative metabolism during periods of low energy availability or oxidative stress. Tumor suppressors are shown in red, and oncogenes are in green. Key metabolic pathways are labeled in purple with white boxes, and the enzymes controlling critical steps in these pathways are shown in blue. Some of these enzymes are candidates as novel therapeutic targets in cancer. Malic enzyme refers to $NADP^+$-specific malate dehydrogenase [systematic name (S)-malate:$NADP^+$ oxidoreductase (oxaloacetate-decarboxylating)].

other synthetic pathways for nucleic acid and amino acid synthesis must be similarly balanced.

The excess generation of lactate that accompanies the Warburg effect would appear to be an inefficient use of cellular resources. Each lactate excreted from the cell wastes three carbons that might otherwise be utilized for either ATP production or macromolecular precursor biosynthesis. Possibly the dumping of excess carbon as lactate is effective because it allows faster incorporation of carbon into biomass, which in turn facilitates rapid cell division. For most proliferating cells, nutrients are not limiting so there is no selective pressure to optimize metabolism for ATP yield. In contrast, a selective pressure for rate of metabolism does exist. Immune responses and wound repair depend on the speed of the proliferative expansion of effector cells. To survive, the organism must signal the responding cells to maximize their rate of anabolic growth. Cells that convert glucose and glutamine into biomass most efficiently will proliferate fastest. For the organism, nutrients may be scarce and there are pathways active in specialized, nonproliferating tissues to recycle the excess lactate and alanine dumped during the rapid cell growth of proliferating cells. The Cori cycle in the liver can recycle lactate generated from actively proliferating tissues to glucose, and analogous pathways exist to recycle the alanine generated from "inefficient" glutamine metabolism (*8*). This ability to recycle the organic waste produced by cell proliferation during an immune response or wound repair results in a minimal impact on the energy reserves of the whole organism. In addition, there is emerging evidence that cellular metabolism within a tumor can be heterogeneous, with some cells using the excess lactate generated as a fuel for mitochondrial oxidative phosphorylation (*19*).

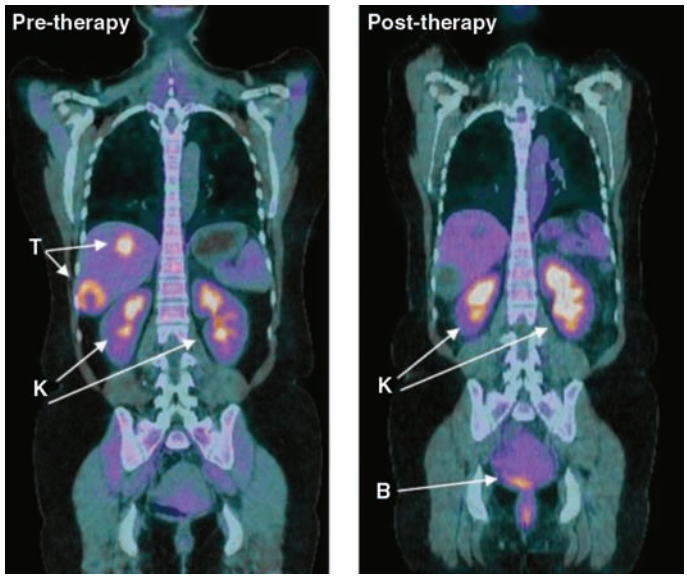

Fig. 4. Decreased metabolism of glucose by tumors, visualized by PET with the glucose analog FDG, predicts response to anticancer therapy. Shown are fused coronal images of FDG-PET and computerized tomography (CT) obtained on a hybrid PET/CT scanner after the infusion of FDG in a patient with a form of malignant sarcoma (gastrointestinal stromal tumor) before and after therapy with a tyrosine kinase inhibitor (sunitinib). The tumor (T) is readily visualized by FDG-PET/CT before therapy (**left**). After 4 weeks of therapy (**right**), the tumor shows no uptake of FDG despite persistent abnormalities on CT. Excess FDG is excreted in the urine, and therefore the kidneys (K) and bladder (B) are also visualized as labeled. [Image courtesy of A. D. Van den Abbeele, Dana-Farber Cancer Institute, Boston]

Metabolic Regulation Is a Component of the Cell Growth Machinery

The phosphoinositide 3-kinase (PI3K) signaling pathway is linked to both growth control and glucose metabolism. In addition to a well-described role in directing available amino acids into protein synthesis via mTOR, the PI3K pathway regulates glucose uptake and utilization (Fig. 3). Even in non–insulin-dependent tissues, PI3K signaling through AKT can regulate glucose transporter expression, enhance glucose capture by hexokinase, and stimulate phosphofructokinase activity (*2*). PI3K pathway activation renders cells dependent on high levels of glucose flux (*20*). Small molecules that disrupt PI3K signaling lead to decreased glucose uptake by tumors as measured by ^{18}F-deoxyglucose positron emission tomography (FDG-PET), and the ability to inhibit tumor FDG uptake correlates with tumor regression (*21*). Glucose withdrawal induces cell death in a manner indistinguishable from that seen upon withdrawal of growth factor signaling, a phenomenon that may contribute to "oncogene addiction" (*22*). Indeed, where it has been examined in cancer patients, response to therapy is predicted by the ability to disrupt glucose metabolism as measured by FDG-PET (*23*) (Fig. 4).

There is growing evidence that metabolic enzymes can directly contribute to carcinogenesis. Germline mutations in the TCA cycle enzymes succinate dehydrogenase and fumarate hydratase have been identified in some forms of human renal cell cancer, paraganglioma, and pheochromocytoma (*24*, *25*). One effect of these mutations is activation of Hif1α-mediated glucose utilization (*26*). A recent analysis of human glioblastoma multiforme, an aggressive brain cancer, revealed that up to 12% of the tumors harbor the same point mutation in the gene encoding cytosolic isocitrate dehydrogenase–1 (IDH1) (*27*). Monoallelic mutation of the same residue in IDH1, or the analogous residue in the related enzyme IDH2, is a common feature of gliomas as more than 80% of indolent gliomas harbor such a mutation (*28*, *29*). IDH1 and IDH2 couple the interconversion of cytosolic isocitrate and α-ketoglutarate in an $NADP^+$/NADPH-dependent reaction. What effect this mutation has on cellular metabolism is not clear; however, given the important requirement for NADPH in macromolecular synthesis and redox control, alterations in NADPH production may affect cellular proliferation or mutation rates (*30*). Alternatively, such mutations may favor the production of citrate from α-ketoglutarate as a carbon precursor for macromolecular synthesis.

Many oncogenes are tyrosine kinases. One common feature of tyrosine kinase signaling associated with cell proliferation is regulation of glucose metabolism. In contrast to differentiated cells, proliferating cells selectively express the M2 isoform of the glycolytic enzyme pyruvate kinase (PK-M2) (*9*). Unlike other pyruvate kinase isoforms, PK-M2 is regulated by tyrosine-phosphorylated proteins (*17*). Phosphotyrosine signaling downstream of a variety of cell growth signals shares the common ability to negatively regulate PK-M2 activity (*17*). In response to phosphotyrosine-protein binding, PK-M2 is induced into a low-activity state. This regulation of enzyme activity may constitute a molecular switch that allows cells to metabolize glucose through glycolysis in a manner that is consistent with proliferating cell metabolism only when growth signals are present (Fig. 3). Although counterintuitive, it is the low-activity form of PK-M2 that is necessary for cell proliferation. This regulation allows PK-M2 to act as a gatekeeper that dictates the flow of carbon into biosynthetic pathways versus complete catabolism for ATP production. In support of this idea, PK-M2 is required for proliferation in vivo (*9*).

Human tumor cells whose growth is driven by the *MYC* oncogene are particularly sensitive to glutamine withdrawal (*31*), and genes involved in glutamine metabolism appear to be under both the direct and indirect transcriptional control of the MYC protein (*32*, *33*). Glutamine depletion from *MYC*-transformed cells results in the rapid loss of TCA cycle intermediates and cell death (*31*). Furthermore, this dependence on glutamine for survival is not related to the generation of ATP by glutamine metabolism.

Tumor suppressor pathways can also regulate cellular metabolism and may act to coordinate nutrient utilization with cell physiology. For instance, p53 expression controls metabolic genes and alters glucose utilization. Expression of *TIGAR*, a gene induced by p53, leads to inhibition of phosphofructokinase, redirection of glucose toward the pentose phosphate shunt, and NADPH production (*34*). This may be an adaptive response that protects the cell from oxidative stress, as NADPH is required to generate the reduced form of glutathione, which is a major intracellular defense against damage mediated by reactive oxygen species (ROS).

Mitochondrial oxidative phosphorylation is the major cellular source of ROS production. Cells with excess nutrient uptake that have not converted to aerobic glycolysis would be predicted to have increased oxidative phosphorylation and ROS

production. This maladaptive metabolic state may underlie the evolutionary selection for induction of apoptosis and/or senescence in the setting of increased ROS. Because some oncogenes drive glucose uptake, this hypothesis may explain oncogene-induced senescence. For instance, oncogenic Ras causes alterations in glucose metabolism (*35*) but causes senescence when expressed in cells without a cooperating oncogene (*36*). Further supporting this hypothesis is the observation that stationary-phase yeast lose viability when exposed to high levels of glucose and no additional nutrients (*37*). Yeast studies have also demonstrated that oxidative phosphorylation stops during S phase to limit ROS-mediated DNA damage, underscoring the importance of limiting oxidative phosphorylation and ROS production in proliferating cells (*38*).

What Triggers the Switch from Oxidative Phosphorylation to Aerobic Glycolysis?

One proposed explanation for Warburg's observation is that tumor hypoxia selects for cells dependent on anaerobic metabolism (*39*). However, cancer cells appear to use glycolytic metabolism before exposure to hypoxic conditions. For example, leukemic cells are highly glycolytic (*40*, *41*), yet these cells reside within the bloodstream at higher oxygen tensions than cells in most normal tissues. Similarly, lung tumors arising in the airways exhibit aerobic glycolysis even though these tumor cells are exposed to oxygen during tumorigenesis (*9*, *42*). Thus, although tumor hypoxia is clearly important for other aspects of cancer biology, the available evidence suggests that it is a late-occurring event that may not be a major contributor in the switch to aerobic glycolysis by cancer cells.

The classic view of metabolism is that of a self-correcting, homeostatic system where a core set of housekeeping enzymes enables the cell to respond to changing bioenergetic demands. However, as described above, the evolving evidence instead points to a dynamically regulated system that is programmed to fit the requirements for cell proliferation or meet the specific needs of each differentiated tissue as appropriate. For normal proliferating tissues, such as in the developing embryo or during an immune response in the adult, signals from growth factors allow cells to utilize nutrients for growth (*41*, *43*). Perhaps one function of oncogenic pathways is to drive cell-autonomous nutrient uptake and program proliferative metabolism, whereas one function of tumor suppressor pathways is to prevent nutrient utilization for anabolic processes. In this model, for cancer to arise, mutations are needed to give cells the ability to acquire nutrients and coordinately regulate metabolic pathways to support proliferation. This alteration in metabolic control may result by reverting to an embryonic program, or evolving the capability to alter existing cell metabolism in a way that supports cell growth.

Cellular Metabolism and Human Cancer

In principle, the metabolic dependencies of cancer cells can be exploited for cancer treatment. For instance, a large fraction of human cancer is dependent on aberrant signaling through the PI3K/Akt pathway, and agents that target PI3K and various downstream signaling molecules are now in clinical trials. The growing evidence that activation of PI3K causes increased dependency on glycolysis suggests that these agents may exert some of their effect by disrupting glucose metabolism. Drugs targeting key metabolic control points important for aerobic glycolysis, such as PK-M2 or LDH-A, might also warrant investigation as potential cancer therapies. In addition, the drugs developed to target metabolic diseases such as type 2 diabetes may have use in treating cancer. A number of retrospective clinical studies have found that the widely used diabetes drug metformin may offer a possible benefit in cancer prevention as well as improved outcomes when used with other cancer therapies (*44*). Metformin and the more potent related compound Phenformin activate AMPK in cells, suggesting that Phenformin or other activators of AMPK might also be used as an adjunct to cancer therapy. Optimal use of these drugs will require a better understanding of cancer cell metabolism and identification of the signaling pathways that represent an Achilles' heel for cell proliferation or survival.

Metabolic tissues in mammals transform ingested food into a near-constant supply of glucose, glutamine, and lipids to balance the metabolic needs of both differentiated and proliferating tissues. Alterations in the appropriate balance of fuels and/or signal transduction pathways that deal with nutrient utilization may underlie the cancer predisposition associated with metabolic diseases such as diabetes and obesity (*45*, *46*). A better understanding of how whole-body metabolism interacts with tumor metabolism may better define these risks and identify potential points of therapeutic intervention. In addition, it is possible that the cachexia associated with many cancers is exacerbated by the excess nutrient consumption by the tumor, which would affect whole-body metabolic regulation. To this end, the potential role of dietary supplements and tight glucose control as adjuncts to cancer treatment is an active field of investigation.

Future Prospects

Metabolism is involved directly or indirectly in essentially everything a cell does. There is mounting evidence for cross-talk between signaling pathways and metabolic control in every multicellular organism studied. There is still much to learn about how proliferating cell metabolism is regulated. Despite a long and rich history of research, the complex connection between metabolism and proliferation remains an exciting area of investigation. Indeed, new metabolic pathways have been discovered as recently as the 1980s (*47*), and it is possible that additional pathways have yet to be described. Understanding this important aspect of biology is likely to have a major impact on our understanding of cell proliferation control and cancer.

References and Notes

1. P. P. Hsu, D. M. Sabatini, *Cell* **134**, 703 (2008).
2. R. J. Deberardinis, J. J. Lum, G. Hatzivassiliou, C. B. Thompson, *Cell Metab.* **7**, 11 (2008).
3. O. Warburg, K. Posener, E. Negelein, *Biochem. Z.* **152**, 319 (1924).
4. O. Warburg, *Science* **123**, 309 (1956).
5. S. Weinhouse, *Z. Krebsforsch. Klin. Onkol. Cancer Res. Clin. Oncol.* **87**, 115 (1976).
6. V. R. Fantin, J. St-Pierre, P. Leder, *Cancer Cell* **9**, 425 (2006).
7. R. Moreno-Sanchez, S. Rodriguez-Enriquez, A. Marin-Hernandez, E. Saavedra, *FEBS J.* **274**, 1393 (2007).
8. A. L. Lehninger, D. L. Nelson, M. M. Cox, *Principles of Biochemistry* (Worth, New York, ed. 2, 1993).
9. H. R. Christofk *et al.*, *Nature* **452**, 230 (2008).
10. D. S. Izyumov *et al.*, *Biochim. Biophys. Acta* **1658**, 141 (2004).
11. M. G. Vander Heiden, N. S. Chandel, P. T. Schumacker, C. B. Thompson, *Mol. Cell* **3**, 159 (1999).
12. R. J. Shaw *et al.*, *Proc. Natl. Acad. Sci. U.S.A.* **101**, 3329 (2004).
13. J. J. Lum *et al.*, *Cell* **120**, 237 (2005).
14. D. G. Hardie, *Nat. Rev. Mol. Cell Biol.* **8**, 774 (2007).
15. Possibly up to four NADPH molecules per glucose can be produced if the products of the pentose phosphate shunt are metabolized via the TCA cycle and malic enzyme or cytosolic isocitrate dehydrogenase 1 (IDH1) to generate two additional NADPH molecules.
16. R. J. DeBerardinis *et al.*, *Proc. Natl. Acad. Sci. U.S.A.* **104**, 19345 (2007).
17. H. R. Christofk, M. G. Vander Heiden, N. Wu, J. M. Asara, L. C. Cantley, *Nature* **452**, 181 (2008).
18. G. Hatzivassiliou *et al.*, *Cancer Cell* **8**, 311 (2005).
19. P. Sonveaux *et al.*, *J. Clin. Invest.* **118**, 3930 (2008).
20. M. Buzzai *et al.*, *Oncogene* **24**, 4165 (2005).
21. J. A. Engelman *et al.*, *Nat. Med.* **14**, 1351 (2008).
22. M. G. Vander Heiden *et al.*, *Mol. Cell. Biol.* **21**, 5899 (2001).
23. S. Ben-Haim, P. Ell, *J. Nucl. Med.* **50**, 88 (2009).
24. B. E. Baysal *et al.*, *Science* **287**, 848 (2000).
25. P. J. Pollard, N. C. Wortham, I. P. Tomlinson, *Ann. Med.* **35**, 634 (2003).
26. M. A. Selak *et al.*, *Cancer Cell* **7**, 77 (2005).
27. D. W. Parsons *et al.*, *Science* **321**, 1807 (2008).
28. F. E. Bleeker *et al.*, *Hum. Mutat.* **30**, 7 (2009).
29. H. Yan *et al.*, *N. Engl. J. Med.* **360**, 765 (2009).
30. C. B. Thompson, *N. Engl. J. Med.* **360**, 813 (2009).
31. M. Yuneva, N. Zamboni, P. Oefner, R. Sachidanandam, Y. Lazebnik, *J. Cell Biol.* **178**, 93 (2007).
32. D. R. Wise *et al.*, *Proc. Natl. Acad. Sci. U.S.A.* **105**, 18782 (2008).
33. P. Gao *et al.*, *Nature* **458**, 762 (2009).
34. K. Bensaad *et al.*, *Cell* **126**, 107 (2006).
35. F. Chiaradonna *et al.*, *Oncogene* **25**, 5391 (2006).
36. M. Serrano, A. W. Lin, M. E. McCurrach, D. Beach, S. W. Lowe, *Cell* **88**, 593 (1997).
37. D. Granot, M. Snyder, *Proc. Natl. Acad. Sci. U.S.A.* **88**, 5724 (1991).
38. Z. Chen, E. A. Odstrcil, B. P. Tu, S. L. McKnight, *Science* **316**, 1916 (2007).
39. R. A. Gatenby, R. J. Gillies, *Nat. Rev. Cancer* **4**, 891 (2004).
40. S. Gottschalk, N. Anderson, C. Hainz, S. G. Eckhardt, N. J. Serkova, *Clin. Cancer Res.* **10**, 6661 (2004).
41. R. L. Elstrom *et al.*, *Cancer Res.* **64**, 3892 (2004).
42. K. B. Nolop *et al.*, *Cancer* **60**, 2682 (1987).
43. H. Kondoh *et al.*, *Antioxid. Redox Signal.* **9**, 293 (2007).
44. J. M. Evans, L. A. Donnelly, A. M. Emslie-Smith, D. R. Alessi, A. D. Morris, *BMJ* **330**, 1304 (2005).
45. E. E. Calle, R. Kaaks, *Nat. Rev. Cancer* **4**, 579 (2004).
46. M. Pollak, *Nat. Rev. Cancer* **8**, 915 (2008).
47. M. R. El-Maghrabi, S. J. Pilkis, *J. Cell. Biochem.* **26**, 1 (1984).

48. We thank A. Van den Abbeele (Department of Imaging, Dana-Farber Cancer Institute, Boston) for the FDG-PET image. We also thank K. D. Courtney, A. J. Shaywitz, and K. D. Swanson for thoughtful discussions and critical reading of the manuscript and the Damon Runyon Cancer Research Foundation for support (to M.G.V.H.). M.G.V.H. receives grant support from the National Cancer Institute (NCI) and NIH; L.C.C. receives grant support from the NIH; and C.B.T. receives grant support from the NCI, NIH, and Abramson Family Cancer Research Institute to study aspects of cancer cell metabolism. M.G.V.H., L.C.C., and C.B.T. hold patents related to the targeting of cancer cell metabolism and have financial interests in Agios Pharmaceuticals, a company that seeks to exploit alterations in cancer metabolism for novel therapeutics.

10.1126/science.1160809

The SOS Response Controls Integron Recombination

Émilie Guerin,[1]* Guillaume Cambray,[2]* Neus Sanchez-Alberola,[3]* Susana Campoy,[3] Ivan Erill,[4] Sandra Da Re,[1] Bruno Gonzalez-Zorn,[5] Jordi Barbé,[3] Marie-Cécile Ploy,[1] Didier Mazel[2]†

Integrons are bacterial genetic elements capable of incorporating and expressing promoterless genes structured as cassettes (*1*). Two subsets of integrons have been described: mobile (or resistance) integrons (MIs), which are located in transposons and contain two to eight cassettes encoding resistance to a broad spectrum of antibiotics, and chromosomal integrons (CIs), which are ancient sedentary elements that may contain hundreds of gene cassettes of mostly unknown function. Several lines of evidence indicate that MIs and their cassettes were derived from CIs (*1*). All integrons contain an integrase gene (*intI*) that mediates the integration of exogenous gene cassettes at the *attI* site and random excision or rearrangement of resident gene cassettes (fig. S1). Despite the importance of integrons in the acquisition and spread of antibiotic resistance determinants, little is known about the dynamics and regulatory control of cassette recombination.

To address this issue, we aligned the upstream region of several CI and MI integrase genes and identified a conserved LexA-binding motif overlapping the putative promoter regions (*2*) (Fig. 1A). LexA is the transcriptional repressor governing the SOS response, a widespread regulatory network aimed at addressing DNA damage by repairing or bypassing lesions (*3*). Derepression of SOS genes results from the autocatalytic cleavage of LexA, a process induced by single-stranded DNA and mediated by RecA. The SOS response has strong links with bacterial adaptation and has been implicated in clinically relevant phenotypes, such as dissemination of virulence factors.

We assessed the functionality of the identified *Vibrio cholerae* LexA-binding site in vitro and found that purified *V. cholerae* LexA specifically bound the identified motif, whereas changes in key site positions prevented this interaction (fig. S2). We analyzed the integrase expression in both the CI of *V. cholerae* and a class 1 MI of *Escherichia coli*. Induction of the SOS response increased the expression of a β-galactosidase reporter of integrase transcription by 4.5-fold in *E. coli* and 37-fold in *V. cholerae*. No induction was observed when either LexA or RecA was impaired or when the LexA boxes were inactivated (Fig. 1, B and C). To verify that the induction of integrase expression results in functional cassette recombination, we measured the frequency of cassette excision. For the class 1 MI and *V. cholerae* CI, the excision rates increased by 141-fold and 340-fold, respectively, upon SOS induction (Fig. 1, B and C). All together, these results demonstrate that the regulation of these integrase genes is strictly dependent on the SOS response and that SOS induction controls the rates of cassette recombination.

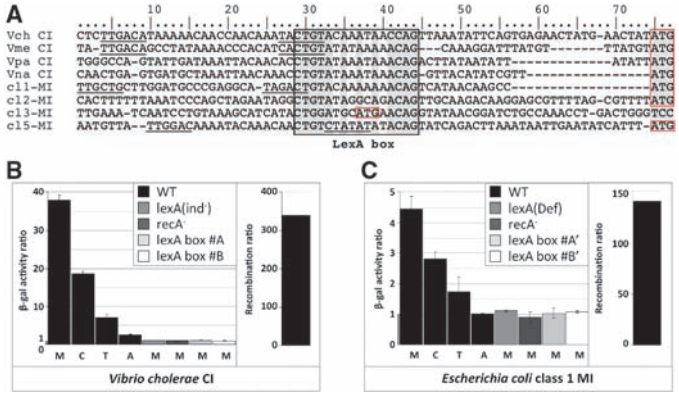

Fig. 1. (**A**) Alignment of the promoter regions of *intI* genes from the CI of *V. cholerae* (Vch), *V. metschnikovii* (Vme), *V. parahaemolyticus* (Vpa), and *V. natriegens* (Vna) and from class 1 (cl1-MI), class 2 (cl2-MI), class 3 (cl3-MI), and class 5 (cl5-MI) MIs (*1*). Putative LexA-binding sequences are boxed, whereas putative σ70 promoter elements (−35 and −10) are underlined and the translation start site of *intI* is boxed in red. (**B** and **C**) *intI* expression and cassette recombination inductions in the *V. cholerae* CI and the *E. coli* pAT674 class 1 MI. Mitomycin (M), ciprofloxacin (C), trimethoprim (T), and ampicilin (A) were used to induce the SOS response in a wild-type background. Induction was validated by using several SOS-defective mutants. Mutants are specified in the insets. The LexA box mutants correspond to substitution of the canonical site known to abolish LexA binding (*2*). *lexA*(ind-), noninducible LexA derivative; *lexA*(Def), inactive LexA mutant.

In integrons, newly acquired cassettes are highly expressed by the *Pc* promoter, but they can be silenced by untimely recombination events that displace the cassettes to distal positions (*4*). Recombination can also activate silenced cassettes or retrieve new cassettes from surrounding bacterial communities (*1*). Under normal conditions, SOS repression of *intI* maintains integron cassette arrays in a steady state. The SOS response can be induced by several stresses (*5*), thus ensuring that the reordering of existing cassettes and the acquisition of exogenous cassettes occur under conditions when innovations are needed. In this respect, it is worth noting that antibiotics known to induce the SOS response, such as trimethoprim, quinolones, and β-lactams, promote integrase expression (Fig. 1, B and C).

Current policies in the fight against antibiotic resistance rely on the assumption that resistance mechanisms are costly to the bacteria that host them, which thus gives these bacteria a selective disadvantage and leads to their loss in the absence of antibiotic exposure (*6*). However, the incorporation of responsive regulation in integrons indicates that antibiotic resistance genes can be silenced at no biological cost until needed, while other adaptive traits continue to be expressed. This being so, there may be little selection acting on MIs, and antibiotic resistance may persist in bacterial populations. Future antibiotic restriction guidelines should take this phenomenon into account.

References and Notes

1. D. Mazel, *Nat. Rev. Microbiol.* **4**, 608 (2006).
2. Materials and methods are available as supporting material on *Science* Online.
3. I. Erill, S. Campoy, J. Barbe, *FEMS Microbiol. Rev.* **31**, 637 (2007).
4. C. M. Collis, R. M. Hall, *Antimicrob. Agents Chemother.* **39**, 155 (1995).
5. A. Aertsen, C. W. Michiels, *Trends Microbiol.* **14**, 421 (2006).
6. D. I. Andersson, *Curr. Opin. Microbiol.* **9**, 461 (2006).
7. M.-C.P. acknowledges support by grants from the Ministère de l'Enseignement Supérieur et de la Recherche, the Conseil Régional du Limousin, the Fondation pour la Recherche Médicale (FRM), and Institut National de la Santé et de la Recherche Médicale; D.M. from the Institut Pasteur, the Centre National de la Recherche Scientifique, the FRM, and the European Union (STREP CRAB, LSHM-CT-2005-019023); J.B. from the Spanish Ministerio de Ciencia e Innovación (MICINN) (BFU2008-01078/BMC) and the Catalunya Generalitat (2005SGR-533); and B.G.Z. from the MICINN (GEN2006-27767-E/PAT) and European Union (MED-VET-NET and FOOD-CT-2004-506122). The GenBank accessions for the sequences shown in Fig. 1 are AF055586 (Vch CI), AY014398 (Vme CI), AY014399 (Vpa CI), AY181034 (Vna CI), AF034958 (cl1-MI), AJ001816 (cl2-MI), AB070224 (cl3-MI), and AJ277063 (cl5-MI).

Supporting Online Material

www.sciencemag.org/cgi/content/full/324/5930/1034/DC1
Materials and Methods
Figs. S1 and S2
Tables S1 to S3
References

2 March 2009; accepted 2 April 2009
10.1126/science.1172914

[1]Université de Limoges, Faculté de Médecine, EA3175; INSERM, Equipe Avenir, 87000 Limoges, France. [2]Institut Pasteur, Plasticité du Génome Bactérien, CNRS URA 2171, 75015 Paris, France. [3]Departament de Genètica i Microbiologia, Universitat Autònoma de Barcelona, 08193 Barcelona, Spain. [4]Biomedical Applications Group, Centro Nacional de Microelectrónica–Instituto de Microelectrónica, Consejo Superior de Investigaciones Cientificas (CNM-IMB, CSIC), 08193 Barcelona, Spain. [5]Departamento de Sanidad Animal and VISAVET (Centro de Vigilancia Sanitaria Veterinaria), Universitat Complutense de Madrid, 28040 Madrid, Spain.

*These authors contributed equally to this work.
†To whom correspondence should be addressed. E-mail: mazel@pasteur.fr

The Genetic Structure and History of Africans and African Americans

Sarah A. Tishkoff,[1,2]* Floyd A. Reed,[1]†‡ Françoise R. Friedlaender,[3]‡ Christopher Ehret,[4] Alessia Ranciaro,[1,2,5]§ Alain Froment,[6]§ Jibril B. Hirbo,[1,2] Agnes A. Awomoyi,[1]‖ Jean-Marie Bodo,[7] Ogobara Doumbo,[8] Muntaser Ibrahim,[9] Abdalla T. Juma,[9] Maritha J. Kotze,[10] Godfrey Lema,[11] Jason H. Moore,[12] Holly Mortensen,[1]¶ Thomas B. Nyambo,[11] Sabah A. Omar,[13] Kweli Powell,[1]# Gideon S. Pretorius,[14] Michael W. Smith,[15] Mahamadou A. Thera,[8] Charles Wambebe,[16] James L. Weber,[17] Scott M. Williams[18]

Africa is the source of all modern humans, but characterization of genetic variation and of relationships among populations across the continent has been enigmatic. We studied 121 African populations, four African American populations, and 60 non-African populations for patterns of variation at 1327 nuclear microsatellite and insertion/deletion markers. We identified 14 ancestral population clusters in Africa that correlate with self-described ethnicity and shared cultural and/or linguistic properties. We observed high levels of mixed ancestry in most populations, reflecting historical migration events across the continent. Our data also provide evidence for shared ancestry among geographically diverse hunter-gatherer populations (Khoesan speakers and Pygmies). The ancestry of African Americans is predominantly from Niger-Kordofanian (~71%), European (~13%), and other African (~8%) populations, although admixture levels varied considerably among individuals. This study helps tease apart the complex evolutionary history of Africans and African Americans, aiding both anthropological and genetic epidemiologic studies.

Modern humans originated in Africa ~200,000 years ago and then spread across the rest of the globe within the past ~100,000 years (*1*). Thus, modern humans have existed continuously in Africa longer than in any other geographic region and have maintained relatively large effective population sizes, resulting in high levels of within-population genetic diversity (*1*, *2*). Africa contains more than 2000 distinct ethnolinguistic groups representing nearly one-third of the world's languages (*3*). Except for a few isolates that show no clear relationship with other languages, these languages have been classified into four major macrofamilies: Niger-Kordofanian (spoken across a broad region of Africa), Afroasiatic (spoken predominantly in Saharan, northeastern, and eastern Africa), Nilo-Saharan (spoken predominantly in Sudanic, Saharan, and eastern Africa), and Khoesan (languages containing click-consonants, spoken by San in southern Africa and by Hadza and Sandawe in eastern Africa) (fig. S1) (*4*).

Despite the importance of African population genetics, the pattern of genome-wide nuclear genetic diversity across geographically and ethnically diverse African populations is largely uncharacterized (*1*, *2*, *5*). Because of considerable environmental diversity, African populations show a range of linguistic, cultural, and phenotypic variation (*1*, *2*, *4*). Characterizing the pattern of genetic variation among ethnically diverse African populations is critical for reconstructing human evolutionary history, clarifying the population history of Africans and African Americans, and determining the proper design and interpretation of genetic disease association studies (*1*, *6*), because substructure can cause spurious results (*7*). Furthermore, variants associated with disease could be geographically restricted as a result of new mutations, genetic drift, or region-specific selection pressures (*1*). Thus, our in-depth characterization of genetic structure in Africa benefits research of biomedical relevance in both African and African-diaspora populations.

We genotyped a panel of 1327 polymorphic markers, consisting of 848 microsatellites, 476 indels (insertions/deletions), and three SNPs (single-nucleotide polymorphisms), in 2432 Africans from 113 geographically diverse populations (fig. S1), 98 African Americans, and 21 Yemenites (table S1). To incorporate preexisting African data and to place African genetic variability into a worldwide context, we integrated these data with data from the panel of markers genotyped in 952 worldwide individuals from the CEPH-HGDP (Centre d'Étude du Polymorphisme Humain–Human Genome Diversity Panel) (*8*–*10*) in 432 individuals of Indian descent (*11*) and in 10 Native Australians (tables S1 and S2).

African variation in a worldwide context. African and African American populations, with the exception of the Dogon of Mali, show the highest levels of within-population genetic diversity ($\theta = 4N_e\mu$, where θ is the level of genetic diversity based on variance of microsatellite allele length, N_e is the effective population size, and μ is the microsatellite mutation rate) (figs. S2 and S3). In addition, genetic diversity declines with distance from Africa (fig. S2, A to C), consistent with proposed serial founder effects resulting from the migration of modern humans out of Africa and across the globe (*9*, *11*–*13*). Within Africa, genetic diversity estimated from expected heterozygosity significantly correlates with estimates from microsatellite variance (fig. S4) (*4*) and varies by linguistic, geographic, and subsistence classifications (fig. S5). Three hunter-gatherer populations (Baka Pygmies, Bakola Pygmies, and San) were among the five populations with the highest levels of genetic diversity based on variance estimates (fig. S2A) (*4*). In addition, more private alleles exist in Africa than in other regions (fig. S6A). Consistent with bidirectional gene flow (*14*), African and Middle Eastern populations shared the greatest number of alleles absent from all other populations (fig. S6B). Within Africa, the most private alleles were in southern Africa, reflecting those in southern African Khoesan (SAK) San and !Xun/Khwe populations (fig. S6C) (*12*). Eastern and Saharan Africans shared the most alleles absent from other African populations examined (fig. S6D).

The proportion of genetic variation among all studied African populations was 1.71% (table S3). In comparison, Native American and Oceanic populations showed the greatest proportion of genetic variation among populations (8.36% and 4.59%, respectively), most likely due to genetic drift (*9*, *15*, *16*). Distinct patterns of the distribution of variation among African populations classified by geography, language, and subsistence were also observed (*4*).

[1]Department of Biology, University of Maryland, College Park, MD 20742, USA. [2]Departments of Genetics and Biology, University of Pennsylvania, Philadelphia, PA 19104, USA. [3]Independent researcher, Sharon, CT 06069, USA. [4]Department of History, University of California, Los Angeles, CA 90095, USA. [5]Dipartimento di Biologia ed Evoluzione, Università di Ferrara, 44100 Ferrara, Italy. [6]UMR 208, IRD-MNHN, Musée de l'Homme, 75116 Paris, France. [7]Ministère de la Recherche Scientifique et de l'Innovation, BP 1457, Yaoundé, Cameroon. [8]Malaria Research and Training Center, University of Bamako, Bamako, Mali. [9]Department of Molecular Biology, Institute of Endemic Diseases, University of Khartoum, 15-13 Khartoum, Sudan. [10]Department of Pathology, Faculty of Health Sciences, University of Stellenbosch, Tygerberg 7505, South Africa. [11]Department of Biochemistry, Muhimbili University of Health and Allied Sciences, Dar es Salaam, Tanzania. [12]Departments of Genetics and Community and Family Medicine, Dartmouth Medical School, Lebanon, NH 03756, USA. [13]Kenya Medical Research Institute, Center for Biotechnology Research and Development, 54840-00200 Nairobi, Kenya. [14]Division of Human Genetics, Faculty of Health Sciences, University of Stellenbosch, Tygerberg 7505, South Africa. [15]Laboratory of Genomic Diversity, National Cancer Institute, Frederick, MD 21702, USA. [16]International Biomedical Research in Africa, Abuja, Nigeria. [17]Marshfield Clinic Research Foundation, Marshfield, WI 54449, USA. [18]Department of Molecular Physiology and Biophysics, Center for Human Genetics Research, Vanderbilt University, Nashville, TN 37232, USA.

*To whom correspondence should be addressed. E-mail: tishkoff@mail.med.upenn.edu

†Present address: Department of Evolutionary Genetics, Max Planck Institute for Evolutionary Biology, 24306 Plön, Germany.

‡These authors contributed equally to this work.

§These authors contributed equally to this work.

‖Present address: Department of Internal Medicine, Ohio State University, Columbus, OH 43210, USA.

¶Present address: Office of Research and Development, National Center for Computational Toxicology, U.S. Environmental Protection Agency, Research Triangle Park, NC 27711, USA.

#Present address: College of Education, University of Maryland, College Park, MD 20742, USA.

Fig. 1. Neighbor-joining tree from pairwise D^2 genetic distances between populations (*65*). African population branches are color-coded according to language family classification. Population clusters by major geographic region are noted; bootstrap values above 700 out of 1000 are indicated by thicker lines and bootstrap number.

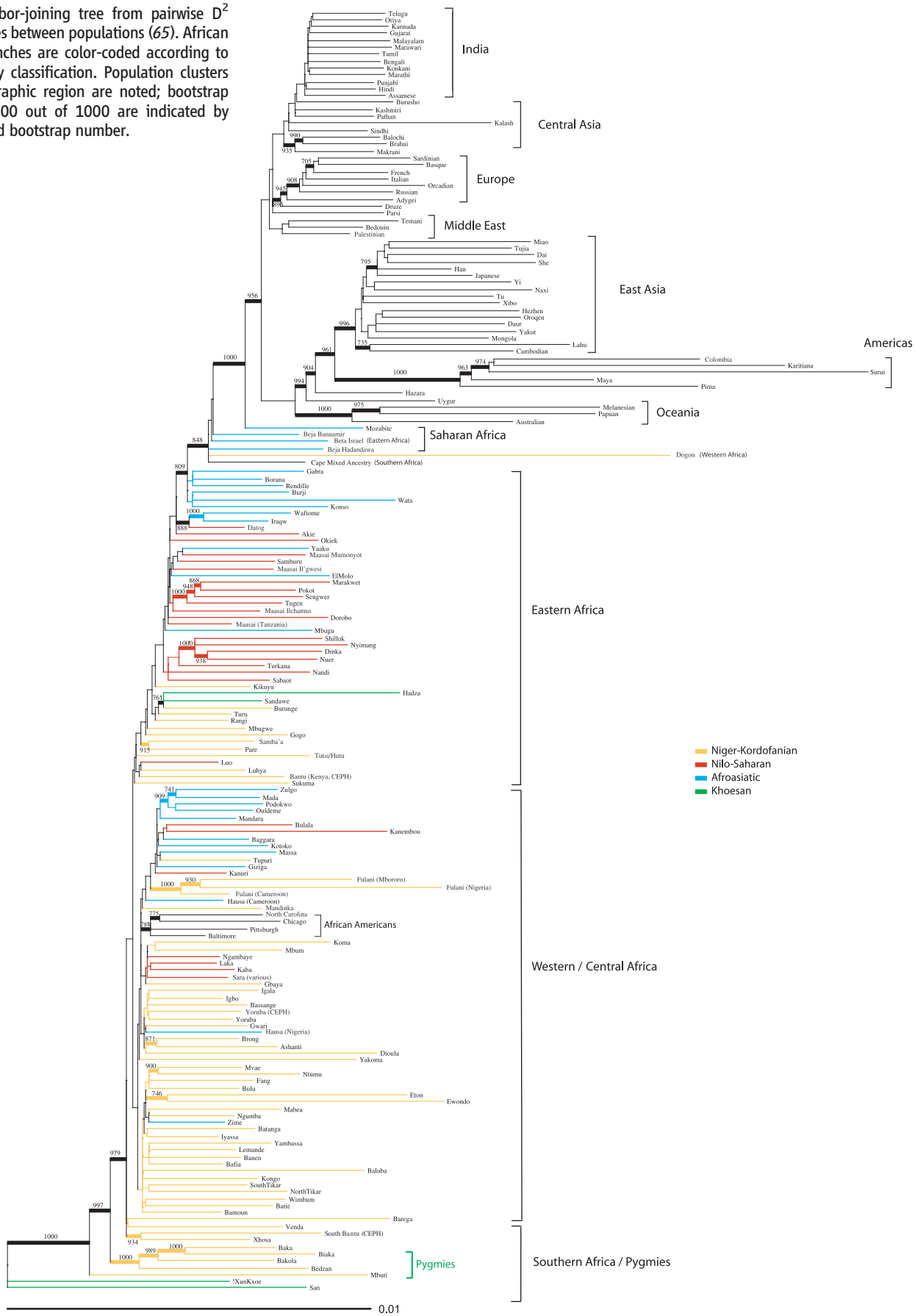

Phylogenetic trees constructed from genetic distances between populations generally showed clustering by major geographic region, both on a global scale and within Africa (Fig. 1 and figs. S7 and S8). Within Africa, the two SAK populations cluster together and are the most distant from other populations, consistent with mitochondrial DNA (mtDNA), Y chromosome, and autosomal chromosome diversity studies, indicating that SAK populations have the most diverged genetic lineages (*12*, *17*–*21*). The Pygmy populations cluster near the SAK populations in the tree constructed from D^2 genetic distances (Fig. 1), whereas the Hadza and Sandawe cluster near the SAK populations in the tree constructed from R_{ST} genetic distances (fig. S8) (*4*). Note that population clustering in the tree may reflect common ancestry and/or admixture. African populations with high levels of non-African admixture [e.g., the Cape Mixed Ancestry (CMA) population, commonly referred to as "Cape Coloured" in South Africa] cluster in positions that are intermediate between Africans and non-Africans, whereas the African American populations, which are relatively less admixed with non-Africans, cluster more closely with West Africans. Additionally, populations with high levels of genetic drift (i.e., the Americas, Oceania, and Pygmy, Hadza, and SAK hunter-gatherers) have longer branch lengths.

Geographic distances (great circle routes) and genetic distances $(\delta\mu)^2$ between population pairs were significantly correlated, consistent with an isolation-by-distance model (figs. S9 to S11 and table S4) (*13*). A heterogeneous pattern of correlations across global regions was observed, consistent with a previous study (*16*); the strongest correlations were in Europe and the Middle East (Spearman's $\rho = 0.88$ and 0.83, respectively; $P \leq 0.0001$ for both), followed by Africa (Spearman's $\rho = 0.40$; $P < 0.0001$). Correlations were not significant for central Asia or India. Within Africa, the strongest correlations between genetic and geographic distances were in Saharan Africa and central Africa (Spearman's $\rho = 0.76$ and 0.55, respectively; $P < 0.0001$ for both) (fig. S11 and table S4). The smallest correlation was observed in eastern Africa ($\rho = 0.19$; $P < 0.0001$).

Genetic structure on a global level. Global patterns of genetic structure and individual ancestry were inferred by principal components analysis (PCA) (*22*) (Fig. 2A) and a Bayesian model-based clustering approach with STRUCTURE (*23*) (Figs. 3 and 4 and figs. S12 to S14). Worldwide, 72 significant principal components (PCs) were identified by PCA ($P < 0.05$) (*22*). PC1 (accounting for 19.5% of the extracted variation) distinguishes Africans from non-Africans. The CMA and African American individuals cluster between Africans and non-Africans, reflecting both African and non-African ancestry. PC2 (5.01%) distinguishes Oceanians, East Asians, and Native Americans from others. PC3 (3.5%) distinguishes the Hadza hunter-gatherers from others. The remaining PCs each extract less than 3% of the variation, and the 22nd to 72nd PCs extract less than 1% combined, with some minor PCs corresponding to regional and/or ethnically defined populations, consistent with STRUCTURE results below.

STRUCTURE analysis revealed 14 ancestral population clusters ($K = 14$) on a global level (Figs. 3 and 4) (*4*). Middle Eastern and Oceanic populations exhibit low levels of East African ancestry up to $K = 8$, consistent with possible gene flow into these regions and with studies suggesting early migration of modern humans into southern Asia and Oceania (*16*, *24*). The Hadza, and to a lesser extent the Pygmy, SAK, and Sandawe hunter-gatherers, are distinguished at $K = 5$. The 11th cluster ($K = 11$) distinguishes Mbuti Pygmy and SAK individuals, indicating common ancestry of these geographically distant hunter-gatherers. A number of Africans (predominantly CMA, Fulani, and eastern Afroasiatic speakers) exhibit low to moderate levels of European–Middle Eastern ancestry, consistent with possible gene flow from those regions. We found more African substructure on a global level (nine clusters) than previously observed (*9*–*12*, *20*). A phylogenetic tree of genetic distances from inferred ancestral clusters (fig. S14) indicates that within Africa, the Pygmy and SAK associated ancestral clusters (AACs) form a clade, as do the Hadza and Sandawe AACs and the Nilo-Saharan and Chadic AACs, reflecting their ancient common ancestries.

Genetic structure within Africa. PCA of genetic variation within Africa indicated the presence of 43 significant PCs ($P < 0.05$ with a Tracy-Widom distribution). PC1 (10.8% of the extracted variation) distinguishes eastern and Saharan Africa from western, central, and southern Africa (Fig. 2B). The second PC (6.1%) distinguishes the Hadza; the third PC (4.9%) distinguishes Pygmy and SAK individuals from other Africans. The fourth PC (3.7%) is associated with the Mozabites, some Dogon, and the CMA individuals, who show ancestry from the European–Middle Eastern cluster. The fifth PC (3.1%) is associated with SAK speakers. The 10th PC was of particular interest (2.2%) because it associates with the SAK, Sandawe, and some Dogon individuals, suggesting shared ancestry.

We incorporated geographic data into a Bayesian clustering analysis, assuming no admixture (TESS software) (*25*) and distinguished six clusters within continental Africa (Fig. 5A). The most geographically widespread cluster (orange) extends from far Western Africa (the Mandinka) through central Africa to the Bantu speakers of South Africa (the Venda and Xhosa) and corresponds to the distribution of the Niger-Kordofanian language family, possibly reflecting the spread of Bantu-speaking populations from near the Nigerian/Cameroon highlands across eastern and southern Africa within the past 5000 to 3000 years (*26*, *27*). Another inferred cluster includes the Pygmy and SAK populations (green), with a noncontiguous geographic distribution in central and southeastern Africa, consistent with the STRUCTURE (Fig. 3) and phylogenetic analyses (Fig. 1). Another geographically contiguous cluster extends across northern Africa (blue) into Mali (the Dogon), Ethiopia, and northern Kenya. With the exception of the

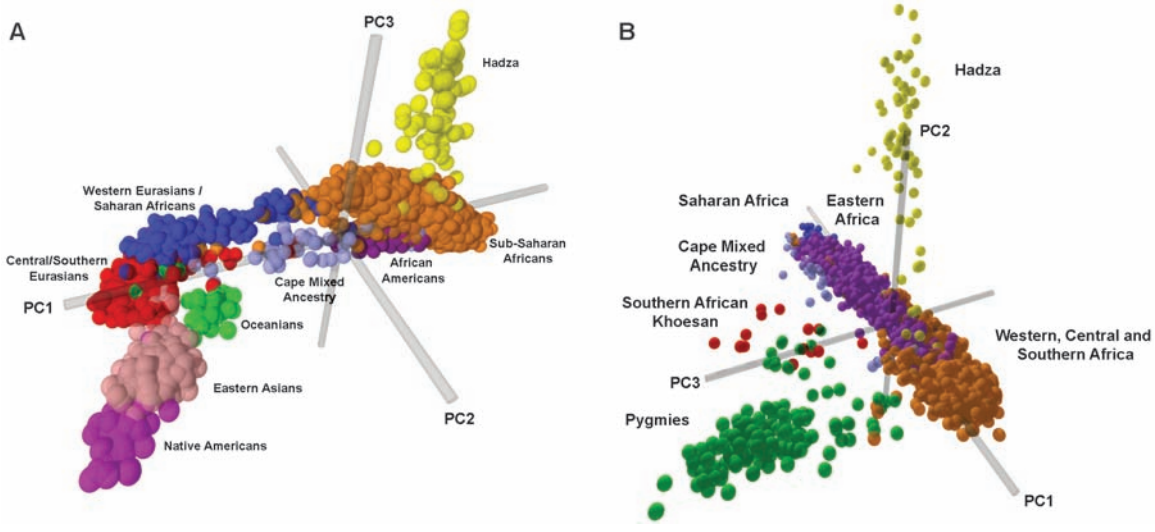

Fig. 2. Principal components analysis (*22*) created on the basis of individual genotypes. (**A**) Global data set and (**B**) African data set.

Dogon, these populations speak an Afroasiatic language. Chadic-speaking and Nilo-Saharan–speaking populations from Nigeria, Cameroon, and central Chad, as well as several Nilo-Saharan–speaking populations from southern Sudan, constitute another cluster (red). Nilo-Saharan and Cushitic speakers from the Sudan, Kenya, and Tanzania, as well as some of the Bantu speakers from Kenya, Tanzania, and Rwanda (Hutu/Tutsi),

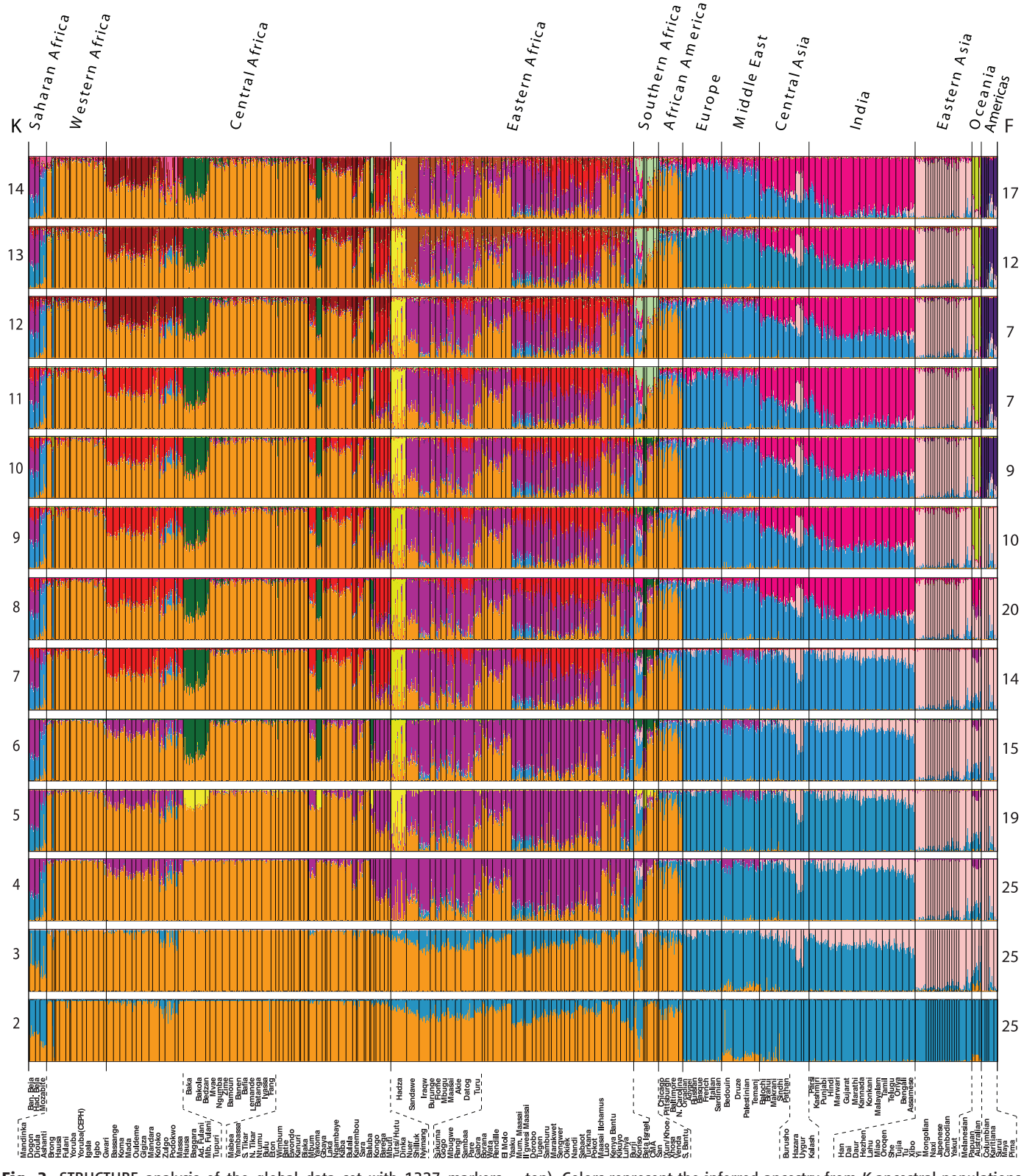

Fig. 3. STRUCTURE analysis of the global data set with 1327 markers genotyped in 3945 individuals. Each vertical line represents an individual. Individuals were grouped by self-identified ethnic group (at bottom) and ethnic groups are clustered by major geographic region (at top). Colors represent the inferred ancestry from *K* ancestral populations. STRUCTURE results for $K = 2$ to 14 (left) are shown with the number of similar runs (F) for the primary mode of 25 STRUCTURE runs at each *K* value (right).

constitute another cluster (purple), reflecting linguistic evidence for gene flow among these populations over the past ~5000 years (*28*, *29*). Finally, the Hadza are the sole constituents of a sixth cluster (yellow), consistent with their distinctive genetic structure identified by PCA and STRUCTURE.

STRUCTURE analysis of the Africa data set indicated 14 ancestral clusters (Fig. 5, B and C, and figs. S15 to S18). Analyses of subregions within Africa indicated additional substructure (figs. S19 to S29). At low K values, the Africa-wide STRUCTURE results (fig. S15) recapitulated the PCA and worldwide STRUCTURE results. However, as K increased, additional population clusters were distinguished (*4*): the Mbugu [who speak a mixed Bantu and Cushitic language (*30*), shown in dark purple]; Cushitic-speaking individuals of southern Ethiopian origin (light purple); Nilotic Nilo-Saharan–speaking individuals (red); central Sudanic Nilo-Saharan–speaking individuals (tan); and Chadic-speaking and Baggara individuals (maroon). At $K = 14$, subtle substructure between East African Bantu speakers (light orange) and West Central African Bantu speakers (medium orange), and individuals from Nigeria and farther west, who speak various non-Bantu Niger-Kordofanian languages (dark orange), was also apparent (Fig. 5, B and C). Bantu speakers of South Africa (Xhosa, Venda) showed substantial levels of the SAK and western African Bantu AACs and low levels of the East African Bantu AAC (the latter is also present in Bantu speakers from Democratic Republic of Congo and Rwanda). Our results indicate distinct East African Bantu migration into southern Africa and are consistent with linguistic and archeological evidence of East African Bantu migration from an area west of Lake Victoria (*28*) and the incorporation of Khoekhoe ancestry into several of the Southeast Bantu populations ~1500 to 1000 years ago (*31*).

High levels of heterogeneous ancestry (i.e., multiple cluster assignments) were observed in nearly all African individuals, with the exception of western and central African Niger-Kordofanian speakers (medium orange), who are relatively homogeneous at large K values (Fig. 5C and fig.

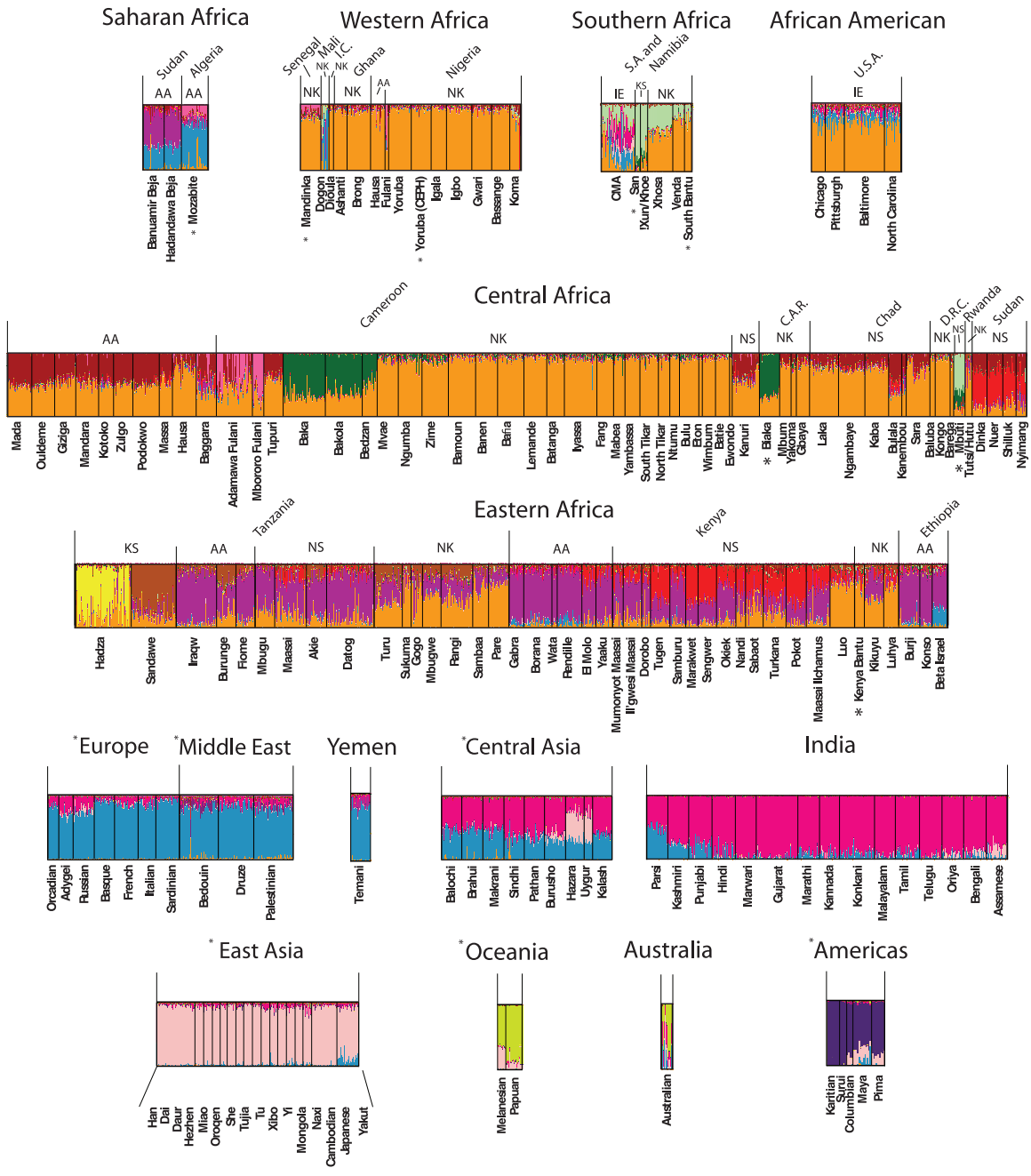

Fig. 4. Expanded view of STRUCTURE results at $K = 14$. Populations from the CEPH diversity panel are identified by asterisks. Languages spoken by populations are classified as Niger-Kordofanian (NK), Nilo-Saharan (NS), Afroasiatic (AA), Khoesan (KS), or Indo-European (IE).

Fig. 5. Geographic and genetic structure of populations within Africa. (**A**) Geographic discontinuities among African populations using TESS, assuming a model of no population admixture (*25*). Circles indicate location of populations included in the study. (**B**) Inferred proportions of ancestral clusters from STRUCTURE analysis at $K = 14$ for individuals grouped by geographic region and language classification. Classifications of languages spoken by self-identified ethnic affiliation in the Africans are as in Fig. 1. (**C**) Inferred proportion of ancestral clusters in individuals from STRUCTURE analysis at $K = 14$.

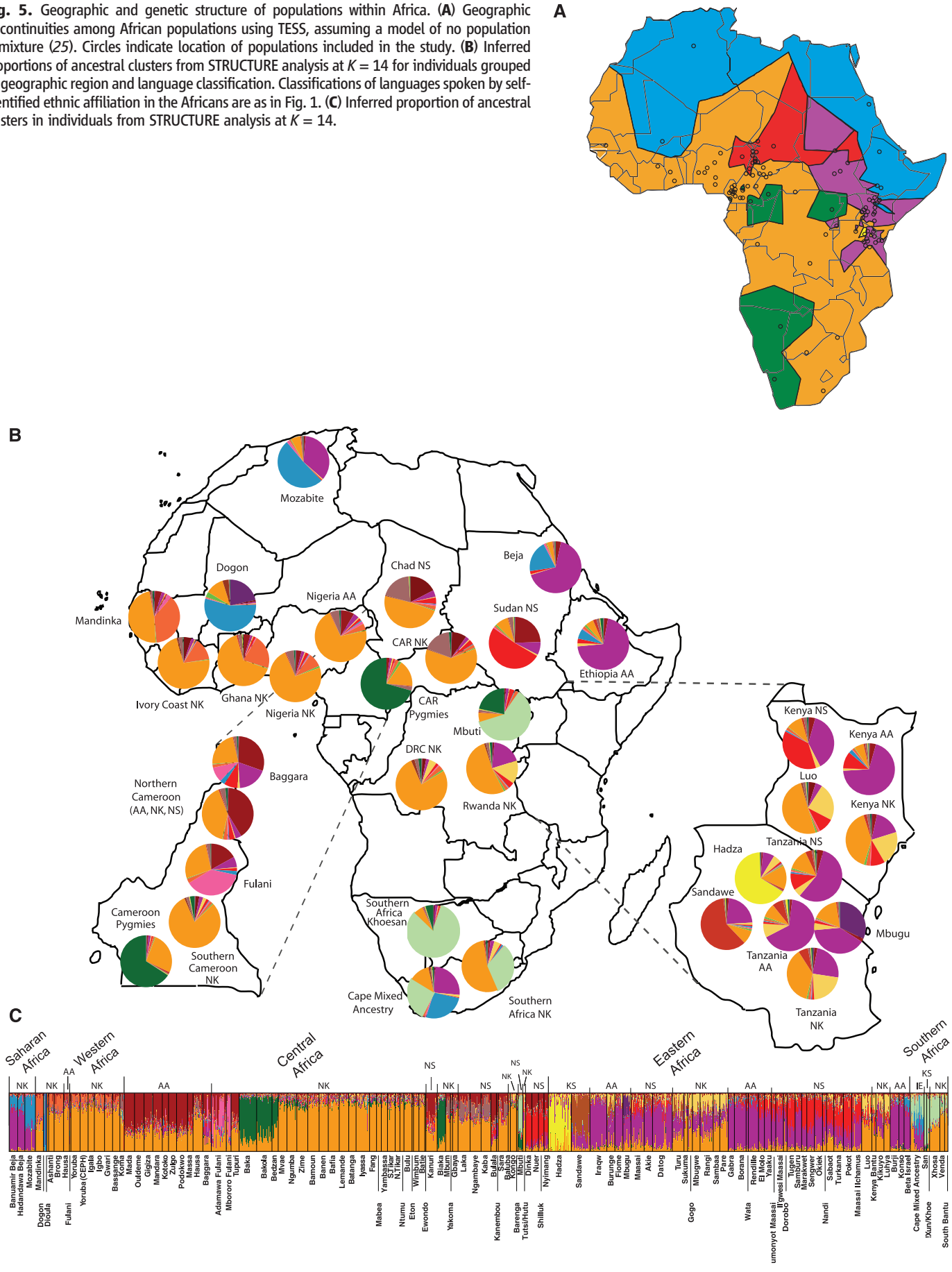

S15). Considerable Niger-Kordofanian ancestry (shades of orange) was observed in nearly all populations, reflecting the recent spread of Bantu speakers across equatorial, eastern, and southern Africa (*27*) and subsequent admixture with local populations (*28*). Many Nilo-Saharan–speaking populations in East Africa, such as the Maasai, show multiple cluster assignments from the Nilo-Saharan (red) and Cushitic (dark purple) AACs, in accord with linguistic evidence of repeated Nilotic assimilation of Cushites over the past 3000 years (*32*) and with the high frequency of a shared East African–specific mutation associated with lactose tolerance (*33*).

Our data support the hypothesis that the Sahel has been a corridor for bidirectional migration between eastern and western Africa (*34*–*36*). The highest proportion of the Nilo-Saharan AAC was observed in the southern and central Sudanese populations (Nuer, Dinka, Shilluk, and Nyimang), with decreasing frequency from northern Kenya (e.g., Pokot) to northern Tanzania (Datog, Maasai) (Fig. 5, B and C, and fig. S15). Additionally, all Nilo-Saharan–speaking populations from Kenya, Tanzania, southern Sudan, and Chad clustered with west central Afroasiatic Chadic–speaking populations in the global analysis at $K \leq 11$ (Fig. 3), which is consistent with linguistic and archeological data suggesting bidirectional migration of Nilo-Saharans from source populations in Sudan within the past ~10,500 to 3000 years (*4*, *29*). The proposed migration of proto-Chadic Afroasiatic speakers ~7000 years ago from the central Sahara into the Lake Chad Basin may have resulted in a Nilo-Saharan to Afroasiatic language shift among Chadic speakers (*37*). However, our data suggest that this shift was not accompanied by large amounts of Afroasiatic gene flow. Other populations of interest, including the Fulani (Nigeria and Cameroon), the Baggara Arabs (Cameroon), the Koma (Nigeria), and Beja (Sudan), are discussed in (*4*).

Genetic structure in East Africa. East Africa, the hypothesized origin of the migration of modern humans out of Africa, has a remarkable degree of ethnic and linguistic diversity, as reflected by the greatest level of regional substructure in Africa (figs. S15, S16, and S19 to S21). The diversity among populations from this region reflects the proposed long-term presence of click-speaking Hadza and Sandawe hunter-gatherers and successive waves of immigration of Cushitic, Nilotic, and Bantu populations within the past 5000 years (*4*, *29*, *32*, *38*, *39*). Within eastern Africa, including southern and central Sudan, clustering is primarily associated with language families, including Niger-Kordofanian, Afroasiatic, Nilo-Saharan, and two click-speaking hunter-gatherer groups: the Sandawe and Hadza (figs. S19 to S21). However, individuals from the Afroasiatic Cushitic Iraqw and Gorowa (Fiome) and the Nilo-Saharan Datog, who are in close geographic proximity, also cluster. Additionally, several hunter-gatherer populations were distinct, including the Okiek, Akie, and Yaaku and El Molo. Of particular interest is the common ancestry of the Akie (who have remnants of a Cushitic language) and the Eastern Cushitic El Molo and Yaaku at $K = 9$, consistent with linguistic data suggesting that these populations originated from southern Ethiopia and migrated into Kenya and Tanzania within the past ~4000 years (*4*, *29*, *32*, *39*).

Origins of hunter-gatherer populations in Africa. Our analyses demonstrate potential shared ancestry of a number of populations who practice (or until recently practiced) a traditional hunting and gathering lifestyle. For example, we observed a Hadza AAC (yellow) at $K = 5$ and $K = 3$ in the global and African STRUCTURE analyses, respectively (Fig. 3 and fig. S15), which is at moderate levels (0.18 to 0.32) in the SAK and Pygmy populations and at low levels (0.03 to 0.04) in the Sandawe and neighboring Burunge with whom the Sandawe have admixed (tables S8 and S9). The SAK and Pygmies continue to cluster at higher K values (Fig. 3 and fig. S15) and in the TESS (Fig. 5A) and phylogenetic (Fig. 1) analyses, consistent with an exclusively shared Y chromosome lineage (B2b4) (*40*). Additionally, we observed clustering of the SAK, Sandawe, and Hadza in the R_{ST} phylogenetic tree (fig. S8) and of the SAK, Sandawe, and Mbuti Pygmies at low K values in the secondary modes of Africa STRUCTURE analyses (fig. S16), consistent with observed low frequency of the Khoesan-specific mitochondrial haplotype (L0d) in the Sandawe (*18*, *19*), the presence of Khoesan-related rock art near the Sandawe homeland (*41*), and similarities between the Sandawe and SAK languages (*42*). These results suggest the possibility that the SAK, Hadza, Sandawe, and Pygmy populations are remnants of a historically more widespread proto–Khoesan-Pygmy population of hunter-gatherers. Analyses of mtDNA and Y chromosome lineages in the Khoesan-speaking populations suggest that divergence may be >35,000 years ago (*4*, *17*–*19*). The shared ancestry, identified here, of Khoesan-speaking populations with the Pygmies of central Africa suggests the possibility that Pygmies, who lost their indigenous language, may have originally spoken a Khoesan-related language, consistent with shared music styles between the SAK and Pygmies (*4*, *43*).

Shared ancestry of western and eastern Pygmies, who do not become differentiated until larger K values in STRUCTURE analyses (Fig. 3 and fig. S15), was also supported by the phylogenetic trees (Fig. 1 and figs. S7 and S8), consistent with mtDNA and autosomal studies indicating that the western and eastern Pygmies diverged >18,000 years ago (*44*–*47*). Western Pygmy populations usually clustered (Fig. 3 and fig. S15), consistent with a proposed recent common ancestry within the past ~3000 years (*48*). However, subtle substructure within the western Pygmies was apparent in the analysis of central Africa (fig. S24), probably due to recent geographic isolation and genetic drift. Asymmetric Bantu gene flow into Pygmy populations was also observed, with Bantu ancestry ranging from 0.13 in Mbuti to 0.54 in the Bedzan (table S8), consistent with prior studies (*40*, *44*, *49*, *50*).

The Hadza, with a census size of ~1000, were genetically distinct on a global level with STRUCTURE, PCA, and TESS (Figs. 2 to 5), consistent with linguistic data indicating that the Hadza language is divergent from or unrelated to other Khoesan languages (*42*, *51*, *52*). The Hadza, who have maintained a traditional hunter-gatherer lifestyle, show low levels of asymmetric gene flow from neighboring populations, whereas the Sandawe, with a census size of >30,000 (*39*), show evidence of bidirectional gene flow with neighboring populations, from whom they may have adopted mixed farming technologies (Figs. 3 to 5 and fig. S15). In fact, we observed high levels of the Sandawe AAC in northern Tanzania and low levels in northern Kenya and southern Ethiopia (Fig. 3 and fig. S15) ($K = 8$ to 13), consistent with linguistic and genetic data suggesting that Khoesan populations may once have extended from Somalia through eastern Africa and into southern Africa (*28*, *38*, *53*–*55*). Although the Hadza and Sandawe show evidence of common ancestry (Fig. 1 and figs. S7, S8, S14, S18, and S21), we observe no evidence of recent gene flow between them despite their geographic proximity, consistent with mtDNA and Y chromosome studies indicating divergence >15,000 years ago (*19*). The origins of other African hunter-gatherer populations (Dorobo, Okiek, Yaaku, Akie, El Molo, and Wata) are discussed in (*4*).

Origins of human migration within and out of Africa. The geographic origin for the expansion of modern humans was inferred, as in (*13*), from the correlation between genetic diversity and geographic position of populations (r) (figs. S30 and S31). Both the point of origin of human migration and waypoint for the out-of-Africa migration were optimized to fit a linear relationship between genetic diversity and geographic distance (*4*). This analysis indicates that modern human migration originated in southwestern Africa, at 12.5°E and 17.5°S, near the coastal border of Namibia and Angola, corresponding to the current San homeland, with the waypoint in northeast Africa at 37.5°E, 22.5°N near the midpoint of the Red Sea (figs. S2C, S30, and S31). However, the geographic distribution of genetic diversity in modern populations may not reflect the distribution of those populations in the past, although our waypoint analysis is consistent with other studies suggesting a northeast African origin of migration of modern humans out of Africa (*1*, *56*).

Correlation between genetic and linguistic diversity in Africa. Genetic clustering of populations was generally consistent with language classification, with some exceptions (Fig. 1 and fig. S32). For example, the click-speaking Hadza and Sandawe, classified as Khoesan, were separated from the SAK populations in the D^2 and $(\delta\mu)^2$ phylogenetic trees (Fig. 1 and fig. S7).

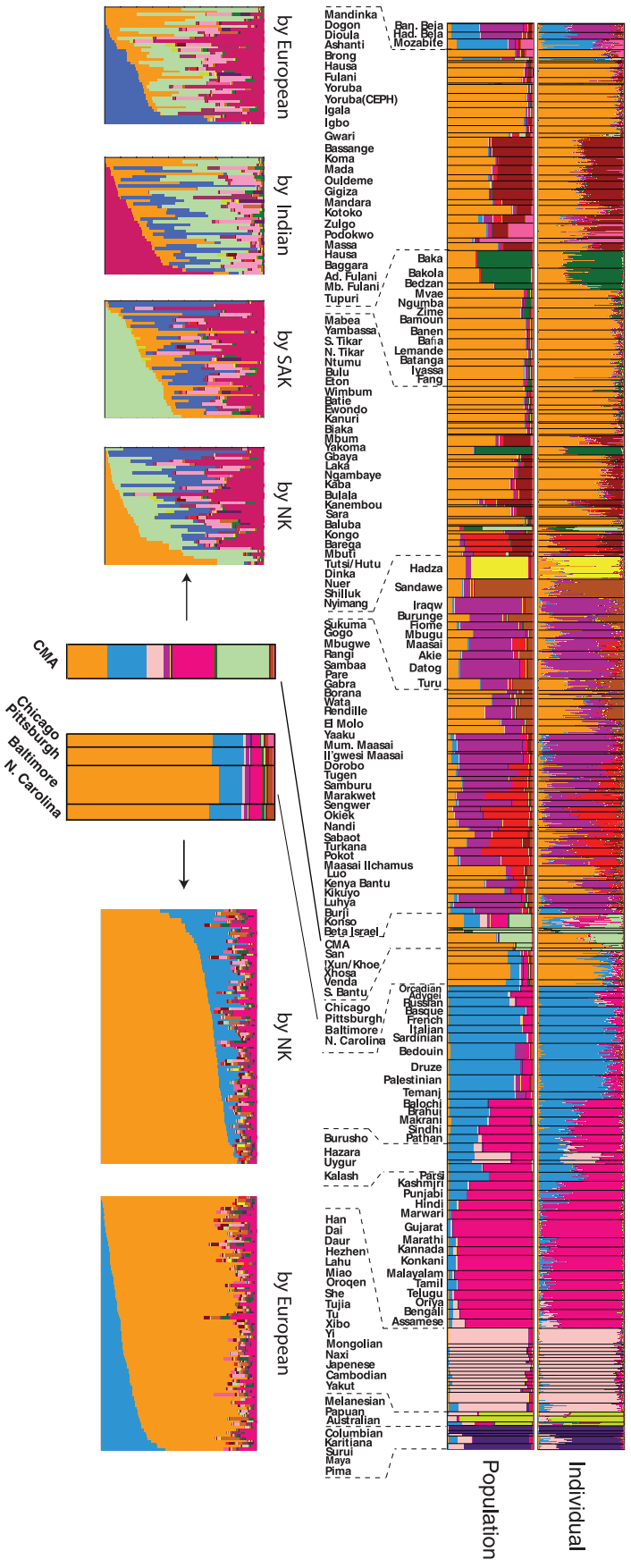

Fig. 6. Analyses of Cape Mixed Ancestry (CMA) and African American populations. Frequencies of inferred ancestral clusters are shown for $K = 14$ with the global data set for individuals (top row) and proportion of AACs in self-identified populations (bottom row). The proportions of AACs in the CMA and African American populations are highlighted in the center bottom row; proportions of AACs in individuals, sorted by Niger-Kordofanian, European, SAK, and/or Indian ancestry, are shown to the left and right, bottom row.

However, this observation is consistent with linguistic studies indicating that these Khoesan languages are highly divergent (*42*, *51*) and may reflect gene flow between the Hadza and Sandawe with neighboring populations in East Africa subsequent to divergence from the SAK. Additionally, the Afroasiatic Chadic–speaking populations from northern Cameroon cluster close to the Nilo-Saharan–speaking populations from Chad, rather than with East African Afroasiatic speakers (Fig. 1), consistent with a language replacement among the Chadic populations.

Other divergences between genetic and linguistic classifications include the Pygmies, who lost their indigenous language and adopted the neighboring Niger-Kordofanian language (*27*), and the Fulani, who speak a West African Niger-Kordofanian language but cluster near the Chadic- and Central Sudanic–speaking populations in the phylogenies (Fig. 1 and figs. S7 and S8), consistent with Y chromosome studies (*34*). Additionally, the Nilo-Saharan–speaking Luo of Kenya show predominantly Niger-Kordofanian ancestry in the STRUCTURE analyses (orange) (Figs. 3 and 4, Fig. 5, B and C, and fig. S15) and cluster together with eastern African Niger-Kordofanian–speaking populations in the phylogenetic trees (Fig. 1 and figs. S7 and S8).

Both language and geography explained a significant proportion of the genetic variance, but differences exist between and within the language families (table S5 and fig. S33, A to C) (*4*). For example, among the Niger-Kordofanian speakers, with or without the Pygmies, more of the genetic variation is explained by linguistic variation ($r^2 = 0.16$ versus 0.11, respectively; $P < 0.0001$ for both) than by geographic variation ($r^2 = 0.02$ for both; $P < 0.0001$ for both), consistent with recent long-range Bantu migration events. The reverse was true for Nilo-Saharan speakers ($r^2 = 0.06$ for linguistic distance versus 0.21 for geographic distance; $P < 0.0001$ for both), possibly due to admixture among Nilo-Saharan–, Cushitic-, and Bantu-speaking populations in eastern Africa, which might reduce the variation explained by language. The Afroasiatic family had the highest r^2 for both linguistic and geographic distances (0.20 and 0.34, respectively). However, when subfamilies were analyzed independently, the Chadic-speaking populations showed a strong association between geography and genetic variation (0.39), but not between linguistic and genetic variation (0.0012), as expected on the basis of a possible language replacement, whereas the Cushitic-speaking populations were significant for both (0.29 and 0.27, respectively) (*4*).

Genetic ancestry of African Americans and CMA populations. In contrast to prior studies of African Americans (*57*–*61*), we inferred African American ancestry with the use of genome-wide nuclear markers from a large and diverse set of African populations. African American populations from Chicago, Baltimore, Pittsburgh, and North Carolina showed substantial ancestry from

the African Niger-Kordofanian AAC, most common in western Africa (means 0.69 to 0.74), and from the European–Middle Eastern AAC (means 0.11 to 0.15) (Fig. 6 and tables S6 and S8), consistent with prior genetic studies and the history of the slave trade (*4*, *57*–*62*). European and African ancestry levels varied considerably among individuals (Fig. 6). We also detected low levels of ancestry from the Fulani AAC (means 0.0 to 0.03, individual range 0.00 to 0.14), Cushitic AAC (means 0.02, individual range 0.00 to 0.10), Sandawe AAC (means 0.01 to 0.03, individual range 0.0 to 0.12), East Asian AAC (means 0.01 to 0.02, individual range 0.0 to 0.08), and Indian AAC (means 0.04 to 0.06, individual range 0.01 to 0.17) (table S6) (*4*). We observed very low levels of Native American ancestry, although other U.S. regions may reveal Native American ancestry (*57*).

Supervised STRUCTURE analysis (fig. S34) (*4*) was used to infer African American ancestry from global training populations, including both Bantu (Lemande) and non-Bantu (Mandinka) Niger-Kordofanian–speaking populations (fig. S34 and table S7). These results were generally consistent with the unsupervised STRUCTURE analysis (table S6) and demonstrate that most African Americans have high proportions of both Bantu (~0.45 mean) and non-Bantu (~0.22 mean) Niger-Kordofanian ancestry, concordant with diasporas originating as far west as Senegambia and as far south as Angola and South Africa (*62*). Thus, most African Americans are likely to have mixed ancestry from different regions of western Africa. This observation, together with the subtle substructure observed among Niger-Kordofanian speakers, will make it a challenge to trace the ancestry of African Americans to specific ethnic groups in Africa, unless considerably more markers are used.

The CMA population shows the highest levels of intercontinental admixture of any global population, with nearly equal high levels of SAK ancestry (mean 0.25, individual range 0.01 to 0.48), Niger-Kordofanian ancestry (mean 0.19, individual range 0.01 to 0.71), Indian ancestry (mean 0.20, individual range 0.0 to 0.69), and European ancestry (mean 0.19, individual range 0.0 to 0.86) (Fig. 6 and tables S6 and S8). The CMA population also has low levels of East Asian ancestry (mean 0.08, individual range 0.0 to 0.21) and Cushitic ancestry (mean 0.03, individual range 0.0 to 0.40). These results are consistent with the supervised STRUCTURE analyses (fig. S34 and table S7) and with the history of the CMA population (*4*, *63*).

The genetic, linguistic, and geographic landscape of Africa. The differentiation observed among African populations is likely due to ethnicity, language, and geography, as well as technological, ecological, and climatic shifts (including periods of glaciation and warming) that contributed to population size fluctuations, fragmentations, and dispersals in Africa (*1*, *4*, *34*, *64*). We observed significant associations between genetic and geographic distance in all regions of Africa, although their strengths varied. We also observed significant associations between genetic and linguistic diversity, reflecting the concomitant spread of languages, genes, and often culture [e.g., the spread of farming during the Bantu expansion (*28*)]. Of interest for future anthropological studies are the cases in which populations have maintained their culture in the face of extensive genetic introgression (e.g., Maasai and Pygmies) and populations that have maintained both cultural and genetic distinction (e.g., Hadza).

Given the extensive amount of ethnic diversity in Africa, additional sampling—particularly from underrepresented regions such as North and Central Africa—is important. Because of the extensive levels of substructure in Africa, ethnically and geographically diverse African populations need to be included in resequencing, genome-wide association, and pharmacogenetic studies to identify population- or region-specific functional variants associated with disease or drug response (*1*). The high levels of mixed ancestry from genetically divergent ancestral population clusters in African populations could also be useful for mapping by admixture disequilibrium. Future large-scale resequencing and genotyping of Africans will be informative for reconstructing human evolutionary history, for understanding human adaptations, and for identifying genetic risk factors (and potential treatments) for disease in Africa.

References and Notes

1. M. C. Campbell, S. A. Tishkoff, *Annu. Rev. Genomics Hum. Genet.* **9**, 403 (2008).
2. F. A. Reed, S. A. Tishkoff, *Curr. Opin. Genet. Dev.* **16**, 597 (2006).
3. Ethnologue (www.ethnologue.com).
4. See supporting material on *Science* Online.
5. S. A. Tishkoff, S. M. Williams, *Nat. Rev. Genet.* **3**, 611 (2002).
6. G. Sirugo *et al*., *Hum. Genet.* **123**, 557 (2008).
7. J. K. Pritchard, M. Stephens, N. A. Rosenberg, P. Donnelly, *Am. J. Hum. Genet.* **67**, 170 (2000).
8. H. M. Cann *et al*., *Science* **296**, 261 (2002).
9. N. A. Rosenberg *et al*., *Science* **298**, 2381 (2002).
10. N. A. Rosenberg *et al*., *PLoS Genet.* **1**, e70 (2005).
11. N. A. Rosenberg *et al*., *PLoS Genet.* **2**, e215 (2006).
12. M. Jakobsson *et al*., *Nature* **451**, 998 (2008).
13. S. Ramachandran *et al*., *Proc. Natl. Acad. Sci. U.S.A.* **102**, 15942 (2005).
14. P. Forster, V. Romano, *Science* **316**, 50 (2007).
15. S. Wang *et al*., *PLoS Genet.* **3**, e185 (2007).
16. J. S. Friedlaender *et al*., *PLoS Genet.* **4**, e19 (2008).
17. D. M. Behar *et al*., *Am. J. Hum. Genet.* **82**, 1130 (2008).
18. M. K. Gonder, H. M. Mortensen, F. A. Reed, A. de Sousa, S. A. Tishkoff, *Mol. Biol. Evol.* **24**, 757 (2007).
19. S. A. Tishkoff *et al*., *Mol. Biol. Evol.* **24**, 2180 (2007).
20. J. Z. Li *et al*., *Science* **319**, 1100 (2008).
21. Y. S. Chen *et al*., *Am. J. Hum. Genet.* **66**, 1362 (2000).
22. N. Patterson, A. L. Price, D. Reich, *PLoS Genet.* **2**, e190 (2006).
23. J. K. Pritchard, M. Stephens, P. Donnelly, *Genetics* **155**, 945 (2000).
24. P. Forster, S. Matsumura, *Science* **308**, 965 (2005).
25. O. Francois, S. Ancelet, G. Guillot, *Genetics* **174**, 805 (2006).
26. C. Ehret, *Int. J. Afr. Hist. Stud.* **34**, 5 (2001).
27. K. A. Klieman, *"The Pygmies Were Our Compass": Bantu and Batwa in the History of West Central Africa, Early Times to c. 1900 C.E.* (Heinemann, Portsmouth, NH, 2003).
28. C. Ehret, *An African Classical Age: Eastern and Southern Africa in World History, 1000 B.C. to A.D. 400* (Univ. Press of Virginia, Charlottesville, VA, 1998).
29. C. Ehret, in *Culture History in the Southern Sudan*, J. Mack, P. Robertshaw, Eds. (British Institute in Eastern Africa, Nairobi, 1983), pp. 19–48.
30. C. Ehret, *The Historical Reconstruction of Southern Cushitic Phonology and Vocabulary* (Reimer, Berlin, 1980).
31. C. Ehret, *Southern African Humanities* **30**, 7 (2008).
32. C. Ehret, *Ethiopians and East Africans: The Problem of Contacts* (East African Publishing House, Nairobi, 1974).
33. S. A. Tishkoff *et al*., *Nat. Genet.* **39**, 31 (2007).
34. H. Y. Hassan, P. A. Underhill, L. L. Cavalli-Sforza, M. E. Ibrahim, *Am. J. Phys. Anthropol.* **137**, 316 (2008).
35. R. E. Bereir *et al*., *Eur. J. Hum. Genet.* **15**, 1183 (2007).
36. V. Cerny, A. Salas, M. Hajek, M. Zaloudkova, R. Brdicka, *Ann. Hum. Genet.* **71**, 433 (2007).
37. C. Ehret, in *West African Linguistics: Studies in Honor of Russell G. Schuh,* P. Newman, L. Hyman, Eds. (Ohio State Univ., Columbus, OH, 2006), pp. 56–66.
38. S. H. Ambrose, in *The Archaeological and Linguistic Reconstruction of African History*, C. Ehret, M. Posnansky, Eds. (Univ. of California Press, Berkeley, CA, 1982), pp. 104–157.
39. J. L. Newman, *The Peopling of Africa* (Yale Univ. Press, New Haven, CT, 1997).
40. E. T. Wood *et al*., *Eur. J. Hum. Genet.* **13**, 867 (2005).
41. L. Lim, thesis, Brown University (1992).
42. C. Ehret, *Sprache Gesch. Afrika* **7**, 105 (1986).
43. A. Lomax *et al*., in *Folk Song Style and Culture* (National Association for the Advancement of Science, Washington, DC, 1968), pp. 16–18, 26, 91–92.
44. L. Quintana-Murci *et al*., *Proc. Natl. Acad. Sci. U.S.A.* **105**, 1596 (2008).
45. C. Batini *et al*., *Mol. Phylogenet. Evol.* **43**, 635 (2007).
46. G. Destro-Bisol *et al*., *Am. Nat.* **163**, 212 (2004).
47. E. Patin *et al*., *PLoS Genet.* **5**, e1000448 (2009).
48. P. Verdu *et al*., *Curr. Biol.* **19**, 312 (2009).
49. G. Destro-Bisol *et al*., *Mol. Biol. Evol.* **21**, 1673 (2004).
50. V. Coia *et al*., *Am. J. Hum. Biol.* **16**, 57 (2004).
51. B. Sands, in *Language, Identity and Conceptualization Among the Khoisan*, M. Schladt, Ed. (Rudiger Kupper, Köln, Germany, 1998), vol. Bd 15, pp. 266–283.
52. E. D. Elderkin, *Sprache Gesch. Afrika* **4**, 67 (1982).
53. R. Scozzari *et al*., *Am. J. Hum. Genet.* **65**, 829 (1999).
54. O. Semino, A. S. Santachiara-Benerecetti, F. Falaschi, L. L. Cavalli-Sforza, P. A. Underhill, *Am. J. Hum. Genet.* **70**, 265 (2002).
55. L. L. Cavalli-Sforza, A. Piazza, P. Menozzi, *History and Geography of Human Genes* (Princeton Univ. Press, Princeton, NJ, 1994).
56. R. C. Walter *et al*., *Nature* **405**, 65 (2000).
57. E. J. Parra *et al*., *Am. J. Phys. Anthropol.* **114**, 18 (2001).
58. A. Salas *et al*., *Am. J. Phys. Anthropol.* **128**, 855 (2005).
59. J. M. Lind *et al*., *Hum. Genet.* **120**, 713 (2007).
60. M. W. Smith *et al*., *Am. J. Hum. Genet.* **74**, 1001 (2004).
61. E. J. Parra *et al*., *Am. J. Hum. Genet.* **63**, 1839 (1998).
62. Trans-Atlantic Slave Trade Database (www.slavevoyages.org/tast/index.faces).
63. G. T. Nurse, J. S. Weiner, T. Jenkins, *The Peoples of Southern Africa and Their Affinities* (Oxford Univ. Press, New York, 1985).
64. P. Mellars, *Proc. Natl. Acad. Sci. U.S.A.* **103**, 9381 (2006).
65. J. B. Reynolds *et al*., *Genetics* **105**, 767 (1983).

66. We thank the thousands of people who donated DNA samples used in this study. We thank D. Bygott, S. J. Deo, D. Guracha, J. Hanby, D. Kariuki, P. Lufungulo, A. Mabulla, A. A. Mohamed, W. Ntandu, L. A. Nyindodo, C. Plowe, and A. Tibwitta for assisting with sample collection; K. Panchapakesan and L. Pfeiffer for assistance in sample preparation; S. Dobrin for assistance with genotyping; J. Giles, J. Bartlett, N. Kodaman, and J. Jarvis for assistance with analyses; and N. Rosenberg, J. Pritchard, A. Brooks, J. S. Friedlaender, J. Jarvis, C. Lambert, B. Payseur, N. Patterson, and J. Plotkin for

helpful suggestions and discussions. Conducted in part using the ACCRE computing facility at Vanderbilt University, Nashville, TN. Supported by L. S. B. Leakey and Wenner Gren Foundation grants, NSF grants BCS-0196183, BSC-0552486, and BCS-0827436, NIH grants R01GM076637 and 1R01GM083606-01, and David and Lucile Packard and Burroughs Wellcome Foundation Career Awards (S.A.T.); NIH grant F32HG03801 (F.A.R.); and NIH grant R01 HL65234 (S.M.W. and J.H.M.). Genotyping was supported by the NHLBI Mammalian Genotyping Service. The content of this publication does not necessarily reflect the views or policies of the Department of Health and Human Services, nor does mention of trade names, commercial products, or organizations imply endorsement by the U.S. government. The project included in this manuscript has been funded in part with federal funds from the National Cancer Institute under contract N01-CO-12400. Original genotype data are available at http://research.marshfieldclinic.org/genetics/genotypingData_Statistics/humanDiversityPanel.asp. Data used for analyses in the current manuscript are available at www.med.upenn.edu/tishkoff/Supplemental/files.html and at http://chgr.mc.vanderbilt.edu/page/supplementary-data.

Supporting Online Material

www.sciencemag.org/cgi/content/full/1172257/DC1
Materials and Methods
SOM Text
Figs. S1 to S35
Tables S1 to S9
References

13 February 2009; accepted 17 April 2009
Published online 30 April 2009;
10.1126/science.1172257
Include this information when citing this paper.

REPORTS

Dispersion of the Excitations of Fractional Quantum Hall States

Igor V. Kukushkin,[1,2] Jurgen H. Smet,[1]* Vito W. Scarola,[3,4] Vladimir Umansky,[5] Klaus von Klitzing[1]

The rich correlation physics in two-dimensional (2D) electron systems is governed by the dispersion of its excitations. In the fractional quantum Hall regime, excitations involve fractionally charged quasi particles, which exhibit dispersion minima at large momenta referred to as rotons. These rotons are difficult to access with conventional techniques because of the lack of penetration depth or sample volume. Our method overcomes the limitations of conventional methods and traces the dispersion of excitations across momentum space for buried systems involving small material volume. We used surface acoustic waves, launched across the 2D system, to allow incident radiation to trigger these excitations at large momenta. Optics probed their resonant absorption. Our technique unveils the full dispersion of such excitations of several prominent correlated ground states of the 2D electron system, which has so far been inaccessible for experimentation.

In two-dimensional electron systems (2DESs) exposed to a strong perpendicular magnetic field B, interaction effects give rise to a remarkable set of quantum fluids. When all electrons reside in the lowest electronic Landau level, the kinetic energy is quenched and the Coulomb interaction then dominates. The strong repulsive interaction gives rise to the incompressible fractional quantum Hall fluids at rational fillings V_p of the lowest Landau level of the form $\nu_p = p/[2p \pm 1]$, $p = 1, 2, 3,\ldots$ (*1*). The appearance of these fluids may also be understood as a result of Landau quantization of a Fermi sea, which forms at filling factor $\nu_{p\to\infty} = 1/2$ and is composed of quasi particles referred to as composite fermions (*2*–*4*). At this filling, these composite fermions experience a vanishing effective magnetic field B_{eff}. When moving away from half filling, the composite fermions are sent into circular cyclotron orbits that they execute with frequency $\omega_{c,\mathrm{CF}} \propto |B_{\mathrm{eff}}|$. Landau quantization of these composite fermion orbits and the successive depopulation of the associated Landau levels give rise to the incompressible fractional quantum Hall fluids. The lowest energy-neutral excitation of these fluids involves a negatively charged quasi particle with a fractional charge of $e/(2p \pm 1)$, where e is the charge on the electron (*5*–*7*), and a positively charged quasi hole that is left behind. This excitation requires an energy that, in the weakly interacting picture, corresponds to the energy gap separating adjacent composite fermion Landau levels (*4*, *8*). According to theory, these neutral excitations at fractional filling ν_p possess an energy dispersion with p minima at large wave vectors q on the order of the inverse of the magnetic length $l_B = \sqrt{e/hB}$, where h is Planck's constant, or about 10^8 m^{-1} for typical densities of gallium arsenide–based 2DESs (*1*, *9*–*14*).

The minima are referred to as magneto-roton minima and are analogous to the roton minimum in the excitation dispersion that was introduced by Landau (*15*) to account for the anomalous heat capacity observed in superfluid He-II (*16*). The magneto-roton minima govern the low-

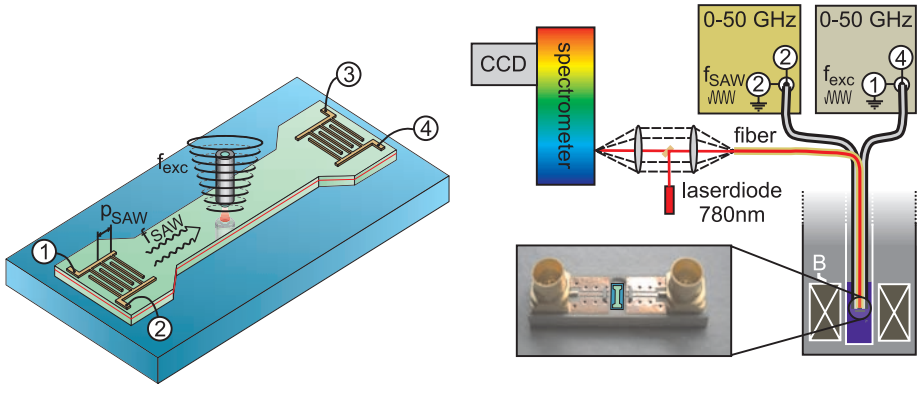

Fig. 1. Experimental arrangement for the detection of resonant microwave absorption at large wave vectors. (Left) Sample geometry consisting of a 0.1-mm-wide and 1-mm-long mesa. At its ends, the mesa widens and hosts two interdigital transducers with period p_{SAW}. High-frequency radiation drives the left transducer. The transducer launches SAWs across the sample. In the active-device region, light from a 780-nm laserdiode triggers a luminescence signal. This region of the sample is also irradiated with a quasi-monochromatic microwave by using a second high-frequency generator. Electrodes 1 and 4, which belong to transducers on opposite sides of the mesa, serve as a dipole antenna. (Right) Schematic of the cryostat configuration and the high-frequency chip carrier.

[1]Max Planck Institute for Solid State Research, D-70569 Stuttgart, Germany. [2]Institute of Solid State Physics, Russian Academy of Science, Chernogolovka 142432, Russia. [3]Department of Chemistry and Pitzer Center for Theoretical Chemistry, University of California at Berkeley, Berkeley, CA 94720, USA. [4]Theoretische Physik, Eidgenössische Technische Hochschule Zürich, 8093 Zürich, Switzerland. [5]Department of Condensed Matter Physics, Weizmann Institute of Science, Rehovot 76100, Israel.

*To whom correspondence should be addressed. E-mail: j.smet@fkf.mpg.de

temperature thermodynamic behavior and the stability of the incompressible fractional quantum Hall fluids because they are the lowest-energy excitations in the dispersion. Rotons at fillings of $p/(2p \pm 1)$ can be understood intuitively as bound states of such negatively charged quasi particles and positively charged quasi holes. These quasi particles are localized charges that move in a magnetic field on top of the p filled composite fermion Landau levels. The excitation wave functions have a nodal structure that gives rise to p oscillations in the electron pair correlation function over length scales on the order of l_B. When imparted with momentum k, the Lorentz force causes the quasi particle and hole to rotate about each other at an intercharge separation that increases with k. At large momenta ($k >> l/l_B$), the charges completely separate. But at intermediate momenta ($k \approx l/l_B$), the pair-correlation oscillations in the host liquid impose an energy gain for the charges so as to nest in one of the p correlation minima and set up a rotating bound state. The center of mass motion of the resulting p bound states, rotons, gives rise to free-particle behavior (a parabolic dispersion) for momenta near the roton minima.

Magneto-rotons in the fractional quantum Hall regime were predicted long ago (*9*–*11*), but direct experimental observation of them has remained elusive. Optical experiments would in principle only probe the excitation energy close to zero momentum. However, Kohn's theorem for a translationally invariant system implies that there is no oscillator strength in this limit. Therefore, excitations emerging from the Coulomb interaction remain invisible for small excitation wave vectors $k \rightarrow 0$ (*12*, *17*). Temperature-dependent transport addresses the opposite limit $k \rightarrow \infty$ because it requires charge separation. Powerful methods applied in other contexts, such as inelastic neutron scattering, in order to explore the regime in between both limits, has helped to confirm experimentally the roton dispersion predicted by Landau in He-II (*18*), but these methods are not useful. Inelastic neutron scattering performs very well on bulk systems, but to address a 2DES with an active region of only 10 nm is still very difficult. A surface-scattering technique such as angle-resolved photoemission spectroscopy cannot be used either because the 2DESs are buried deep underneath the crystal surface so as to obtain the highest-purity samples. Inelastic light scattering is one approach that has been applied successfully; however, control over the momentum is limited to $k < 4\pi/\lambda$ (where λ is the wavelength of the incident light). In the case of GaAs, optical excitation takes place at a wavelength of 800 nm, and the maximum momentum that can be transferred is only 1.6×10^7 m^{-1}. Roton excitations occur at larger momenta. The inevitable short-range disorder of the sample also permits inelastic light scattering to probe such large momenta; however, only extrema in the dispersion will be visible, and it is not possible to assign the observed features to a specific wave number. Even so, such studies led to the first evidence for rotons in the fractional quantum Hall regime (*19*, *20*). Also, specific heat-capacity studies that were based on the absorption of ballistic phonons have revealed signatures of magneto-rotons (*21*). Here too, the momentum dispersion remained inaccessible.

To trace the dispersion as a function of wave vector, one may impose a periodic modulation of the dielectric constant with different periodicities. Incident light is then not perceived as homogeneous by the sample, and the light can couple at the nonzero wave vector defined by the modulation. This idea has been implemented in the past in order to investigate plasmons (*22*). Similarly, inelastic light scattering studies performed at large values of k with metallic gratings were reported in the integer quantum Hall regime (*23*). However, these metallic gratings on top of the active device region are not benign. They block a large part of the incident optical radiation. The metal also screens the Coulomb interaction and modifies the physics under study.

We achieved a periodic modulation by launching surface acoustic waves (SAWs) across the 2DES. The experimental arrangement (Fig. 1) uses metallic interdigital transducers placed far away from the active device region (*24*, *25*). Three different waves are simultaneously incident on the sample: (i) A SAW propagates along the sample surface in order to impose a slowly varying modulation of the dielectric constant. The periodicity of the interdigital transducer p_{SAW} fixes the SAW wavelength at $\lambda_{SAW} = p_{SAW}$ and the resonance frequency at $f_{SAW} = v_{sound}/\lambda_{SAW}$, where v_{sound} is the velocity of sound in GaAs (approximately 2850 m s^{-1}). The modulation period λ_{SAW} defines the momentum k_{SAW} at which the excitations are probed. We repeated the experiments

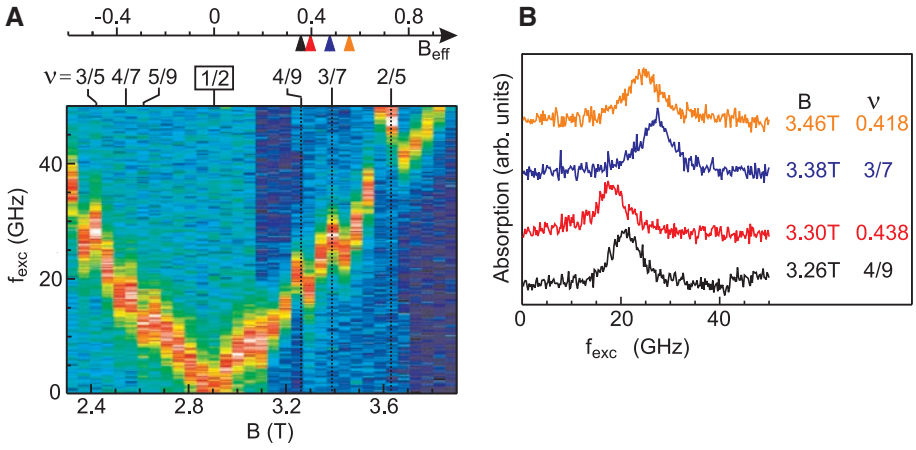

Fig. 2. The absorption of microwave radiation with frequency f_{exc} in the vicinity of filling factor 1/2 as a function of the magnetic field B for $k_{SAW} = 3.9 \times 10^5$ cm^{-1} ($f_{SAW} = 18$ GHz) and a carrier density of 3.5×10^{10} cm^{-2}. (**A**) Color rendition of the absorption strength as a function of the magnetic field and the incident microwave radiation f_{exc}. Blue colors correspond to weak absorption. Absorption maxima appear in red. The differential luminescence spectra were recorded at 30 mK. Prominent fractional states are marked at the top. (**B**) Vertical cuts through the data of (A) for filling factors smaller than 1/2. The absorption peak does not monotonically shift to a higher frequency with an increase of the effective magnetic field.

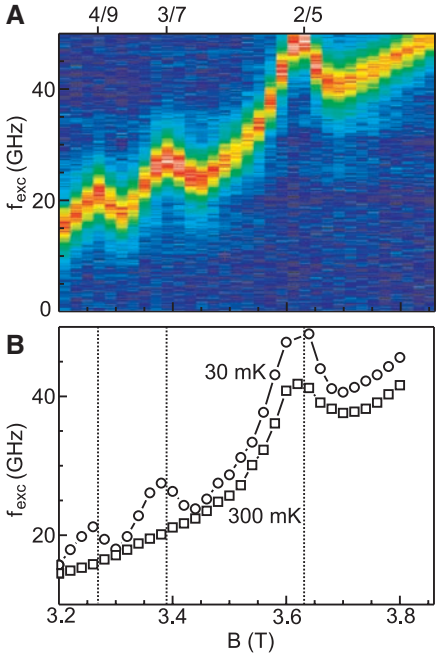

Fig. 3. The absorption strength of microwave radiation with frequency f_{exc} recorded with higher resolution as a function of the magnetic field B for $k_{SAW} = 3.9 \times 10^5$ cm^{-1} ($f_{SAW} = 18$ GHz) and a density of 3.5×10^{10} cm^{-2}. (**A**) Color rendition of the absorption strength in the magnetic field versus the frequency plane. Blue colors correspond to weak absorption. Absorption maxima appear in red. The resonance frequency oscillates with the magnetic field and reaches maxima at prominent fractional filling factors. (**B**) The resonant absorption frequency as a function of the applied magnetic field for two different temperatures, 30 and 300 mK.

for transducers with different periodicities down to 120 nm (24 GHz). By driving these transducers in a contactless fashion at double the frequency in order to preferentially excite their second harmonic (*24*), it is possible to cover momenta up to 10.4×10^8 m^{-1}. (ii) A second high-frequency generator irradiates the active-device region with a wave at frequency f_{exc}. When the photon energy hf_{exc} matches the energy of an excitation at wave vector k_{SAW} of the 2DES, resonant absorption may occur. Resonant absorption heats up the system and causes a thermal redistribution of charge carriers. (iii) Incident laser light at a wavelength of 780 nm triggers luminescence. Its spectrum is sensitive to the thermal distribution of the charge carriers. By comparing the luminescence in the absence and presence of the microwave radiation f_{exc}, we built the differential spectrum so as to reveal the resonant absorption profile. The integral of the absolute value of the differential spectrum across the recorded spectral range serves as a measure of the absorption strength.

This technique (and its derivatives) can also be applied to detect the electron-spin resonance and the composite fermion cyclotron resonance mode at a large nonzero wave vector (*26*, *27*). Studies on the well-known magnetoplasmon excitations at moderate magnetic fields have confirmed that with this technique, excitations are triggered at a wave vector with magnitude k_{SAW}. A typical example of such investigations has been included as supporting online material (SOM) text. The influence of the SAW seems to be limited to aiding the transfer of momentum. Apparently, no absorption of the SAW phonon takes place, as is demonstrated in the SOM for the electron-spin resonance (SOM text). Figure 2 plots an example of the microwave absorption strength as a function of the applied magnetic field and the incident microwave frequency f_{exc} at large magnetic fields around filling factor 1/2. Figure 2A displays a color rendition covering the magnetic field and frequency parameter space, and Fig. 2B highlights selected line scans at fixed values of the magnetic field. At low values of the effective magnetic field, two resonances or maxima in the absorption strength appear for each frequency f_{exc}. They are symmetrically arranged around filling factor 1/2. They have a width of ~10 GHz or less (which corresponds to 40 μeV) and can be attributed to the cyclotron resonance of composite fermions at the nonzero wave vector defined by the SAW (*26*). The frequency drops approximately linearly to zero as these resonances approach filling factor 1/2. It reflects the linear dependence of the composite fermion cyclotron frequency $\omega_{c,CF}$ on the effective magnetic field.

Further away from filling factor 1/2, however, deviations from a linear dependence are apparent in Fig. 2A. The resonance frequency starts to oscillate as the effective magnetic field increases. Some prominent fractional fillings have been marked in Fig. 2A and reveal that the largest deviations from a linear dependence occur at fields in which the 2DES is expected to condense into a fractional quantum Hall fluid. Figure 3A depicts a smaller region of the (B, f_{exc})–parameter space. It has been recorded with longer accumulation times and with a smaller magnetic field step size in order to better bring out the oscillatory features. For the parameters of the experiment, the maxima at fillings 2/5, 3/7, and 4/9 are the optical signatures for the formation of an incompressible fractional quantum Hall state that can be interpreted as an integer quantum Hall state of composite fermions. The resonance frequency yields the energy gap, which is the energy cost required to create a neutral quasi particle–quasi hole excitation at momentum k_{SAW}. The strongest fractional filling factor, 1/3, is out of reach because the energy gap exceeds the maximum accessible frequency f_{exc} of 50 GHz.

We emphasize that the oscillatory features in the absorption due to the correlation-driven condensation of composite fermions in incompressible states are only observable at the lowest temperatures. These features vanish for the 4/9 and 3/7 fractional quantum Hall states upon increasing the temperature (T) to 300 mK, whereas the feature is strongly reduced for the 2/5 state. This temperature-dependent behavior is illustrated in Fig. 3B. Even though the increase in T to 300 mK destroyed the formation of the more fragile fractional quantum Hall states, the composite particles themselves survive because at the cyclotron resonance frequency, resonant absorption can be observed up to considerably higher temperatures. Further temperature-dependent features of the resonances are deferred to the SOM text.

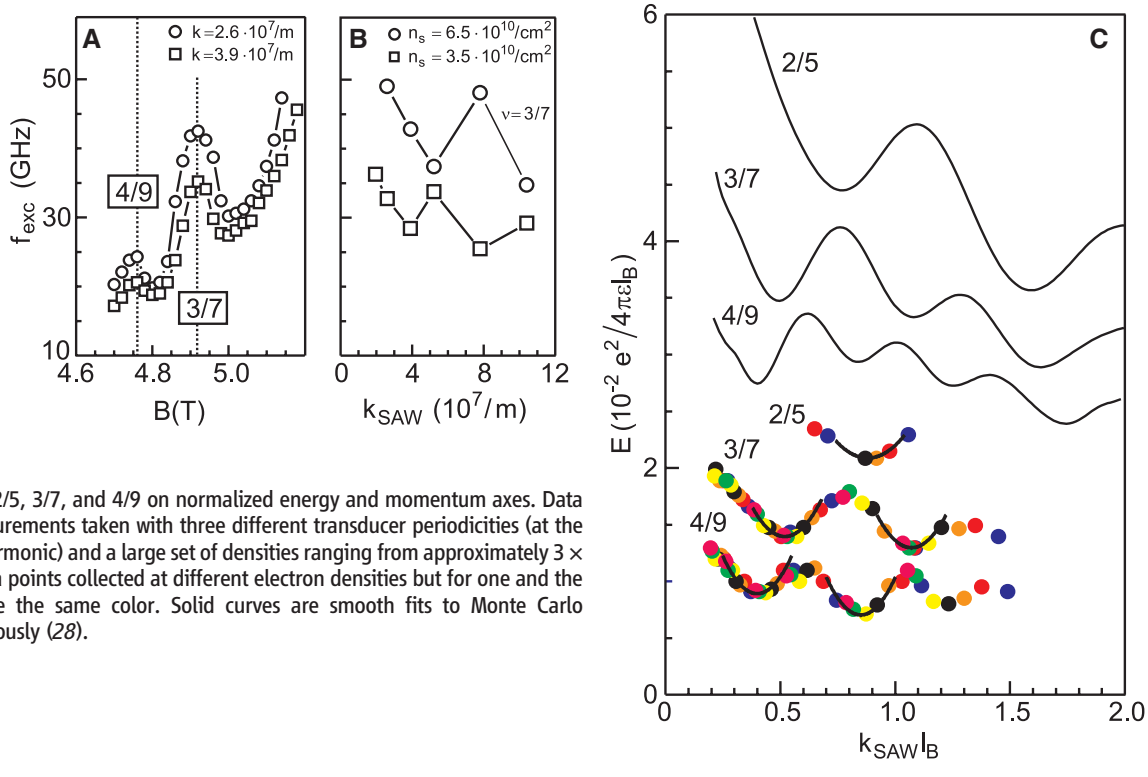

Fig. 4. Roton dispersion at filling factors 2/5, 3/7, and 4/9. (**A**) Resonant absorption frequency as a function of the applied magnetic field for two different momentum values $k_{SAW} = 2.6 \times 10^7$ m^{-1} and 3.9×10^7 m^{-1} at an electron density of 5.1×10^{10} cm^{-2} and a temperature of 30 mK. (**B**) Resonance frequency at filling factor 3/7 as a function of momentum k_{SAW} for two different values of the carrier density. (**C**) Dispersion of the resonance frequency at filling factors 2/5, 3/7, and 4/9 on normalized energy and momentum axes. Data points originate from measurements taken with three different transducer periodicities (at the fundamental and second harmonic) and a large set of densities ranging from approximately 3×10^{10} to 7×10^{10} cm^{-2}. Data points collected at different electron densities but for one and the same k_{SAW} transducer have the same color. Solid curves are smooth fits to Monte Carlo simulations described previously (*28*).

The oscillatory features were observed at all investigated values of the electron density as well as for the different momentum values k_{SAW} supplied by the SAW transducers. Example traces in Fig. 4A depict the magnetic field–dependence of the resonant microwave frequency for two different values of k_{SAW} (2.6×10^7 m^{-1} and 3.9×10^7 m^{-1}) and a density of 5.1×10^{10} cm^{-2} and $T = 30$ mK. Evidently, the energy gaps of the incompressible states substantially depend on the transferred momentum k_{SAW}. Figure 4B plots the resonant frequency at fractional filling 3/7 for the different values of k_{SAW} covered by the fabricated set of transducers (p_{SAW} = 120, 160, and 240 nm and contactless excitation of the second harmonic). Data sets are shown for two electron densities: 3.5×10^{10} cm^{-2} and 6.5×10^{10} cm^2. Despite the limited number of data points, the dispersion of the gap excitation at filling 3/7 is clearly a nonmonotonic function of k_{SAW}. Several minima are present, indicating that residual quasi particle–quasi hole correlations modify the absorption frequency. We assigned these minima to roton minima in the quasi particle dispersion. Varying the electron density influences the position of these minima. In order to compose a curve with more data points, the same experiment was repeated at several carrier densities. The circles in Fig. 4C display our primary results, the measured dispersions for the fractional states at filling factors 2/5, 3/7, and 4/9. These traces were compiled from data points taken at electron densities between 3×10^{10} and 7×10^{10} cm^{-2}. The energy is plotted in units of the Coulomb interaction strength $E_C = e^2/4\pi\varepsilon l_B$, the relevant energy scale in the lowest Landau level. Here, e is the electron charge and ε is the permittivity of GaAs. Usually, density-induced changes in the width of the electron wave function introduce complications for such a normalization procedure. However, in the investigated range of densities, the interparticle separation is considerably larger than the width of the electron wave function, and the form factor remains close to 1 (*28*). According to theory, the gap excitations of fractional quantum Hall states possess a parabolic dispersion near the roton minimum wave vector k_{roton}. For fractional fillings of the form $p/(2p + 1)$, a total of p minima is expected. In the accessible range of momenta, a single roton-like minimum is observed for the fractional quantum Hall state at filling 2/5, two minima are distinguishable for the 3/7 state, and three minima appear for the 4/9 state. We are unable to reach the last minimum for each of these fractional quantum Hall states because the required momentum transfer exceeds our present capabilities. The SOM text illustrates how the dispersion at fractional filling 3/7 changes with temperature and as one moves away from the quantized Hall state. At 300 mK, the roton features largely vanish. They also disappear at filling factors at which the system does not condense in a fractional quantum Hall state.

In the vicinity of each minimum, the dispersion is described well by a parabola, $E(k)/E_C = E_{roton}/E_C + \frac{\hbar^2(kl_B - k_{roton}l_B)^2}{2l_B^2 E_C m_{roton}}$, as illustrated by the solid black lines in Fig. 4C. Here, E_{roton} is the gap energy at the minimum and m_{roton} is referred to as the roton mass. Minima belonging to one and the same fractional quantum Hall state are fitted well, assuming the same roton mass. Table S1 in the supporting material lists the experimentally determined normalized values of E_{roton}, k_{roton}, and the inverse roton mass $1/m_{roton}$ for each minimum.

We compared our experimentally determined dispersion with the dispersion obtained from the composite fermion wave functions (*28*). These calculations are included as solid lines in Fig. 4C. They are smooth fits through Monte Carlo simulation data with typical uncertainties of $\leq 0.002E_C$. The simulations have no fitting parameters and take into account the finite thickness of the 30-nm-wide square quantum well at a density of 7×10^{10} cm^{-2}. The right panel of Table S1 shows roton parameters of the theoretical dispersion curves extracted by using a nonlinear least-square parabolic fit to the Monte Carlo data near the roton minima. The positions of the roton minima match well with the experimentally obtained values. For the 2/5 state, the deviation from the theoretical estimate of the roton mass falls within the experimental accuracy. However, the energy E_{roton} is systematically smaller in experiment by roughly a factor of 2 for the well-developed 2/5 and 3/7 fractional quantum Hall states. Because the nonzero width of the wave function was included, disorder broadening as well as Landau-level mixing are the remaining suspects for this discrepancy between theory and experiment. Landau-level mixing may cause a deviation on the order of 10% but not 100%. Hence, disorder, not included in existing theory, is probably responsible for the substantial reduction of the gap.

The fractional quantum Hall effect ground states are uniform liquids, whereas excitations lead to spatial oscillations in charge density over distances on the order of the magnetic length l_B. Charge disorder will couple to excited states more strongly than to a uniform state, lowering the energy difference between these two states; that is, disorder lowers the gap. If disorder perturbs the 2DES on length scales much longer than the magnetic length, then this just results in an overall energy shift. If disorder perturbs the 2DES on shorter length scales, we would expect a k-dependent distortion of the roton dispersion and therefore altered effective masses. The agreement between theory and experiment in comparison of the roton masses and the position of the minima suggests that disorder length scales are much larger than the magnetic length. Because the magnetic length is on the order of 10 nm, this is plausible for these high-quality structures. Also, a nearby conducting plane may strongly affect the energy gap. Such a parallel layer may indeed exist in the doped region of the heterostructure because of the optical excitation during the experiment. Here, this layer is located at a distance of 80 nm from the 2DES. Image charges would screen the Coulomb interaction and lower the gap.

References and Notes

1. R. E. Prange, S. M. Girvin, Eds., *The Quantum Hall Effect* (Springer, New York, 1990).
2. J. K. Jain, *Phys. Rev. Lett.* **63**, 199 (1989).
3. B. I. Halperin, P. A. Lee, N. Read, *Phys. Rev. B* **47**, 7312 (1993).
4. O. Heinonen, Ed., *Composite Fermions: A Unified View of the Quantum Hall Regime* (World Scientific Publishing Company, Singapore, 1998).
5. R. B. Laughlin, *Phys. Rev. Lett.* **50**, 1395 (1983).
6. R. de-Picciotto *et al.*, *Nature* **389**, 162 (1997).
7. L. Saminadayar, D. C. Glattli, Y. Jin, B. Etienne, *Phys. Rev. Lett.* **79**, 2526 (1997).
8. B. I. Halperin, P. A. Lee, N. Read, *Phys. Rev. B* **47**, 7312 (1993).
9. C. Kallin, B. I. Halperin, *Phys. Rev. B* **30**, 5655 (1984).
10. F. D. M. Haldane, E. H. Rezayi, *Phys. Rev. Lett.* **54**, 237 (1985).
11. S. M. Girvin, A. H. MacDonald, P. M. Platzman, *Phys. Rev. Lett.* **54**, 581 (1985).
12. S. M. Girvin, A. H. MacDonald, P. M. Platzman, *Phys. Rev. B* **33**, 2481 (1986).
13. M. Rasolt, A. H. MacDonald, *Phys. Rev. B* **34**, 5530 (1986).
14. S. H. Simon, B. I. Halperin, *Phys. Rev. B* **48**, 17368 (1993).
15. L. Landau, *Phys. Rev.* **60**, 356 (1941).
16. P. L. Kapitza, *Phys. Rev.* **60**, 354 (1941).
17. W. Kohn, *Phys. Rev.* **123**, 1242 (1961).
18. J. L. Yarnell, G. P. Arnold, P. J. Bendt, E. C. Kerr, *Phys. Rev.* **113**, 1379 (1959).
19. A. Pinczuk, B. Denis, L. N. Pfeiffer, K. West, *Phys. Rev. Lett.* **70**, 3983 (1993).
20. A. Pinczuk *et al.*, *Am. Phys. Soc.* **40**, 515 (1995).
21. U. Zeitler *et al.*, *Phys. Rev. Lett.* **82**, 5333 (1999).
22. E. Batke, D. Heitmann, J. P. Kotthaus, K. Ploog, *Phys. Rev. Lett.* **54**, 2367 (1985).
23. L. L. Sohn *et al.*, *Solid State Commun.* **93**, 897 (1995).
24. I. V. Kukushkin *et al.*, *Appl. Phys. Lett.* **85**, 4526 (2004).
25. Materials and methods are available as supporting material on *Science* Online.
26. I. V. Kukushkin *et al.*, *Phys. Rev. Lett.* **96**, 126807 (2006).
27. I. V. Kukushkin *et al.*, *Phys. Rev. Lett.* **98**, 066403 (2007).
28. V. W. Scarola, K. Park, J. K. Jain, *Phys. Rev. B* **61**, 13064 (2000).

29. We acknowledge financial support from the Deutsche Forschungsgemeinschaft, the German Israeli Foundation, and the Bundesministerium für Bildung und Forschung.

Supporting Online Material

www.sciencemag.org/cgi/content/full/1171472/DC1
Materials and Methods
SOM Text
Figs. S1 to S4
Table S1
References

27 January 2009; accepted 3 April 2009
Published online 30 April 2009;
10.1126/science.1171472
Include this information when citing this paper.

Real-Time Infrared Detection of Cyanide Flip on Silver-Alumina NO_x Removal Catalyst

Frédéric Thibault-Starzyk,[1]* Etienne Seguin,[1] Sébastien Thomas,[1] Marco Daturi,[1] Heike Arnolds,[2] David A. King[3]

Spectroscopic studies of the mechanistic steps that occur on supported precious metal catalysts used in industrial and automotive applications are hampered by a dearth of suitable experimental methods. We used femtosecond laser excitation followed by nanosecond time-resolved in situ Fourier-transform infrared spectroscopy to initiate a catalytic reaction on alumina-supported silver catalysts, which are of interest in minimizing nitrogen oxide emissions from fuel-efficient lean-burn engines. We found that the key intermediate step in the reaction between carbon monoxide and nitric oxide is the flip of a cyanide group from a silver nanoparticle to the alumina support (with a lifetime of 2 microseconds), which indicates the central role played by the interface between the metal particle and the oxide support.

Fuel-efficient lean-burn engines help to conserve fossil fuels and limit the rate of CO_2 emissions from motor vehicles. These engines also introduce an environmental problem of their own: The standard three-way catalysts cannot reduce NO_x (= NO + NO_2) under an excess of oxygen in the lean-burn engine exhaust, as they rely on unburnt hydrocarbons to reduce NO_x. The removal of NO_x from modern engines is one of the greatest challenges facing car manufacturers, who must meet ever-tougher U.S., Japanese, and European emission standards (*1*). Some of the most successful strategies are the development of NO_x storage and reduction catalysts, where NO_x is reduced by reductants created in a fuel-rich spike, and selective catalytic reduction using fuel injection in the afterburning systems. Silver-alumina catalysts are particularly adaptable to this task, as they have excellent properties for hydrocarbon activation, NO_x reduction, and sulfur tolerance (*2*, *3*) and have successfully passed diesel engine bench tests (*4*). One of the central reactions is that between NO and CO, but there is still much speculation as to the mechanistic details of NO_x reduction on silver-alumina catalysts.

Some of us succeeded in establishing the importance of isocyanate species in the pathway from C_2H_5OH + NO + O_2 reaction to N_2 formation on a Ag/Al_2O_3 sample (*5*), especially concerning the coordination and transformation sites, via the use of isotopically labeled species in infrared (IR) spectroscopy (*6*). We had proposed a tentative reaction mechanism involving intermediates between –CN and –NCO species on the basis of acid-base considerations (Scheme 1). Nonetheless, no clear evidence for these intermediates has been reported, presumably because they are too short-lived to be detected with conventional methods, which only allow millisecond time resolution (*5*). Thus, we have developed a spectroscopic technique with higher time resolution, and we show that the key intermediate in the reduction of NO by CO is a CN group in a bridge formation between a silver particle and the alumina support with a lifetime of only 2 μs.

Step-scan Fourier-transform infrared spectroscopy (*7*, *8*) is capable of submicrosecond time resolution (*9*) needed to study this reaction, but the challenge is to find a short enough trigger for its initiation. Processes initiated by photolysis can be investigated, as ultrashort laser pulses are readily available (*10*, *11*). Pulsed reactant gives access to a much broader class of reactions, but it only allows a time resolution of seconds to milliseconds because of its mechanical origin (*12*). Another broadly applicable trigger in heterogeneous catalysis is temperature, which is easily amenable to initiation by laser pulses. One maturing field of investigation involves catalytic processes triggered by femtosecond laser heating on single-crystalline metal surfaces under ultrahigh vacuum (*13*). Normally, these surface processes are followed on a subpicosecond to picosecond time scale by a time-delayed probe pulse—for example, visible-IR sum frequency generation—to monitor the progress of the reaction. Recently, some of us used this technique to follow the first few picoseconds of the NO dissociation and the reaction between CO and NO on an iridium surface (*14*, *15*). Here, in the CO + NO reaction on Ag/Al_2O_3, we are trying to detect a longer-lived intermediate, for which submicrosecond time resolution that can be obtained by step-scan IR spectroscopy is most appropriate.

The choice of a femtosecond over a nanosecond laser pulse for heating the substrate was motivated by our experience that heating of metals on a time scale of a few nanoseconds can destroy the substrate through high induced strain (*16*). Nanosecond laser heating of alumina (*17*) produces microcracks, unlike femtosecond laser heating. The generation of microcracks is a special concern because we use self-supporting wafers of micrometer thickness. After more than 10,000 laser shots on the sample used here, we did not find any irreversible visible change of the laser-treated area relative to the untreated areas.

Heating of alumina by a femtosecond laser is a largely unexplored area, unlike femtosecond heating of single crystals or of dispersed silver nanoclusters in an alumina matrix, which is well understood (*18*–*20*). Femtosecond laser heating of metal surfaces or metal clusters generally occurs in three stages. Initially, absorption of photons leads to the creation of nascent electrons, with energies up to the photon energy. Within a few hundred femtoseconds, these nascent electrons equilibrate via electron-electron scattering and form a hot electron bath, with temperatures up to several thousand kelvin (*21*, *22*). These hot electrons then equilibrate with the lattice phonons on a time scale of a few picoseconds. Finally, the phonons cool down on a time scale of several hundred picoseconds. The cooling time of metal clusters depends strongly on the thermal conductivity of the matrix they are embedded in (*22*). Although more precise time scales would be available via femtosecond pump-probe spectroscopy, from the wide variety of systems investigated in this way we can be confident that all large-scale laser-induced temperature changes in the electron and phonon baths pass too quickly to be recorded at 33-ns time resolution.

The perturbation of the surface by the laser pulse appears on a microsecond time scale as an offset in the interferogram measured by the step-scan spectrometer. The interferogram is shown in Fig. 1 for gentle excitation by a 3-μJ laser pulse (higher pulse energies lead to saturation of the detector). Such perturbation can be caused by direct heating of the solid and blackbody radiation combined with delayed luminescence, but on this time scale and at this pulse energy (3 μJ) the temperature increase caused by the laser is likely to be less than 0.1 K. The microsecond time scale points to a different potential cause: luminescence from trapped electrons in the alumina lattice (*23*). During the actual experiment at 3-mJ pulse energy, a low-pass filter with a cutoff at 4000 cm^{-1} was inserted to block all energy emitted in the near-IR and avoid saturating the detector. We can estimate the maximum temperature reached after the first nanosecond

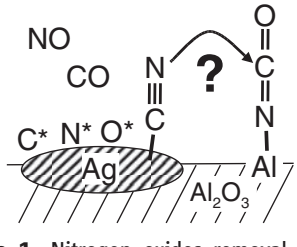

Scheme 1. Nitrogen oxides removal (deNO_x) reaction on alumina-supported Ag catalysts.

[1]Laboratoire Catalyse et Spectrochimie, ENSICAEN-Université de Caen-CNRS, Boulevard Maréchal Juin, 14050 Caen Cedex, France. [2]Surface Science Research Centre, Department of Chemistry, University of Liverpool, Oxford Street, Liverpool L69 3BX, UK. [3]Department of Chemistry, University of Cambridge, Lensfield Road, Cambridge CB2 1EW, UK.

*To whom correspondence should be addressed. E-mail: fts@ensicaen.fr

as ΔT = 38 K (fig. S1) from the known heat capacity of alumina (900 J kg^{-1} K^{-1}), the laser pulse energy, the laser spot size (1 mm), and the density of the wafer (7.5 mg/cm^2). The laser spot size was only estimated, not actually measured. A higher temperature would be obtained on a smaller spot, and 38 K is thus only a minimal estimation. We modeled heat transport from the laser-heated spot to the surrounding area of the wafer (*8*) and found that the complete heat cycle between two laser pulses occurs on a time scale of tens of milliseconds (fig. S1). The average base temperature of the wafer increases by ~10 K in the first 10 s after the start of the laser shots (fig. S2). Data were recorded after this stabilization period.

As an aid to band assignment, we present a brief summary of stable surface species as a function of temperature (Fig. 2A). We know from previous studies (*5*, *6*) that the essential reaction steps should be observable between 2300 and 2100 cm^{-1}. At room temperature, bulk silver cyanide is characterized by an IR band at 2165 cm^{-1}. Heating of a physical mixture of AgCN and the Ag/Al_2O_3-supported catalyst (Fig. 2A) leads to a new band at 2130 cm^{-1} for AgCN supported on alumina. This species progressively disappears under stronger heating, forming isocyanates on alumina with two bands at 2240 and 2265 cm^{-1} for isocyanates on Al^{IV} and on Al^{VI}, respectively (*6*) [aluminum sites with several possible coordination states, tetrahedral Al^{IV} and octahedral Al^{VI}, were reported to greatly influence catalytic behavior in NO_x removal on Ag/Al_2O_3 (*24*)]. The same species and IR bands are usually observed in the reaction of CO and NO on the supported catalyst. NO and CO dissociate on Ag and form a stable silver cyanide with a characteristic frequency around 2130 cm^{-1} that can be observed when the temperature is kept below 523 K. Our experiments are carried out at a base temperature of 473 K, where NO and CO have dissociated on the catalyst to form AgCN. The laser pulse initiates reaction of the cyanide to form isocyanate species on alumina. Other CO and NO molecules are dissociated again to form additional cyanide on Ag, and cyanide can be observed again on Ag before the next laser pulse arrives.

In an ideal pump-probe experiment, the catalyst returns to the same state after each laser pulse, but our catalyst is slowly saturated because the maximum temperature is not high enough to desorb the final product. This slow buildup of product does not appear to block the catalytic cycle, as only a fraction of available sites is involved at each laser pulse; however, it does affect subsequent runs (12,000 pulses each). We present the results of two subsequent runs at time resolutions of 100 ns and 33 ns. In the spectra we present, we calculate the average spectrum before the laser pulse and subtract this from each spectrum at later times.

On the fresh catalyst at 100-ns time resolution (Fig. 3), the intensity change for the band at 2130 cm^{-1} shows a decrease of surface concentration of supported AgCN during the first 20 μs. After ~5 μs, a band becomes visible at 2240 cm^{-1}, caused by the appearance of isocyanates on Al^{IV} sites, which continuously increases up to 40 μs after the laser pulse. The kinetics for isocyanate creation does not match that of the disappearance of supported AgCN, which points to a missing intermediate species.

After the laser experiment with 100-ns time resolution, we recorded a second run on a now

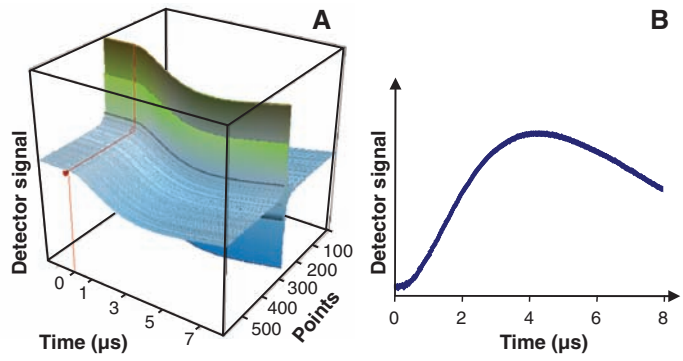

Fig. 1. (**A**) Changes in the interferogram recorded at 33-ns time resolution after a laser pulse at 3 μ]. (**B**) Change in maximum intensity of the interferogram versus time. This reflects the changes under the whole of the IR measurement zone, not under the laser spot, where the reaction takes place (*8*).

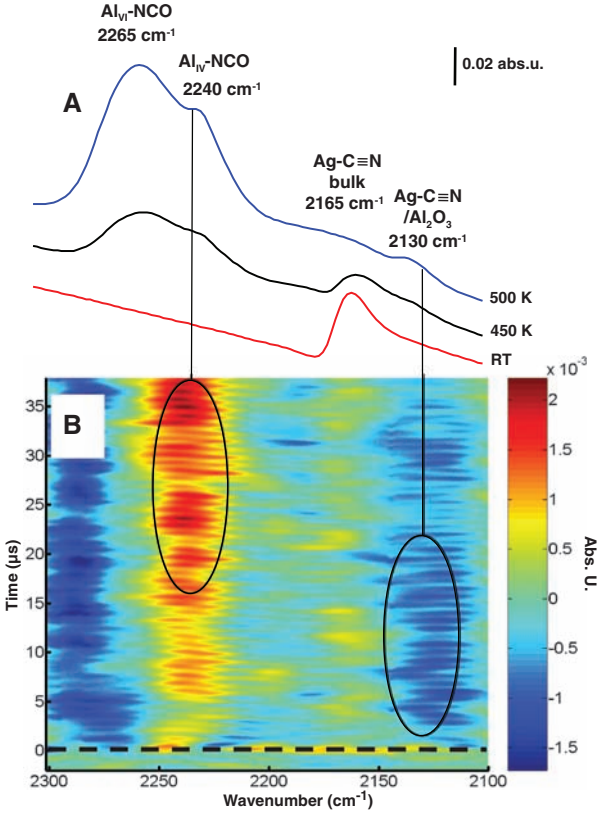

Fig. 2. (**A**) IR spectra of AgCN mixed with Ag/Al_2O_3 and progressively heated to 500 K to identify stable surface species. (**B**) Spectra recorded at 100-ns time resolution during the reaction induced by the laser pulse (3 mJ). Red corresponds to IR bands with intensities higher than at time 0; blue shows regions where the IR intensity decreased.

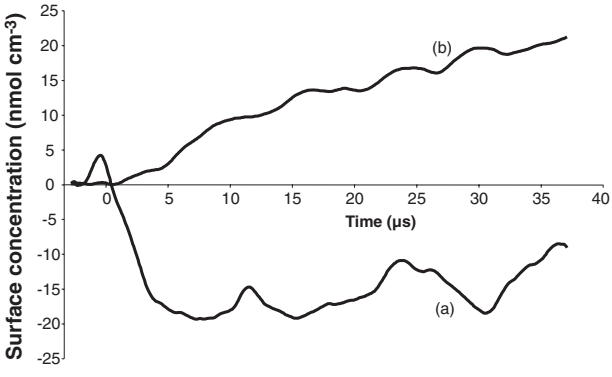

Fig. 3. Time trace (100-ns time resolution) of IR band intensities for $AgCN/Al_2O_3$ (a) and isocyanates on alumina (b) after the laser pulse.

partly saturated catalyst with 33-ns time resolution (Fig. 4). At 33-ns time resolution, the signal is also noisier than at 100-ns resolution. We have nonetheless been able to follow intensity changes lower than 10^{-3} absorbance units. The surface composition has changed relative to the 100-ns experiment. We now see increased intensity at the frequency of the isocyanates on Al^{VI} around 2265 cm^{-1}, indicating that the Al^{IV} sites have been mostly saturated in the previous experiment. This is also borne out in the smaller absorbance changes detected. In this experiment, we observe the appearance of a new band at 2205 cm^{-1}. This band reaches its maximum intensity 2 μs after the laser pulse.

The frequency of the band does not fit a cyanide or an isocyanide, but rather corresponds to a bridged cyanide between the Ag cluster and an aluminum atom on the surface of alumina. One of the earliest observations of such a bridged cyanide was that of a complex between nickel and BF_3, 100 cm^{-1} higher than the frequency of NiCN (*25*). BF_3 is a strong Lewis acid, as is the aluminum cation in alumina. Bridging cyanides in cyano–transition metal complexes have a ~30 cm^{-1} higher frequency than those in terminal CN groups, an effect ascribed to the constraint of motion and the backdonation from the C- and N-bonded metal atoms (*26*). The situation is similar here, with a frequency increase of 75 cm^{-1} relative to terminal CN on silver.

In agreement with the hard-soft acid-base theory (*27*), the cyanide is initially linked to Ag because of the rather hard properties of both carbon and silver, whereas on the softer aluminum atom the bonding via the nitrogen atom is favored. When the cyanide moiety flips from silver to alumina, it can form an isocyanide (attached to aluminum Al^{VI}, which is statistically the most accessible site), which in turn is quickly oxidized into an isocyanate and transferred to the stronger Lewis acid Al^{IV}. The isocyanate observed immediately after the cyanide flip corresponds to a band at 2265 cm^{-1}, typical for an Al^{VI} atom. The saturation of isocyanates on Al^{IV} in the previous experiment might have aided the detection of the intermediate by slowing down transfer of the isocyanate from the Al^{VI} site. This change would also account for the different kinetics observed in the two experiments. The detection of such a bridged cyanide between Ag clusters and alumina support gives evidence for the reaction mechanism (Scheme 2).

The experiments were repeated with frequency-doubled laser pulses at 400 nm wavelength (photon energy 3.1 eV, pulse energy 140 μJ), with no detected changes in any of the bands, and at lower pulse energy (1 and 2 mJ instead of 3 mJ), with overall reduced responses. A photochemical mechanism caused by nascent electrons is thus unlikely, and the reaction initiation by the laser is more probably due to a thermalized hot electron or hot phonon distribution, which would relax on a time scale of a few hundred femtoseconds or a few hundred picoseconds, respectively. In this case, any reaction caused by direct action of the laser pulse should have ended before we reach the nanosecond time scale. Our microsecond transients must therefore involve a much slower mechanism involving, for example, an activated AgCN species. This activated species then proceeds to form the bridged intermediate, which converts to isocyanate. Because the conversion of the intermediate into the isocyanate begins before the end of its formation from the cyanide, the maximum concentration of the bridged intermediate is reached before the minimum concentration of the cyanide.

The much faster recovery of the AgCN band on the aged catalyst relative to the fresh catalyst suggests that the reaction rate to form AgCN from gas-phase CO and NO has increased. One possible explanation is the formation of smaller, more reactive Ag clusters through interaction with the femtosecond laser (*28*). It might also indicate that our one-way reaction scheme is still incomplete; it might be necessary to consider back-reactions for some of the steps (for example, the bridged intermediate could revert back to AgCN). In terms of reaction rate, we estimate from the measured transient changes a consumption rate of cyanides of 70 mmol s^{-1} g^{-1} just after the laser

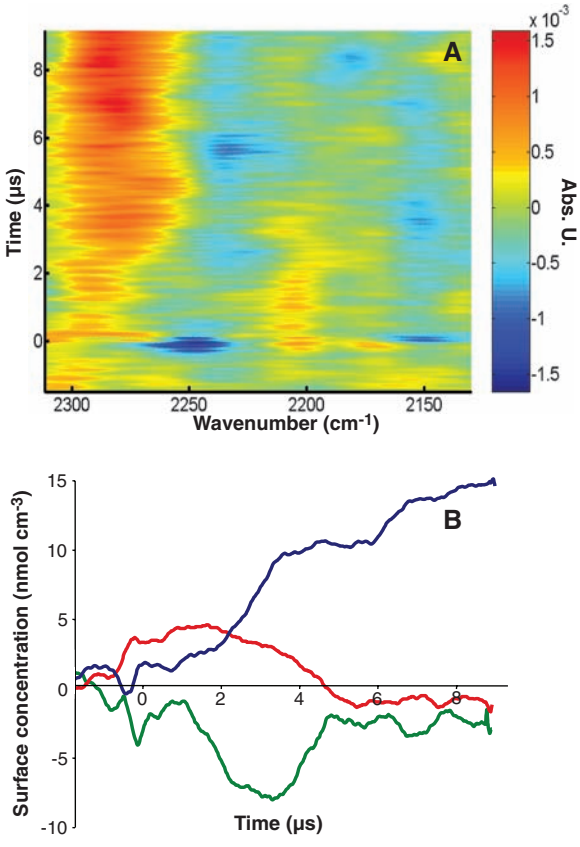

Fig. 4. (**A**) IR spectra recorded at 33-ns time resolution on the catalyst in the presence of CO and NO during the first 7 μs after the laser pulse (3 mJ). (**B**) Time traces for the bands detected for supported AgCN (green), isocyanates (blue), and the short-lived reaction intermediate (red). The noise around time 0 is due to electronic perturbation of the recording by the switching of the Pockel's cells in the laser amplifier (*8*).

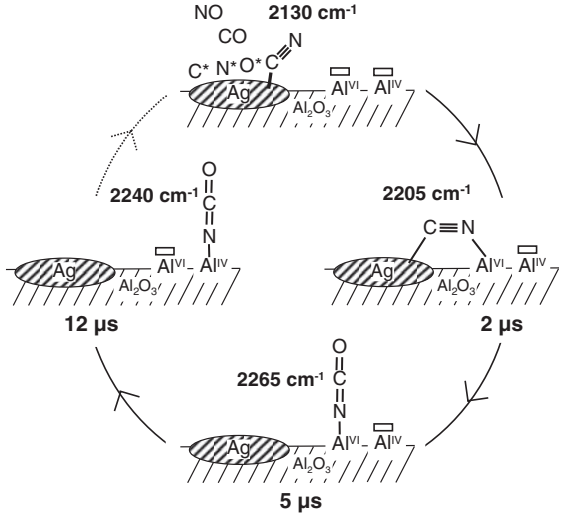

Scheme 2. Reaction mechanisms for the deNO$_x$ reaction on an alumina-supported silver catalyst.

shot in the 33-ns experiment. This value is much higher than rates obtained in steady-state conditions with a similar catalyst and temperature range (*29*). The rate-determining step in the steady-state complete reaction of NO conversion in N_2 at 200°C would probably be the reaction of isocyanate (which is fairly stable on alumina in the absence of water at this temperature), and our intermediate step is clearly much faster than that (when performed independently).

Scheme 2 should only be regarded as the most comprehensive version of the reaction cycle that can be deduced from the data. Our measurements show the key role of the interface between Ag nanoparticles and the alumina support, the structure of which controls the catalytic reaction. Although metal-support interactions have long been recognized as vital for catalytic performance, a microscopic understanding of the precise role of the metal-support interface has emerged only recently (*30*, *31*). In our case, the difference between octahedrally and tetrahedrally coordinated Al sites must strongly influence the reaction speed. The preparation procedure and the thermal treatment of the solid are known to affect this difference (*24*).

The mechanism we demonstrate here is an indication that improved catalytic activity for NO conversion could be obtained by, for instance, tuning the ratio of Al^{VI} versus Al^{IV} with the calcination temperature of alumina. The alumina support has been shown to have a profound influence on the dispersion of silver clusters on the catalyst (*32*), and catalytically active Ag_n^+ clusters form on acid sites on the alumina support. The bridged intermediate reported here can only be formed at the interface between the silver cluster and the support, and the corresponding reaction mechanism explains the key role of the size of silver clusters in catalytic activity.

References and Notes

1. Summary of Worldwide Diesel Emission Standards (www.dieselnet.com/standards).
2. R. Burch, J. P. Breen, F. C. Meunier, *Appl. Catal. B* **39**, 283 (2002).
3. F. Ouyang, M. Haneda, W. Sun, Y. Kindaichi, H. Hamada, *Kinet. Catal.* **49**, 236 (2008).
4. H. He, Y. Yu, *Catal. Today* **100**, 37 (2005).
5. N. Bion, J. Saussey, M. Haneda, M. Daturi, *J. Catal.* **217**, 47 (2003).
6. N. Bion, J. Saussey, C. Hedouin, T. Seguelong, M. Daturi, *Phys. Chem. Chem. Phys.* **3**, 4811 (2001).
7. T. J. Johnson, A. Simon, J. M. Weil, G. W. Harris, *Appl. Spectrosc.* **47**, 1376 (1993).
8. See supporting material on *Science* Online.
9. Y. H. Yeom, H. Frei, in *In-Situ Spectroscopy of Catalysts*, B. Weckhuysen, Ed. (American Scientific, San Diego, CA, 2004), pp. 33–46.
10. S. E. Bromberg *et al.*, *Science* **278**, 260 (1997).
11. G. Sansone *et al.*, *Science* **314**, 443 (2006).
12. A. Wille, E. Fridell, *Appl. Catal. Environ.* **70**, 294 (2007).
13. C. Frischkorn, M. Wolf, *Chem. Rev.* **106**, 4207 (2006).
14. I. M. Lane, D. A. King, Z. P. Liu, H. Arnolds, *Phys. Rev. Lett.* **97**, 186105 (2006).
15. H. Arnolds, D. A. King, I. M. Lane, *Chem. Phys.* **350**, 94 (2008).
16. G. Hoogers, D. C. Papageorgopoulos, D. A. King, *Surf. Sci.* **310**, 147 (1994).
17. W. Perrie, A. Rushton, M. Gill, P. Fox, W. O'Neill, *Appl. Surf. Sci.* **248**, 213 (2005).
18. E. Carpene, *Phys. Rev. B* **74**, 024301 (2006).
19. M. Bonn *et al.*, *Phys. Rev. B* **61**, 1101 (2000).
20. C. Voisin *et al.*, *Phys. Rev. Lett.* **85**, 2200 (2000).
21. M. Lisowski *et al.*, *Appl. Phys. A* **78**, 165 (2004).
22. Y. Bigot, V. Halté, J.-C. Merle, A. Daunois, *Chem. Phys.* **251**, 181 (2000).
23. J. K. Thomas, *Chem. Rev.* **105**, 1683 (2005).
24. Z.-M. Wang, M. Yamaguchi, I. Goto, M. Kumagai, *Phys. Chem. Chem. Phys.* **2**, 3007 (2000).
25. D. F. Shriver, *J. Am. Chem. Soc.* **84**, 4610 (1962).
26. A. Palazzi *et al.*, *J. Organomet. Chem.* **689**, 2324 (2004).
27. R. G. Pearson, *J. Am. Chem. Soc.* **85**, 3533 (1963).
28. J. Sung *et al.*, *J. Phys. Chem. C* **112**, 5707 (2008).
29. P. Bera, K. C. Patil, M. S. Hegde, *Phys. Chem. Chem. Phys.* **2**, 3715 (2000).
30. Z. P. Liu, S. J. Jenkins, D. A. King, *Phys. Rev. Lett.* **93**, 156102 (2004).
31. F. Thibault-Starzyk, M. Daturi, P. Bazin, O. Marie, in *Nanoparticles and Catalysis*, D. Astruc, Ed. (Wiley-VCH, Weinheim, Germany, 2007), pp. 508–528.
32. K. Sato, T. Yoshinari, Y. Kintaichi, M. Haneda, H. Hamada, *Appl. Catal. B* **44**, 67 (2003).

33. We thank K. Jewkes and P. Turner from Bruker Optics for their technical help. Supported by a fellowship from Churchill College, Cambridge (F.T.S.) and an Engineering and Physical Sciences Research Council Advanced Research Fellowship (H.A.).

Supporting Online Material

www.sciencemag.org/cgi/content/full/324/5930/1048/DC1
Materials and Methods
SOM Text
Figs. S1 and S2
References

26 November 2008; accepted 19 March 2009
10.1126/science.1169041

Fabricating Genetically Engineered High-Power Lithium-Ion Batteries Using Multiple Virus Genes

Yun Jung Lee,[1]* Hyunjung Yi,[1]* Woo-Jae Kim,[2] Kisuk Kang,[3,4] Dong Soo Yun,[1] Michael S. Strano,[2] Gerbrand Ceder,[1] Angela M. Belcher[1,5]†

Development of materials that deliver more energy at high rates is important for high-power applications, including portable electronic devices and hybrid electric vehicles. For lithium-ion (Li^+) batteries, reducing material dimensions can boost Li^+ ion and electron transfer in nanostructured electrodes. By manipulating two genes, we equipped viruses with peptide groups having affinity for single-walled carbon nanotubes (SWNTs) on one end and peptides capable of nucleating amorphous iron phosphate (a-$FePO_4$) fused to the viral major coat protein. The virus clone with the greatest affinity toward SWNTs enabled power performance of a-$FePO_4$ comparable to that of crystalline lithium iron phosphate (c-$LiFePO_4$) and showed excellent capacity retention upon cycling at 1C. This environmentally benign low-temperature biological scaffold could facilitate fabrication of electrodes from materials previously excluded because of extremely low electronic conductivity.

Lithium-ion battery electrodes store and release electrical energy by insertion and extraction of Li^+ ions and electrons through the electrode materials. Therefore, increasing transport of Li^+ ions and electrons in electrodes can enhance energy storage at high charge and discharge rates. Controlling nanostructure has become a critical process in developing electrode materials to boost transport in composite electrodes (*1*, *2*), especially for the electrically insulating transition metal phosphate cathode materials. Among them, iron phosphate–based materials have elicited attention as promising Li^+-ion battery positive electrode materials due to their lower toxicity, lower cost, and improved safety through improved chemical, thermal, and structural stability for high-power applications (*3*). However, their practical use has been constrained due to kinetic limitations, which result in poor charge- and discharge-rate capability and fading of capacity upon prolonged cycling. To address the rate limitation of these materials, most researchers have focused on tailoring particle size (*4*, *5*) to reduce both the ionic and electronic path within the particles and enhancing electronic conductivity with surface carbon-coating layers (*6*) or conducting nanoparticles additives (*7*, *8*). However, the fabrication of nanosized particles is still challenging because the materials require at least 350°C for crystallization and carbon coating. Despite the recent advances in synthesis methods, the smallest particle size remains 20 to 40 nm (*5*).

Biological systems offer capabilities for environmentally benign materials synthesis. An M13 virus–based biological toolkit has been developed for the design of nanoarchitectured structures and materials (*9*–*12*). Our group has

[1]Department of Materials Science and Engineering, Massachusetts Institute of Technology, Cambridge, MA 02139, USA. [2]Department of Chemical Engineering, Massachusetts Institute of Technology, Cambridge, MA 02139, USA. [3]Department of Materials Science and Engineering, Korea Advanced Institute of Science and Technology, 335, Gwahangno, Yuseong-gu, Daejeon, Korea, 305-701. [4]KAIST Institute for Eco-Energy, 335, Gwahangno, Yuseong-gu, Daejeon, Korea, 305-701. [5]Department of Biological Engineering, Massachusetts Institute of Technology, Cambridge, MA 02139, USA.

*These authors contributed equally to this work.
†To whom correspondence should be addressed. E-mail: belcher@mit.edu

shown that M13 bacteriophage (phage or virus) can be used for battery device fabrication with improved performance by synthesizing electrochemically active anode nanowires and organizing the virus on a polymer surface (*11*, *13*). However, in designing nanostructured electrodes with better electrical wiring for high-power batteries, multifunctionality of the virus is required. Multifunctional viruses have been engineered with desired modifications on different positions of the protein coat (*10*, *12*, *14*). Here we demonstrate a genetically programmed multifunctional virus as a versatile scaffold for the synthesis and assembly of materials for high-power batteries.

Virus-enabled nanostructured cathode materials were first demonstrated by templating amorphous anhydrous iron phosphate (a-$FePO_4$) on the E4 virus. E4 is a modified M13 virus that has tetraglutamate (EEEE) fused to the N terminus of each copy of pVIII major coat protein. Due to the presence of extra carboxylic acid groups compared with wild-type M13 virus (M13KE), the E4 virus exhibits increased ionic interactions with cations and can serve as a template for materials growth (*11*, *13*, *15*). Because only one gene (gVIII in Fig. 2A) has been modified for the desired peptide motif on pVIII, we call this E4 clone a one-gene system. a-$FePO_4$ nanowires were produced on silver nanoparticles (Ag NPs)–loaded E4 virus. Details of the synthesis procedure are given in the supporting online material (*16*). Loading of uniformly distributed Ag NPs along the coat protein of E4 virus (fig. S1) was initially intended to increase electronic conductivity (*7*, *8*, *11*). The chemical analysis by direct current plasma atomic emission spectroscopy confirmed the atomic ratio of Fe to P as 1:1. Although viruses themselves have phosphate groups in their DNA (7270 phosphate groups per virus particle), the fraction of phosphate groups from DNA is <1%. Figure 1A shows transmission electron microscope (TEM) images of a-$FePO_4$ nanowires with particle sizes of 10 to 20 nm in diameter templated on the virus. Generally, hydrated a-$FePO_4$ (a-$FePO_4{\cdot}nH_2O$, n = 2 to 4) is precipitated in aqueous solutions containing Fe^{3+} and PO_4^{3-} ions around pH = 7 to 8, and anhydrous structures can be obtained through the dehydration of a-$FePO_4{\cdot}nH_2O$ by thermal annealing at 400°C.

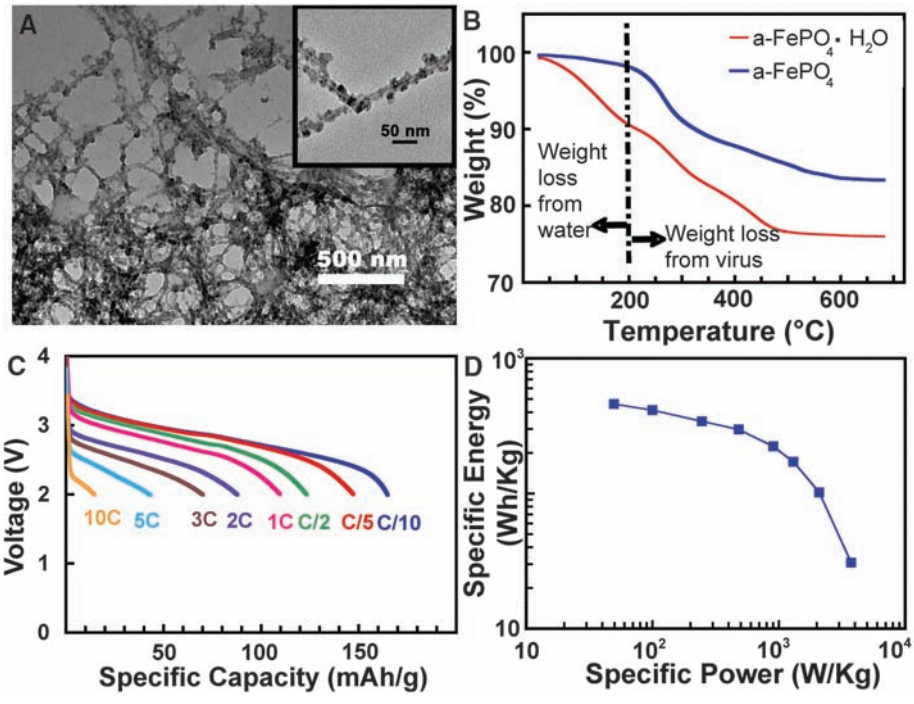

Fig. 1. Characterization of a-$FePO_4$ nanowire cathodes in a one-gene viral system (E4). (**A**) TEM images of templated a-$FePO_4$ nanowires on E4 viruses. (Inset) Magnified images of the same nanowires. (**B**) TGA curve of a-$FePO_4$ nanowires synthesized on Ag NP–loaded E4. For comparison, a TGA curve of a-$FePO_4 \cdot H_2O$ grown on E4 virus (without Ag NPs) is also presented. (**C** and **D**) Electrochemical performance of a-$FePO_4$ viral nanowires on E4 tested between 2.0 and 4.3 V. Active materials loading was 2.63 mg/cm^2. (**C**) First discharge curves at different rates. (**D**) The Ragone plot representing rate performance in terms of specific power versus specific energy (only the active electrode mass is included in the weight).

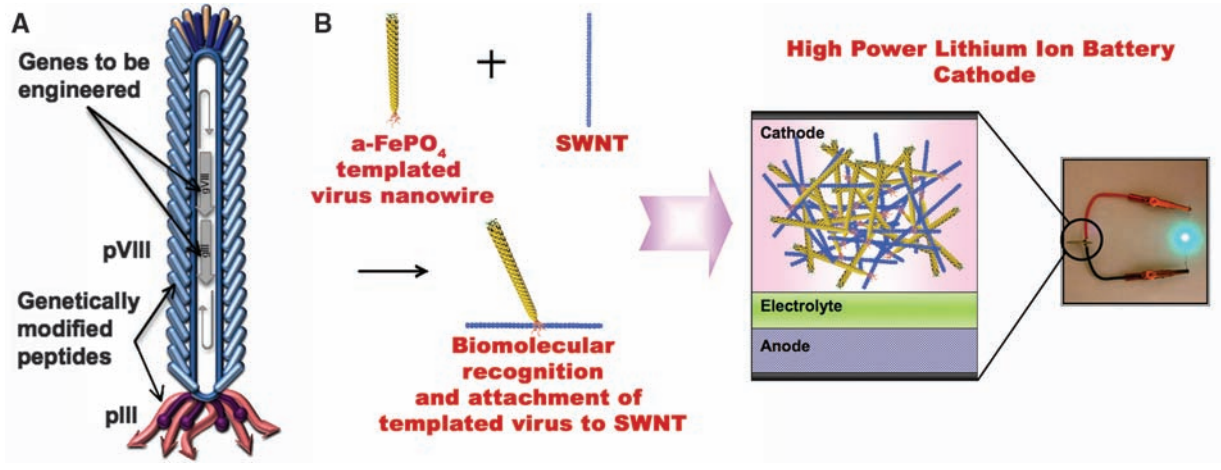

Fig. 2. Biological toolkits: genetic engineering and biomolecular recognition. (**A**) A schematic presentation of the multifunctional M13 virus is shown with the proteins genetically engineered in this study. The gene VIII protein (pVIII), a major capsid protein of the virus, is modified to serve as a template for a-$FePO_4$ growth, and the gene III protein (pIII) is further engineered to have a binding affinity for SWNTs. (**B**) A schematic diagram for fabricating genetically engineered high-power lithium-ion battery cathodes using multifunctional viruses (two-gene system) and a photograph of the battery used to power a green LED. The biomolecular recognition and attachment to conducting SWNT networks make efficient electrical nanoscale wiring to the active nanomaterials, enabling high power performance. These hybrid materials were assembled as a positive electrode in a lithium-ion battery using lithium metal foil as a negative electrode to power a green LED. Active cathode materials loading was 3.21 mg/cm^2. The 2016 Coin Cell, which is 2 cm in diameter and 1.6 mm in thickness, was used. LED power dissipation was 105 mW.

Most structural water in a-$FePO_4 \cdot nH_2O$ is removed from the structure around 200°C (*17*). Surprisingly, the viral nanowires produced on Ag NP-loaded E4 were anhydrous as synthesized, as shown by thermogravimetric analysis (TGA) (Fig. 1B and fig. S2). Without Ag NPs, nanowires have about 10 weight percent (wt %) structural water, which corresponds to $n = 1$ in a-$FePO_4 \cdot nH_2O$. X-ray powder diffraction of a-$FePO_4$ nanowires on Ag NPs-loaded E4 (fig. S3A) showed only peaks indexed as silver chloride (AgCl). We speculate that the dehydration of $FePO_4 \cdot nH_2O$ is related to the chlorination of Ag NPs, which could occur during the incubation with the iron chloride precursor. Part of the chlorinated AgCl was reduced to metallic Ag after electrochemical test (fig. S3B). The reduced metallic Ag could enhance local electronic conductivity as Au nanoparticles could in Co_3O_4/Au heterostructured nanowires (*11*). Although the exact mechanism of dehydration is under investigation, dehydration of structural water without thermal treatment was accomplished by low-temperature and environmentally benign chemistry. The dehydrated structure increases the theoretical capacity to 178 mAh/g, making it a good cathode material.

The electrochemical performance of viral a-$FePO_4$ nanowires as a lithium-ion battery cathode was evaluated (Fig. 1, C and D). Positive electrodes were prepared by mixing viral a-$FePO_4$ with Super P (TIMCAL, SUPER P Li) carbon black and polytetrafluoroethylene (PTFE) binder in a mass ratio of 70:25:5. Details of the weight ratio of components are given in the supporting online material (*16*). The first discharge capacity at a low discharge rate of C/10 (*18*) was 165 mAh/g (93% of the theoretical value) and that of 1C discharge rate was 110 mAh/g (Fig. 1C) (*19*). The rate performance is also presented as a Ragone plot (Fig. 1D). In most electrode materials, specific energy decreases substantially as one applies more power (high rates), drawing more current from the electrodes (*20*). These rate performance values are similar to the best reported values for a-$FePO_4$ synthesized at high temperature (*21*). Even with this one-gene system, the nanostructuring of a-$FePO_4$ nanowires by the virus enabled an enhanced performance. However, high-power performance and capacity retention upon cycling of both the biologically and traditionally synthesized electrodes are still inferior to commercially available c-$LiFePO_4$ cathodes.

Because our particles were already 10 to 20 nm in diameter, our strategy for improved performance was to increase the electronic conductivity in the cathode by achieving better electrical contact between the active materials. Although metallic Ag NPs can locally enhance the electronic conductivity, more important for improved high-power performance is a percolating network throughout the electrodes. It is known that incorporation of well-dispersed materials with high conductivity and high aspect ratio leads to efficient percolating networks (*22*, *23*). Carbon nanotubes (CNTs) have been shown to meet these needs (*23*); thus, well-dispersed single-walled CNTs (SWNTs) in water were used. However, conventional composite electrode fabrication processes inevitably suffer from aggregation of carbon particles, thereby diminishing contact with the active materials (*23*). To achieve better electrical wiring to our biologically derived a-$FePO_4$, we engineered a specific affinity between the conducting material and active material.

Because the major coat protein of the E4 virus serves only as a template for a-$FePO_4$ nanowire growth, additional genetic modification was required to engineer the E4 virus to have a binding affinity for SWNTs. In this context, the gene III protein (pIII), a minor coat protein located at one end of the virus (Fig. 2A), is an ideal tool because gene III can be controlled independently of gene VIII to insert foreign DNA encoding pIII-displayed peptides. Moreover, the peptide sequences identified through the phage display with a pIII phage-display library can be directly inserted into the E4 virus without losing functionality (*12*). Therefore, phage-display experiments to search for peptide sequences with a strong binding affinity for SWNTs were done first, followed by genetic engineering into the E4 virus to produce a

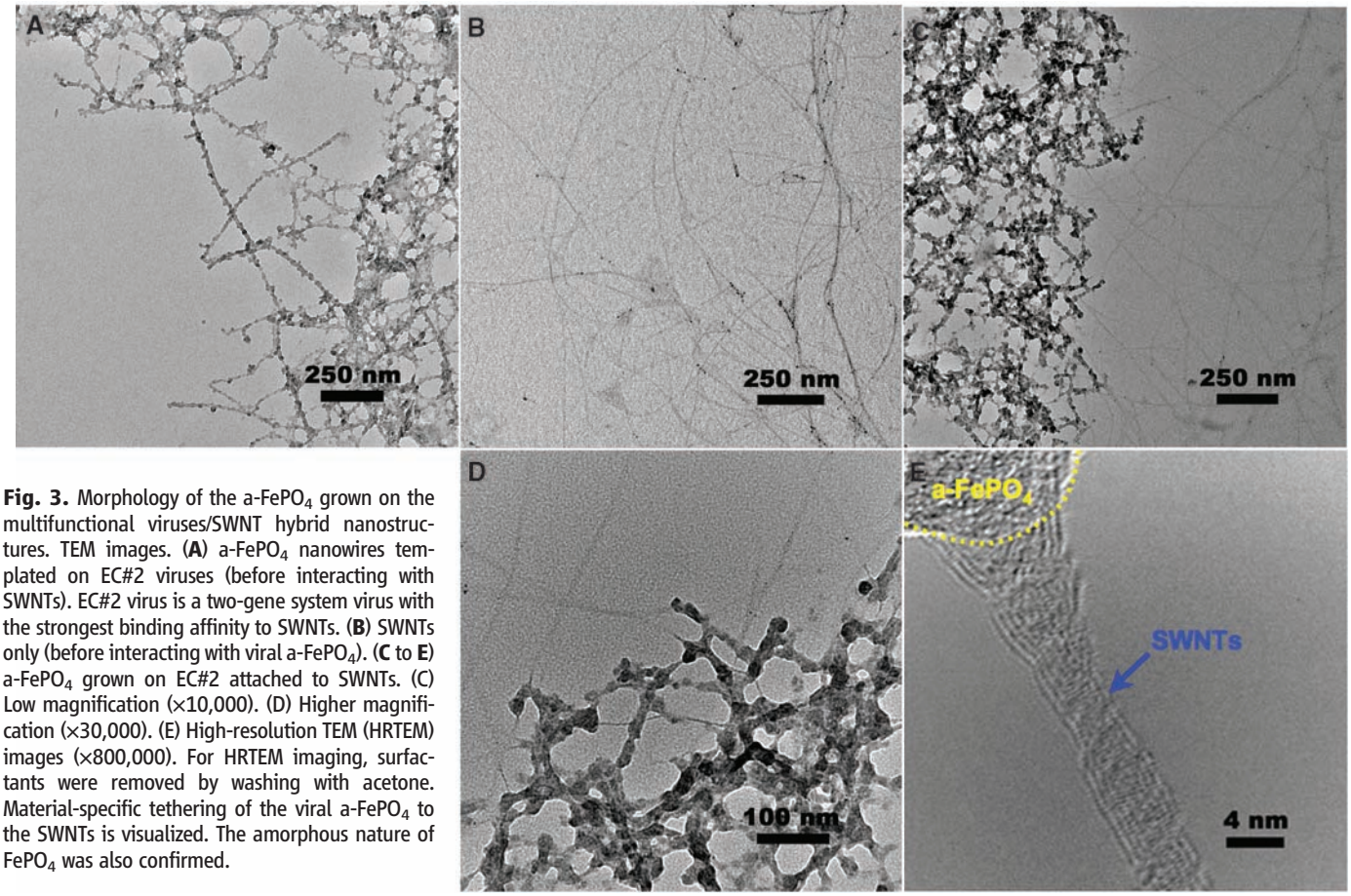

Fig. 3. Morphology of the a-$FePO_4$ grown on the multifunctional viruses/SWNT hybrid nanostructures. TEM images. (**A**) a-$FePO_4$ nanowires templated on EC#2 viruses (before interacting with SWNTs). EC#2 virus is a two-gene system virus with the strongest binding affinity to SWNTs. (**B**) SWNTs only (before interacting with viral a-$FePO_4$). (**C** to **E**) a-$FePO_4$ grown on EC#2 attached to SWNTs. (C) Low magnification (×10,000). (D) Higher magnification (×30,000). (E) High-resolution TEM (HRTEM) images (×800,000). For HRTEM imaging, surfactants were removed by washing with acetone. Material-specific tethering of the viral a-$FePO_4$ to the SWNTs is visualized. The amorphous nature of $FePO_4$ was also confirmed.

multifunctional virus structure [see Methods for details of the procedure (*16*)]. Several consensus sequences were obtained from separate phage-display screening experiments. Among them, sequences N′-HGHPYQHLLRVL-C′ (*24*) (named MC#1) and N′-DMPRTTMSPPPR-C′ (MC#2) were selected for further experiments. The sequence MC#1 started with histidine (H), whose appearance in the first position was often observed in CNT-binding sequences (*25*). Also, it contained several aromatic residues (H and Y), which were expected to bind favorably to the graphene surface via π-stacking interaction (*26*). The sequence MC#2 is quite different from MC#1, and the binding affinity of clone MC#2 was approximately four times as high as that of clone MC#1, whose binding affinity was already two-and-a-half times as high as that of wild-type M13KE in the binding-affinity tests (*27*) (fig. S4, A and B). The strong binding of sequence MC#2 can be explained by the location of the hydrophobic segments of the sequence. The calculated hydrophobicity plot (fig. S5) shows a tri-block structure with hydrophilic regions on both ends and the hydrophobic region in the middle of the sequence. A tri-block structure of hydrophilic-hydrophobic-hydrophilic polymers was effective when used to suspend SWNTs (*25*, *28*).

To genetically engineer E4 virus as a multifunctional biological platform, we fused the selected sequences, MC#1 and MC#2, independently onto the N-terminus of pIII of E4 virus, producing clones EC#1 and EC#2, respectively (*16*). Because two genes (gIII and gVIII in Fig. 2A) were engineered with the desired modification on both pIII and pVIII proteins, we called it a two-gene system.

A schematic diagram for constructing the genetically engineered high-power lithium-ion battery using the multifunctional two-gene virus system is illustrated in Fig. 2B. All viruses were loaded with Ag NPs to synthesize anhydrous a-$FePO_4$. Formation of anhydrous a-$FePO_4$ on pVIII preceded the interaction with SWNTs. The synthesis procedure of anhydrous a-$FePO_4$ nanowires on the multifunctional viruses was the same for growth on the one-gene system. Viral a-$FePO_4$ solutions were then incubated with the SWNT suspensions to form a-$FePO_4$/SWNTs hybrid nanostructures (*16*). The photograph in Fig. 2B is the actual assembled lithium-ion battery powering a light-emitting diode (LED) using Li metal as a negative electrode. The virus-enabled high-power battery could power a green LED with a small amount of active materials loading of 3.21 mg/cm^2. Although this cell was assembled with lithium foil as negative electrode, we have successfully made full virus-based 3-V batteries with various negative electrode materials (fig. S6).

The morphology of hybrid a-$FePO_4$/SWNT nanowires on the EC#2 virus is shown in Fig. 3, C to E. In the high-resolution TEM image (Fig. 3E), six to eight SWNTs are bundled with diameters of 4 to 5 nm. The TEM images show that a-$FePO_4$ nanowires templated on the multifunctional virus were tethered to SWNTs mainly through the pIII attachment; however, they made multiple contacts with neighboring SWNTs because of close positioning. To explore the effect of specificity, we also mixed the one-gene system (E4) viral nanowires solution with SWNTs. Most viral a-$FePO_4$ nanowires on E4 did not make contact with SWNTs, and even if they did, the contact did not seem to be due to specific binding with SWNTs (fig. S7). Moreover, SWNTs aggregated by themselves when there was no specific binding on pIII, suggesting that SWNT-specific viruses enhanced dispersion of SWNTs in solution. Similar observation has been reported showing that SWNT-specific peptides can disperse SWNTs, whereas nonspecific peptides cannot (*25*).

The electrochemical properties of viral a-$FePO_4$/SWNT hybrid materials with 5 wt % SWNTs were evaluated and compared (Fig. 4). Positive electrodes were prepared by mixing viral a-$FePO_4$/SWNT hybrid composites with Super P carbon black and PTFE binder in a mass ratio of 90:5:5 (*16*). The addition of 5 wt % extra carbon was used to increase the total volume, making the powder easier to handle. Without extra carbon, the electrodes showed slightly higher polarization at high rates, but the difference was not substantial. As demonstrated in the first discharge profiles (see Fig. 4A and fig. S8A for full discharge/charge curves) (*19*), electrochemical performances improve markedly as the binding affinity to the SWNTs increases. Specific capac-

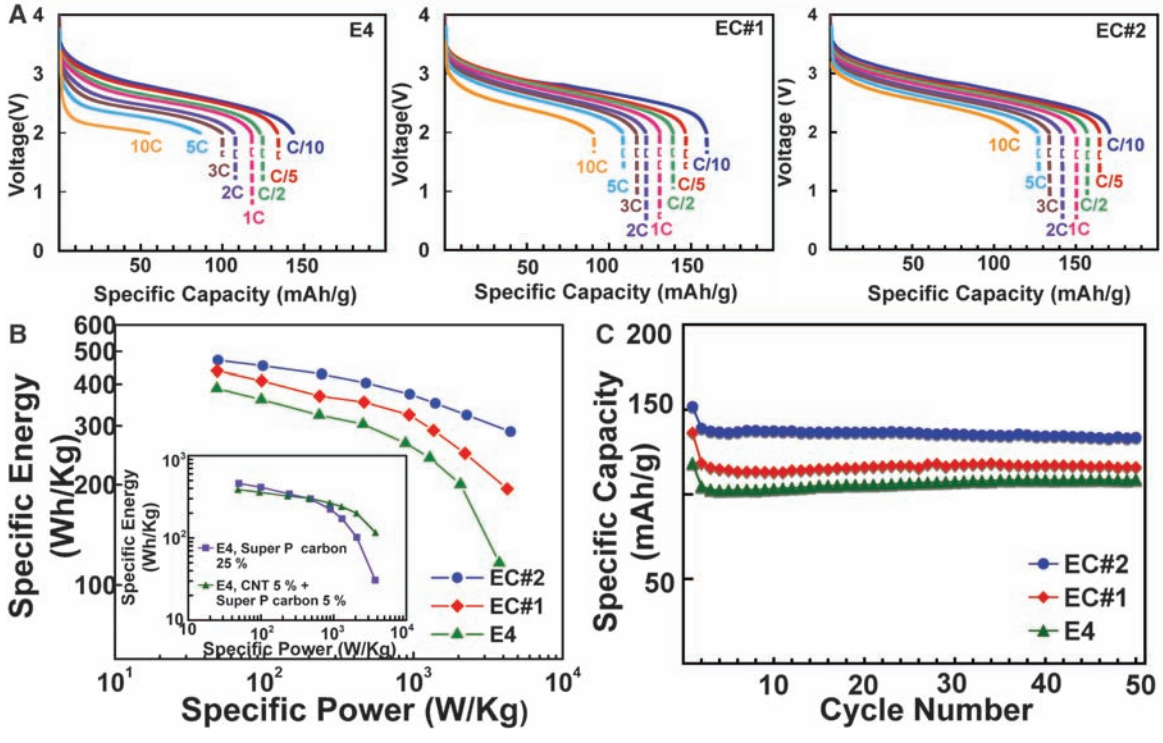

Fig. 4. Electrochemical properties of the a-$FePO_4$ viral nanowires in two-gene systems tested between 2.0 and 4.3 V. Rate capabilities and capacity retention upon cycling of the a-$FePO_4$ nanowires/SWNTs hybrid electrodes templated on different clones are presented. All a-$FePO_4$/SWNT hybrid materials had 5 wt % SWNTs. EC#2 virus is a two-gene system virus with the strongest binding affinity to SWNTs; EC#1 is a two-gene system virus with moderate binding affinity; and E4 is a one-gene system virus with no insert on pIII. (**A**) First discharge curves at different rates. Active materials loading: E4, 2.34 mg/cm^2; EC#1, 2.31 mg/cm^2; and EC#2, 2.62 mg/cm^2. (**B**) Ragone plot showing improvement in high-power performance with higher binding affinity toward SWNTs (only active electrode mass is included in the weight). (Inset) Comparison of rate capability of E4 virus–based cathodes with either Super P carbon or SWNTs. Electrodes with well-dispersed SWNTs, even with much smaller amounts, exhibited improved rate performance due to better percolation networks than carbon black powders. (**C**) Capacity retention for 50 cycles at 1C rate. There was no obvious fading for at least 50 cycles. Active materials loading: E4, 2.90 mg/cm^2; EC#1, 2.22 mg/cm^2; and EC#2, 2.27 mg/cm^2.

ity at a low discharge rate of C/10 increased from 143 mAh/g (E4) to 160 mAh/g with EC#1 and to 170 mA·hour/g with EC#2. The performance improvement is more pronounced at higher rates. Discharge profiles of the two-gene system show much lower polarization and maintain much higher capacity than those of the one-gene system at high rates. When compared with the best reported capacity for a-$FePO_4$ at a high rate of 3C (80 mAh/g) (*21*), EC#2 showed a capacity of 134 mAh/g, confirming substantially improved high-power performance. Moreover, when we cycled EC#2 between 1.5 and 4.3 V, the first discharge capacity at 10C reached 130 mAh/g. No published data for a-$FePO_4$ are available for comparison at rates higher than 3C, but this capacity value obtained for the two-gene system is comparable to the capacity from state-of-the-art c-$LiFePO_4$. The power performance of the multifunctional virus-based cathode was further compared with a Ragone plot. Figure 4B shows that two-gene system–based materials delivered much higher energy than the one-gene system at high power. At a specific power of 4000 W/kg (corresponding to a rate of ~10C), the energy density of EC#1 and EC#2 was two times and three times as high, respectively, as that of E4. Again, the high-power performance scales with binding affinity. In Fig. 4B (inset), the rate performance of E4 virus–based cathodes with either Super P carbon or SWNTs was tested. Well-dispersed SWNTs by themselves make better electrical wiring to active materials due to better percolation networks than carbon black powders (*23*), confirming the importance of nanoscale electrical wiring. Figure 4C shows the stable capacity retention of a-$FePO_4$/SWNT hybrid electrodes upon cycling at 1C. Up to 50 cycles, virtually no capacity fade was observed. A slight capacity loss after the first cycle is a characteristic of a-$FePO_4$ materials (*17*, *21*). When cycled at C/10 rate again after the sample was tested for several cycles at rates from C/10 to 10C, the original capacity was recovered, confirming structural stability (fig. S8B). Structural stability of viral a-$FePO_4$/SWNT hybrid nanostructures was induced by materials-specific binding and stiff, robust carbon nanotubes, leading to excellent retention at a low SWNT content of 5 wt %. Because the density of SWNTs is 1.33 g/cm^3 (*23*), it would decrease the volumetric energy density of the hybrid electrodes. However, although we adopted SWNTs to show that we can achieve nanoscale wiring by genetic engineering, we expect that we could optimize the fraction of the conducting additives by using even better-conducting nanowires with high aspect ratio and higher density.

There have been efforts to electrically address electrode materials with poor electronic conductivity through nanoscale wiring of active materials (*8*, *29*, *30*). However, the wiring tools used so far were functionalized for a single component, either active materials (*8*, *30*) or conducting materials (*29*). The wiring did not completely exploit specificity but depended on the random occurrence of contacts between conducting networks and active materials. By developing a two-gene system with a universal handle to pick up electrically conducting carbon nanotubes, we devised a method to realize nanoscale electrical wiring for high-power lithium-ion batteries using basic biological principles. This biological scaffold could further extend possible sets of electrode materials by activating classes of materials that have been excluded because of their extremely low electronic conductivity.

References and Notes

1. P. G. Bruce, B. Scrosati, J. M. Tarascon, *Angew. Chem. Int. Ed.* **47**, 2930 (2008).
2. M. Armand, J. M. Tarascon, *Nature* **451**, 652 (2008).
3. S. Y. Chung, J. T. Bloking, Y. M. Chiang, *Nat. Mater.* **1**, 123 (2002).
4. C. Delacourt, P. Poizot, S. Levasseur, C. Masquelier, *Electrochem. Solid-State Lett.* **9**, A352 (2006).
5. D. H. Kim, J. Kim, *Electrochem. Solid-State Lett.* **9**, A439 (2006).
6. J. M. Tarascon *et al.*, *Dalton Trans.* 2988 (2004).
7. F. Croce *et al.*, *Electrochem. Solid-State Lett.* **5**, A47 (2002).
8. Y. S. Hu *et al.*, *Adv. Mater.* **19**, 1963 (2007).
9. S. R. Whaley, D. S. English, E. L. Hu, P. F. Barbara, A. M. Belcher, *Nature* **405**, 665 (2000).
10. K. T. Nam, B. R. Peelle, S. W. Lee, A. M. Belcher, *Nano Lett.* **4**, 23 (2004).
11. K. T. Nam *et al.*, *Science* **312**, 885 (2006).
12. Y. Huang *et al.*, *Nano Lett.* **5**, 1429 (2005).
13. K. T. Nam *et al.*, *Proc. Natl. Acad. Sci. U.S.A.* **105**, 17227 (2008).
14. A. S. Khalil *et al.*, *Proc. Natl. Acad. Sci. U.S.A.* **104**, 4892 (2007).
15. K. T. Nam, Y. J. Lee, E. M. Krauland, S. T. Kottmann, A. M. Belcher, *ACS Nano* **2**, 1480 (2008).
16. Materials and methods are available as supporting material on *Science* Online.
17. P. P. Prosini *et al.*, *J. Electrochem. Soc.* **149**, A297 (2002).
18. Rates are reported in C-rate convention, where C/*n* is the rate (current per gram) corresponding to complete charging or discharging to the theoretical capacity of the materials in *n* hours. Here, 1C corresponds to 178 mA/g.
19. In the rate test, the cell was charged at C/10 rate to 4.3 V and then held at 4.3 V until the current density was lower than C/100 and discharged at different rates.
20. K. Kang, Y. S. Meng, J. Breger, C. P. Grey, G. Ceder, *Science* **311**, 977 (2006).
21. Z. C. Shi *et al.*, *Electrochim. Acta* **53**, 2665 (2008).
22. S. Ahn, *Electrochem. Solid-State Lett.* **1**, 111 (1998).
23. J. S. Sakamoto, B. Dunn, *J. Electrochem. Soc.* **149**, A26 (2002).
24. Abbreviations for the amino acid residues are as follows: D, Asp; G, Gly; H, His; L, Leu; M, Met; P, Pro; Q, Gln; R, Arg; S, Ser; T, Thr; V, Val; and Y, Tyr.
25. S. Wang *et al.*, *Nat. Mater.* **2**, 196 (2003).
26. M. Zheng *et al.*, *Science* **302**, 1545 (2003).
27. E. Ryan, U.S. patent (2002).
28. V. C. Moore *et al.*, *Nano Lett.* **3**, 1379 (2003).
29. L. Kavan, *Chem. Mater.* **19**, 4716 (2007).
30. Q. Wang, N. Evans, S. M. Zakeeruddin, I. Exnar, M. Gratzel, *J. Am. Chem. Soc.* **129**, 3163 (2007).

31. This work was supported by the Army Research Office Institute of the Institute of Collaborative Biotechnologies (ICB) and U.S. NSF through the Materials Research Science and Engineering Centers program. H.Y. is grateful for Korean Government Overseas Scholarship. W.-J.K. is grateful for support from the Korea Research Foundation Grant funded by the Korean Government (MOEHRD) (KRF-2005-214-D00260). K.K is grateful for funding support from Korea Science and Engineering Foundation of the Ministry of Education, Science and Technology (No. R01-2008-000-10913-0) and Energy Resource Technology Development program by the Ministry of Knowledge Economy (No. 2008-E-EL11-P-08-3-010). M.S.S. is grateful for funding from the NSF and the Office of Naval Research Young Investigator Grant.

Supporting Online Material

www.sciencemag.org/cgi/content/full/1171541/DC1
Materials and Methods
Figs. S1 to S8
References

28 January 2009; accepted 25 March 2009
Published online 2 April 2009;
10.1126/science.1171541
Include this information when citing this paper.

Greater Transportation Energy and GHG Offsets from Bioelectricity Than Ethanol

J. E. Campbell,[1,2]* D. B. Lobell,[3] C. B. Field[4]

The quantity of land available to grow biofuel crops without affecting food prices or greenhouse gas (GHG) emissions from land conversion is limited. Therefore, bioenergy should maximize land-use efficiency when addressing transportation and climate change goals. Biomass could power either internal combustion or electric vehicles, but the relative land-use efficiency of these two energy pathways is not well quantified. Here, we show that bioelectricity outperforms ethanol across a range of feedstocks, conversion technologies, and vehicle classes. Bioelectricity produces an average of 81% more transportation kilometers and 108% more emissions offsets per unit area of cropland than does cellulosic ethanol. These results suggest that alternative bioenergy pathways have large differences in how efficiently they use the available land to achieve transportation and climate goals.

Concerns over petroleum prices and greenhouse gas (GHG) emissions are driving research investments into alternative transportation technologies, but the preferred technology is still being debated (*1*–*5*). There is surging interest in the use of agriculture lands to grow energy feedstocks for these alternative transportation technologies. Two leading technology developments, cellulosic ethanol and electric vehicle batteries, provide alternative pathways for bioenergy-

based transportation. Biomass can be converted into ethanol to power internal combustion vehicles (ICVs) or converted into electricity to power battery electric vehicles (BEVs). It is uncertain which pathway could reach technical and economic maturity first. The cellulosic ethanol pathway benefits from commercially available flex-fuel vehicles but requires substantial investments in infrastructure as well as technology advancements to reduce costs for energy conversion (*6*). The bioelectricity pathway shows promise in existing distribution infrastructure and emerging commercial offerings of BEVs that meet technology challenges of range, cost, and charging time. Electricity produced from biomass is a near-term renewable energy source that can be implemented with biomass boilers, integrated gasification combined cycle (IGCC) power plants, or co-combustion with coal (*7*, *8*).

Although both of these bioenergy pathways have real potential to meet transportation goals, their relative performance with respect to land-use efficiency is not well quantified. Given the limited area of land that is available to grow biofuels crops without causing direct or indirect land-use impacts (*9*–*12*), bioenergy applications should maximize the efficiency with which a given land area is used to meet transportation and climate change goals. In one study, the use of willow biomass for electricity was shown to have greater transportation fuel displacement and GHG offsets than corn ethanol (*13*). A quantification of the transportation output and GHG offset per unit area of cropland, across a range of feedstocks, energy conversion technologies, and vehicle types, is needed to assess the land-use efficiency of these alternative energy pathways.

Here, we present a life-cycle assessment comparing the performance of bioelectricity and ethanol with respect to transportation kilometers and GHG offsets achieved per unit area of biofuels cropland. The Energy and Resources Group Biofuel Analysis Meta-Model (EBAMM) is used to consider scenarios that cover a range of feedstocks and energy conversion technologies, including corn and cellulosic ethanol (*14*). A range of vehicle classes is evaluated with published U.S. Environmental Protection Agency (EPA) efficiencies for highway and city driving of ICVs and BEVs (*15*). The life-cycle assessment includes accounting of the fuel-cycle energy (energy input needed to grow the feedstock and convert it to either electricity or ethanol) (*14*) and vehicle-cycle energy (energy input needed to manufacture and dispose of vehicles) (*16*–*18*). Co-product credits in EBAMM favor the ethanol pathway by accounting for ethanol co-products but not potential bioelectricity co-products, including steam for heat and fly ash for cement. Whereas new corn ethanol refineries may have higher efficiencies than those used in EBAMM (*19*, *20*), the cellulosic case provides a much higher ethanol efficiency case for comparing ethanol to bioelectricity (biomass is used to power the cellulosic ethanol conversion process). Because crop yields (*21*, *22*) and land-use impacts (*12*) vary beyond those applied in the EBAMM model, our analysis is best suited for a comparison of these two pathways rather than quantification of the total land area needed for an individual pathway. Although burning kernels for electricity is an unlikely pathway, the kernels of the corn plant are harvested for energy use in the corn scenarios for comparison of the ethanol and bioelectricity pathways (*23*). Detailed methods and results are provided in the supporting online material.

The net transportation output per hectare is larger for the bioelectricity case. With BEVs and ICVs of similar size, one can travel farther on biomass grown on a hectare of land when it is converted to electricity than when it is converted to ethanol. To illustrate the transportation results, we show the various inputs and outputs in Fig. 1 for the case of the switchgrass feedstock with a small sport utility vehicle (SUV) driving on the highway. For this case, the gross transportation output per hectare is 85% greater for bioelectricity than for cellulosic ethanol. This is largely due to the fact that the small SUV BEV has an electric motor that is 3.1 times as efficient as the internal combustion engine of the small SUV ICV for highway driving (*24*). The fuel cycle and vehicle cycle account for the energy inputs and co-products during the production of the biomass, fuel, and vehicles. Gross transportation output is converted to net transportation output by subtracting the fuel-cycle and vehicle-cycle costs. Input costs were converted from energy units (megajoules per hectare per year) to transportation distance units (kilometers per hectare per year) using the ICV efficiency for petroleum inputs and the BEV efficiency for coal, natural gas, and electricity inputs. The vehicle-cycle inputs per hectare of cropland (costs to manufacture, maintain, and dispose of the vehicle over its lifetime) are large for the bioelectricity case for two reasons (*24*): First, the vehicle-cycle costs per hectare are calculated by scaling the lifetime vehicle costs by the gross distance traveled per hectare, and the gross distance is larger for bioelectricity than for ethanol. Second, the lifetime vehicle costs are larger for the BEV than the ICV because of the cost of the batteries. The net transportation output per hectare is 56% greater for the bioelectricity pathway than the ethanol pathway for this case of a switchgrass feedstock with a small SUV driving on the highway.

The gross and net transportation outputs for a range of feedstocks and vehicle classes are shown in Fig. 2. For the gross transportation distance, the bioelectricity output is, on average, 112% greater than the ethanol output for the full range of feedstocks, energy conversions, and vehicle efficiencies. For the net transportation distance, several of the corn ethanol cases result in negative distances because the distance that could be traveled with the net fuel-cycle inputs (petroleum via ICV and electricity; coal and natural gas via BEV) is greater than the distance that could be traveled with the gross ethanol output. The average net transportation distance for the switchgrass feedstock was 81% larger (SE = 21%) for bioelectricity than for ethanol. Whereas bioelectricity generally performed better than ethanol, the bioelectricity and ethanol pathways had similar results for highway driving with the small car and full-size SUV. The two BEVs tested by the EPA for these vehicle classes had particularly low highway efficiencies and low ranges (<166 km). This suggests that these specific BEVs were not designed for highway driving, as opposed to the midsize car BEV and small SUV BEV, which perform well for city and highway driving. A high-efficiency case (hybrid ICVs, IGCC power plant, excluding low-range BEV) results in 95% greater net transportation output for bioelectricity than for ethanol (*24*). The relative efficiency of these pathways may be altered in the future with new powertrain technologies (*5*), heating co-products,

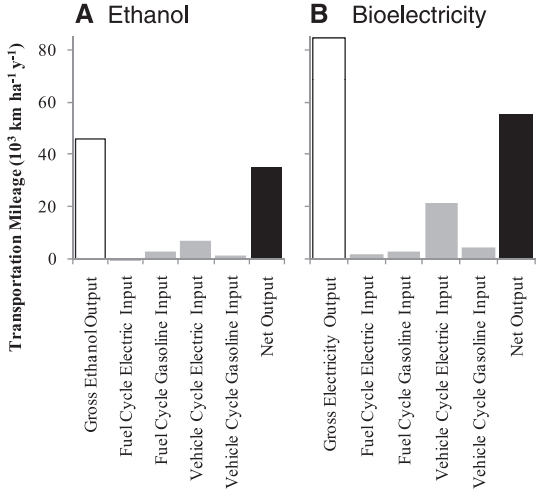

Fig. 1. Transportation for ethanol (**A**) and bioelectricity (**B**) using the switchgrass feedstock with highway driving in a small SUV. Electric inputs account for natural gas, coal, and electricity used in the fuel cycle and vehicle cycle. The liquid fuel inputs are accounted for as transportation input using the ICV efficiency, and the electric inputs are accounted for using the BEV efficiency. Co-products in the ethanol pathway are subtracted from the ethanol inputs in the EBAMM. Vehicle-cycle inputs are scaled by the total vehicle lifetime distance relative to the distance traveled with the gross fuel minus the fuel-cycle inputs (*24*).

[1]College of Engineering, University of California, Merced, CA 95344, USA. [2]Sierra Nevada Research Institute, University of California, Merced, CA 95344, USA. [3]Program on Food Security and the Environment, Stanford University, Stanford, CA 94305, USA. [4]Department of Global Ecology, Carnegie Institution of Washington, Stanford, CA 94305, USA.

*To whom correspondence should be addressed. E-mail: ecampbell3@ucmerced.edu

and electricity storage approaches (*25*). However, on the basis of the efficiencies of deployed bioelectricity technologies and emerging cellulosic ethanol technologies, the bioelectricity pathway consistently produces more transportation kilometers than the ethanol pathway.

The gross and net GHG offsets for a range of feedstocks and vehicle classes are shown in Fig. 2. For the switchgrass feedstock, the average net offset for bioelectricity is 108% greater (SE = 28%) than the offset for ethanol. For both pathways, these GHG offsets could only be achieved if land-use impacts are avoided (*9*–*12*). For the bioelectricity pathway, the GHG offsets could be greatly increased by accounting for the steam coproducts during electricity generation. Furthermore, the application of carbon capture and sequestration (CCS) technologies with bioelectricity could result in a carbon-negative energy source. By sequestering the flue gas CO_2 at the power plant, the bioelectricity pathway could result in a net removal of CO_2 from the air.

The life-cycle assessment considered here suggests that a limited area of cropland would deliver more transportation and GHG offsets with a bioelectricity pathway than with an ethanol pathway. These results provide further support for general bioelectricity applications, which are already thought to have greater climate mitigation benefits than ethanol (*26*–*28*). Electric transportation may also provide a bridge that connects transportation to future renewable energy sources such as solar and wind power. Combining CCS with the bioelectricity pathway could result in a carbon-negative energy source that removes CO_2 from the atmosphere. On the other hand, electric transportation also provides a bridge to the use of conventional coal energy for transportation. These results do not indicate that bioelectricity is the preferred pathway over ethanol because there are numerous other criteria that need to be evaluated, such as impacts on regional water resources (*29*), battery toxicity and recycling (*30*), air pollution (*7*), and economic constraints (*18*). The optimal pathway for biomass will also depend on how efficiently other feedstocks can be converted to both liquid fuels and electricity. Specifically, the competitiveness of biomass ethanol depends on the cost of petroleum, whereas the competitiveness of biomass electricity depends on the cost of coal, wind, hydro, solar, and nuclear power. These results do suggest, however, that alternative bioenergy pathways have large differences in how efficiently they use the limited available land to maximize transportation and climate benefits.

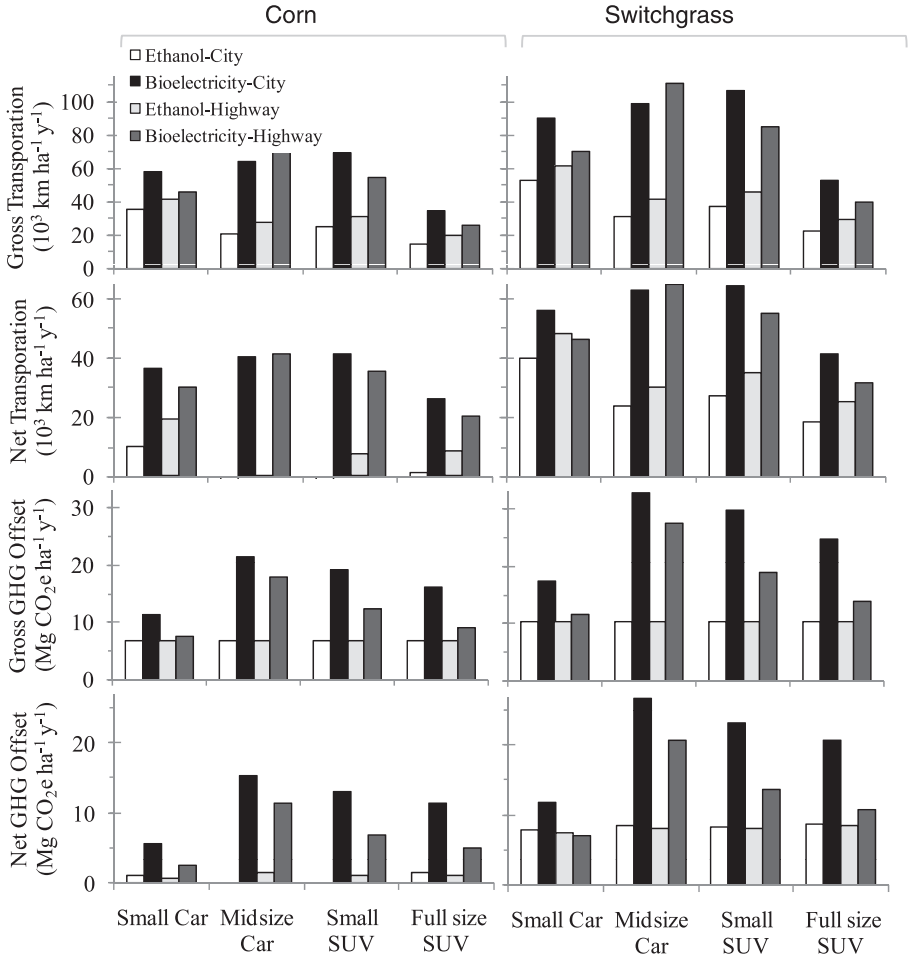

Fig. 2. Transportation and GHG offsets from bioelectricity and ethanol, based on a range of vehicle classes, agriculture systems, and energy conversion technologies. The net output accounts for coproducts as well as for input in the fuel cycle and vehicle cycle. Results are not plotted for cases when a further distance could be traveled with input energy than with gross output energy (*24*).

References and Notes

1. C. A. Amann, *Int. J. Veh. Des.* **17**, 510 (1996).
2. R. Gilbert, A. Perl, *Energy Policy* **35**, 3053 (2007).
3. H. L. Maclean, *Int. J. Veh. Des.* **35**, 27 (2004).
4. J. Romm, *Energy Policy* **34**, 2609 (2006).
5. M. A. Kromer, J. B. Heywood, "Electric Powertrains: Opportunities and Challenges in the U.S. Light-Duty Vehicle Fleet" *Tech. Report No. LFEE 2007-03 RP* (MIT Laboratory for Energy and the Environment, Cambridge, MA, 2007).
6. C. E. Wyman, *Trends Biotechnol.* **25**, 153 (2007).
7. L. Baxter, *Fuel* **84**, 1295 (2005).
8. A. E. Farrell, A. R. Gopal, *MRS Bull.* **33**, 373 (2008).
9. J. E. Campbell, D. B. Lobell, R. C. Genova, C. B. Field, *Environ. Sci. Technol.* **42**, 5791 (2008).
10. C. B. Field, J. E. Campbell, D. B. Lobell, *Trends Ecol. Evol.* **23**, 65 (2008).
11. D. Tilman, J. Hill, C. Lehman, *Science* **314**, 1598 (2006).
12. J. Fargione, J. Hill, D. Tilman, S. Polasky, P. Hawthorne, *Science* **319**, 1235 (2008); published online 5 February 2008 (10.1126/science.1152747).
13. K. Hedegaard, K. A. Thyø, H. Wenzel, *Environ. Sci. Technol.* **42**, 7992 (2008).
14. A. E. Farrell *et al.*, *Science* **311**, 506 (2006).
15. *Fuel Economy Guide* (U.S. Department of Energy/U.S. EPA, Washington, DC, 2008).
16. A. Burnham, M. Wang, Y. Wu, "Development and Applications of GREET 2.7—The Transportation Vehicle-Cycle Model" *Tech. Report No. ANL/ESD/06-5* (Argonne National Laboratory, Argonne, IL, 2006).
17. M. A. Delucchi, "A Multi-Country Analysis of Lifecycle Emissions from Transportation Fuels and Motor Vehicles" *Tech. Report No. UCD—ITS—RR—05—10* (Univ. of California, Davis, CA, 2005).
18. M. A. Delucchi, T. E. Lipman, *Transp. Res. Part D Trans. Environ.* **6**, 371 (2001).
19. A. J. Liska, K. G. Cassman, *J. Biobased Mat. Bioenergy* **2**, 187 (2008).
20. M. Wang, M. Wu, H. Huo, *Environ. Res. Lett.* **2**, 024001 (2007).
21. E. A. Heaton, F. G. Dohleman, S. P. Long, *Glob. Change Biol.* **14**, 2000 (2008).
22. H. K. Gibbs *et al.*, *Environ. Res. Lett.* **3**, 034001 (2008).
23. R. V. Morey, D. G. Tiffany, D. L. Hatfield, *Appl. Eng. Agric.* **22**, 723 (2006).
24. See supporting material on *Science* Online.
25. M. Armand, J. M. Tarascon, *Nature* **451**, 652 (2008).
26. G. Marland, S. Marland, *Water Air Soil Pollut.* **64**, 181 (1992).
27. G. Marland, B. Schlamadinger, *Biomass Bioenergy* **13**, 389 (1997).
28. R. Samson *et al.*, *Crit. Rev. Plant Sci.* **24**, 461 (2005).
29. C. W. King, M. E. Webber, *Environ. Sci. Technol.* **42**, 4305 (2008).
30. N. L. C. Steele, D. T. Allen, *Environ. Sci. Technol.* **32**, 40A (1998).

31. This work was supported by University of California, Merced start-up funds, the Stanford University Global Climate and Energy Project, the Carnegie Institution, and NASA New Investigator grant no. NNX08AV25G to D.B.L. We thank K. Gillingham and C. Weber for critical comments on the manuscript.

Supporting Online Material

www.sciencemag.org/cgi/content/full/1168885/DC1
Tables S1 to S13
References

24 November 2008; accepted 15 April 2009
Published online 7 May 2009;
10.1126/science.1168885
Include this information when citing this paper.

Exploration of Victoria Crater by the Mars Rover Opportunity

S. W. Squyres,[1]* A. H. Knoll,[2] R. E. Arvidson,[3] J. W. Ashley,[4] J. F. Bell III,[1] W. M. Calvin,[5] P. R. Christensen,[4] B. C. Clark,[6] B. A. Cohen,[7] P. A. de Souza Jr.,[8] L. Edgar,[9] W. H. Farrand,[10] I. Fleischer,[11] R. Gellert,[12] M. P. Golombek,[13] J. Grant,[14] J. Grotzinger,[9] A. Hayes,[9] K. E. Herkenhoff,[15] J. R. Johnson,[15] B. Jolliff,[3] G. Klingelhöfer,[11] A. Knudson,[4] R. Li,[16] T. J. McCoy,[17] S. M. McLennan,[18] D. W. Ming,[19] D. W. Mittlefehldt,[19] R. V. Morris,[19] J. W. Rice Jr.,[4] C. Schröder,[11] R. J. Sullivan,[1] A. Yen,[13] R. A. Yingst[20]

The Mars rover Opportunity has explored Victoria crater, a ~750-meter eroded impact crater formed in sulfate-rich sedimentary rocks. Impact-related stratigraphy is preserved in the crater walls, and meteoritic debris is present near the crater rim. The size of hematite-rich concretions decreases up-section, documenting variation in the intensity of groundwater processes. Layering in the crater walls preserves evidence of ancient wind-blown dunes. Compositional variations with depth mimic those ~6 kilometers to the north and demonstrate that water-induced alteration at Meridiani Planum was regional in scope.

The Mars Exploration Rover Opportunity examined a small bedrock outcrop at its landing site in Eagle crater (*1*) and ~7.5 m of stratigraphy at Endurance crater, 800 m to the east (*2*). Here, we report on a third stratigraphic section, more than 10 m thick, at Victoria crater, 6 km south of Eagle and Endurance.

Exploration of Victoria (Fig. 1) began on sol 952 (*3*) with a traverse along the crater's northern rim, imaging cliff faces to document stratigraphy. Opportunity then drove to Duck Bay and descended into the crater on sol 1293 to begin in situ observations. Opportunity exited the crater on sol 1634.

Victoria crater is ~750 m in diameter and ~75 m deep. Its outline is serrated, with sharp, steep promontories separated by rounded, less steep alcoves. The crater rim is ~4 to 5 m high and ~120 to 220 m wide. It is surrounded by an annulus of smooth terrain that extends approximately one crater diameter from the rim, suggesting that the annulus is derived from the crater's ejecta blanket. Such characteristics, along with observed morphology and ejecta thickness, indicate that Victoria formed as a primary crater ~600 m in diameter and ~125 m deep (*4*). On the crater floor is a dune field. The crater has been widened by erosion, and its depth has been reduced by deposition of wind-blown sand and material released from the crater walls. Eolian erosion and mass wasting have contributed to the development of alcoves and promontories.

The sulfate-rich sedimentary rocks at Meridiani are easily eroded by eolian abrasion (*1*, *2*). Therefore, the annulus, although derived from the original ejecta blanket, preserves no perched ejecta blocks; they have been planed off by eolian abrasion. Ejecta currently is exposed only in the uppermost interior walls of the crater and near the rim where soil cover is discontinuous. There is no evidence that the impact excavated through the sediments into an underlying nonsedimentary basement unit.

Small hematite-rich spherules interpreted as concretions characterize sedimentary rocks throughout Meridiani (*1*, *2*). Opportunity gained more than 30 m of elevation during the traverse from Endurance to Victoria; because regional outcrop is approximately flat-lying, this may have been a traverse up-section. Spherule size observed in outcrop shows a systematic decrease with elevation (*5*–*7*) (fig. S1), documenting regional and/or stratigraphic variation in the intensity of groundwater processes (e.g., less water higher in the section) after sulfate-rich sand deposition.

Once Opportunity entered Victoria's annulus, large spherules reappeared in the soil. The source of these spherules is suggested by ejecta blocks at the Cape of Good Hope that exhibit purple-gray colors in Pancam (*8*) false-color views (*9*), distinct from typical outcrop rocks (Fig. 2). Pancam spectra of these blocks are correspondingly unusual, exhibiting negative 754- to 1009-nm slopes and weaker 535-nm band depths than typical "purple" rocks (*10*). We chose one, Cercedilla, for study, which unlike nearby bedrock contains large (~6 mm) spherules.

Cercedilla was abraded using the Rock Abrasion Tool (RAT) (*11*) (Fig. 2c) and imaged with the Microscopic Imager (MI) (*12*). The elemental chemistry of Cercedilla revealed by the Alpha Particle X-Ray Spectrometer (APXS) (*13*) is similar to that in the deepest part of Endurance crater (*14*) and is distinct from that in the examined section in Victoria crater, in having lower FeO_T/Al_2O_3 (where FeO_T is total iron expressed as FeO) and no Cl enrichment.

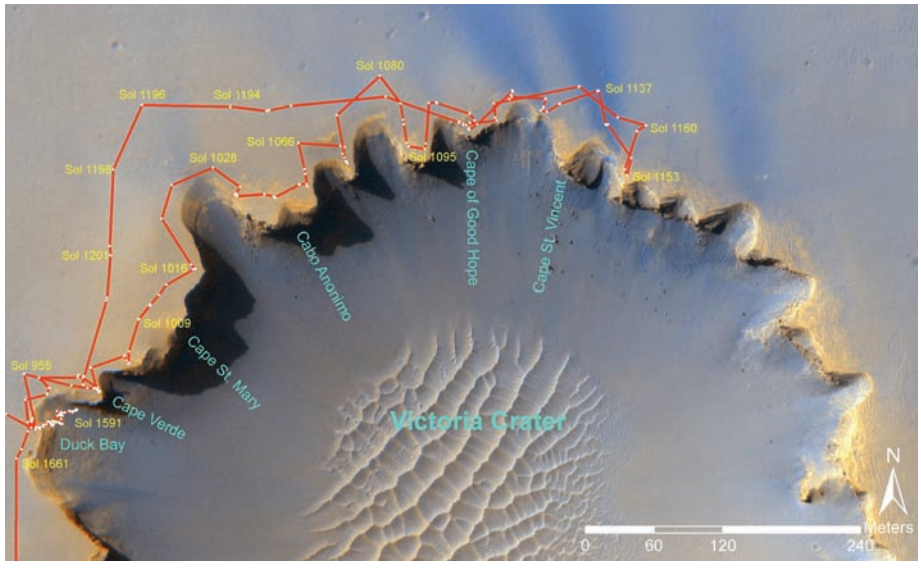

Fig. 1. Opportunity's traverse at Victoria crater. Image acquired by the Mars Reconnaissance Orbiter High Resolution Imaging Science Experiment camera.

[1]Department of Astronomy, Space Sciences Building, Cornell University, Ithaca, NY 14853, USA. [2]Botanical Museum, Harvard University, Cambridge, MA 02138, USA. [3]Department of Earth and Planetary Sciences, Washington University, St. Louis, MO 63031, USA. [4]School of Earth and Space Exploration, Arizona State University, Tempe, AZ 85287, USA. [5]University of Nevada, Reno, Geological Sciences, Reno, NV 89557, USA. [6]Lockheed Martin Corporation, Littleton, CO 80127, USA. [7]National Aeronautics and Space Administration, Marshall Space Flight Center, Huntsville, AL 35812, USA. [8]Tasmanian Information and Communication Technologies Centre, Commonwealth Scientific and Industrial Research Organisation, Castray Esplanade, Hobart TAS 7000, Australia. [9]Division of Geological and Planetary Sciences, California Institute of Technology, Pasadena, CA 91125, USA. [10]Space Science Institute, Boulder, CO 80301, USA. [11]Institut für Anorganische und Analytische Chemie, Johannes Gutenberg-Universität, Mainz, Germany. [12]Department of Physics, University of Guelph, Guelph, ON, N1G 2W1, Canada. [13]Jet Propulsion Laboratory, California Institute of Technology, Pasadena, CA 91109, USA. [14]Center for Earth and Planetary Studies, Smithsonian Institution, Washington, DC 20560, USA. [15]U.S. Geological Survey, Flagstaff, AZ 86001, USA. [16]Department of Civil and Environmental Engineering and Geodetic Science, Ohio State University, Columbus, OH 43210, USA. [17]Department of Mineral Sciences, National Museum of Natural History, Smithsonian Institution, Washington, DC 20560, USA. [18]Department of Geosciences, State University of New York, Stony Brook, NY 11794, USA. [19]Astromaterials Research and Exploration Science, NASA Johnson Space Center, Houston, TX 77058, USA. [20]Natural and Applied Sciences, University of Wisconsin Green Bay, Green Bay, WI 54311, USA.

*To whom correspondence should be addressed. E-mail: squyres@astro.cornell.edu

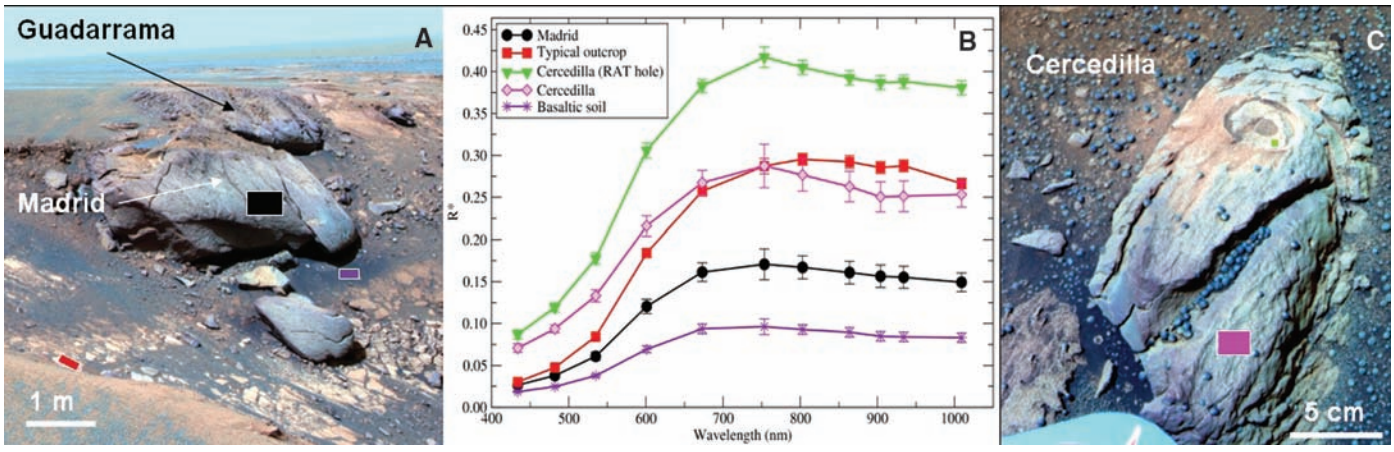

Fig. 2. (**A**) Pancam false-color image (red, 753 nm; green, 535 nm; blue, 432 nm) of Madrid and Guadarrama (sequence p2579, sol 1097). (**B**) Pancam spectra [*R** = absolute reflectivity/cos(incidence angle)] of regions outlined in (A) and (C). (**C**) Pancam false-color image of Cercedilla (sequence p2564, sol 1184).

Cercedilla and other spectrally similar blocks probably represent materials excavated during crater formation from a deeper stratigraphic unit within Victoria crater. The abundance of large spherules in Cercedilla supports the idea that the spherules in the annulus were released by erosion from deeply sourced, spherule-rich ejecta, consistent with the hypothesis that the systematic decrease in spherule size from Endurance to Victoria reflects stratigraphic variation.

As Opportunity drove south toward Victoria, large eolian ripples became prominent as mean spherule size declined. The Victoria annulus is covered by large spherules eroded from ejecta and lacks large ripples, which suggests that accumulations of larger spherules create dense, protective lags that impede eolian transport, stabilizing the soil and inhibiting ripple development.

Opportunity encountered a field of loose rocks at Cabo Anonimo. All have similar Pancam spectral properties, including absorption features consistent with the presence of olivine and/or low-Ca pyroxene. Miniature Thermal Emission Spectrometer (Mini-TES) (*15*) spectra of the 12 rocks observed are also similar to one another; together these observations imply a common composition for all the rocks in the field.

One of the largest rocks, Santa Catarina (~11 by 14 cm), was chosen for detailed analysis. MI images show brecciation, with some clasts exhibiting possible igneous quench textures (fig. S2). Mössbauer (*16*) spectra confirm olivine and pyroxene and reveal troilite. The elemental chemistry of Santa Catarina is unusual for Meridiani but closely approximates that of Barberton (*17*), a pebble at the rim of Endurance crater. Kamacite, an iron-nickel alloy, was identified in Barberton, which suggests that it is a meteorite. Its composition is consistent with a mesosiderite silicate clast (*17*). We infer that Santa Catarina and the other rocks in the field on Cabo Anonimo are also meteoritic. Presumably, they are better preserved than the friable ejecta blocks because their achondritic composition makes them more resistant to erosion. Troilite is more abundant than metal in silicate clasts of the Vaca Muerta mesosiderite (*18*), and some troilite in Santa Catarina may have remained while the metal phase was altered [although alteration may have required several hundred million years of water exposure (*19*)]. Santa Catarina Mössbauer spectra reveal proportionally more ferric iron than in Barberton, which may indicate greater alteration. Alternatively, Santa Catarina may contain kamacite clasts that went undetected because of heterogeneity in the breccia. Santa Catarina and Barberton may be related, because mesosiderites are rare and these rocks were found within a few kilometers of one another. Santa Catarina and nearby rocks may be fragments of the impactor that created Victoria crater.

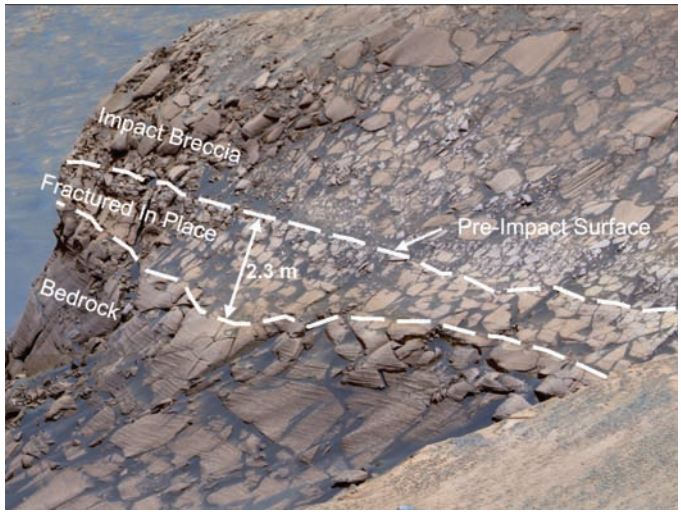

Fig. 3. Pancam false-color image of the east face of Cape Verde, showing typical impact-related stratigraphy (sequence p2429, sol 1006).

The lowest materials in the crater walls are intact bedrock (Fig. 3). These beds grade upward into rock that is fractured but in place, as shown by bedding planes that retain their original orientation. The fracturing probably took place during the impact, as the shock wave impinged on the free surface, loading rocks in tension. Immediately above the pre-impact surface is an abrupt transition to ejecta blocks with bedding planes in random orientations.

The crater walls exhibit distinctive horizontal color and albedo banding immediately below the pre-impact surface (fig. S3). The uppermost unit (Steno) has a blue-to-red slope and a 535-nm band depth that are low compared with the underlying unit (Smith). The color properties of these units are similar, respectively, to darker-toned and lighter-toned rocks observed elsewhere at Meridiani (*10*). The next lower unit (Lyell) is spectrally similar to Steno. This color sequence was also observed at Endurance crater (*10*).

Cape St. Mary, Cape St. Vincent, and Cape Verde were imaged from the crater rim using techniques that combine information from multiple images (*20*) to enhance resolution. The three promontories are dominated by eolian facies. No clasts are visible at Pancam resolution, consistent with the exclusively sand-sized grains in all outcrops observed by Opportunity. Bedding is clearly distinguishable everywhere. Meter-scale eolian cross-stratification is visible in several promontories, including Cape St. Mary and Cape St. Vincent (Fig. 4). Elsewhere bedding is massive, planar, or observed as low-angle climbing translatent cross-strata.

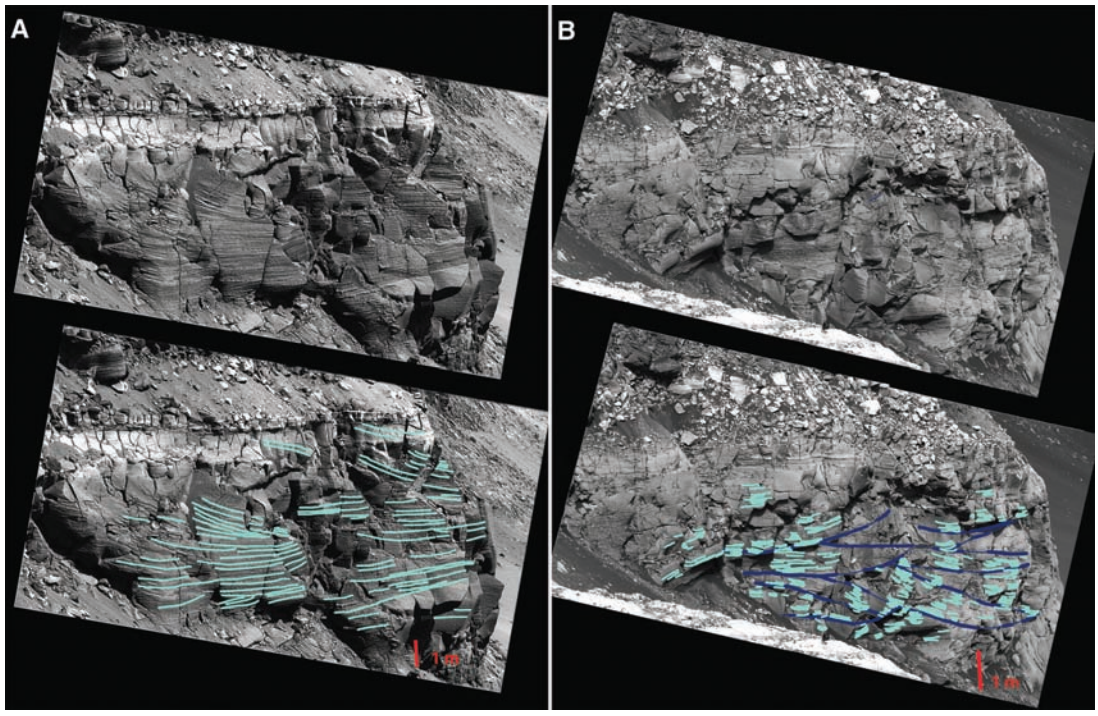

Fig. 4. Pancam images of Cape St. Vincent (**A**), sequence p2417, sol 1167, and Cape St. Mary (**B**), sequence p2444, sol 1213. Lower images have bedding and cross-stratification highlighted.

Cape St. Vincent presents a west-facing outcrop dominated by an 8-m vertical exposure of large-scale cross-strata. The stratification suggests subcritical climbing bedforms with decameter-scale dune heights that migrated approximately parallel to the outcrop face. Color and albedo banding below the pre-impact surface is prominent. The banding is nearly horizontal and cut by bedding at a high angle, so it is diagenetic in origin rather than a primary depositional feature.

Cape St. Mary presents a south-facing outcrop dominated by a 6-m vertical exposure of meter-scale sets of trough cross-bedding (bedding concordant with set boundaries). This layering is indicative of decameter-scale, sinuous-crested, eolian dunes that migrated approximately perpendicular to the outcrop face. No erosional contacts are observed.

Cape Verde shows evidence for an erosional contact at its base (fig. S4). The lowermost unit is dominated by thickly bedded dune toeset laminae. Evidence for diagenesis at Cape Verde includes truncated and cross-cutting facture fills, preferentially eroded bedding, and a ribbed weathering pattern superimposed on cross-strata, suggesting differential cementation.

The cross-stratification at Victoria is comparable in scale (several meters) to Jurassic eolian deposits of the western United States, implying a dry dune field. The grain size, scale, angle of exposed bedding, and lack of volcanic bombs or other outsized clasts are inconsistent with a pyroclastic or impact origin (*21*, *22*).

Opportunity performed in situ observations of the Steno, Smith, and Lyell units at Duck Bay. All are sulfate-rich sandstone. Steno has a vertical thickness of ~70 cm and is fine-to-medium-grained, with well-defined laminae. Centimeter-to-meter–scale cross-bedding is visible, and spherules are abundant. Steno and Smith are separated by a low-angle disconformity. Smith has a vertical thickness of ~80 cm and is smoother and lighter-toned than Steno and Lyell, with fine planar laminations.

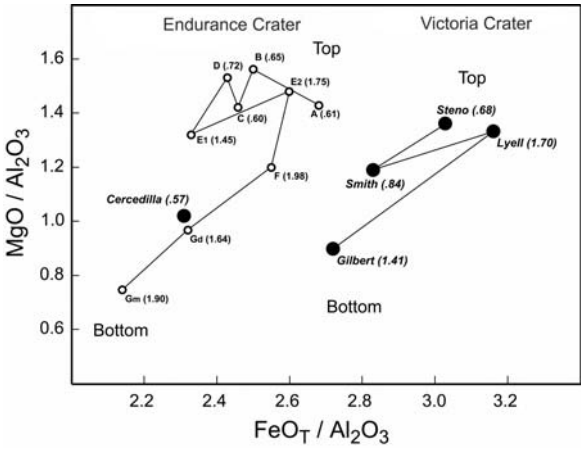

Fig. 5. Plot of MgO/Al_2O_3 versus FeO_T/Al_2O_3 for abraded targets from Endurance crater (open circles) and Victoria crater (closed circles). Samples are joined in stratigraphic order. Cl concentrations in weight percent are in parentheses.

The Smith-Lyell contact is gradational. Lyell is darker than Smith because of basaltic sand trapped in surface porosity. It is a well-sorted, fine-grained sandstone with a vertical thickness of 1.85 m, prominent millimeter-to-centimeter–scale laminations, and cross-bed sets up to several meters thick. Spherules are more common than in Smith and Steno. The porosity comes partly from tabular prismatic vugs, similar to those at Eagle crater (*23*).

Elemental compositions at Duck Bay (Fig. 5) fall mostly within established ranges for Meridiani, but with more Fe; the lowermost unit investigated (Gilbert, immediately below Lyell) has more Fe than previously measured in Meridiani bedrock. Other elements commonly associated with Fe, including Ti, Mn, Cr, and Ni, display no enhancements. All rocks are sulfate-rich; Steno has more S than previously observed at Meridiani.

Higher Fe aside, stratigraphic trends in outcrop chemistry compare closely to those at Endurance. Both sections show down-section decreases in S, Fe, and Mg, and corresponding Al and Si enrichment. Both also show a sharp discontinuity in Cl content; lower parts of the sections at both craters are 2 to 3 times as high as uppermost units. At Duck Bay, the main chemical discontinuity coincides with the Smith-Lyell contact, likely corresponding to a diagenetic boundary. Cl discontinuities occur slightly above the level at which decreases in MgO/Al_2O_3 and FeO_T/Al_2O_3 begin (Fig. 5).

Measured sections at Endurance and Victoria are similar in character but differ in detail, consistent with the hypothesis that Victoria rocks lie stratigraphically above those at Endurance. On

the basis of cross-cutting relationships, textural features at Endurance crater suggest relatively late diagenetic events (*24*) that record chemical interaction with a local groundwater table (*21*, *24*). If correct, the observation of comparable vertical trends in sections that may represent distinct stratigraphic levels could imply that a set of depositional and early diagenetic processes recurred through time during regional stratigraphic development. Alternatively, chemostratigraphic trends at Endurance may reflect downward-penetrating diagenesis related to surface exposure (*25*). This would allow chemical trends in both sections to reflect a single alteration event that took place during or after development of the current land surface. In either case, the wettest conditions occurred during deposition and early diagenesis, with drying thereafter (*26*).

Opportunity's investigation of Victoria crater shows that depositional, diagenetic, and erosional processes documented locally at Eagle and Endurance craters acted regionally. These processes include (i) chemical interaction of basalts and acidic water to produce sulfate salts; (ii) production of sands, transport and deposition by wind, and subsequent groundwater-influenced cementation; (iii) later diagenetic alteration of outcrop surfaces under increasingly arid conditions; and (iv) erosion of friable sedimentary rocks by persistent wind action, continuing to the present.

References and Notes

1. S. W. Squyres *et al.*, *Science* **306**, 1698 (2004).
2. S. W. Squyres *et al.*, *Science* **313**, 1403 (2006).
3. A sol is defined as one martian solar day.
4. J. A. Grant *et al.*, *J. Geophys. Res.* **113**, E11010; 10.1029/2008JE003155 (2008).
5. C. Weitz *et al.*, *J. Geophys. Res.* **111**, E12S04; 10.1029/2005JE002541 (2006).
6. W. M. Calvin *et al.*, *J. Geophys. Res.* **113**, E12S37; 10.1029/2007JE003048 (2008).
7. K. E. Herkenhoff *et al.*, *J. Geophys. Res.* **113**, E12S32; 10.1029/2008JE003100 (2008).
8. J. F. Bell III *et al.*, *J. Geophys. Res.* **108**, 8063; 10.1029/2003JE002070 (2003).
9. Colors based on contrast-stretched red-green-blue composites from Pancam's 673-, 535-, and 432-nm filters.
10. W. H. Farrand *et al.*, *J. Geophys. Res.* **112**, E06S02; 10.1029/2006JE002773 (2007).
11. S. Gorevan *et al.*, *J. Geophys. Res.* **108**, 8068; 10.1029/2003JE002061 (2003).
12. K. E. Herkenhoff *et al.*, *J. Geophys. Res.* **108**, 8065; 10.1029/2003JE002076 (2003).
13. R. Rieder *et al.*, *J. Geophys. Res.* **108**, 8066; 10.1029/2003JE002150 (2003).
14. B. C. Clark *et al.*, *Earth Planet. Sci. Lett.* **240**, 73 (2005).
15. P. R. Christensen *et al.*, *J. Geophys. Res.* **108**, 8064; 10.1029/2003JE002117 (2003).
16. G. Klingelhöfer *et al.*, *J. Geophys. Res.* **108**, 8067; 10.1029/2003JE002138 (2003).
17. C. Schröder *et al.*, *J. Geophys. Res.* **113**, E06S22; 10.1029/2007JE002990 (2008).
18. M. Kimura *et al.*, *Proc. NIPR Symp. Antarct. Meteorites* **4**, 263 (1991).
19. P. A. Bland, T. B. Smith, *Icarus* **144**, 21 (2000).
20. J. F. Bell III *et al.*, *J. Geophys. Res.* **111**, E02S03; 10.1029/2005JE002444 (2006).
21. J. P. Grotzinger *et al.*, *Earth Planet. Sci. Lett.* **240**, 11 (2005).
22. K. E. Herkenhoff *et al.*, *J. Geophys. Res.* **113**, E12S32; 10.1029/2008JE003100 (2008).
23. S. W. Squyres *et al.*, *Science* **306**, 1709 (2004).
24. S. M. McLennan *et al.*, *Earth Planet. Sci. Lett.* **240**, 95 (2005).
25. R. Amundson *et al.*, *Geochim. Cosmochim. Acta* **72**, 3845 (2008).
26. A. H. Knoll *et al.*, *J. Geophys. Res.* **113**, E06S16; 10.1029/2007JE002949 (2008).

27. This research was carried out for the Jet Propulsion Laboratory, California Institute of Technology, under a contract with NASA.

Supporting Online Material

www.sciencemag.org/cgi/content/full/324/5930/1058/DC1
Figs. S1 to S4

29 December 2008; accepted 31 March 2009
10.1126/science.1170355

Bone Assemblages Track Animal Community Structure over 40 Years in an African Savanna Ecosystem

David Western[1] and Anna K. Behrensmeyer[2]

Reconstructing ancient communities depends on how accurately fossil assemblages retain information about living populations. We report a high level of fidelity between modern bone assemblages and living populations based on a 40-year study of the Amboseli ecosystem in southern Kenya. Relative abundance of 15 herbivorous species recorded in the bone assemblage accurately tracks the living populations through major changes in community composition and habitat over intervals as short as 5 years. The aggregated bone sample provides an accurate record of community structure time-averaged over four decades. These results lay the groundwork for integrating paleobiological and contemporary ecological studies across evolutionary and ecological time scales. Bone surveys also provide a useful method of assessing population changes and community structure for modern vertebrates.

Accurate reconstructions of ancient community ecology depend on how closely fossil assemblages match species richness and relative abundances in the original living communities. Many taphonomic and methodological biases relating to morphology, body size, and life habit can affect the presence or absence of taxa and their relative abundance in fossil assemblages (*1*–*4*). Vertebrates and shelly invertebrates have durable remains that can accumulate over long periods of time, raising questions about how such remains record properties of the original community, especially during periods of marked population and habitat change (*2*–*5*). Data quality issues have been addressed through studies of living populations and their death assemblages in marine invertebrates (*3*, *4*, *6*, *7*) and terrestrial vertebrates (*8*–*10*). These "live:dead" studies show that single-census death assemblages can approximate ecological snapshots but typically include durable remains representing varying intervals of accumulation, or time averaging. Time averaging usually inflates species richness relative to live samples, but under stable population and environmental conditions can accurately represent rank abundances of the dominant species in shelly invertebrate assemblages (*3*, *4*, *6*, *7*).

Earlier, single-census live:dead research in the Amboseli ecosystem demonstrated preburial fidelity of the surface bone assemblage with respect to large (15 to 4000 kg) herbivore populations and their habitat distributions (*8*, *11*–*13*). Birth and death rates among species, and hence the production of skeletal remains, are inversely scaled to species body weight (*12*). Consequently, the greater numbers of dead smaller animals were offset by allometrically scaled bone destruction

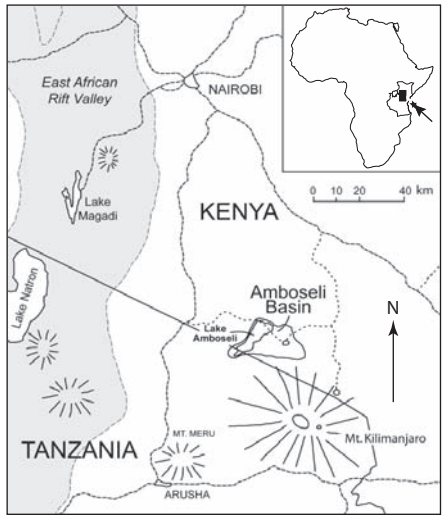

Fig. 1. Regional map of southern Kenya showing the physiographic context of the Amboseli Basin north of Mount Kilimanjaro. Lake Amboseli is a shallow, seasonal playa with wetlands fed by springs from Mount Kilimanjaro.

[1]African Conservation Center, Box 62844, Nairobi, Kenya. [2]Department of Paleobiology, MRC 121, National Museum of Natural History, Smithsonian Institution, Post Office Box 37012, Washington, DC 20013–7012, USA.

E-mail: dwestern@africaonline.co.ke (D.W.); behrensa@si.edu (A.K.B.)

rates, such that the relative abundances and size-frequency distributions of species in the bone and living assemblages matched (*8*, *13*). The question remains, however, whether cumulative bone assemblages accurately reflect time-averaged community structure, especially during periods of rapid population and environmental change.

The 8500 km^2 Amboseli ecosystem straddling the Kenya-Tanzania border (Fig. 1) lies at an altitude of 1200 m and receives an annual rainfall of 250 to 300 mm, distributed in two seasons (*14*, *15*). The ecosystem encompasses the migrations of the large ungulates and pastoral livestock that concentrate seasonally around permanent swamps in the Amboseli Basin (*11*, *16*, *17*) [supporting online material (SOM) text S1]. In the 1960s, the ecosystem was dominated by dense woodlands and bushland interspersed with grasslands and swamps. By the 1990s, woodlands had given way to open grassland and scrubland and the swamps had doubled in size (*18*). Amboseli's ungulate populations have fluctuated widely in response to drought cycles and human impact over the past four decades (*18*) (table S1). Overall, the abundance of grazers increased relative to browsers, and species richness declined in response to the habitat changes (*18*).

Amboseli thus provides a test of the response of a large vertebrate community to decadal-scale ecological changes and the fidelity of bones in reflecting these changes. The large herbivore counts and vegetation maps give a continuous picture of the changing numbers and distributions of animals in relation to habitat from 1967 to 2004 (SOM text S1.1). The bone sampling protocol (*8*, *13*) targeted the main areas and habitats used by the living vertebrate species. Bones of vertebrate species were recorded along 96 ground transects in 1975 to 1976, and a subset of 44 of these transects in 2002 to 2004 (SOM text S1.2). Bone survey data for 15 regularly censused abundant wild ungulates (14 mammals and ostrich) were used for comparison with the live population counts (Table 1 and table S1).

We tested how well recent bone assemblages represent abundances of the parent populations by tracking correlations between dead and living populations of large herbivores over 40 years (1964 to 2004) that span some of the most rapid habitat changes and herbivore population fluxes recorded in the African savannas (*16*, *18*) (table S1). We use live population counts versus bone surveys to test three hypotheses: (i) bone surveys accurately track community structure through successive time intervals and record the time-averaged structure for all intervals combined, (ii) bone surveys accurately record live species abundance distributions in different habitats, and (iii) ecological properties of the living community can be deduced from its bone assemblage.

Counts of individuals for each bone sampling period include identifiable remains of animals dying up to ~10 years before the sampling years (*19*) (SOM text S1.3). Sampling was done in two phases (1975 to 1976 and 2002 to 2004); thus, the surveys recorded fresh to weathered bones representing time intervals of 11 to 12 years before these dates, that is, 1964 to 1976 and 1993 to 2004. Based on established bone weathering stages (WS) in Amboseli (*19*), each of these two intervals can be divided into two subintervals. Bones in WS 0 to 2 (~5 years since death) represent animals that died in 1970 to 1976 and 1998 to 2004, and WS 3 and 4 (~6 to 12 years since death) represent deaths in 1964 to 1969 and 1993 to 1998 (SOM text S1.3 and table S2). The bone survey data thus are grouped in four time intervals: 1964 to 1969, 1970 to 1976, 1993 to 1998, and 1999 to 2004 (table S2), representing ~25 out of 40 years or ~60% of the total time span (SOM text S1.3). Live census data were selected to match these same multiyear intervals (table S2). Counts of live and dead individuals of each species are expressed as a proportion of all individuals in each habitat and time interval (table S1).

Spearman's rank order coefficient (r_s) and reduced major axis (RMA) regressions (SOM text S2.1) show highly significant correlations of species abundances in live populations and bone counts for each time interval separately, and for the time-averaged counts over the entire study (Table 1, Fig. 2, and fig. S1). These results show that the bone assemblage closely tracks population changes in the parent community and also gives an accurate averaged record of herbivore community structure over time. The match of live:dead abundances confirms that size-related death (turnover) rates among species in Amboseli herbivores are nearly balanced by size-related bone destruction rates (*8*, *12*). The time-averaged live:dead RMA regression (Fig. 2), as well as each of the four time-interval samples, have slopes slightly (but insignificantly) below 1 (Table 1 and table S1). Body size frequency distribution of species in the living large herbivore community is therefore retained by the bone assemblage, although the cluster of large-bodied species to the left of the regression line in Fig. 2 suggests a slight bias in the survival of their larger, more durable bones (SOM text S2.3).

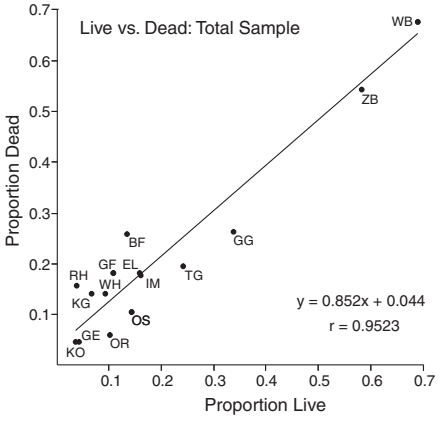

Fig. 2. RMA regression of total live (N = 169,235 counted individuals) against the total dead (N = 1502 individuals), using transformed {ASIN[SQRT(Proportion)]} relative abundances of 15 herbivore species between 20 and 4000 kg (14 mammal species and ostrich). Codes for species: BF, Cape buffalo; EL, elephant; GE, gerenuk; GF, giraffe; GG, Grant's gazelle; IM, impala; KG, kongoni; KO, waterbuck; OR, oryx; OS, ostrich; RH, black rhino; TG, Thomson's gazelle; WB, wildebeest; WH, warthog; ZB, Burchell's zebra. This relationship is significant at the $P < 0.001$ level (Table 1) (*29*). ArcSin transformation equalizes variances of proportional data and thus is appropriate for RMA analysis. See table S1 for numerical data and fig. S1.

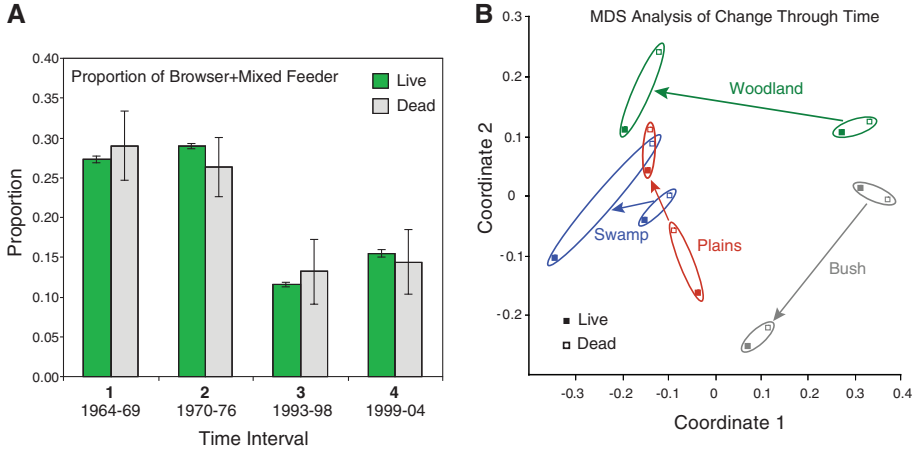

Fig. 3. (**A**) Change through time in Amboseli's browser+mixed feeder guild (N = 7 species) as shown by the live versus dead abundance data. Proportions are based on the total sample of 15 species; the relative abundance of grazers (N = 8 species) increased as the browsers declined, reflecting the loss of wooded habitats since the 1960s. See table S3 for numerical data. The 95% confidence limits are based on the normal approximation to a binomial distribution. (**B**) Results of a nonmetric MDS analysis of transformed relative abundance data for live and dead data sets, using the lower weathering stage subset (bone weathering stages 0 to 2), i.e., time intervals 1970 to 1976 and 1999 to 2004 (table S4). Live:dead pairs are connected by ovals; habitat samples are connected by arrows to show shifts through time. Calculated stress for this analysis using Euclidean distances = 0.1617.

Spearman *r* tests (Table 2) of living versus bone census data in four different habitats are significant for live:dead correlations in all but 3 of the 16 habitat cells and when time-averaged over four decades for each of these habitats. Nonmetric multidimensional scaling (MDS) analysis shows differing herbivore subcommunities in the four habitats, with similar shifts through time in both the live and dead samples (Fig. 3B and SOM text S2.1). These results show that Amboseli's bone assemblages distinguish habitat differences among living populations and tracked population changes during the transition from woodland to open grasslands.

Given the highly significant correlation between the relative species abundance in the live:dead censuses for the four discrete time periods and time-averaged over four decades, the bone assemblage also should accurately predict ecological properties of the Amboseli community. We tested this prediction using standard ecological measures of community structure (Table 3). Ecological indices are similar for live versus dead data sets through the four time intervals (SOM text S2.2 and fig. S3) but show slightly higher diversity (greater evenness) for the bone survey data. The Shannon H and Simpson D indices are slightly higher for the bone samples but accurately track the living population through time despite 2 orders of magnitude smaller sample size for bone versus live survey data (SOM text S1 and S2.2, Table 3, table S1, and fig. S3). Bone data also closely track changes in guild composition (Fig. 3A) that resulted from woodland collapse (*18*).

Our results show that relative abundance and habitat distribution of species in a modern bone assemblage accurately represent the composition and changes in large herbivore community structure over intervals as short as 5 years and reflect aggregate structure over four decades of rapid ecological change (SOM text S2.3). A subsample of partially buried bones (SOM text S2.4) shows that the prefossil assemblage also records accurate information on species abundances.

Amboseli provides a reasonable facsimile for live:dead fidelity preserved in a fossil assemblage time-averaged over decades to millennia through continual burial of surface bones in a land-surface soil (SOM text S2.3 and S2.4). The vertebrate record includes many fossil bone assemblages preserved in strata representing buried land surfaces or floodplain paleosols (*20*, *21*), and these assemblages could retain ecological information similar to that captured in the Amboseli live:dead study. Broad application of our results to the vertebrate fossil record depends on how initial high live:dead fidelity survives additional taphonomic processes such as fluvial reworking of surface-accumulated bone assemblages and long-term diagenesis.

The close tracking of community structure shown by the bone assemblages in this study enriches the range of ecological inferences that can be drawn from both ancient and modern vertebrate communities. Evidence of high fidelity in species relative abundance and habitat tracking in bone assemblages makes it possible to use a common framework for inferring the ecological properties of both contemporary and paleontological bone

Table 1. Sample sizes, Spearman's *r* and probability (*P*) values, and RMA results for comparisons of relative abundances of the living population and bone assemblage data for 15 ungulate species sampled in the Amboseli Basin. Proportional abundance data were transformed using ASIN[SQRT(Proportion)] for each species to equalize variance for residuals for the RMA (*29*). Slope 95% confidence interval (C.I.) estimated using the ±2* (least-squares) SE (*29*). See also table S1 and fig. S1.

Time interval	Years	*N* live	*N* dead	Spearman		RMA (transformed data)			
				r_s	*P*	*r*	Slope	95% C.I.	*P* (slope = 1)
1	1964–1969	36,326	417	**0.666**	**0.008**	0.8617	0.8682	0.624–1.113	**0.2674**
2	1970–1976	72,741	535	**0.682**	**0.006**	0.9420	0.9405	0.765–1.116	**0.4782**
3	1993–1998	35,597	265	**0.664**	**0.008**	0.9072	0.8950	0.686–1.104	**0.3000**
4	1999–2004	24,571	285	**0.880**	**<0.0001**	0.9513	0.9174	0.761–1.074	**0.2785**
1 + 2 + 3 + 4	1964–1976 + 1993–2004	169,235	1,502	**0.823**	**0.0002**	0.9523	0.8951	0.744–1.047	**0.1609**

Table 2. Probability (*P*) values from correlation tests using Spearman's *r* comparing live and dead survey data for the four major habitat types in Amboseli in the four different time intervals and the total sample, based on proportions of a maximum possible 15 species per habitat and time interval. Significant values ($P \leq 0.05$) in bold. See table S3 for live and dead abundances by habitat.

Time Interval	Years	Spearman *P* values				r_s Values			
		Swamp	Plains	Bush	Woodland	Swamp	Plains	Bush	Woodland
1	1964–1969	0.529	**0.002**	**0.029**	0.093	–0.0253	**0.9669**	**0.8890**	0.6890
2	1970–1976	**0.012**	**<0.001**	**0.026**	**0.001**	**0.9720**	**0.9061**	**0.9618**	**0.9616**
3	1993–1998	**0.022**	**0.002**	0.110	**0.006**	**0.7472**	**0.8586**	0.4804	**0.9766**
4	1999–2004	**0.006**	**0.003**	**<0.001**	**<0.0001**	**0.8487**	**0.9892**	**0.9292**	**0.8950**
1 + 2 + 3 + 4	1964–1976 + 1993–2004	**<0.001**	**<0.001**	**0.011**	**<0.001**	**0.9683**	**0.9725**	**0.9675**	**0.9419**

Table 3. Comparison of diversity indices, evenness, and feeding guild structure (proportions of total *N*) based on live versus dead census data of the Amboseli large herbivore community between 1964 and 2004. See also table S1 and fig. S3.

Time interval	Years	Diversity indices						Browser+mixed		Grazer	
		Simpson live	Simpson dead	Shannon H live	Shannon H dead	Evenness _e^H/S live	Evenness _e^H/S dead	Prop. live	Prop. dead	Prop. live	Prop. dead
1	1964–1969	0.7577	0.7967	1.73	1.951	0.4029	0.4692	0.273	0.290	0.727	0.710
2	1970–1976	0.7441	0.7661	1.74	1.862	0.3798	0.4290	0.289	0.264	0.711	0.736
3	1993–1998	0.6372	0.6624	1.291	1.542	0.2597	0.3339	0.116	0.132	0.884	0.868
4	1999–2004	0.6869	0.7301	1.458	1.623	0.3071	0.4606	0.154	0.144	0.846	0.856
1 + 2 + 3 + 4	1964–1976 +1993–2004	0.7269	0.7627	1.657	1.862	0.3496	0.4290	0.230	0.225	0.770	0.775

assemblages. Given that body size is a unifying concept in macroecological theory (*22*), a preserved size-frequency distribution of species in a modern or fossil bone assemblage provides a quantitative basis for reconstructing population and community structure. Measures of ecological properties such as species richness, diversity, productivity, turnover, guild composition, resilience, and resistance can be deduced from allometrically scaled history traits (*22*, *23*). Species size-frequency structure therefore offers a common metric for calculating the ecological and energetic properties of both fossil and contemporary communities (*12*, *22*–*25*).

Amboseli and other similar taphonomic studies (*10*, *26*–*28*) demonstrate that bone surveys can be used to monitor modern vertebrate populations and community structure, document unusual mortality levels, and correct bias in habitat use patterns resulting from diurnal live population counts. Bone assemblages also can give a baseline against which to measure disruptions to contemporary animal communities caused by human impact (*4*).

References and Notes

1. C. E. Badgley, *Palaios* **1**, 328 (1986).
2. A. K. Behrensmeyer, S. M. Kidwell, R. A. Gastaldo, *Paleobiology* **26** (suppl.), 103 (2000).
3. S. M. Kidwell, *Science* **294**, 1091 (2001).
4. S. M. Kidwell, *Proc. Natl. Acad. Sci. U.S.A.* **104**, 17701 (2007).
5. S. M. Kidwell, S. M. Holland, *Annu. Rev. Ecol. Syst.* **33**, 561 (2002).
6. E. N. Powell, R. J. Stanton Jr., A. Logan, M. A. Craig, *Palaeogeogr. Palaeoclimatol. Palaeoecol.* **95**, 209 (1992).
7. A. Tomasovych, S. M. Kidwell, *Paleobiology* **35**, 94 (2009).
8. A. K. Behrensmeyer, D. Western, D. E. Dechant, *Paleobiology* **5**, 12 (1979).
9. E. A. Hadly, *Palaeogeogr. Palaeoclimatol. Palaeoecol.* **149**, 389 (1999).
10. R. C. Terry, *Palaios* **23**, 402 (2008).
11. D. Western, *East Afr. Wildl. J.* **13**, 265 (1975).
12. D. Western, in *Fossils in the Making*, A. K. Behrensmeyer, A. Hill, Eds. (Univ. of Chicago Press, Chicago, 1980), pp. 41–54.
13. A. K. Behrensmeyer, D. E. Dechant, in *Fossils in the Making*, A. K. Behrensmeyer, A. Hill, Eds. (Univ. of Chicago Press, Chicago, 1980), pp. 72–93.
14. J. Altmann, S. C. Albert, S. A. Altmann, *Afr. J. Ecol.* **40**, 248 (2002).
15. D. Western, C. van Praet, *Nature* **241**, 104 (1973).
16. D. Western, D. Maitumo, *Afr. J. Ecol.* **42**, 111 (2004).
17. C. J. Pennycuick, D. Western, *East Afr. Wildl. J.* **10**, 175 (1972).
18. D. Western, *Afr. J. Ecol.* **45**, 302 (2006).
19. A. K. Behrensmeyer, *Paleobiology* **4**, 150 (1978).
20. A. K. Behrensmeyer, R. W. Hook, in *Terrestrial Ecosystems Through Time*, A. Behrensmeyer *et al.*, Eds. (Univ. of Chicago Press, Chicago, 1992), pp. 15–136.
21. R. Potts, A. K. Behrensmeyer, P. Ditchfield, *J. Hum. Evol.* **37**, 747 (1999).
22. J. H. Brown, *Macroecology* (Univ. of Chicago Press, Chicago, 1995).
23. D. Western, *Afr. J. Ecol.* **17**, 185 (1979).
24. R. M. Sibly, J. H. Brown, *Proc. Natl. Acad. Sci. U.S.A.* **104**, 17707 (2007).
25. J. Damuth, B. J. MacFadden, Eds., *Body Size in Mammalian Paleobiology* (Cambridge University Press, Cambridge, 1990).
26. D. Reed, in *Hominin Environments in the East African Pliocene: An Assessment of the Faunal Evidence*, R. Bobe, Z. Alemseged, A. K. Behrensmeyer, Eds. (Springer, Dordrecht, Netherlands, 2007), pp. 217–255.
27. J. Miller, *J. Vertebr. Paleontol.* **28**, 116A (2008).
28. J. T. Faith, Abstract for the biennial meeting of the Paleontological Society of South Africa, Matjiesfontein, South Africa, 11 to 14 September, 2008.
29. Statistical and diversity indices analysis used Palaeontological Statistics software package for education and data analysis (PAST) version 1.55 (*30*). Slope C.I. estimated based on (*31*).
30. O. Hammer, D. A. T. Harper, P. D. Ryan, *Palaeontol. Electronica* **4**, 9 (2001); http://folk.uio.no/ohammer/past.
31. R. Sokal, F. Rohlf, *Biometry* (Freeman, New York, 1995).

32. D.W.'s ecological studies have been supported by the Ford Foundation, Wildlife Conservation Society, and Liz Claiborne Art Ortenberg Foundation. We acknowledge the statistical assistance of V. Mose, T. Faith, G. Hunt, S. Kidwell, and A. Tomasovych and the field support of D. Maitumo. A.K.B's taphonomic research has been supported by the National Geographic Society (grants 1508, 4339-90, and 7525-03) and the Smithsonian Institution. Particular thanks are due to D. D. Boaz, J. Altmann, E. Kanga, F. Odock, and many other individuals who provided essential advice and help with the bone surveys. Permission for the studies was granted by the Office of the President, Kenya, and institutional support over the years was provided by the Kenya Wildlife Service and the National Museums of Kenya.

Supporting Online Material

www.sciencemag.org/cgi/content/full/324/5930/1061/DC1
Materials and Methods
SOM Text
Figs. S1 to S3
Tables S1 to S4
References

21 January 2009; accepted 16 March 2009
10.1126/science.1171155

Regulators of PP2C Phosphatase Activity Function as Abscisic Acid Sensors

Yue Ma,* Izabela Szostkiewicz,* Arthur Korte,* Danièle Moes,† Yi Yang,‡ Alexander Christmann, Erwin Grill§

The plant hormone abscisic acid (ABA) acts as a developmental signal and as an integrator of environmental cues such as drought and cold. Key players in ABA signal transduction include the type 2C protein phosphatases (PP2Cs) ABI1 and ABI2, which act by negatively regulating ABA responses. In this study, we identify interactors of ABI1 and ABI2, which we have named regulatory components of ABA receptor (RCARs). In *Arabidopsis*, RCARs belong to a family with 14 members that share structural similarity with class 10 pathogen-related proteins. RCAR1 was shown to bind ABA, to mediate ABA-dependent inactivation of ABI1 or ABI2 in vitro, and to antagonize PP2C action in planta. Other RCARs also mediated ABA-dependent regulation of ABI1 and ABI2, consistent with a combinatorial assembly of receptor complexes.

The phytohormone abscisic acid (ABA) serves as an endogenous messenger in biotic and abiotic stress responses (*1*–*4*). ABA responses include a redirection of gene expression, reduced transpiration, protection of photosynthesis, and control of plant growth (*2*, *4*–*6*). A variety of proteins has been reported to function as ABA receptors (*7*–*9*), but their ability to bind to ABA, to transduce the ABA signal, and thereby to regulate diverse ABA responses has not been unequivocally established (*10*–*15*).

Major players in ABA signaling are a subclass of Mg^{2+}- and Mn^{2+}-dependent serine-threonine phosphatases type 2C (PP2Cs) (*16*–*21*). Prototypes of these PP2Cs are ABI1 and its close structural homolog ABI2, which act in partially overlapping ways to repress ABA responses (*22*). ABI1 has emerged as a hub in the network of ABA signal transduction (*23*–*25*). The link between ABA perception and the regulation of ABI1 and ABI2 has not been elucidated.

As key regulators of ABA responses, the ABI1 and ABI2 protein phosphatases are of central importance for elucidating the integrative network of ABA signaling. We used the yeast two-hybrid system to screen for *Arabidopsis* proteins interacting with ABI2 (*18*). One of the interacting proteins (At1g01360.1) had no annotated function, and we named it regulatory component of ABA receptor 1 (RCAR1). The RCAR1 protein shares 75% and 74% amino acid identity to poplar and grape vine homologs, respectively, and its predicted structure is similar to the protein Bet v 1 of birch pollen (Fig. 1, A and B). RCAR1 belongs to a protein family with 14 members in *Arabidopsis* (Fig. 1C).

The interaction between RCAR1 and ABI2 (Fig. 2A) was almost completely abolished by the single–amino acid exchange present in abi2 ($ABI2^{G168D}$) (*26*). The mutations in abi2 and abi1 ($ABI1^{G180D}$) confer dominant ABA insensitivity. The single point mutation present in abi1 also impaired RCAR1 binding, and the interaction was abrogated with a carboxyl terminally truncated $ABI1^{1\text{-}180}$. There are more than 50 PP2Cs in *Arabidopsis*. Of these, HAB1, a PP2C involved in ABA signaling and structurally related to ABI1/2 (*19*), physically interacted with RCAR1 in the yeast assay. In contrast, two additional PP2Cs we

Lehrstuhl für Botanik, Technische Universität München, Am Hochanger 4, D-85354 Freising, Germany.

*These authors contributed equally to this work.
†Present address: Plant Molecular Biology Laboratory, Public Research Centre for Health, 84, Val Fleuri, L-1526 Luxembourg, Luxembourg.
‡Present address: College of Life Sciences, Sichuan University, Chengdu, Sichuan 610064, P. R. China.
§To whom correspondence should be addressed. E-mail: erwin.grill@wzw.tum.de

tested, which belong to other subfamilies, did not significantly interact with RCAR1 (fig. S1). The protein interactions between RCAR1 and ABI1 or ABI2 were confirmed in plant cells by bimolecular fluorescence complementation (*27*).

Coexpression of RCAR1-YFP^N and PP2C-YFP^C in *Arabidopsis* protoplasts (*27*) yielded yellow fluorescent protein (YFP) signals both in the cytosol and in the nucleus (Fig. 2B). Fluorescence-activated cell distribution analysis of RCAR1-YFP^N– and ABI1-YFP^C–transfected protoplasts provides evidence for the formation of functional YFP complexes (fig. S2). Expression of a protein fusion between RCAR1 and green fluorescent protein (GFP) was localized to the same intracellular compartments as the RCAR1-PP2C complex (Fig. 2C).

In previous analyses, we consistently observed an up to 20% reduction of ABI1 phosphatase activity in the presence of micromolar levels of ABA, although no PP2C-bound ABA was detected (*28*). The inhibition indicated that the PP2C is to some extent capable of sensing ABA, but that an essential component that provides high affinity and stereo-selectivity for the ligand is missing. The missing constituent is RCAR1. In the presence of RCAR1, ABA instantaneously and almost fully blocked the phosphatase activity of purified ABI2 (Fig. 3A). Half-maximal inhibition of ABI1 and ABI2 occurred at ~60 nM and ~70 nM of physiologically active (*S*)-ABA, respectively (Fig. 3, B and C). In the absence of RCAR1, a residual PP2C inhibition of ~15 to 20% was observed at 1 to 30 μM (*S*)-ABA (Fig. 3C).

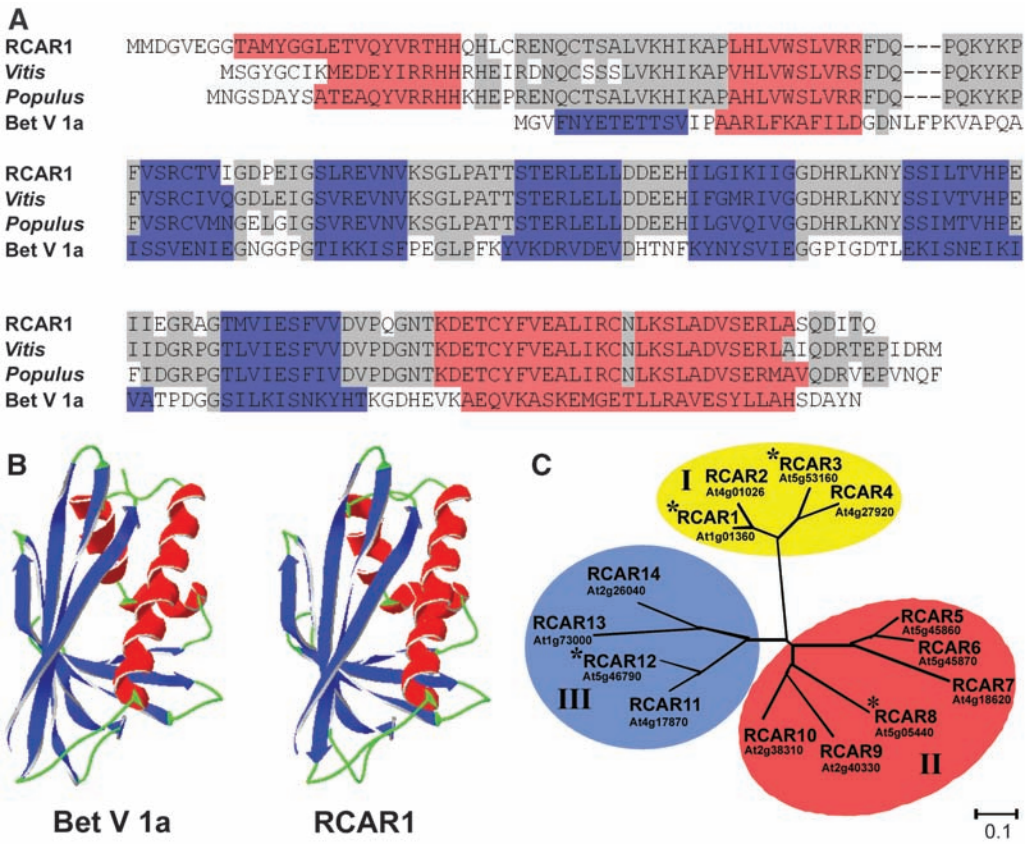

Fig. 1. Structural similarities between RCAR1 and the pollen allergen Bet v 1a. (**A**) Identical amino acid residues are shaded in gray, and predicted α-helical and β-sheet structures are highlighted in red and blue, respectively. The two RCAR1 homologs are from *Populus* (ABK92491) and *Vitis* (CAO65816). (**B**) Superimposition of the RCAR1 primary structure (RCAR1$^{L28\text{-}T186}$) onto the three-dimensional structure of Bet v 1a. (**C**) Phylogenetic tree of the RCAR proteins of *Arabidopsis* with 14 members and three subfamilies (I, II, and III). Asterisks identify members of the family analyzed in the study.

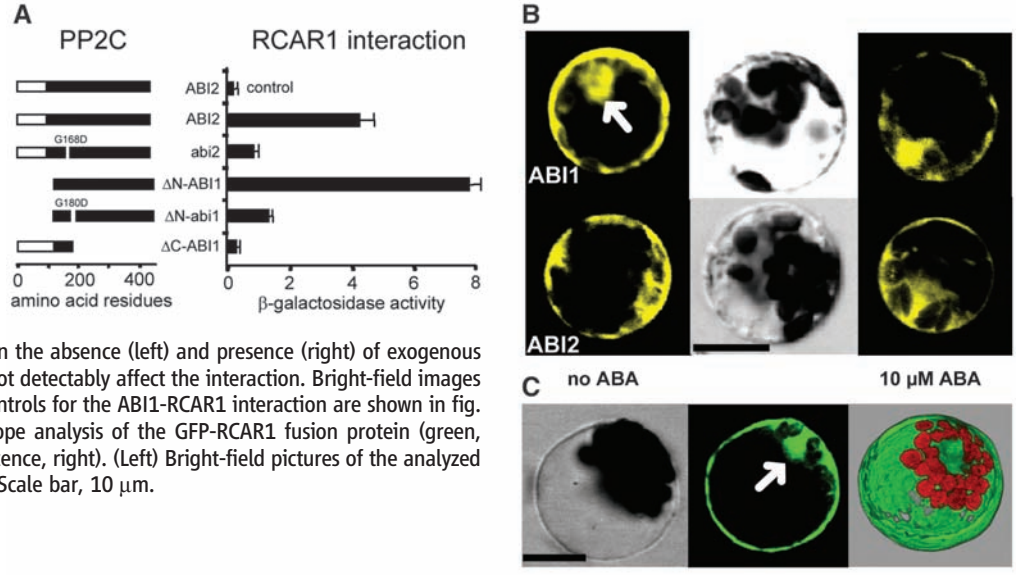

Fig. 2. Physical interaction between RCAR1 and ABI1/2. (**A**) (Left) Yeast two-hybrid analysis with different bait variants of ABI1 and ABI2 (wild-type versus mutant). (Right) Binding of RCAR1 to the PP2Cs is seen as a stimulation of reporter activity above basal levels. The galactosidase activity is given in Miller units. (**B**) Interaction analysis in *Arabidopsis* protoplasts by bimolecular fluorescence complementation. RCAR1-YFP^N was analyzed for YFP complementation with ABI1-YFP^C and ABI2-YFP^C (top and bottom, respectively). YFP complementation in the absence (left) and presence (right) of exogenous ABA. Administration of ABA (10 μM) did not detectably affect the interaction. Bright-field images (middle) correspond to the left images. Controls for the ABI1-RCAR1 interaction are shown in fig. S2C. (**C**) Confocal laser scanning microscope analysis of the GFP-RCAR1 fusion protein (green, middle), and chloroplasts (red autofluorescence, right). (Left) Bright-field pictures of the analyzed protoplasts. The arrows mark the nucleus. Scale bar, 10 μm.

The residual inhibition was also recorded in the presence of either (*R*)-ABA or *trans*-ABA and RCAR1. Supplementation of (*R*)-ABA and *trans*-ABA with (*S*)-ABA yielded the (*S*)-ABA–dependent inhibition, whereas heat-inactivation of RCAR1 abrogated ABA regulation of ABI2 (fig. S3A).

To ascertain that the ABA-stereoselective inhibition of phosphatase activity by RCAR1 was not specific to the umbelliferylphosphate substrate, we also used an alternative phosphopeptide substrate and obtained comparable results (compare fig. S3A with S3B). The RCAR1-related proteins RCAR3, 8, and 12 (Fig. 1C) were also able to block both PP2Cs in an ABA-dependent manner (fig. S3, C and D). In the presence of RCAR1, 30 μM (*R*)-ABA and *trans*-ABA were not able to inhibit the phosphatase activity of ABI1 and ABI2 to a level evoked by 30 nM (*S*)-ABA (Fig. 3, B and C).

Isothermal titration calorimetry revealed binding of (*S*)-ABA to RCAR1 and ABI2 with an apparent binding affinity (K_d) of ~64 ± 8 nM ABA (Fig. 3D) and a single binding site (n = 1.08 ± 0.05). The analysis for binding of (*S*)-ABA to RCAR1 yielded lower energy changes and a higher apparent K_d of ~0.66 ± 0.08 μM ABA (fig. S4, A and B).

To define the stoichiometry of the RCAR1-PP2C interaction, a fixed concentration of ABI2 was titrated with increasing levels of RCAR1 in the presence of 1 mM ABA. Half-maximal inhibition occurred at an RCAR1 to ABI2 ratio of ~0.5 (Fig. 3E). This value ranged between 0.4 and 0.8 for different protein preparations. Combined, the data are indicative of a one-to-one ratio of the heteromeric protein complex. The PP2C inhibition imposed by ABA and RCAR1 is independent of substrate concentration (fig. S5A). The Michaelis-Menten constant of the ABI2-catalyzed reaction was not affected by increasing RCAR1-enzyme ratios, whereas v_{max} was reduced (fig. S5B). Thus, the mode of inhibition relies on a noncompetitive inactivation of the enzyme. The Scatchard analysis of the PP2C inactivation in the presence of RCAR1 tentatively indicates a nanomolar dissociation rate for ABA with an apparent K_d of ~ 35 and 26 nM (*S*)-ABA for ABI1 and ABI2, respectively (Fig. 3F and fig. S5C). The K_d values are somewhat lower than the data from thermal measurements but fall within a comparable range. In the presence of saturating ABA levels, serial dilutions of an RCAR1-containing ABI2 solution maintained a constant inhibition level of up to 5 nM ABI2 (fig. S5D).

The transient expression of RCAR1 in *Arabidopsis* protoplasts resulted in an enhanced ABA-response at the level of gene regulation (Fig. 4A). An eightfold stimulation of ABA signaling was observed in the absence of exogenous ABA. Analyses of the ABA-deficient *aba2-1* mutant supported our conclusion that RCAR1 expression activates ABA signaling in response to endogenous ABA levels (Fig. 4B). Coexpression of a construct targeting RCAR1 and related transcripts with RNA interference (RNAi) counteracted the ABA response (Fig. 4, C and D), whereas cytokinin signaling was not affected (fig. S6). The concomitant expression of PP2Cs antagonized the RCAR1- and ABA-stimulated reporter expression (Fig. 4E) in a dose response–dependent manner, as shown for ABI2 (Fig. 4F).

Regulation of stomatal aperture, seed dormancy, and growth are major physiological control nodes of ABI1 and ABI2 action. Transgenic *Arabidopsis* plants with high transcript levels of RCAR1 were generated, and these plants were hypersensitive to ABA. The characterization of two independent lines, in which RCAR1 transcript levels were up-regulated (Fig. 4G), is depicted in Fig. 4, H to J. Regulation of stomatal aperture was impaired in the RCAR1 transgenic plants. In the absence of exogenous ABA, stomatal aperture ratios differed marginally between the RCAR1-2 and RCAR1-5 lines (0.42 ± 0.06) and control plants (0.45 ± 0.06) (Fig. 4H). Stomatal closure in response to ABA was enhanced in the RCAR1 overexpressors (compare an aperture of 0.05 ± 0.07 in RCAR1-2 to one of 0.33 ± 0.03 in the control line at 0.3 μM ABA, $P < 0.001$). Higher ABA levels (~10-fold) were required to close the stomata of the control to the extent observed at 0.3 μM ABA in the overexpressors. Similarly, the RCAR1–overexpressing lines were ABA-hypersensitive with respect to seed germination and root elongation. The median inhibitory concentration (IC_{50} value) for (*S*)-ABA–mediated inhibition of germination was shifted from 0.6 ± 0.15 μM ABA in the control to 0.2 ± 0.07 μM in the RCAR1-2–overexpressing line (Fig. 4I). ABA (1 μM) inhibited root growth by more than 80% in RCAR1-2 and RCAR1-5 plantlets, as compared with 40% in control plants (Fig. 4J). The IC_{50} value of (*S*)-ABA to inhibit root growth was 0.4 ± 0.2 μM for RCAR1-2 seedlings as compared with 3 ± 0.3 μM for the control line. RCAR1 is expressed in various parts of *Arabidopsis* including roots, stomata, and parenchymal cells of the vasculature (fig. S7, A to F).

In conclusion, the manipulation of RCAR1 transcript levels via RNAi or overexpression affected all facets of ABA signaling examined: gene expression, adjustment of stomatal aperture, seed germination, and vegetative growth. RCAR-related proteins from *Vigna* and lupine have been linked to phytohormone homeostasis (*29*–*31*), and the crystal structure analyses of the proteins revealed a cavity in the center encaged by seven β sheets and two α-helical domains. Ligands such as the steroid deoxycholate and cytokinins can be bound within the cavity and, by analogy, possibly ABA. Our analyses indicate binding of a single ABA molecule per RCAR1 and a dissociation constant in the nanomolar range for the complex of RCAR1-PP2C with ABA. The considerably lower K_d value of the heteromeric protein–ABA complex argues for a ligand-induced complex stabilization similar to FLS2 and BAK1 receptor stabilization by flagellin (*32*). The heteromeric complex of PP2C and RCAR1 protein has the hallmark of a receptor, i.e., selective recognition and transmission of the signal, in this case, via ABA-exerted control on protein phosphatase activity. The ABA receptor complex was detected both in the cytosol and in the nucleus. There is strong evidence for a cytosolic perception site of ABA (*5*) and a control of ABA signaling by nuclear ABI1 (*21*).

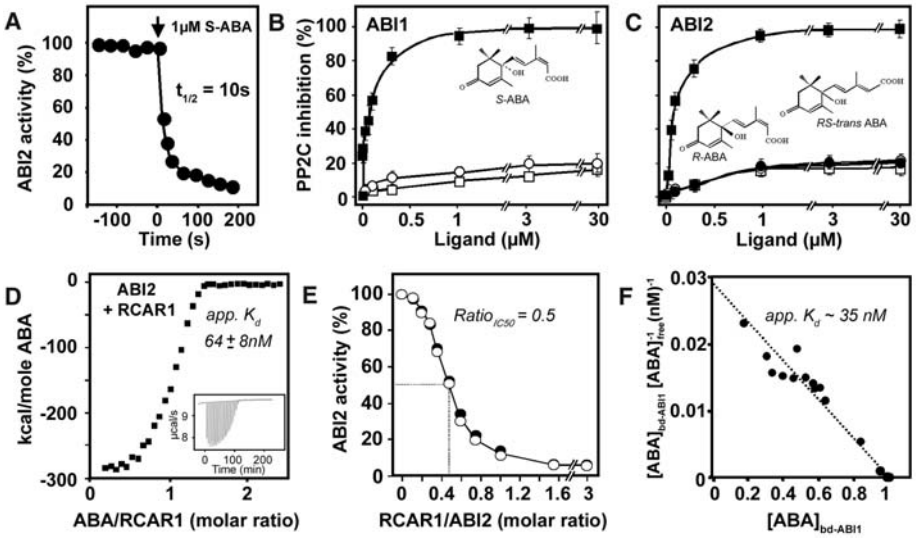

Fig. 3. Binding of ABA to RCAR1 and ABI1/2 and the regulation of PP2C phosphatase activity. (**A**) Time course of inhibition of ABI2 activity. S-ABA, (*S*)-ABA. (**B**) Inhibition of ABI1 and (**C**) ABI2 by (*S*)-ABA (filled squares), (*R*)-ABA (open squares), and *trans*-(*R*,*S*)-ABA (open circles) in the presence of RCAR1. The effect of (*S*)-ABA on ABI2 activity is marked by filled circles in the absence of RCAR1 in (C). (**D**) Interaction analysis by isothermal titration calorimetry of RCAR1 + ABI2 (4 μM). (**E**) Stoichiometric analysis of RCAR1-mediated inhibition of ABI2 (30 nM) in the presence of 1 mM (*S*)-ABA and 1 mM (open circles) or 4 mM (filled circles) of substrate (SD < 5%). (**F**) Scatchard plot of ABI1 inhibition by (*S*)-ABA. $[ABA]_{bd}$ is the concentration of bound ABA.

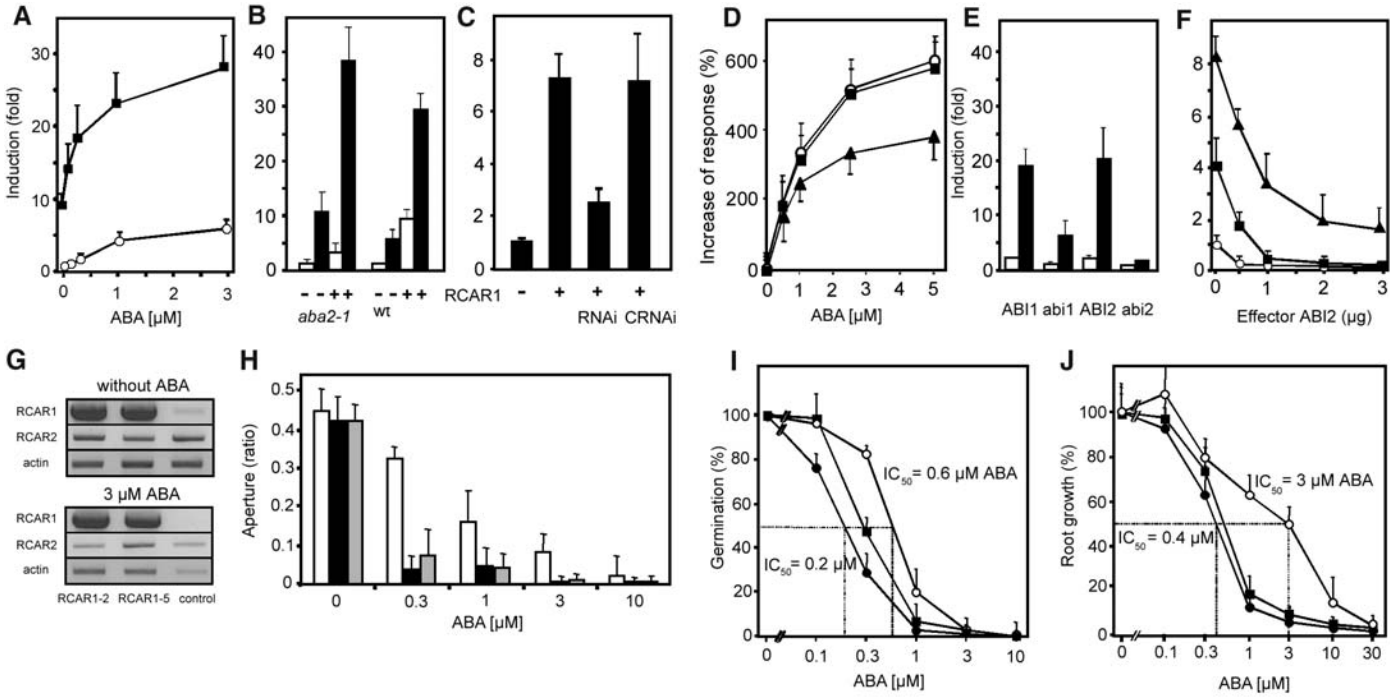

Fig. 4. ABA responses and RCAR1. (A to F) The ABA-induced up-regulation of gene expression was monitored with the ABA-responsive reporter constructs *pRD29B::LUC* (A, B, and D to F) and *pRAB18::LUC* (C) in *Arabidopsis* protoplasts and was measured as relative light units (RLU/RFU; $n > 3$). (**A**) Activation of the ABA response by ectopic expression of RCAR1 (1 μg, filled squares) in comparison with the control (open circles). (**B**) Regulation of gene expression by the effector RCAR1 (3 μg) in the absence (white bars) and presence of 3 μM (*S*)-ABA (black bars). (Left) ABA-deficient *aba2-1* protoplasts; (right) wild-type protoplasts. (**C** and **D**) The RCAR1-mediated stimulation of the ABA response is antagonized by coexpression of an RNAi construct (1 μg) targeting RCAR1. CRNAi: control RNAi. Control, empty vector plasmid, open circles; CRNAi, filled squares; RNAi, filled triangles. (**E**) The RCAR1- and ABA-stimulated reporter expression is antagonized by concomitant expression of various PP2Cs (1 μg) in the absence (white bars) and presence of 3 μM (*S*)-ABA (black bars). (**F**) The RCAR1-mediated stimulation of the ABA response is antagonized by coexpression of ABI2. The levels of RCAR1 effector constructs were 0, 1, and 10 μg plasmid (open circles, filled squares, and triangles, respectively). (**G**) Comparative reverse transcriptase polymerase chain reaction analysis of transgenic lines RCAR1-2, RCAR1-5, and of a control line for transcripts of RCAR1 and RCAR2 (At4g01026) in the absence and presence of 3 μM (*S*)-ABA. (**H** to **J**) Analysis of transgenic lines overexpressing RCAR1. (H) Stomatal response of 5-day-old seedlings exposed to (*S*)-ABA ($n > 50$). (I) Seed germination after 5 days of incubation ($n > 140$). (J) Inhibition of root growth of the transgenic lines in the presence of (*S*)-ABA (3 days, $n > 60$). In the absence of ABA, root growth equaled 15.4 ± 1.8 mm, 15.2 ± 1.6 mm, and 14.9 ± 1.2 mm for RCAR1-2, RCAR1-5, and the control line, respectively. RCAR1-2 black bar in (H) and filled circles in (I and J); RCAR1-5 (gray bar, filled squares), control line (white bar, open circles).

Recently, two homologous G proteins, GTG1 and GTG2, have been characterized as plasma membrane–localized ABA receptors that are structurally related to a mammalian anion channel (*9*). Hence, ABA receptors seem to display a diversity not known for any other phytohormone. The capacity of RCAR1 and other RCAR1-like proteins to regulate ABI1 and ABI2 in an ABA-dependent manner indicates a combinatorial complexity of ABA receptors. The RCAR proteins examined are from different clades within the protein family, which supports the notion that all 14 members might represent ABA receptor components. This 14-member RCAR gene family has been independently identified by Park *et al*. (*33*), who analyzed the genes' role in ABA signaling and named the genes *PYRABACTIN RESISTANCE* and *PYR1-Like* (*PYR1* and *PYL1* through *PYL13*, respectively). Members of the RCAR family seem to interact with other PP2Cs, such as HAB1, involved in ABA signaling (*33*). The functional knockout of RCAR1 in *Arabidopsis* did not reveal altered ABA responses consistent with functional redundancy among the RCAR proteins. However, multiple knockouts of RCAR11-PYR1 and other RCARs-PYLs generated an ABA-insensitive phenotype (*33*). The regulation of the receptor complexes for (*S*)-ABA at the nanomolar level is in the range of ABA levels under conditions of mild stress, which already limit transpiration (*34*, *35*). Future studies will reveal whether a combinatorial assembly of different receptor complexes provides a mechanism to adjust the sensitivity of ABA perception for optimal gas exchange and performance.

References and Notes

1. M. Melotto, W. Underwood, J. Koczan, K. Nomura, S. Y. He, *Cell* **126**, 969 (2006).
2. A. Christmann *et al*., *Plant Biol (Stuttgart)* **8**, 314 (2006).
3. B. A. Adie *et al*., *Plant Cell* **19**, 1665 (2007).
4. T. Hirayama, K. Shinozaki, *Trends Plant Sci.* **12**, 343 (2007).
5. V. Levchenko, K. R. Konrad, P. Dietrich, M. R. Roelfsema, R. Hedrich, *Proc. Natl. Acad. Sci. U.S.A.* **102**, 4203 (2005).
6. T. Vahisalu *et al*., *Nature* **452**, 487 (2008).
7. Y. Y. Shen *et al*., *Nature* **443**, 823 (2006).
8. X. Liu *et al*., *Science* **315**, 1712 (2007).
9. S. Pandey, D. C. Nelson, S. M. Assmann, *Cell* **136**, 136 (2009).
10. Y. Gao *et al*., *Plant J.* **52**, 1001 (2007).
11. C. A. Johnston *et al*., *Science* **318**, 914c (2007).
12. X. Liu, Y. Yue, W. Li, L. Ma, *Science* **318**, 914d (2007).
13. J. Guo, Q. Zeng, M. Emami, B. E. Ellis, J. G. Chen, *PLoS One* **3**, e2982 (2008).
14. P. McCourt, R. Creelman, *Curr. Opin. Plant Biol.* **11**, 474 (2008).
15. A. H. Müller, M. Hansson, *Plant Physiol.* Published online 28 January 2009. 10.1104/pp.109.135277.
16. T. Yoshida *et al*., *Plant Physiol.* **140**, 115 (2006).
17. J. M. Kuhn, A. Boisson-Dernier, M. B. Dizon, M. H. Maktabi, J. I. Schroeder, *Plant Physiol.* **140**, 127 (2006).
18. Y. Yang *et al*., *Proc. Natl. Acad. Sci. U.S.A.* **103**, 6061 (2006).
19. A. Saez *et al*., *Plant Physiol.* **141**, 1389 (2006).
20. N. Nishimura *et al*., *Plant J.* **50**, 935 (2007).
21. D. Moes, A. Himmelbach, A. Korte, G. Haberer, E. Grill, *Plant J.* **54**, 806 (2008).
22. S. Merlot, F. Gosti, D. Guerrier, A. Vavasseur, J. Giraudat, *Plant J.* **25**, 295 (2001).
23. R. Yoshida *et al*., *J. Biol. Chem.* **281**, 5310 (2006).
24. Y. Guo *et al*., *Dev. Cell* **3**, 233 (2002).
25. A. Himmelbach, T. Hoffmann, M. Leube, B. Hohener, E. Grill, *EMBO J.* **21**, 3029 (2002).
26. Single-letter abbreviations for the amino acid residues are as follows: A, Ala; C, Cys; D, Asp; E, Glu; F, Phe; G, Gly; H, His; I, Ile; K, Lys; L, Leu; M, Met; N, Asn; P, Pro; Q, Gln; R, Arg; S, Ser; T, Thr; V, Val; W, Trp; and Y, Tyr.
27. Materials and methods are available as supporting material on *Science* Online.
28. M. P. Leube, E. Grill, N. Amrhein, *FEBS Lett.* **424**, 100 (1998).
29. Z. Markovic-Housley *et al*., *J. Mol. Biol.* **325**, 123 (2003).
30. O. Pasternak *et al*., *Plant Cell* **18**, 2622 (2006).
31. H. Fernandes *et al*., *J. Mol. Biol.* **378**, 1040 (2008).
32. D. Chinchilla *et al*., *Nature* **448**, 497 (2007).

33. S.-Y. Park *et al.*, *Science* **324**, 1068 (2009); published online 30 April 2009 (10.1126/science.1173041).
34. D. M. Priest *et al.*, *Plant J.* **46**, 492 (2006).
35. A. Christmann, E. W. Weiler, E. Steudle, E. Grill, *Plant J.* **52**, 167 (2007).
36. This study was funded by the Deutsche Forschungsgemeinschaft CH-182/5, European Union Marie-Curie-Program MEST-CT-2005-020232, and the Fonds der Chemischen Industrie. We thank J. Berger, C. Heidersberger, and C. Kornbauer for technical assistance. We are grateful to D. Weinfurtner, Chemistry Department TUM, and K. Berendzen, University of Tübingen, for help in conducting the ITC and FACS analysis, respectively. The cytokinin reporter and the At5g46790 cDNA clone were kindly provided by J. Sheen, Harvard University, and the *Arabidopsis* Biological Resource Center, USA, respectively. We thank F. Assaad for critical reading of the manuscript. This contribution is dedicated to Hubert Ziegler, who passed away on 17 April 2009.

Supporting Online Material
www.sciencemag.org/cgi/content/full/1172408/DC1
Materials and Methods
Figs. S1 to S7
References

27 October 2008; accepted 17 April 2009
Published online 30 April 2009;
10.1126/science.1172408
Include this information when citing this paper.

Abscisic Acid Inhibits Type 2C Protein Phosphatases via the PYR/PYL Family of START Proteins

Sang-Youl Park,[1]* Pauline Fung,[2]* Noriyuki Nishimura,[4]† Davin R. Jensen,[8]† Hiroaki Fujii,[1] Yang Zhao,[2] Shelley Lumba,[2] Julia Santiago,[5] Americo Rodrigues,[5] Tsz-fung F. Chow,[2] Simon E. Alfred,[2] Dario Bonetta,[6] Ruth Finkelstein,[7] Nicholas J. Provart,[2,3] Darrell Desveaux,[2,3] Pedro L. Rodriguez,[5] Peter McCourt,[2] Jian-Kang Zhu,[1] Julian I. Schroeder,[4] Brian F. Volkman,[8] Sean R. Cutler[1,9,10,11]‡

Type 2C protein phosphatases (PP2Cs) are vitally involved in abscisic acid (ABA) signaling. Here, we show that a synthetic growth inhibitor called pyrabactin functions as a selective ABA agonist. Pyrabactin acts through *PYRABACTIN RESISTANCE 1* (*PYR1*), the founding member of a family of START proteins called PYR/PYLs, which are necessary for both pyrabactin and ABA signaling in vivo. We show that ABA binds to PYR1, which in turn binds to and inhibits PP2Cs. We conclude that PYR/PYLs are ABA receptors functioning at the apex of a negative regulatory pathway that controls ABA signaling by inhibiting PP2Cs. Our results illustrate the power of the chemical genetic approach for sidestepping genetic redundancy.

Abscisic acid (ABA), identified in plants in the 1960s, is a small molecule that functions to inhibit growth and to regulate plant stress responses. Genetic analyses have identified many factors involved in ABA signaling (*1*), including the group A type 2C protein phosphatases (PP2Cs), which negatively regulate ABA signaling at an early step in the pathway (*2*), and the SNF1-related kinase 2 (SnRK2 kinases), which are positive regulators (*3*–*5*). Several (+)-ABA (**1**) binding proteins have been reported (*6*–*8*) (Fig. 1A); however, their roles are not fully understood, and they do not appear to work via the genetically defined signaling pathway (*9*) or bind to the nonnatural but bioactive stereoisomer (–)-ABA (**2**) (*10*–*12*). The genetic dissection of ABA perception has not identified proteins resembling receptors, which suggests that the ABA receptor(s) may be functionally redundant or may be required for viability (*13*). We therefore pursued a chemical genetic strategy (*14*), because chemicals can bypass redundancy by inducing phenotypes not revealed by single-locus mutations (*15*). For example, an antagonist with low selectivity can perturb the function of an entire protein family, whereas a selective agonist can illuminate the function of one member of normally redundant receptors, as we describe here with pyrabactin (**3**) (Fig. 1A), a synthetic seed germination inhibitor (*14*). The analysis of analogs revealed that pyrabactin's activity requires its pyridyl nitrogen, because the analog apyrabactin (**4**) is biologically inactive (fig. S1) (*16*). Further investigation of pyrabactin's action revealed reduced sensitivity in ABA-insensitive mutants, but not ABA biosynthesis or gibberellic acid–perception mutants (fig. S2), which suggests it is an agonist of ABA signaling that inhibits germination in response to environmental stress (*17*). Aside from ABA analogs, no synthetic agonists of this stress pathway are known. Microarray analyses of the ABA and pyrabactin responses of seeds and seedlings revealed that, in seeds, both compounds induce highly correlated transcriptional responses (r = 0.98; Fig. 1B; table S1). Three unrelated germination inhibitors (*18*) failed to induce ABA-like effects (fig. S2), which demonstrates that an indirect germination effect

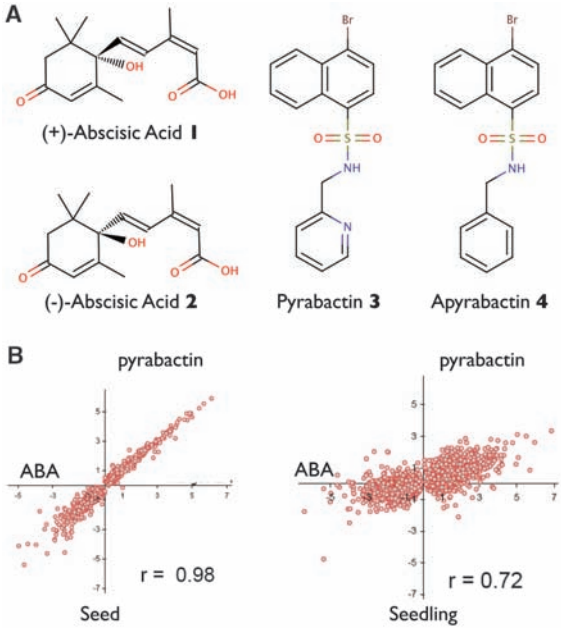

Fig. 1. Pyrabactin is a seed-selective ABA agonist. (**A**) Structures of molecules described in this study. (**B**) ATH1 microarray comparison of pyrabactin and ABA effects on seeds and seedlings. The axes plot $\log_2$-transformed values for probe responses to pyrabactin (y axis) or ABA (x axis), relative to control samples. The Pearson correlation coefficient (r) for each comparison is shown within the graph. Probes selected for analyses were those significantly responsive to either ABA or pyrabactin. Germination-responsive transcripts were removed for seed analyses. Detailed methods are provided in (*16*).

[1]Department of Botany and Plant Sciences, University of California at Riverside, Riverside, CA 92521, USA. [2]Department of Cell and Systems Biology, University of Toronto, 25 Willcocks Street, Toronto, ON, M5S 3B2, Canada. [3]Centre for the Analysis of Genome Evolution and Function, University of Toronto, 25 Willcocks Street, Toronto, ON, M5S 3B2, Canada. [4]Division of Biological Sciences, Cell and Developmental Biology Section, University of California at San Diego, 9500 Gilman Drive, La Jolla, CA 92093, USA. [5]Instituto de Biología Molecular y Celular de Plantas, Universidad Politécnica de Valencia, Avenida de los Naranjos, Edificio CPI, 8E, ES-46022 Valencia, Spain. [6]Faculty of Science, University of Ontario Institute of Technology, 2000 Simcoe Street North, Oshawa, ON, L1H 7K4, Canada. [7]Department of Molecular, Cellular, and Developmental Biology, University of California at Santa Barbara, Santa Barbara, CA 93106, USA. [8]Department of Biochemistry, Medical College of Wisconsin, 8701 Watertown Plank Road, Milwaukee, WI 53226, USA. [9]Center for Plant Cell Biology, University of California at Riverside, Riverside, CA 92521, USA. [10]Institute for Genome Biology, University of California at Riverside, Riverside, CA 92521, USA. [11]Department of Chemistry, University of California at Riverside, Riverside, CA 92521, USA.

*These authors contributed equally to the work described. †These authors contributed equally to the work described. ‡To whom correspondence should be addressed. E-mail: sean.cutler@ucr.edu

is not sufficient to account for pyrabactin's agonist activity in seeds. In contrast to seed responses, seedling ABA and pyrabactin responses show poorer correlation ($r = 0.72$) (Fig. 1C), and few ABA-responsive genes significantly respond to pyrabactin (table S1). Thus, pyrabactin affects some, but not all, of the pathways regulated by ABA and is therefore a selective agonist.

Selective agonists have a long history as reagents for receptor identification, so we used pyrabactin for genetic dissection and isolated 12 *PYRABACTIN RESISTANCE 1* (*Pyr1*) mutant alleles. *Pyr1*, isolated by map-based cloning, encodes a member of the cyclase subfamily of the START domain superfamily. START proteins share a conserved hydrophobic ligand–binding pocket (*19*–*21*). There are 13 genes in the *Arabidopsis* genome having marked similarity to *Pyr1* (fig. S1), which we have named *Pyl1* to *Pyl13* (for *PYR1-Like*). This 14-member gene family (Fig. 4B) has been independently identified as ABI1-interacting proteins (called "regulatory component of ABA receptor," RCAR1 through RCAR14) by Ma *et al.* (*22*), and their role in ABA signaling is characterized there. The *pyr1* mutant alleles we isolated are predicted to produce a variety of defects in PYR1 (fig. S3). Gene expression databases (*23*–*27*) show that *Pyr* and *Pyl* mRNAs are expressed at high levels in seeds and guard cells and respond to ABA (Fig. 2A), which is consistent with a role in ABA signaling. However, all of the *pyr1* mutants isolated, including putative null alleles, reduce pyrabactin, but not ABA, sensitivity. To examine if functional redundancy might obscure a role for *Pyr1* in ABA signaling, we isolated *Pyl1*, *Pyl2*, and *Pyl4* insertion alleles and constructed multilocus mutants. Triple (*pyr1;pyl1;pyl4*) and quadruple (*pyr1;pyl1;pyl2;pyl4*) mutant lines display strong ABA insensitivity (Fig. 2B), which can be reversed by introducing PYR1- or PYL4-expressing transgenes (fig. S3). The quadruple mutant is less sensitive to (+)-ABA as measured by seed germination, root growth, and quantitative reverse transcription polymerase chain reaction (qRT-PCR) (Fig. 2C), and SnRK2 kinase assays (Fig. 2D and fig. S4). Collectively, our genetic data show that *Pyr1* and *Pyl*s are necessary for multiple ABA responses in vivo and illustrate the differential behavior that natural and synthetic agonists can display in genetic screens.

Because PYR1 is predicted to be a ligand-binding START protein necessary for pyrabactin activity, we hypothesized that pyrabactin might

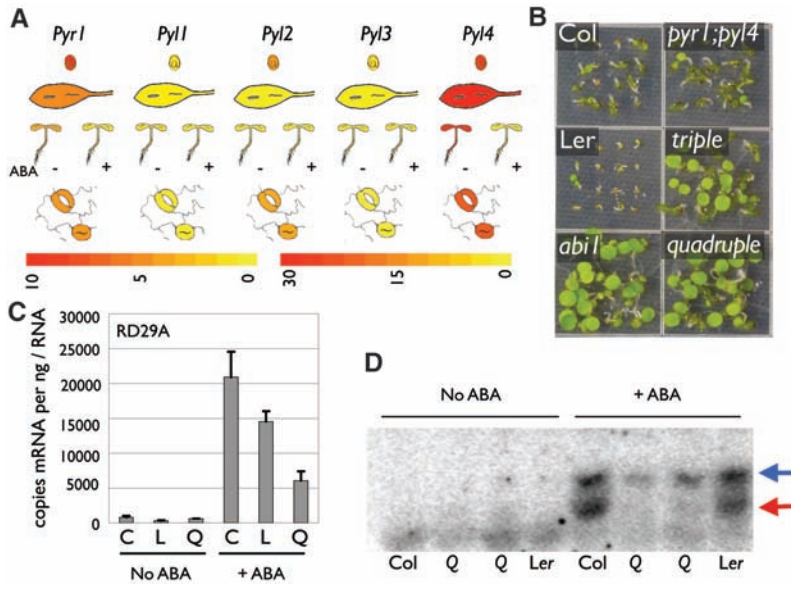

Fig. 2. Pyr/Pyls are necessary for ABA signaling. (**A**) Pyr1 and Pyl1 to Pyl4 expression levels. Plots were made with the eFP browser (*24*); these heat maps show normalized ATH1 microarray expression values (divided by 100) according to the color scales shown; the right color scale is for the guard cell data only. (**B**) Genes for Pyr/Pyl act redundantly in ABA signaling. Genotypes shown were germinated on medium containing 0.9 μM (+)-ABA and were documented 7 days post imbibition. (**C**) Pyr/Pyls are required for normal ABA-induced gene expression in seedlings. Shown are qRT-PCR results for the ABA-responsive gene RD29. L, Ler; C, Col; and Q, quadruple mutant. (**D**) The Pyr/Pyls are required for normal SnRK2 kinase activity. In-gel kinase assays were conducted on extracts made from control or ABA-treated plants of the genotypes shown; extracts from two separate quadruple (Q) mutant lines are shown. Red arrow corresponds to SnRK2.2 and 2.3; blue to SnRK2.6 (OST1), as described (*37*).

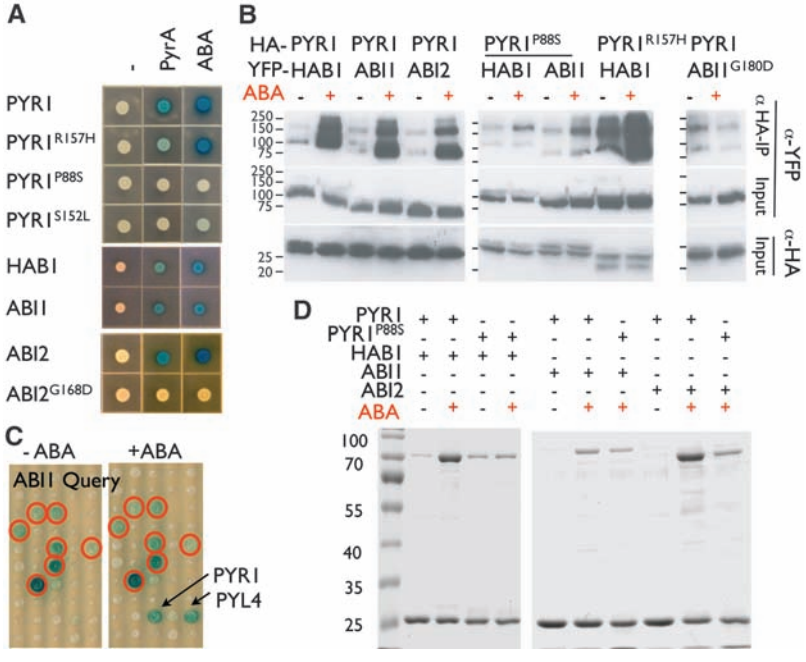

Fig. 3. PYR/PYLs bind to group A PP2Cs in response to ABA. (**A**) Wild-type and mutant PYR1-PP2C interactions. PYR1 and three different pyrabactin-insensitive substitution mutants were constructed as binding-domain (BD) fusion proteins and were tested for their interactions with activation domain (AD)–fused HAB1 with the yeast two-hybrid assay by using the compounds shown at top (top panel). In the two bottom panels, AD fusions of HAB1, ABI1, ABI2, or ABI2^{G168D} were tested for ABA- and pyrabactin-induced interactions with BDPYR1. (**B**) ABA promotes PYR1 to PP2C interactions in planta. Total protein extracts (input) were made from *N. benthamiana* leaves transformed with the indicated constructs and/or treatments, immunoprecipitated with antibody against HA-agarose, and immunodetected with antibodies against green fluorescent protein (GFP) or HA. YFP-PP2Cs migrate at ~100 kD and HA-PYR1 at ~25 kD. (**C**) ABA-orfeome analysis of ABI1 interactions. Shown are subsets of an ABA-orfeome queried with ABI1; autoactivators are circled and ABA-dependent interactors are indicated with arrows. (**D**) Reconstitution of ABA responses in vitro. Pull-down assays using glutathione *S*-transferase (GST)–HAB1 (~80 kD) and His_6-tagged PYR1 (~25 kD) were conducted with purified recombinant proteins. GST-ABI1 and ABI2 tests were done with protein in crude lysates. Pyrabactin (10 μM, PyrA) was used in (A), 10 μM (+)-ABA was used in (A) and (D), and 100 μM ABA (mixed stereoisomers) in (B) and (C).

promote a protein-protein interaction between PYR1 and a downstream effector. To test this, ~2 million prey cDNA clones were screened against PYR1 yeast two-hybrid bait on medium containing pyrabactin. This revealed that the PP2C HAB1 (*28*, *29*) interacts with PYR1 in response to pyrabactin and (+)-ABA, but not the inactive analog apyrabactin or several other plant hormones (Fig. 3A and fig. S4). HAB1 resides in the group A subfamily of plant PP2Cs, which contains nine partially redundant members that negatively regulate ABA signaling (*30*, *31*). To examine the relevance of the yeast two-hybrid data, we next performed a series of control experiments. First, we investigated the effects of defective PYR1 and PP2C amino acid substitution mutants on ABA-responsive interactions in the yeast two-hybrid assay (*32*). PYR1^{S152L} and PYR1^{P88S}, isolated because they cause pyrabactin insensitivity in planta, reduce ABA-induced PYR1-PP2C interactions (Fig. 3A); similarly, the dominant ABA-insensitive ABI2^{G168D} mutant (Fig. 3B) disrupts the PYR1-ABI2 interaction. Second, we investigated in planta interactions by coexpressing a panel of yellow fluorescent protein (YFP)–tagged PP2Cs and hemagglutinin (HA)-tagged PYR1 constructs in *N. benthamiana*. Coimmunoprecipitation experiments performed on ABA or mock-treated plants recapitulated the PYR1-PP2C interactions observed in yeast and also showed that PYR1 does not interact with ABI1^{G180D}, encoded by *abi1-1* (Fig. 3C). Third, we used PYR1 and ABI1 as bait in a yeast two-hybrid screen against a set of 258 ABA-responsive open reading frames and observed that interactions between PYR1 and group A PP2C proteins occur only in the presence of ABA (Fig. 3D and table S2). Fourth, we successfully reconstituted the ABA-induced PYR1-PP2C interactions in vitro using recombinant proteins (Fig. 3E). Thus, we conclude that ABA promotes a biologically meaningful interaction between PYR1 and group A PP2Cs.

Given the redundancy observed in our genetic analyses, it is likely that other PYR/PYLs interact with PP2Cs in response to ABA. We therefore used the yeast two-hybrid assay to explore interactions of HAB1 and PP2CA (AHG3) (ABA-hypersensitive germination gene 3) with a panel of 12 PYR/PYLs, which shows that (+)-ABA promotes interactions between PYR1, PYL1 to PYL4, and HAB1 (Fig. 4A). We next used this PYR/PYL panel to examine ligand response selectivities, which shows that these five (+)-ABA–responsive PYR/PYLs do not all bind HAB1 in response to nonnatural agonists. For example, PYL2, PYL3, and PYL4 respond to both (+)-ABA and (–)-ABA (Fig. 4A), which makes these proteins candidates for the dual-stereoisomer receptors predicted by earlier studies (*12*). Consistent with this hypothesis, our quadruple mutant has greatly reduced (–)-ABA sensitivity (fig. S3). Ligand-selective interactions are also observed for pyrabactin, which promotes interactions between HAB1 and PYR1, PYL1, or PYL3 (Fig. 4A). Of these, only *Pyr1* is highly transcribed in seeds (Fig. 2B), which likely explains why mutations in *Pyr1* cause the seeds to be insensitive to pyrabactin. Last, we observe that PYL12 interacts with PP2CA (AHG3) in response to ABA (fig. S4). Thus, at least 6 of the 14 PYR/PYLs confer ABA responsiveness to yeast. We hypothesize that the entire PYR/PYL gene family participates in ABA-promoted interactions, as these six genes are distributed across the PYR/PYL phylogenetic tree (Fig. 4B). The specificity with which *pyr/pyl* genes control which ligands trigger ABA signaling suggests that the ABA pathway may be dissected using selective PYR/PYL agonists.

Given the role of PYR/PYLs in controlling ligand responses, we explored whether (+)-ABA binds PYR1 by using ^{15}N-labeled PYR1 and PYR1^{P88S} in heteronuclear single quantum coherence (HSQC) nuclear magnetic resonance (NMR) experiments, which probe chemical shifts of protein amide–NH bonds in response to ligands (*33*). Because START proteins contain a conserved ligand-binding cavity (*34*), binding should selectively perturb residues lining this cavity. Addition of (+)-ABA altered the HSQC signals for many PYR1 and PYR1^{P88S} residues (Fig. 4C and figs. S5 and S6), which showed that ABA binds PYR1 and likely induces a conformational change. We also investigated the PYR1-HAB1 interaction in the presence of ABA, because our NMR experiments showed that PYR1^{P88S} is not defective in ABA binding. Addition of unlabeled HAB1 caused peak broadening for PYR1, but not PYR1^{P88S}, HSQC signals (fig. S7), which localized the PYR1^{P88S} defect to binding HAB1 after ABA perception. Because PP2Cs are negative regulators of ABA signaling, we hypothesized that ABA-promoted PYR/PYL–PP2C interactions would inhibit phosphatase activity. To test this, we examined the effects of (+)-ABA on PP2C enzyme

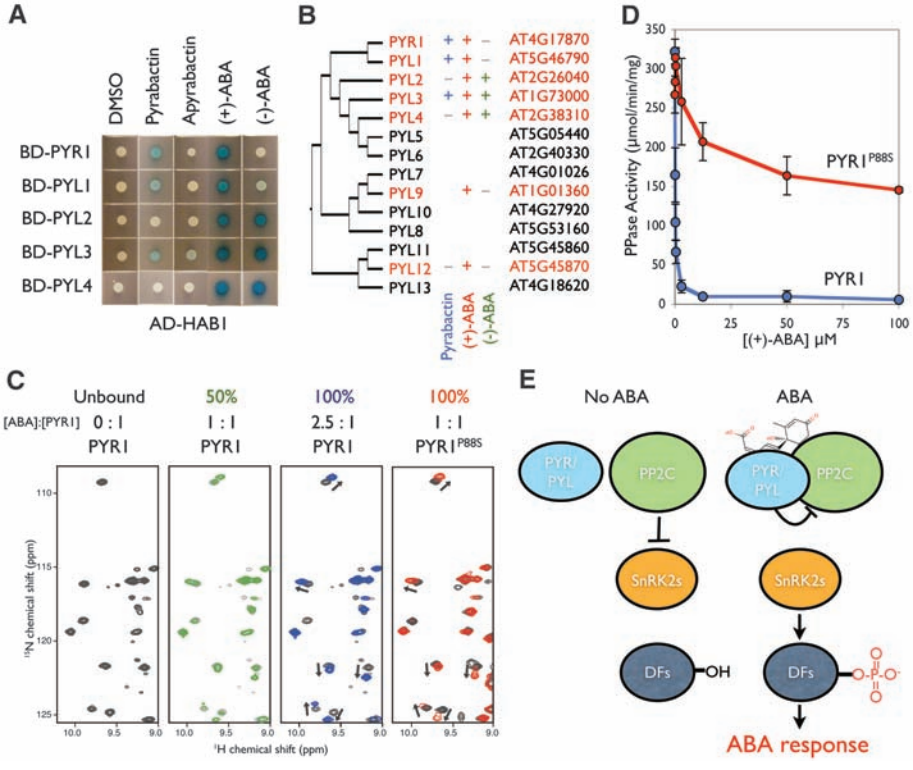

Fig. 4. PYR1 is an ABA-binding protein that regulates PP2C activity. (**A**) PYR/PYL proteins determine selectivities for responses to different ligands. A panel of PYR/PYL genes were constructed as BD fusions and tested in yeast for interactions with HAB1 and AHG3 in response to (+)-ABA, (–)-ABA, pyrabactin, or apyrabactin (all 10 µM), dimethyl sulfoxide (DMSO) (carrier solvent, 1%). Shown are results for five PYR/PYLs that interact with HAB1 in response to ABA. (**B**) ABA response activity is distributed throughout the PYR/PYL family. Shown is a neighbor-joining tree of the PYR/PYL family. (Middle) Ligand selectivity data derived from yeast two-hybrid experiments. (+)-ABA–responsive PYR/PYLs are colored red, *Arabidopsis* Genome Initiative (AGI) annotations are shown at right; PYL9 colored red, on the basis of data from Ma *et al.* (*22*). (**C**) ABA binds to PYR1 and PYR1^{P88S}. Shown are subregions of HSQC spectra for ^{15}N-labeled PYR1 and PYR1^{P88S} in response to increasing amounts of ABA. Arrows indicate amide protons whose chemical environments shift in response to ABA. (**D**) PYR1 inhibits PP2C activity in the presence of ABA. Initial reaction velocities of recombinant GST-HAB1 were tested in the presence of PYR1 or PYR1^{P88S}, and differing ABA concentrations using the colorimetric substrate *p*-nitrophenyl phosphate (pNPP). The measured IC_{50} values are 125 nM for PYR1 and 50 µM for PYR1^{P88S}. (**E**) Hypothesized model for PYR/PYL control of ABA signaling. We propose the following model: In the absence of ABA (left), PYR/PYL proteins are not bound to PP2Cs, and therefore, PP2C activity is high, which prevents phosphorylation and activation of SnRK2s and downstream factors (DFs). In the presence of ABA, PYR/PYLs bind and inhibit PP2Cs. This allows accumulation of phosphorylated downstream factors and ABA transcriptional responses. The regulation of SnRK2s by PYR/PYLs may be indirect or may involve other factors.

kinetics using recombinant HAB1, PYR1, or PYR1^{P88S}. These experiments show that (+)-ABA acts as a potent and saturable inhibitor of phosphatase activity in the presence of PYR1 [median inhibitory concentration (IC_{50}) = 125 nM], but not PYR1^{P88S} (IC_{50} = 50 μM) (Fig. 4D and fig. S8). Similarly, ABA displays saturable inhibition of HAB1 PP2C activity in the presence of recombinant PYL4 (fig. S8). Thus, PYR/PYLs regulate PP2Cs in response to ABA, which defines an unprecedented mechanism for ligand-mediated regulation of PP2C activity.

Collectively, we have shown that PYR1 binds (+)-ABA, PYR/PYLs bind to and inhibit PP2Cs in response to (+)-ABA, and PYR/PYLs control which ligands trigger PP2C interactions. We conclude that the PYR/PYLs are a family of ABA receptors. However, the precise site of ABA binding remains unclear, because the ABA-binding site may be shared with the PP2C. Discriminating between these receptor and co-receptor models will require structural studies of cocrystallized PYR/PYLs, PP2Cs, and ligands. Note that the PYR/PYLs interact directly with PP2Cs, which are core components of the ABA signaling pathway. Because SnRK2 activity is decreased in the PYR/PYL quadruple mutant, we propose a hypothetical model (Fig. 4D) for ABA action in which ABA and PYR/PYLs inhibit PP2Cs, which in turn relieves repression of positive factors, such as the SnRK2s. Consistent with this model, we observed interaction of SnRK2.2 with PP2CA (AHG3), AHG1, and ABI1 when we used the yeast two-hybrid assay (fig. S4). This suggested that the low SnRK2 activity observed in the PYR/PYL quadruple mutant may be a direct consequence of PP2C-SnRK2 interactions. Understanding of the role of PP2Cs in ABA signaling has been complicated by observations from *abi1-1* and *abi2-1* mutations. Their dominant phenotypes suggest that they encode hypermorphic proteins (*35*), but they paradoxically reduce, but do not abolish, PP2C activity (*36*). Our data show that these mutants do not bind PYR1 in response to ABA. We therefore hypothesize that ABA normally lowers wild-type PP2C activity through PYR/PYL proteins, but *abi* PP2Cs escape this and disrupt signaling because of their residual activity. Consistent with this model, a second site mutation that abolishes *abi1-1*'s catalytic activity suppresses its dominant ABA-insensitive phenotype (*36*).

The redundancy in the *Pyr/Pyl* gene family, typical of many plant genes, has kept these genes from emerging as factors necessary for ABA response. We leveraged pyrabactin's selectivity for a subset of the PYR/PYL family to bypass the genetic redundancy that masks ABA phenotypes in single mutants. Thus, our results demonstrate the power of synthetic molecules to expose phenotypes for otherwise redundant genes.

References and Notes

1. R. R. Finkelstein, S. S. L. Gampala, C. D. Rock, *Plant Cell* **14**, S15 (2002).
2. G. J. Allen, K. Kuchitsu, S. P. Chu, Y. Murata, J. I. Schroeder, *Plant Cell* **11**, 1785 (1999).
3. H. Fujii, P. E. Verslues, J. K. Zhu, *Plant Cell* **19**, 485 (2007).
4. A. C. Mustilli, S. Merlot, A. Vavasseur, F. Fenzi, J. Giraudat, *Plant Cell* **14**, 3089 (2002).
5. R. Yoshida *et al.*, *Plant Cell Physiol.* **43**, 1473 (2002).
6. X. Liu *et al.*, *Science* **315**, 1712 (2007).
7. Y. Y. Shen *et al.*, *Nature* **443**, 823 (2006).
8. S. Pandey, D. C. Nelson, S. M. Assmann, *Cell* **136**, 136 (2009).
9. P. McCourt, R. Creelman, *Curr. Opin. Plant Biol.* **11**, 474 (2008).
10. D. Huang *et al.*, *Plant J.* **50**, 414 (2007).
11. E. Sondheimer, E. C. Galson, Y. P. Chang, D. C. Walton, *Science* **174**, 829 (1971).
12. E. Nambara *et al.*, *Genetics* **161**, 1247 (2002).
13. P. McCourt, *Annu. Rev. Plant Physiol. Plant Mol. Biol.* **50**, 219 (1999).
14. Y. Zhao *et al.*, *Nat. Chem. Biol.* **3**, 716 (2007).
15. S. Cutler, P. McCourt, *Plant Physiol.* **138**, 558 (2005).
16. Materials and methods are available as supporting material on *Science* Online.
17. S. Toh *et al.*, *Plant Physiol.* **146**, 1368 (2008).
18. G. W. Bassel *et al.*, *Plant Physiol.* **147**, 143 (2008).
19. L. M. Iyer, E. V. Koonin, L. Aravind, *Proteins* **43**, 134 (2001).
20. C. Radauer, P. Lackner, H. Breiteneder, *BMC Evol. Biol.* **8**, 286 (2008).
21. B. Lytle *et al.*, *Proteins*, published online 2 February 2009, 10.1002/prot.22396, in press.
22. Y. Ma *et al.*, *Science* **324**, 1064 (2009); published online 30 April 2009 (10.1126/science.1172408).
23. M. Schmid *et al.*, *Nat. Genet.* **37**, 501 (2005).
24. K. Nakabayashi, M. Okamoto, T. Koshiba, Y. Kamiya, E. Nambara, *Plant J.* **41**, 697 (2005).
25. H. Goda *et al.*, *Plant J.* **55**, 526 (2008).
26. D. Winter *et al.*, *PLoS One* **2**, e718 (2007).
27. Y. Yang, A. Costa, N. Leonhardt, R. S. Siegel, J. I. Schroeder, *Plant Methods* **4**, 6 (2008).
28. A. Saez *et al.*, *Plant J.* **37**, 354 (2004).
29. N. Leonhardt *et al.*, *Plant Cell* **16**, 596 (2004).
30. N. Nishimura *et al.*, *Plant J.* **50**, 935 (2007).
31. A. Saez *et al.*, *Plant Physiol.* **141**, 1389 (2006).
32. Single-letter abbreviations for the amino acid residues are as follows: A, Ala; C, Cys; D, Asp; E, Glu; F, Phe; G, Gly; H, His; I, Ile; K, Lys; L, Leu; M, Met; N, Asn; P, Pro; Q, Gln; R, Arg; S, Ser; T, Thr; V, Val; W, Trp; and Y, Tyr.
33. B. Meyer, T. Peters, *Angew. Chem. Int. Ed.* **42**, 864 (2003).
34. J.-J. Liu, A. K. M. Ekramoddoullah, *Physiol. Mol. Plant Pathol.* **68**, 3 (2006).
35. N. Robert, S. Merlot, V. N'Guyen, A. Boisson-Dernier, J. I. Schroeder, *FEBS Lett.* **580**, 4691 (2006).
36. F. Gosti *et al.*, *Plant Cell* **11**, 1897 (1999).
37. H. Fujii, J. K. Zhu, *Proc. Natl. Acad. Sci. U.S.A.*, in press; 10.1073/pnas.0903144106.

38. We thank N. Raikhel, J. Bailey-Serres, and C. Larive for comments; K. Nito and T. Demura for materials. Supported by CRC (S.R.C., P.M., D.D.); NSERC (S.R.C., D.D., N.J.P.); NSF awards IOS0820508 (S.R.C.) and MCB0417118 (J.I.S.); NIH awards R01GM060396 (J.I.S.), 01GM59138 (J.-K.Z.), and U54GM074901 (B.V.). S.R.C. thanks J. R. Coleman for early support. Patent application "Control of plant stress tolerance, water use efficiency and gene expression using novel ABA receptor proteins and synthetic agonists" inventors: S. R. Cutler, S. Y. Park, N. Nishimura, J. I. Schroeder, and A. Defries. Author contributions are as follows. Microarrays: P.F. and N.J.P.; pyr1 mutants: P.F.; mutant analyses: P.F. and T.F.C.; yeast two-hybrid assays, biochemistry, and Pyr/Pyl genetics: S.Y.P.; pyr1 complementation and allele sequencing: Y.Z.; in planta pull-downs: N.N. and J.I.S.; PYL12-AHG3 and SnRK2-PP2C interactions: R.F.; HSQC experiments: D.J. and B.V.; SnRK2 assays: H.F. and J.-K.Z.; GFP-PYR1 localization: S.E.A.; PP2C assays: S.Y.P., J.S., A.R., and P.R.; EMS seed: D.B.; ABA orfeome: S.L., D.D., and P.M.; project conception, positional cloning, phone calls, and writing: S.R.C.

Supporting Online Material

www.sciencemag.org/cgi/content/full/1173041/DC1
Materials and Methods
Figs. S1 to S8
Tables S1 and S2
References

27 October 2008; accepted 16 April 2009
Published online 30 April 2009;
10.1126/science.1173041
Include this information when citing this paper.

Understanding the Spreading Patterns of Mobile Phone Viruses

Pu Wang,[1,2] Marta C. González,[1] César A. Hidalgo,[1,2,3] Albert-László Barabási[1,4]*

We modeled the mobility of mobile phone users in order to study the fundamental spreading patterns that characterize a mobile virus outbreak. We find that although Bluetooth viruses can reach all susceptible handsets with time, they spread slowly because of human mobility, offering ample opportunities to deploy antiviral software. In contrast, viruses using multimedia messaging services could infect all users in hours, but currently a phase transition on the underlying call graph limits them to only a small fraction of the susceptible users. These results explain the lack of a major mobile virus breakout so far and predict that once a mobile operating system's market share reaches the phase transition point, viruses will pose a serious threat to mobile communications.

Lacking a standardized operating system, traditional cellphones have been relatively immune to viruses. Smart phones, however, can share programs and data with each other, representing a fertile ground for virus writers (*1*–*4*). Indeed, since 2004 more than 420 smart phone viruses have been identified (*2*, *3*), the newer ones having reached a state of sophistication that took computer viruses about two decades to achieve (*2*). Although smart phones currently represent less than 5% of the mobile market, given their reported fast annual growth rate (*4*) they are poised to become the dominant communication device in the near future, raising the possibility of virus breakouts that could overshadow the disruption caused by traditional computer viruses (*5*).

[1]Center for Complex Network Research, Departments of Physics, Biology, and Computer Science, Northeastern University, Boston, MA 02115, USA. [2]Center for Complex Network Research and Department of Physics, University of Notre Dame, Notre Dame, IN 46556, USA. [3]Center for International Development, Kennedy School of Government, Harvard University, Cambridge, MA 02139, USA. [4]Department of Medicine, Harvard Medical School, and Center for Cancer Systems Biology, Dana Farber Cancer Institute, Boston, MA 02115, USA.

*To whom correspondence should be addressed. E-mail: barabasi@gmail.com

The spread of mobile viruses is aided by two dominant communication protocols. First, a Bluetooth (BT) virus can infect all BT-activated phones within a distance from 10 to 30 m, resulting in a spatially localized spreading pattern similar to the one observed in the case of influenza (*3*, *6*, *7*), severe acute respiratory syndrome (SARS) (*8*, *9*), and other contact-based diseases (Fig. 1A) (*10*). Second, a multimedia messaging system (MMS) virus can send a copy of itself to all mobile phones whose numbers are found in the infected phone's address book, a long-range spreading pattern previously exploited only by computer viruses (*11*, *12*). Thus, in order to quantitatively study the spreading dynamics of mobile viruses we need to simultaneously track the location (*13*), the mobility (*14*–*17*), and the communication patterns (*18*–*21*) of mobile phone users. We achieved this by studying the anonymized billing record of a mobile phone provider and recording the calling patterns and the coordinates of the closest mobile phone tower each time a group of 6.2 million mobile subscribers used their phone. Thus, we do not know the users' precise locations within the tower's reception area, and no information is available about the users between calls.

The methods we used to simulate the spreading of a potential BT and MMS virus are described in (*22*). Briefly, once a phone becomes infected with an MMS virus, within 2 min it sends a copy of itself to each mobile phone number found in the handset's phone book, approximated with the list of numbers with which the handset's user communicated during a month-long observational period. A BT virus can infect only mobile phones within a distance $r = 10$ m. To simulate this process, we assigned to each user an hourly location that was consistent with its travel patterns (*13*) and followed the infection dynamics within each mobile tower area using the susceptible infected (SI) model (*23*). That is, we consider that an infected user (I) infects a susceptible user (S), so that the number of infected users evolves in time (t) as $dI/dt = \beta SI/N$, where the effective infection rate is $\beta = \mu\langle k\rangle$ with $\mu = 1$, N is the number of users in the tower area, and the average number of contacts is $\langle k\rangle = \rho A = NA/A_{\text{tower}}$, where $A = \pi r^2$ represents the BT communication area and $\rho = N/A_{\text{tower}}$ is the population density inside a tower's service area. Once an infected user moves into the vicinity of a new tower, it will serve as a source of a BT infection in its new location.

A cell phone virus can infect only the phones with the operating system (OS) for which it was designed (*2*, *3*), making the market share m of an OS an important free parameter in our study. The current market share of various smart phone OSs vary widely, from as little as 2.6% for Palm OS to 64.3% for Symbian. Given that smart phones together represent less than 5% of all phones, the overall market share of these OSs among all mobile phones is in the range of $m = 0.0013$ for Palm OS and $m = 0.032$ for Symbian, numbers that are expected to dramatically increase as smart phones replace traditional phones. To maintain the generality of our results, we treat m as a free parameter, finding that the spreading of both BT and

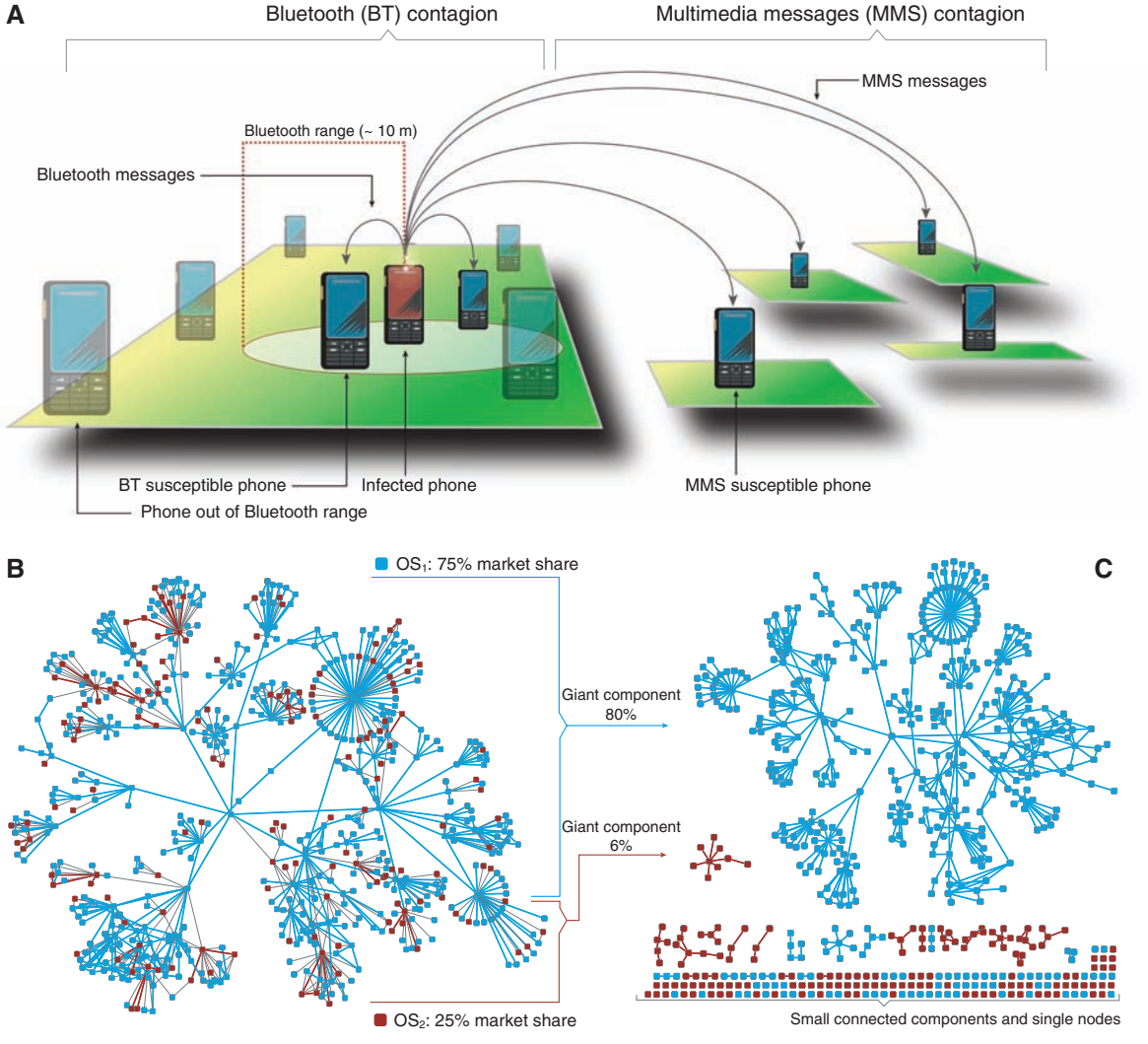

Fig. 1. The spreading mechanisms of mobile viruses. (**A**) A BT virus can infect all phones found within BT range from the infected phone, its spread being determined by the owner's mobility patterns. An MMS virus can infect all susceptible phones whose number is found in the infected phone's phonebook, resulting in a long-range spreading pattern that is independent of the infected phone's physical location. (**B**) A small neighborhood of the call graph constructed starting from a randomly chosen user and including all mobile phone contacts up to four degrees from it. The color of the node represents the handset's OS, which in this example are randomly assigned so that 75% of the nodes represent OS_1, and the red are the remaining handsets with OS_2 (25%). (**C**) The clusters in the call graph on which an MMS virus affecting a given OS can spread, illustrating that an MMS virus can reach at most the number of users that are part of the giant component of the appropriate handset. As the example for the OS shows, the size of the giant component highly depends on the handset's market share (see also Fig. 2C).

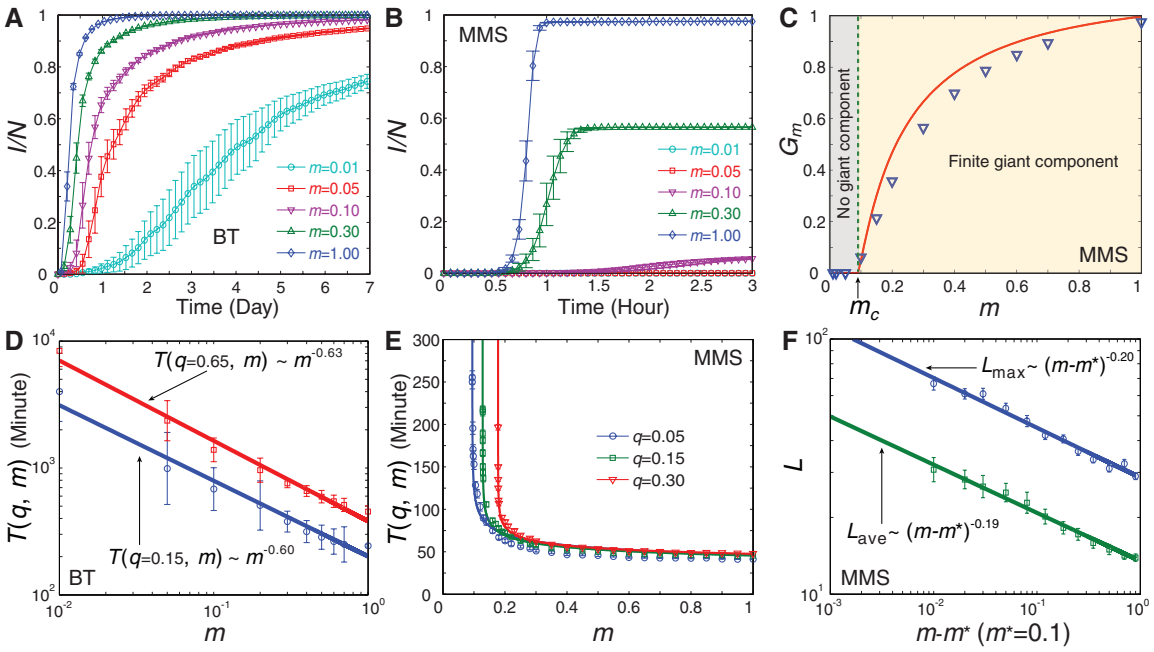

Fig. 2. The spreading patterns of BT and MMS viruses. (**A**) The changes in the ratio of infected and susceptible handsets (I/N) with time in the case of a BT virus affecting handsets with different m. (**B**) Same as in panel (A) but for MMS viruses. The saturation in I/N indicates that an MMS virus can reach only a finite fraction of all susceptible phones. (**C**) The size of the giant component G_m in a function of m. The blue triangles correspond to the saturation values measured in Fig. 2B, whereas the red line is the theoretical prediction according to percolation theory (the deviations are mainly attributed to finite size effects and degree correlations because the calculation assumed an infinite call graph). (**D**) The latency time needed to infect $q = 0.65$ or $q = 0.15$ fraction of susceptible handsets via a BT virus, approximated with $T(q = 0.65, m) \sim m^{-0.63\pm0.05}$ and $T(q = 0.15, m) \sim m^{-0.60\pm0.04}$ (continuous lines). (**E**) The latency time for an MMS virus for $q = 0.05$, 0.15, and 0.30. The continuous lines correspond to $T(q,m) \sim (m - m_q^*)^{-\alpha(q)}$, where the best fits indicate a systematic q-dependence: $\alpha(0.05) = 0.20 \pm 0.02$, $\alpha(0.15) = 0.17 \pm 0.01$, and $\alpha(0.30) = 0.14 \pm 0.01$. (**F**) Log-log plot showing L_{ave} and L_{max} for the largest cluster. The fits correspond to $L_{max} \sim (m - m^*)^{-0.20\pm0.02}$ and $L_{ave} \sim (m - m^*)^{-0.19\pm0.02}$. The curves in (A), (B), and (D) are obtained from 10 independent simulations, and (E) and (F) represent an average over 100 runs. For more statistical analysis of the fits in (D) to (F), see the detailed discussion in (*22*).

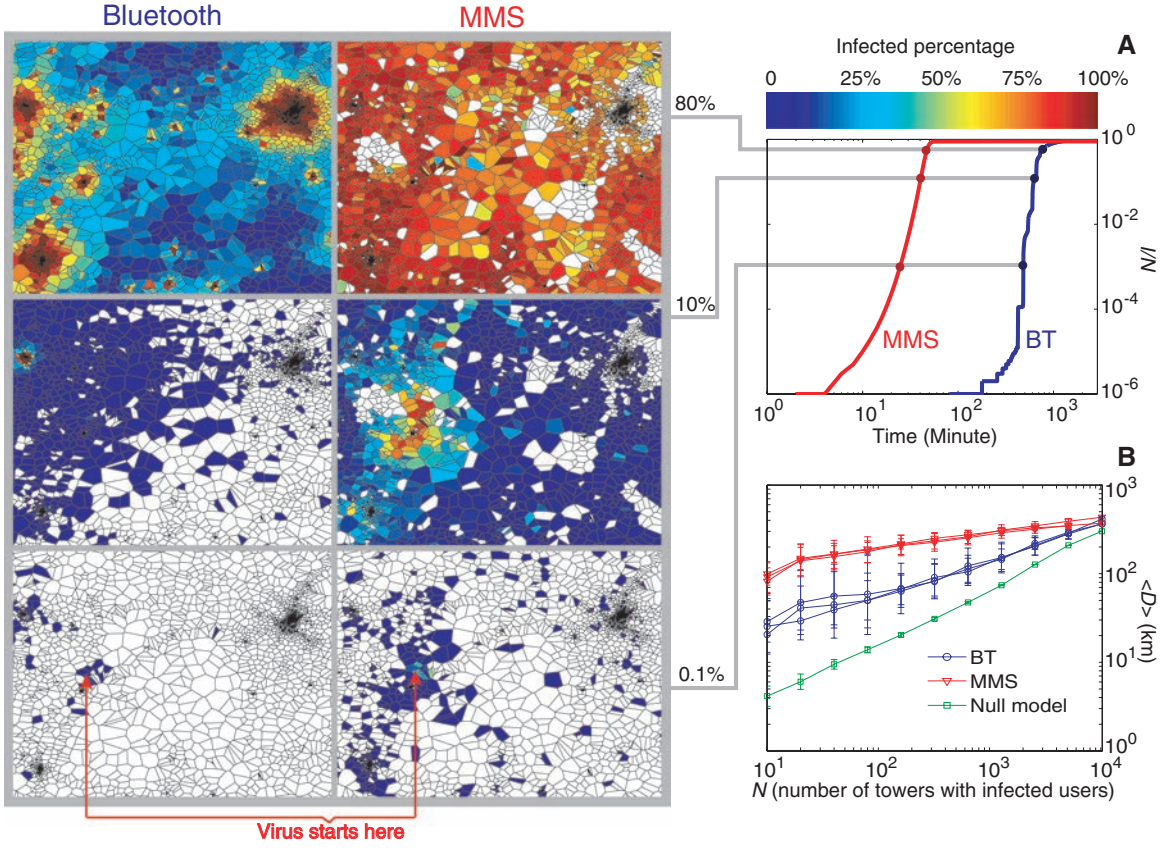

Fig. 3. Spatial patterns in the spread of BT and MMS viruses. (**A**) The virus starts from the same user located at the tower marked by the red arrows (left). The three panels show the percentage of infected users in the vicinity of each mobile phone tower (denoted by the voronoi cell that approximates each tower's service area). In the right panel, we show the corresponding time-dependent infection curves, marking the moments when the spatial distribution was recorded. (**B**) Average distance between the tower where the infection was originally started and the most currently infected phone as a function of N, the number of towers with at least one infected user, used as a proxy of time (three red and blue curves correspond to $m = 0.1$, $m = 0.5$, and $m = 1$). The green line is obtained from a null model that assumes that the virus can only spread from one tower's service area to its neighbor towers' service areas. The curves in (B) are obtained from 100 independent simulations.

MMS viruses is highly sensitive to the market share of the susceptible handsets (Fig. 2, A and B). Our simulations indicate that given sufficient time, a BT virus can reach all susceptible handsets because user mobility guarantees that sooner or later each susceptible handset will find itself in the vicinity of an infected handset. The spreading rate strongly depends, however, on the handset's market share. For example, if the handset's market share is $m = 0.01$ it takes several months for a BT virus to reach all susceptible handsets. In contrast, for $m = 0.30$ the BT virus could infect 85% of susceptible handsets in a few hours and 99.8% in less than a week (Fig. 2A).

The most striking difference between BT and MMS viruses comes in the time scales that their spread requires. Indeed, given that it takes approximately 2 min for a typical MMS virus to copy itself into a new handset (*24*), an MMS epidemic reaches saturation in a few hours, in contrast with the few days that the BT virus requires to infect all susceptible handsets (Fig. 2B). Thus, although there is plenty of time to deploy an antiviral software for a BT virus before it could reach a large fraction of users, it is largely impossible to achieve the same for MMS viruses, given their explosive spread. The good news is that an MMS virus can reach only a small m-dependent fraction of users with a susceptible handset, as indicated by the saturation of the infection curves in Fig. 2B. The origin of this saturation is the fragmentation of the underlying call network. Indeed, in Fig. 1B we show a subset of the real call network and assume for the illustration that the handsets can have only two OSs, OS_1 and OS_2, with market shares $m_1 = 0.75$ and $m_2 = 0.25$, respectively. Although the underlying call network itself is fully connected, the call graph of the users that share the same handset is fragmented into many islands (Fig. 1C). For $m_1 = 0.75$, we observed a giant component (the largest connected cluster) (Fig. 1C) of size $G_m = 0.80$, meaning that it contains 80% of the users with the OS_1 handset; the rest of the OS_1 users are scattered in small isolated clusters. In contrast, for the OS_2 handsets the giant component is tiny ($G_m = 0.06$). If an MMS virus is released from a single handset, it can only reach the handsets in the cluster where the original handset is located, which indicates that an MMS virus can infect at most a G_m fraction of all susceptible handsets, which is 80% for OS_1 and 6% for OS_2 in the example of Fig. 1.

We found that the handset-based fragmentation of the call graph (Fig. 1, B and C) is governed by a percolation phase transition at the market share $m_c = 0.095$ (Fig. 2C) (*25*). That is, for $m < m_c$ the user base is fragmented into many small isolated islands, making a major MMS virus viral outbreak impossible. In contrast, for handsets with $m > m_c$ there is a giant component, allowing the MMS virus to reach all handsets that are part of it. The value of m_c and G_m for $m > m_c$ can be calculated by using the generating function formalism (*26*), requiring as input only the network's degree distribution $P(k)$. With $P(k)$ characterizing our user base, we found a reasonable agreement between the analytical predictions and the direct measurements of the saturation value of the MMS virus spreading in the mobile phone data set (Fig. 2C); the small systematic deviation is rooted in the fact that the generating function formalism ignores the correlations in the call graph's structure. The value of Fig. 2C is its ability to explain why we have not observed a substantial MMS outbreak so far: Currently, the market share of the largest OS is less than $m = 0.03$, well under the predicted percolation transition point $m_c = 0.095$ (*27*, *28*). For a more detailed discussion on the factors affecting m and m_c, see (*22*).

The differences between MMS and BT viruses have a strong impact on their spreading dynamics as well. To see this, we denote the latency time with $T(q,m)$, representing the average time necessary for a virus affecting a handset with market share m to reach a q fraction of all susceptible handsets. For a BT virus, $T(q,m)$ is finite for any q and m combination, given that with time the virus can reach all susceptible users (Fig. 2A). We found, however, that the latency time is highly sensitive to m, a dependency well approximated by $T(q,m) \sim m^{-0.6}$ [coefficient of multiple determination (R^2) > 0.99] (Fig. 2D) (*22*), implying that the smaller a handset's market share the longer a virus will take to reach a q fraction of susceptible users. The observed divergence at $m = 0$ indicates that for handsets with a small market share, the spreading process is exceptionally slow because an infected user takes a very long time to come in contact with another user with a similar handset.

Once again, the behavior of MMS viruses is qualitatively different: We found that $T(q,m)$ di-

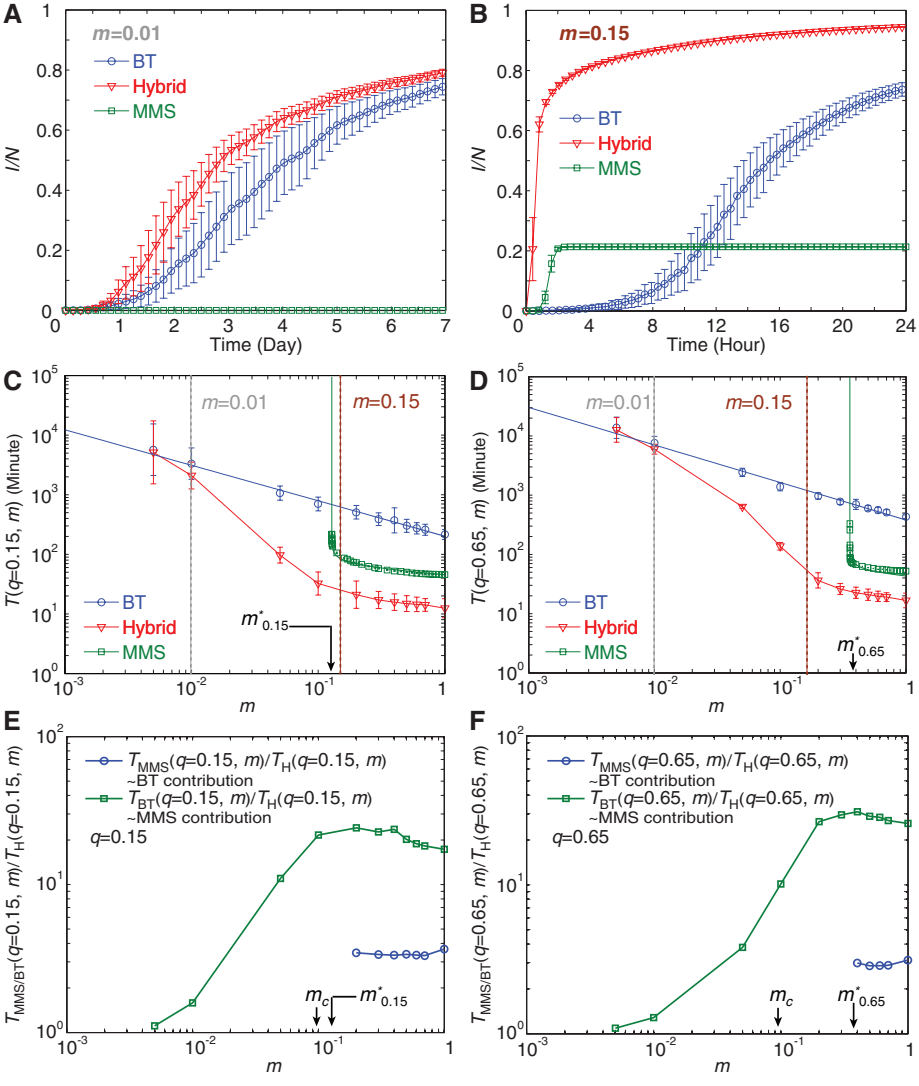

Fig. 4. The spreading patterns of hybrid viruses. (**A** and **B**) The time-dependent fraction of infected users for a hybrid virus spreading on a handset with (A) $m = 0.01$ and (B) $m = 0.15$ market share, compared with the BT and MMS spreading modes. (**C** and **D**) The m-dependence of latency time for hybrid, MMS, and BT viruses for (C) $q = 0.15$ and (D) $q = 0.65$. (**E** and **F**) Ratio between the time it takes a BT or MMS virus to reach (E) 15% and (F) 0.65% of the population divided by the time it takes a hybrid virus to reach the same fraction of the population as a function of m. The curves in (A) to (F) are obtained from 10 independent simulations.

verges not at $m = 0$ but at a finite m_q^* value (Fig. 2E), meaning that for handsets with $m < m_q^*$ the virus is unable to reach a q fraction of users. Indeed, an MMS virus can reach at most a G_m fraction of eligible handsets (Fig. 2C), implying that G_m acts as a critical point for the dynamical spreading process and $T(q > G_m, m) = \infty$. To characterize the observed singularity, the maximum amount of time it takes an MMS virus to invade the giant component should be determined by the length of the longest minimal path (L_{max}) characterizing the susceptible giant cluster (*29*, *30*). As Fig. 2F shows, we found that both L_{max} and the average minimal path length (L_{ave}) diverge as $(m - m^*)^{-\alpha}$ with $\alpha = 0.2$ ($R^2 > 0.97$) (*22*), a singularity that potentially drives the observed divergence of $T(q,m)$ near m_q^* given by the equation $q = G_{m_q}^*$. A more detailed measurement indicates, however, a systematic q-dependence of $\alpha(q)$ in $T(q,m) \sim (m - m_q^*)^{-\alpha(q)}$ in the vicinity of the critical point (Fig. 2E) (*22*), hinting that there are factors beyond L_{max} that contribute to the divergence of $T(q,m)$.

As shown in Fig. 3, we followed the spread of an MMS and BT infection starting from the same user, illustrating that BT and MMS viruses differ in their spatial spreading patterns as well: A BT virus follows a wave-like pattern, predominantly infecting users in the vicinity of the virus's release point, whereas an MMS virus follows a more delocalized pattern, given that the users' address books often contain phone numbers of individuals who are far away. To quantify the observed differences, we measured the average distance between the cell phone tower where the first infected user is located and the location of towers servicing the newly infected users. A null model in which the virus always diffuses to the noninfected towers bordering the already infected towers, thus following a classical two-dimensional diffusion process, was used as a reference. As Fig. 3B indicates, the typical source-infection distances observed in the local model are substantially smaller than the distances recorded for either BT or MMS viruses, indicating the impact of a few long-distance travellers that incubate outbreaks in distant cells (*13*) in the BT spreading process. The average distance is the highest for MMS viruses, underlying the delocalized pattern characterizing its spread. Figure 3B also shows that the dependence of the average source-infection distance ($<D>$) on N is mainly a function of the spreading technology and appears to be independent of m.

BT and MMS viruses have their relative limitations: Although the spread of a BT virus is rather slow because of human mobility, an MMS virus can reach only a small fraction of users because of the fragmentation of the call graph. Both limitations are avoided by hybrid viruses that can simultaneously use both BT and MMS connections to spread; the first of many such viruses was the "CommWarrior," released in 2005 (*2*, *3*). We found, however, that the spreading dynamics of a hybrid virus also displays a complex market share dependence (Fig. 4, A and B), resulting from a nontrivial superposition of the BT and MMS spreading modes. For example, for $m = 0.15$, when there is a giant component aiding the MMS spreading mode (Fig. 2C), the early stage of the spreading process is dominated by the rapid invasion of the MMS cluster. Subsequently, the BT mechanism allows the virus to invade the rest of the independent MMS clusters as well. For $m = 0.01$, however, there is no MMS giant component; thus, the spreading is dominated entirely by the BT capability, resulting in a substantially slower spreading pattern (see the different horizontal axes in Fig. 4, A and B).

The relative role of the BT and the MMS spreading patterns for hybrid viruses is illustrated in Fig. 4, C and D, which shows the latency time $T(q,m)$ for $q = 0.15$ and $q = 0.65$. We find that for high m, the MMS mechanism dominates the hybrid virus's spreading pattern. As m decreases below m_q^* given by $q = G_{m_q}^*$ (Fig. 2E), the giant component becomes smaller than q, so $T(q,m)$ for MMS diverges (green curve) and the BT mechanism starts dominating the spreading rate of a hybrid virus. Therefore, for small values of m the latency time of the hybrid virus converges to the latency time of a BT virus. We found, however, that the phase transition that governs the fragmentation of the call graph plays a key role in the spread of hybrid viruses as well, delimiting the rapid MMS-dominated and slow human mobility–driven spreading modes.

As shown in Fig. 4, E and F, we explored the additional infective power of a hybrid (H) virus, defined as the ratio $T_{MMS}(q,m)/T_H(q,m)$ relative to its pure MMS counterpart or $T_{BT}(q,m)/T_H(q,m)$ relative to its pure BT counterpart. We found that hybrid viruses are about three times faster than an MMS virus at a constant market share for $m > m_c$. The contribution of BT technology for a hybrid virus dominates for $m \leq m_c$ because MMS viruses are unable to spread in this region [$T_{MMS}(q,m) = \infty$]. The additional infective power of a hybrid virus as compared with a BT virus achieves its highest value close to m_q^*, decreasing quickly for $m \to 0$ and mildly for $m \to 1$, once again underlying the importance of the critical behavior near m_q^*.

Taken together, our results offer a comprehensive picture of the potential dangers posed by mobile viruses. We found that although a BT virus can reach the full susceptible user base, its spread is constrained by human mobility, offering ample time for developing and deploying countermeasures. In contrast, MMS viruses can reach most susceptible users within hours. Their spread is limited, however, by the market share–driven phase transition that fragments the underlying call graph, which allows us to predict that no major virus breakout is expected for OSs with market shares under the critical point associated with the user base. Therefore, the current lack of a major mobile virus outbreak cannot be attributed to the absence of effective mobile viruses, but is mainly rooted in the fragmentation of the call graph. Given, however, the rapid growth in the number of smart phones and the increasing market share of a few OSs, it is not inconcievable that the phase transition point will be reached in the near future, raising the possibility of major viral outbreaks. Although the greatest danger is posed by hybrid viruses that take advantage of both BT and MMS protocols, we found that their spread is also limited by the phase transition: Hybrid viruses designed for OSs with small market shares are forced into the slow BT spreading mode, offering time to develop proper countermeasures. We believe that the understanding of the basic spreading patterns presented here could help estimate the realistic risks carried by mobile viruses and aid in the development of proper measures so as to avoid the costly impact of future outbreaks.

References and Notes

1. J. Kleinberg, *Nature* **449**, 287 (2007).
2. A. Shevchenko, "An overview of mobile device security"; available at www.viruslist.com/en/analysis?pubid=170773606 (2005).
3. M. Hypponen, *Sci. Am.* **295**, 70 (2006).
4. J. Cheng, S. Wong, H. Yang, S. Lu, *Proc. 5th ACM Int. Conf. Mob. Syst. Appl. Serv.* (ACM, New York, 2007).
5. D. F. Zucker, M. Uematsu, T. Kamada, *Proc. XTech 2005* May (2005), pp. 25–27.
6. V. Colizza, A. Barrat, M. Barthelemy, A.-J. Valleron, A. Vespignani, *PLoS Med.* **4**, 95 (2007).
7. S. Riley, *Science* **316**, 1298 (2007).
8. R. M. Anderson *et al.*, *Philos. Trans. R. Soc. London Ser. B* **359**, 1091 (2004).
9. L. Hufnagel, D. Brockmann, T. Geisel, *Proc. Natl. Acad. Sci. U.S.A.* **101**, 15124 (2004).
10. S. Eubank *et al.*, *Nature* **429**, 180 (2004).
11. J. Balthrop, S. Forrest, M. E. J. Newman, M. M. Williamson, *Science* **304**, 527 (2004).
12. R. Pastor-Satorras, A. Vespignani, *Phys. Rev. Lett.* **86**, 3200 (2001).
13. M. C. González, C. A. Hidalgo, A.-L. Barabási, *Nature* **453**, 779 (2008).
14. D. Brockmann, L. Hufnagel, T. Geisel, *Nature* **439**, 462 (2006).
15. J. Su *et al.*, *Proc. 5th ACM Workshop Rapid Malcode* (ACM, New York, 2006), pp. 9–16.
16. G. Yan *et al.*, *Proc. 2nd ACM Symposium on Information, Computer and Communications Security* (ACM, New York, 2007).
17. J. W. Mickens, B. D. Nobel, *Proc. ACM Workshop Wireless Security* (ACM, New York, 2005), pp. 77–86.
18. J.-P. Onnela *et al.*, *Proc. Natl. Acad. Sci. U.S.A.* **104**, 7332 (2007).
19. C. A. Hidalgo, C. Rodriguez-Sickert, *Physica A* **387**, 3017 (2008).
20. R. Lambiotte *et al.*, *Physica A* **387**, 5317 (2008).
21. G. Palla, A.-L. Barabási, T. Vicsek, *Nature* **446**, 664 (2007).
22. Materials and methods are available as supporting material on *Science* Online.
23. R. M. Andersen, R. M. May, *Infectious Diseases of Humans: Dynamics and Control* (Oxford Univ. Press, New York, 1992).
24. A. Bose, K. G. Shin, *SecureComm* (SecureComm and Workshops, Baltimore, MD, 2006), pp. 1–10.
25. S. N. Dorogovtsev, J. F. F. Mendes, *Phys. Rev. E Stat. Nonlin. Soft Matter Phys.* **64**, 025101 (2001).
26. D. S. Callaway, M. E. J. Newman, S. H. Strogatz, D. J. Watts, *Phys. Rev. Lett.* **85**, 5468 (2000).
27. R. Cohen, K. Erez, D. ben-Avraham, S. Havlin, *Phys. Rev. Lett.* **85**, 4626 (2000).
28. A. Bunde, S. Havlin, Eds., *Physica A* **266** (1999).
29. Y. Chen *et al.*, *Phys. Rev. E Stat. Nonlin. Soft Matter Phys.* **75**, 046107 (2007).
30. G. Caldarelli, *Scale-Free Networks: Complex Webs in Nature and Technology* (Oxford Univ. Press, New York, 2007).
31. The human mobility data that were used as a basis for the simulations relied on an anonymized billing data set that was previously recorded by a mobile provider as required by law and for billing purposes and not for the purpose of this project. We thank D. Brockmann,

M. Hypponen, J. Park, Z. Qu, C. Song, A. Vazquez, A. Vespignani, and G. Xiao for discussions and comments on the manuscript. We also thank M. Hypponen for providing us the valuable mobile phone virus records data. This work was supported by the James S. McDonnell Foundation 21st Century Initiative in Studying Complex Systems; NSF within the Dynamic Data Driven Applications Systems (CNS-0540348), Information Technology Research (DMR-0426737), and IIS-0513650 programs; the Defense Threat Reduction Agency Award HDTRA1-08-1-0027; and the U.S. Office of Naval Research Award N00014-07-C.

Supporting Online Material
www.sciencemag.org/cgi/content/full/1167053/DC1
Materials and Methods
Figs. S1 to S8
Tables S1 to S3
References

10 October 2008; accepted 24 March 2009
Published online 2 April 2009;
10.1126/science.1167053
Include this information when citing this paper.

ATP-Citrate Lyase Links Cellular Metabolism to Histone Acetylation

Kathryn E. Wellen,* Georgia Hatzivassiliou,*† Uma M. Sachdeva, Thi V. Bui, Justin R. Cross, Craig B. Thompson‡

Histone acetylation in single-cell eukaryotes relies on acetyl coenzyme A (acetyl-CoA) synthetase enzymes that use acetate to produce acetyl-CoA. Metazoans, however, use glucose as their main carbon source and have exposure only to low concentrations of extracellular acetate. We have shown that histone acetylation in mammalian cells is dependent on adenosine triphosphate (ATP)–citrate lyase (ACL), the enzyme that converts glucose-derived citrate into acetyl-CoA. We found that ACL is required for increases in histone acetylation in response to growth factor stimulation and during differentiation, and that glucose availability can affect histone acetylation in an ACL-dependent manner. Together, these findings suggest that ACL activity is required to link growth factor–induced increases in nutrient metabolism to the regulation of histone acetylation and gene expression.

The accessibility of DNA in eukaryotic cells is determined by its organization in a DNA-protein complex known as chromatin. Chromatin structure is regulated in part through dynamic modifications of the constituent proteins, primarily histones. Histone acetylation has critical roles in regulating global chromatin architecture and gene transcription (*1*–*3*). Acetylation of histones can provide binding sites for proteins containing bromodomains, alter chromatin subnuclear localization and structure, and neutralize histone positive charge, which may loosen interactions between histones and DNA (*2*, *4*–*6*). Histone acetylation can be dynamically regulated by several classes of histone deacetylases (HDACs) and families of histone acetyltransferases (HATs), which act both on targeted regions of chromatin to regulate specific gene transcription and in a more global manner (*1*, *3*, *7*).

Studies of the nicotinamide adenine dinucleotide (NAD^+)–dependent sirtuins (class III HDACs), which target both histone and nonhistone proteins, have demonstrated that deacetylation is responsive to metabolic cues (*8*–*12*). Sirtuins are dependent on NAD^+ hydrolysis for their deacetylase activity, and their activity is sensitive to changes in the intracellular NAD^+/NADH ratio. HATs have not been shown to be regulated by the bioenergetic status of the cell, but production of acetyl-CoA by the enzyme acetyl-CoA synthetase (Acs2p), which generates acetyl-CoA from acetate, is linked to the regulation of histone acetylation in the yeast *Saccharomyces cerevisiae* (*13*). This enzyme is itself regulated in a nutrient-responsive manner, and it is activated by sirtuin-dependent deacetylation (*14*). Although mammalian cells contain a homolog to Acs2p, AceCS1, which synthesizes acetyl-CoA from acetate and is also regulated by sirtuins (*15*), most mammalian cells do not use acetate as a major bioenergetic substrate. Rather, the major carbon source in mammalian cells is glucose. Acetyl-CoA can be produced from glucose by the enzyme adenosine triphosphate (ATP)–citrate lyase (ACL), which generates acetyl-CoA from mitochondria-derived citrate. ACL-dependent production of acetyl-CoA for lipogenesis is important for the proliferation of glycolytically converted tumor cells (*16*).

In yeast, Acs2p localizes to both the cytoplasm and the nucleus, suggesting that acetyl-CoA is produced in both compartments in this organism (*13*). Using deconvolution microscopy to image enhanced green fluorescent protein (EGFP)–tagged ACL, we detected EGFP-ACL in the nucleus, in addition to the cytoplasm, in two different mammalian cell lines (Fig. 1A and fig. S1A). Similar results were obtained with myc-tagged ACL in murine FL5.12 hematopoietic cells (fig. S1B). Subcellular fractionation of HCT116 human colon carcinoma cells confirmed the presence of endogenous ACL in the nucleus as well as the cytoplasm (Fig. 1B). AceCS1 was largely cytoplasmic in HCT116 cells, with a small but significant amount of protein detected in the nuclear fractions (Fig. 1B). Because both citrate and acetate are small molecules able to diffuse freely through the nuclear pore complex (*17*), these data suggest

Department of Cancer Biology, Abramson Family Cancer Research Institute, University of Pennsylvania, Philadelphia, PA 19104, USA.

*These authors contributed equally to this work.
†Present address: Genentech Inc., South San Francisco, CA 94080, USA.
‡To whom correspondence should be addressed. E-mail: craig@mail.med.upenn.edu

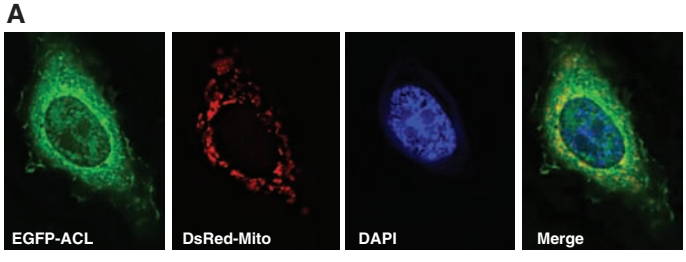

Fig. 1. ACL localizes to the nucleus and cytoplasm. (**A**) Subcellular localization of EGFP-tagged ACL in LN229 cells imaged by deconvolution microscopy. EGFP-ACL, visible in both nucleus and cytoplasm, is contrasted to DsRed mitochondrial marker, which is excluded from the nucleus. DAPI (4′,6′-diamidino-2-phenylindole) staining of nuclear DNA is restricted to the nucleus. (**B**) Western blot analysis of cytoplasmic and nuclear protein extracts from HCT116 cells. Quantitation represents mean ± SD from four (ACL and AceCS1) or eight [poly(ADP-ribose) polymerase (PARP) and tubulin] nuclear and cytoplasmic samples. ACL and AceCS1 are both significantly (***, $P < 0.0001$) enriched in the nuclear fraction as compared with tubulin.

that acetyl-CoA production may occur in both the cytoplasmic and nuclear compartments in mammalian cells.

To investigate whether ACL or AceCS1 is important for the maintenance of global histone acetylation in mammalian cells, we analyzed global histone acetylation after small interfering RNA (siRNA)–mediated silencing of ACL, AceCS1, or both. Silencing of ACL significantly decreased the amount of histone acetylation for all core histones assessed (Fig. 2A). In contrast, suppression of AceCS1 had less of an effect on net histone acetylation, and the reduction failed to reach statistical significance (Fig. 2A). In the absence of physiologic ACL levels, incubation of cells with supraphysiologic levels of acetate, the substrate used by AceCS1, rescued histone acetylation in a dose-dependent and AceCS1-dependent manner (Fig. 2, A and B). Thus, ACL is a major source of acetyl-CoA for global histone acetylation under normal growth conditions in HCT116 cells, but AceCS1 also participates and can compensate for loss of ACL function when its substrate is available.

We next sought to determine whether ACL-dependent production of acetyl-CoA selectively affects acetylation of histones or has equivalent effects on the acetylation of other cellular proteins. Upon DNA damage, p53 K^{382} acetylation is catalyzed by p300 and may increase the ability of p53 to bind DNA and perform its functions as a transactivator (*18*). We assessed the efficiency of p53 acetylation in response to treatment with the DNA-damaging agent doxorubicin and found that acetylation of p53 K^{382} was unaffected by silencing of ACL (Fig. 2C). Thus, high ACL activity is not a general requirement for cellular acetylation events, and acetylation of histones might be specifically linked to the pool of citrate-derived acetyl-CoA produced by ACL. Further investigation will be required to ascertain the relative contributions of different acetyl-CoA sources to acetylation of nonhistone cellular proteins.

Net histone acetylation represents a balance between rates of acetylation and deacetylation catalyzed by HATs and HDACs, respectively. We therefore investigated whether the decrease in global histone acetylation observed upon silencing of ACL could be rescued by inhibition of HDACs. Treatment of cells with the HDAC inhibitor trichostatin A (TSA) suppressed the effects of ACL deficiency on histone acetylation (Fig. 2D). Thus, in the absence of substantial histone deacetylation, ACL activity has less impact on the net acetylation of the core histones.

To better evaluate the scale of the histone acetylation defects observed upon ACL suppression, we compared the relative decrease in histone acetylation upon siRNA silencing of ACL to that upon silencing of GCN5, a HAT with an important role in the maintenance of global histone acetylation (*19*, *20*). Under these conditions, suppression of either ACL or GCN5 led to a statistically significant reduction in the acetylation of histones H2B, H3, and H4 (Fig. 2E and fig. S2). Suppression of both ACL and GCN5 did not lead to additive inhibition of the acetylation of the histones examined, suggesting that the two enzymes may function within the same pathway to regulate chromatin structure. Differences between the effects of silencing ACL and GCN5 may reflect the involvement of other HATs and production of acetyl-CoA by AceCS1. Acetylation of tubulin was unaffected by silencing of either GCN5 or ACL, again emphasizing that production of acetyl-CoA by ACL is not a general requirement for cellular protein acetylation (Fig. 2E).

Regulation of histone acetylation levels may depend on both the cell type and the state of cellular differentiation or activation (*21*–*26*). For example, we observed that apoptosis-deficient cells subjected to extended growth factor withdrawal exhibited low levels of histone acetylation that progressively increased upon growth factor add-back, correlating with increasing protein levels of ACL (fig. S3A). We thus examined the effect of ACL silencing on two cellular processes associated with changes in global histone acetylation: mitogenic stimulation of quiescent cells and adipocyte differentiation.

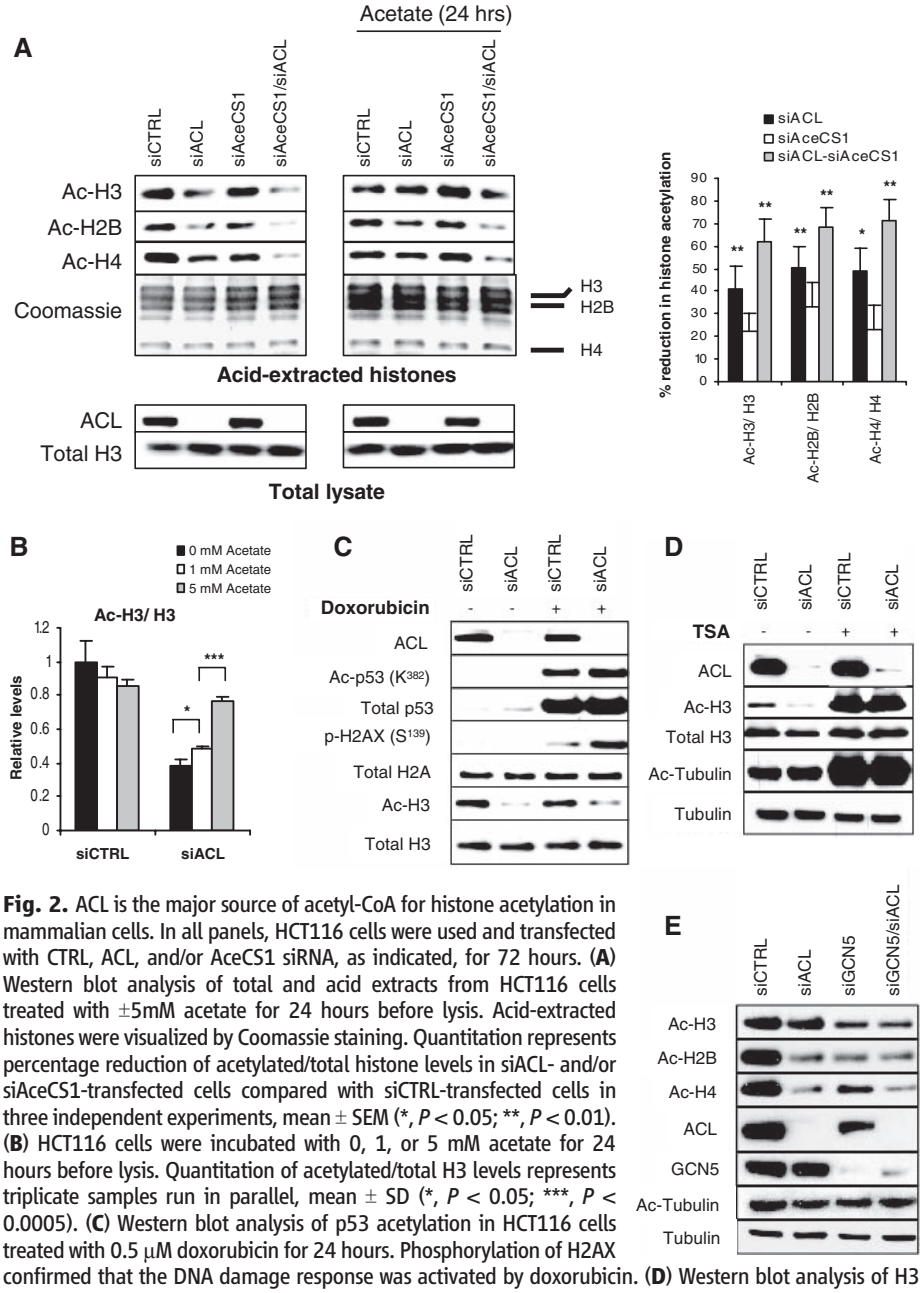

Fig. 2. ACL is the major source of acetyl-CoA for histone acetylation in mammalian cells. In all panels, HCT116 cells were used and transfected with CTRL, ACL, and/or AceCS1 siRNA, as indicated, for 72 hours. (**A**) Western blot analysis of total and acid extracts from HCT116 cells treated with ±5mM acetate for 24 hours before lysis. Acid-extracted histones were visualized by Coomassie staining. Quantitation represents percentage reduction of acetylated/total histone levels in siACL- and/or siAceCS1-transfected cells compared with siCTRL-transfected cells in three independent experiments, mean ± SEM (*, $P < 0.05$; **, $P < 0.01$). (**B**) HCT116 cells were incubated with 0, 1, or 5 mM acetate for 24 hours before lysis. Quantitation of acetylated/total H3 levels represents triplicate samples run in parallel, mean ± SD (*, $P < 0.05$; ***, $P < 0.0005$). (**C**) Western blot analysis of p53 acetylation in HCT116 cells treated with 0.5 μM doxorubicin for 24 hours. Phosphorylation of H2AX confirmed that the DNA damage response was activated by doxorubicin. (**D**) Western blot analysis of H3 and tubulin acetylation in HCT116 cells treated with 500 nM trichostatin A (TSA) for 24 hours. (**E**) Western blot analysis of histone acetylation in total extracts of HCT116 cells transfected for 72 hours with CTRL, ACL, and/or GCN5 siRNAs. Results are representative of four independent experiments. For quantitation, see fig. S2.

Acetylation of histones is regulated in a cell cycle–dependent manner and can contribute to normal cell cycle progression (*27*–*29*). Serum starvation followed by reintroduction can synchronize cells within a population by inducing them to collectively exit and re-enter the cell cycle (*30*). This mitogenic stimulation is accompanied by a net increase in histone acetylation, as cells enter and progress through *S* phase (*24*). We assessed the ability of cells to induce histone acetylation in response to mitogenic stimulation in immortalized mouse embryo fibroblasts (MEFs). In control cells, acetylation of histone H3 increased after serum stimulation, and silencing of ACL inhibited this response (Fig. 3A). Levels of acetylated tubulin were unaffected by ACL suppression. To assess whether this ACL-dependent increase in histone acetylation could be regulated by glucose availability, serum stimulation was repeated in the presence or absence of glucose. Indeed, serum-induced changes in histone acetylation were dependent on glucose and failed to occur in the absence of ACL (Fig. 3, B and C). Under glucose deprivation conditions, cells can use fatty acid oxidation to support their bioenergetic needs. However, fatty acid oxidation results in the production of mitochondrial but not nucleocytoplasmic acetyl-CoA. Consistent with this, supplementation of glucose-starved cells with fatty acids failed to rescue histone acetylation, supporting the model that only nucleocytoplasmic acetyl-CoA is available to participate in histone acetylation (fig. S3B). Reduced histone acetylation after silencing of ACL was also observed during proliferation of MEFs in culture (fig. S3C), which suggests that ACL is also involved in maintaining histone acetylation during proliferative expansion, even when sufficient acetyl-CoA is present to support cell growth.

Histone acetylation increases have also been observed during differentiation of murine 3T3-L1 preadipocytes into adipocytes (*25*). Silencing of ACL reduced histone acetylation in adipocytes, whereas suppression of AceCS1 had little effect (Fig. 4A). Tubulin acetylation was unchanged upon silencing of either ACL or AceCS1 (Fig. 4a). In addition, the increase in histone acetylation observed during adipocyte differentiation was almost entirely suppressed upon ACL silencing and could be rescued by acetate in a dose-dependent manner, which suggests that AceCS1 can compensate in this model, depending on acetate availability (Fig. 4B).

We next sought to determine whether ACL silencing specifically affected differentiation-induced histone acetylation or whether it more broadly impaired the ability of the cell to implement the differentiation program. Using Oil Red O staining to assess differentiation-induced lipid accumulation, we observed that cells depleted of ACL contained visibly less lipid than control cells, whereas silencing of AceCS1 had minimal effects on lipid accumulation (Fig. 4C). Lipid accumulation in ACL-deficient cells, however, could be partially rescued by incubation of cells with acetate (fig. S4A), which suggests that the reduced lipid accumulation was primarily due to low availability of acetyl-CoA rather than impaired differentiation and that, in the absence of supraphysiological acetate, acetyl-CoA is derived mainly from citrate in adipocytes.

These observations raised the possibility that ACL-dependent changes in histone acetylation are required for adipocytes to take up and metabolize the amounts of glucose needed to engage in fat storage. Transcriptional profiling in yeast has previously indicated that a reduction in global histone acetylation as a result of GCN5 deficiency results in altered expression of multiple carbohydrate metabolism genes (*31*). Therefore, we examined whether the expression of genes involved in glucose uptake and metabolism was affected in cells in which ACL is silenced. We found that expression of the insulin-responsive glucose transporter, Glut4, as well as three key regulators of glycolysis, hexokinase 2 (HK2), phosphofructokinase-1 (PFK-1), and lactate dehydrogenase A (LDH-A), were all significantly suppressed upon ACL silencing and rescued by acetate (Fig. 4D). These transcriptional effects correlated well with cellular glycolytic activity; ACL silencing resulted in a 32% decrease in glucose consumption ($P < 0.001$), which was reversed by acetate supplementation. In addition, expression of genes involved in conversion of glucose into nonessential amino acids and fatty acids, including soluble glutamate oxaloacetate transaminase (Got1) and carbohydrate responsive element-building protein (ChREBP), were similarly regulated (Fig. 4D). These effects on glucose metabolism genes appeared to be selective, since the HAT GCN5, as well as markers of adipocyte differentiation such as aP2, were not

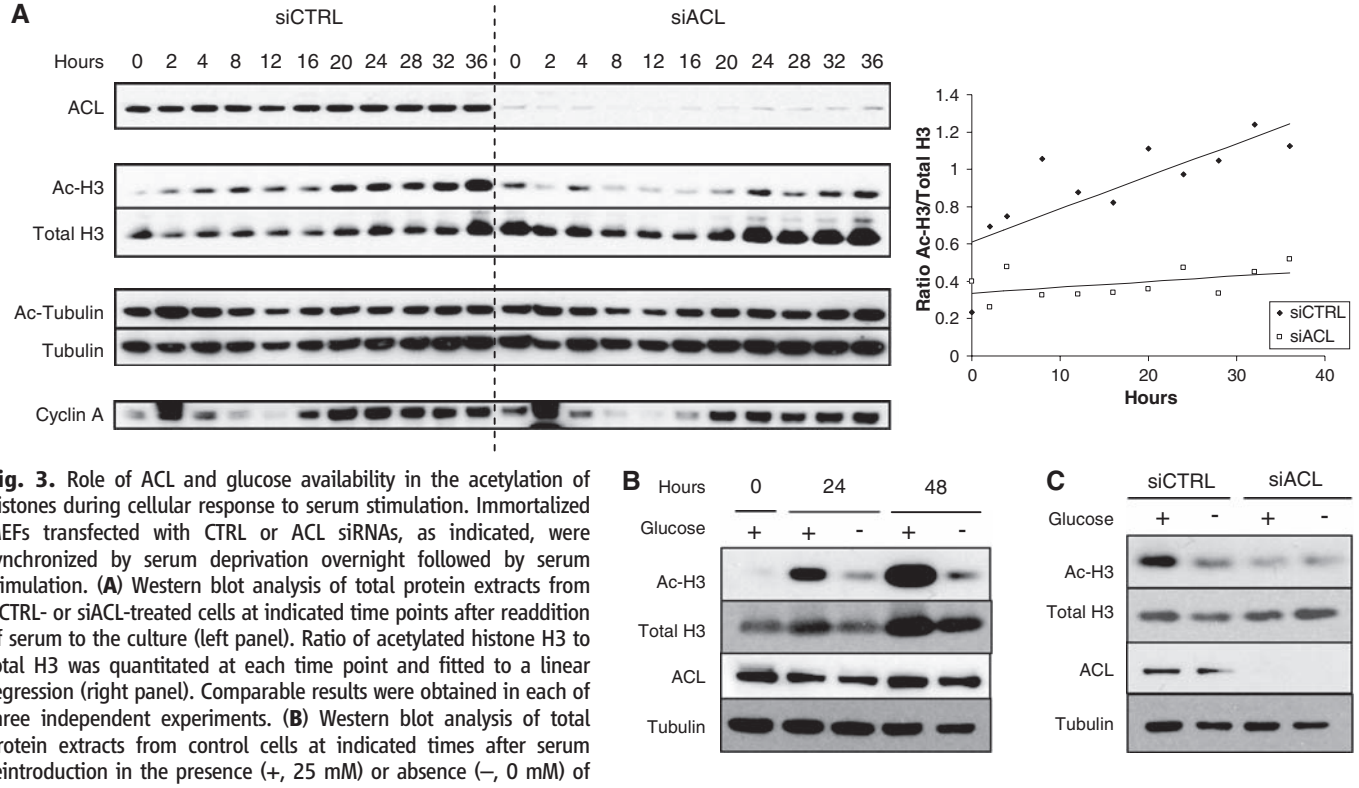

Fig. 3. Role of ACL and glucose availability in the acetylation of histones during cellular response to serum stimulation. Immortalized MEFs transfected with CTRL or ACL siRNAs, as indicated, were synchronized by serum deprivation overnight followed by serum stimulation. (**A**) Western blot analysis of total protein extracts from siCTRL- or siACL-treated cells at indicated time points after readdition of serum to the culture (left panel). Ratio of acetylated histone H3 to total H3 was quantitated at each time point and fitted to a linear regression (right panel). Comparable results were obtained in each of three independent experiments. (**B**) Western blot analysis of total protein extracts from control cells at indicated times after serum reintroduction in the presence (+, 25 mM) or absence (–, 0 mM) of glucose. (**C**) Western blot analysis of total protein extracts from cells transfected with siCTRL or siACL, as described in (*33*) and cultured for 48 hours in the presence or absence of glucose.

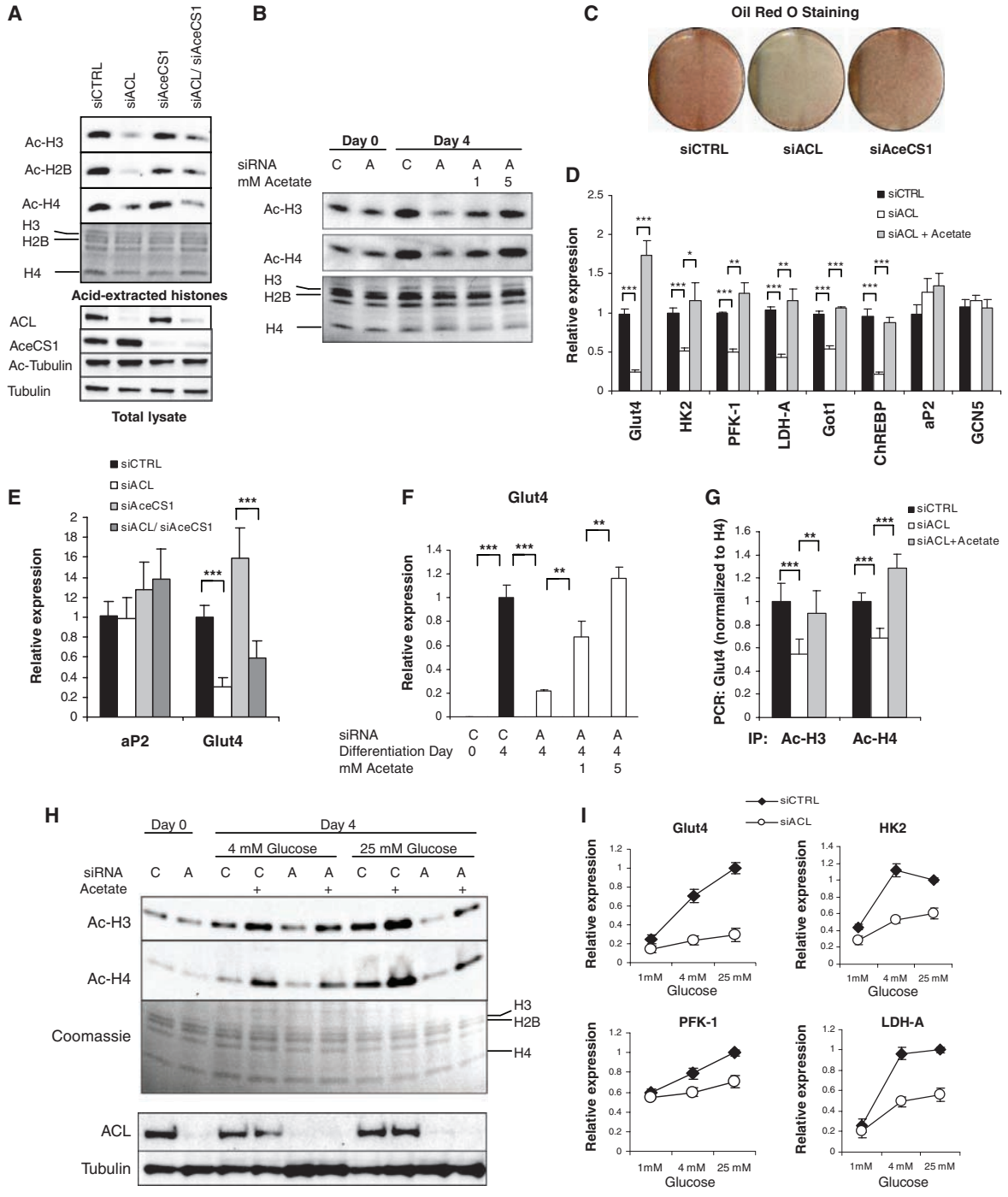

Fig. 4. Regulation of acetylation of histones during adipocyte differentiation by ACL and nutrient availability. 3T3-L1 preadipocytes were transfected with control, ACL, and/or AceCS1 siRNAs and 2 days later stimulated to differentiate into adipocytes. (**A**) Total lysates and acid extracts from 3T3-L1 cells 4 days after induction of differentiation, analyzed by Western blot. (**B**) Acid extracts from 0 and 4 days after induction of differentiation in the presence of 0, 1, or 5 mM sodium acetate were analyzed by Western blot. (**C**) Cells were fixed and Oil Red O lipid staining was performed 5 days after induction of differentiation. Similar results were obtained in each of three independent experiments. (**D**) RNA was isolated 4 days after induction of differentiation in the presence or absence of 5 mM sodium acetate. Gene expression was analyzed by quantitative reverse transcription polymerase chain reaction (RT-PCR) and normalized to 18*S* ribosomal RNA (rRNA) (mean ± SD of triplicate samples). (**E**) Gene expression 4 days after induction of differentiation was quantified by Taqman quantitative RT-PCR and normalized to 18*S* rRNA. Data represent triplicate wells from two independent experiments, mean ± SD. (**F**) RNA was isolated 4 days after induction of differentiation in the presence of 0, 1, or 5 mM sodium acetate. Glut4 expression was analyzed by Taqman RT-PCR and normalized to 18*S* rRNA (mean ± SD of triplicate samples). (**G**) Chromatin immunoprecipitation was performed using antibodies to Ac-H3 and Ac-H4. Immunoprecipitated Glut4 promoter sequence was analyzed by quantitative PCR. H4 genomic sequence was used as an endogenous control. The amount of immunoprecipitated H4 DNA was unchanged upon ACL silencing. Data represent mean ± SD of triplicate samples from each of two independent experiments. (**H**) Western blots of cells differentiated 0 or 4 days in 4 or 25 mM glucose, ±5 mM sodium acetate. (**I**) Gene expression in cells 4 days after induction of differentiation in 1, 4, or 25 mM glucose was assessed by Taqman quantitative RT-PCR and normalized to 18*S* rRNA. Data are the averages of three independent experiments (mean ± SEM). All statistical analyses are comparisons of two data sets and were performed using *t* tests (*, $P < 0.05$; **, $P < 0.005$; ***, $P < 0.0005$). C, siCTRL; A, siACL.

regulated upon either ACL suppression or acetate supplementation (Fig. 4D).

Glut4 expression was selected for further examination because it is a well-characterized determinant of adipocyte glucose consumption. The reduction in Glut4 expression was specific for ACL silencing and was not observed upon silencing of AceCS1 (Fig. 4E). Notably, other differentiation markers including aP2, adiponectin, and fatty acid synthase were expressed at equal or higher levels upon silencing of either ACL or AceCS1, indicating that the adipogenic program is successfully initiated without physiologic levels of ACL or AceCS1 (Fig. 4E and fig. S4B). Upon silencing of ACL, Glut4 expression could be rescued in a dose-dependent manner by acetate supplementation (Fig. 4F), in concert with total histone acetylation levels (Fig. 4B). Furthermore, chromatin immunoprecipitation experiments revealed that acetylation of histones H3 and H4 at the Glut4 promoter was specifically reduced upon ACL silencing and could be rescued by acetate (Fig. 4G).

We next investigated whether the regulation of histone acetylation and Glut4 expression by ACL in differentiating adipocytes is nutrient-dependent by exposing the cells to various concentrations of glucose during differentiation. Standard medium for adipocyte differentiation contains 25 mM glucose, but 3T3-L1 cells can also differentiate at lower concentrations of glucose, although they accumulate lower amounts of lipid (*32*). We differentiated adipocytes in 1, 4, and 25 mM glucose and observed that they accumulated increasing amounts of lipid when exposed to higher levels of glucose, correlating with increasing Glut4 expression (fig. S4, C and D). Cells exposed to either 4 or 25 mM glucose exhibited similar increases in expression of the differentiation marker aP2, whereas 1 mM glucose resulted in lower levels of aP2 gene expression (fig. S4, C and D).

Histone acetylation was regulated during differentiation in a nutrient-dependent manner, increasing according to both glucose and acetate availability (fig. S4E). Glucose-dependent regulation of histone acetylation was dependent on ACL, whereas supraphysiologic concentrations of acetate increased histone acetylation in the presence or absence of ACL (Fig. 4H). Similarly, the expression of Glut4 and the glycolytic genes HK2, PFK-1, and LDH-A were regulated according to glucose availability, in an ACL-dependent manner (Fig. 4I). These results demonstrate that, during adipocyte differentiation, global histone acetylation is determined by glucose availability through an ACL-dependent pathway and that supraphysiologic levels of acetate can also contribute through AceCS1. Our data also suggest that nutrient-responsive histone acetylation may selectively affect the expression of genes required to reprogram intracellular metabolism to use glucose for ATP production and macromolecular synthesis.

We have demonstrated that ACL plays a critical role in determining the total amount of histone acetylation in multiple mammalian cell types. ACL-dependent production of acetyl-CoA contributes to increased histone acetylation during cellular response to growth factor stimulation and during adipocyte differentiation, both energy-intensive processes in which nuclear activity needs to be coordinated with cellular metabolic state. ACL-dependent acetylation can also contribute to the selective regulation of genes involved in glucose metabolism. Our data indicate that ACL activity is required to link growth factor–induced nutrient uptake and metabolism to the regulation of histone acetylation. Thus, it appears that histone acetylation can be dynamically regulated by physiologic changes in concentrations of acetyl-CoA produced by ACL. Our results also suggest that the current model for metabolic regulation of histone acetylation should be expanded to include not only redox regulation of deacetylases but also regulation of HATs by physiologic changes in the generation of acetyl-CoA.

References and Notes

1. S. K. Kurdistani, M. Grunstein, *Nat. Rev. Mol. Cell Biol.* **4**, 276 (2003).
2. B. Li, M. Carey, J. L. Workman, *Cell* **128**, 707 (2007).
3. D. E. Sterner, S. L. Berger, *Microbiol. Mol. Biol. Rev.* **64**, 435 (2000).
4. C. R. Brown, C. J. Kennedy, V. A. Delmar, D. J. Forbes, P. A. Silver, *Genes Dev.* **22**, 627 (2008).
5. A. L. Clayton, C. A. Hazzalin, L. C. Mahadevan, *Mol. Cell* **23**, 289 (2006).
6. R. Schneider, R. Grosschedl, *Genes Dev.* **21**, 3027 (2007).
7. M. A. Glozak, E. Seto, *Oncogene* **26**, 5420 (2007).
8. H. Y. Cohen *et al.*, *Science* **305**, 390 (2004).
9. S. J. Lin, L. Guarente, *Curr. Opin. Cell Biol.* **15**, 241 (2003).
10. B. Schwer, E. Verdin, *Cell Metab.* **7**, 104 (2008).
11. H. Yang *et al.*, *Cell* **130**, 1095 (2007).
12. A. Vaquero, R. Sternglanz, D. Reinberg, *Oncogene* **26**, 5505 (2007).
13. H. Takahashi, J. M. McCaffery, R. A. Irizarry, J. D. Boeke, *Mol. Cell* **23**, 207 (2006).
14. V. J. Starai, I. Celic, R. N. Cole, J. D. Boeke, J. C. Escalante-Semerena, *Science* **298**, 2390 (2002).
15. W. C. Hallows, S. Lee, J. M. Denu, *Proc. Natl. Acad. Sci. U.S.A.* **103**, 10230 (2006).
16. G. Hatzivassiliou *et al.*, *Cancer Cell* **8**, 311 (2005).
17. P. L. Paine, L. C. Moore, S. B. Horowitz, *Nature* **254**, 109 (1975).
18. A. M. Bode, Z. Dong, *Nat. Rev. Cancer* **4**, 793 (2004).
19. P. S. Knoepfler *et al.*, *EMBO J.* **25**, 2723 (2006).
20. Z. Nagy, L. Tora, *Oncogene* **26**, 5341 (2007).
21. K. L. Rice, I. Hormaeche, J. D. Licht, *Oncogene* **26**, 6697 (2007).
22. A. S. Alberts, O. Geneste, R. Treisman, *Cell* **92**, 475 (1998).
23. J. M. Sun, H. Y. Chen, J. R. Davie, *J. Biol. Chem.* **276**, 49435 (2001).
24. O. Knosp, H. Talasz, B. Puschendorf, *Mol. Cell. Biochem.* **101**, 51 (1991).
25. E. J. Yoo, J. J. Chung, S. S. Choe, K. H. Kim, J. B. Kim, *J. Biol. Chem.* **281**, 6608 (2006).
26. V. Shukla, T. Vaissiere, Z. Herceg, *Mutat. Res.* **637**, 1 (2008).
27. W. Zhang, J. R. Bone, D. G. Edmondson, B. M. Turner, S. Y. Roth, *EMBO J.* **17**, 3155 (1998).
28. P. C. Megee, B. A. Morgan, M. M. Smith, *Genes Dev.* **9**, 1716 (1995).
29. R. E. Sobel, R. G. Cook, C. A. Perry, A. T. Annunziato, C. D. Allis, *Proc. Natl. Acad. Sci. U.S.A.* **92**, 1237 (1995).
30. C. B. Thompson, P. B. Challoner, P. E. Neiman, M. Groudine, *Nature* **319**, 374 (1986).
31. A. Johnsson, Y. Xue-Franzen, M. Lundin, A. P. Wright, *Eukaryot. Cell* **5**, 1337 (2006).
32. Y. Lin *et al.*, *J. Biol. Chem.* **280**, 4617 (2005).
33. Materials and methods are available as supporting material on *Science* Online.

34. We thank members of the Thompson laboratory for helpful comments and discussion and A. Stout for assistance with the deconvolution microscopy. Supported by grants to C.B.T. from NIH and the National Cancer Institute. K.E.W. is a Damon Runyon Fellow supported by the Damon Runyon Cancer Research Foundation, DRG-1955-07. U.M.S. is supported in part by a training grant from NIH, T32-HL07439-27.

Supporting Online Material

www.sciencemag.org/cgi/content/full/324/5930/1076/DC1
Materials and Methods
Figs. S1 to S4
References

1 August 2008; accepted 2 April 2009
10.1126/science.1164097

Phasic Firing in Dopaminergic Neurons Is Sufficient for Behavioral Conditioning

Hsing-Chen Tsai,[1,2]* Feng Zhang,[2]* Antoine Adamantidis,[3] Garret D. Stuber,[4] Antonello Bonci,[4] Luis de Lecea,[3] Karl Deisseroth[2,3]†

Natural rewards and drugs of abuse can alter dopamine signaling, and ventral tegmental area (VTA) dopaminergic neurons are known to fire action potentials tonically or phasically under different behavioral conditions. However, without technology to control specific neurons with appropriate temporal precision in freely behaving mammals, the causal role of these action potential patterns in driving behavioral changes has been unclear. We used optogenetic tools to selectively stimulate VTA dopaminergic neuron action potential firing in freely behaving mammals. We found that phasic activation of these neurons was sufficient to drive behavioral conditioning and elicited dopamine transients with magnitudes not achieved by longer, lower-frequency spiking. These results demonstrate that phasic dopaminergic activity is sufficient to mediate mammalian behavioral conditioning.

Dopaminergic (DA) neurons have been suggested to be involved in the cognitive and hedonic underpinnings of motivated behaviors (*1*–*4*). Changes in the firing pattern of DA neurons between low-frequency tonic activity and phasic bursts of action potentials could encode reward prediction errors and incentive salience (*5*). Consistent with the reward prediction-error hypothesis, DA neuron firing activity is depressed by aversive stimuli (*6*).

However, it remains unclear whether DA neuron activation alone is sufficient to elicit reward-related behaviors. Lesion, electrical stimulation, and psychopharmacology studies have been important but have not allowed causal and temporally precise control of DA neurons in freely moving mammals; for example, electrical stimulation inevitably activates multiple classes of neurons within heterogeneous brain tissue, and pharmacological stimulation does not allow delivery of defined patterns of DA neuron spikes in vivo.

To control DA neurons selectively, we used a Cre-inducible adeno-associated virus (AAV) vector (*7*, *8*) carrying the gene encoding the light-activated cation channel channelrhodopsin-2 (ChR2) in-frame fused to enhanced yellow fluorescent protein (ChR2-EYFP) (*9*–*11*). To ensure that there would be no substantial expression leak in nontargeted cell types, we designed the Cre-inducible AAV vector with a double-floxed inverted open reading frame (ORF), wherein the ChR2-EYFP sequence is present in the antisense orientation (Fig. 1A). Stereotactic delivery of this vector into the VTA of tyrosine hydroxylase (TH):: internal ribosomal entry site (IRES)–Cre transgenic mice enables DA neuron-specific expression of ChR2-EYFP. Upon transduction, Cre-expressing TH cells invert the ChR2-EYFP ORF in irreversible fashion and thereby activate sustained ChR2-EYFP expression under the strong, constitutively active elongation factor 1α (EF-1α) promoter.

We validated the specificity and efficacy of this targeting strategy in vivo. In coronal VTA sections of transduced TH::IRES-Cre brains, ChR2-EYFP specifically co-localized with endogenous TH (Fig. 1B). Greater than 90% of TH-immunopositive cells were positive for ChR2-EYFP near virus injection sites, and more than 50% were positive overall, demonstrating highly efficacious transduction of the TH cells. Of ChR2-EYFP–expressing cells, 98.3 ± 0.5% were co-labeled by TH staining (Fig. 1C), demonstrating high specificity. Expression was stable and persistent for at least 2 months, and ChR2-EYFP–expressing neurons displayed robust projections; EYFP-positive fibers richly innervated local neurons in downstream nucleus accumbens (NAc) (Fig. 1D) (*12*).

To assess the potential for optogenetic control of transduced cells, we used whole-cell patch clamps to measure light-induced membrane currents in ChR2-expressing DA neurons (Fig. 2A). ChR2-EYFP–expressing cells in the VTA displayed typical electrophysiological properties of DA neurons with a mean resting membrane potential of –56.0 ± 1.8 mV and a mean membrane resistance of 372.3 ± 19.3 megohm (n = 10 cells), consistent with previously reported values for VTA DA neurons (*13*) and indicating that expression of ChR2 alone does not affect their basic physiology. Under blue light (473 nm) illumination, all patched cells exhibited prominent inward photocurrents (Fig. 2, B and C; n = 10 cells). Trains of light flashes drove action potential firing in ChR2-EYFP neurons; with use of low- and high-frequency light trains, we evoked tonic and phasic DA neuron firing, respectively (Fig. 2D). DA neurons typically do not maintain high-frequency spiking (*14*); 1- to 5-Hz light pulses drove long DA neuron spike trains reliably, whereas bursting at 20 Hz or greater for prolonged trains evoked action potentials in <50% of light pulses (Fig. 2E and fig. S1; bursts maintaining the >15-Hz spiking characteristic of phasic firing could be elicited simply by using higher-frequency light pulse trains). Optrode recording confirmed that optical stimulation of VTA DA neurons in vivo evoked broad spike waveforms consistent with extracellular waveforms for VTA DA neurons (*6*) (Fig. 2F and fig. S2).

We next tested the behavioral conditioning effects of phasic DA neuron activity via the conditioned place preference (CPP) paradigm (Fig. 3A and fig. S3), with use of phasic optogenetic stimulation (*15*) of DA neurons as our conditioning stimuli (Fig. 3, B and C). As a control, we paired the opposite chamber with the same number of light pulses delivered instead at 1 Hz. Mice were subjected to 2 days of conditioning, and conditioned preference was determined by comparing time spent in each chamber of the apparatus. In the first round of experiments, mice received phasic (50-Hz optical stimulation) conditioning in one chamber on the first day of conditioning (day 2), and 1-Hz optical stimulation in the other chamber on the second day of conditioning (day 3); two cohorts of mice were used with the chamber-stimulation pairing reversed to control for spontaneous preference shifts (fig. S3). Mice developed a clear place

[1]Neuroscience Program, W080 Clark Center, 318 Campus Drive West, Stanford University, Stanford, CA 94305, USA. [2]Department of Bioengineering, W083 Clark Center, 318 Campus Drive West, Stanford University, Stanford, CA 94305, USA. [3]Department of Psychiatry and Behavioral Sciences, W083 Clark Center, 318 Campus Drive West, Stanford University, Stanford, CA 94305, USA. [4]Ernest Gallo Clinic and Research Center, Department of Neurology, Wheeler Center for the Neurobiology of Drug Addiction, University of California San Francisco, San Francisco, CA 94158, USA.

*These authors contributed equally to this work.
†To whom correspondence should be addressed. E-mail: deissero@stanford.edu

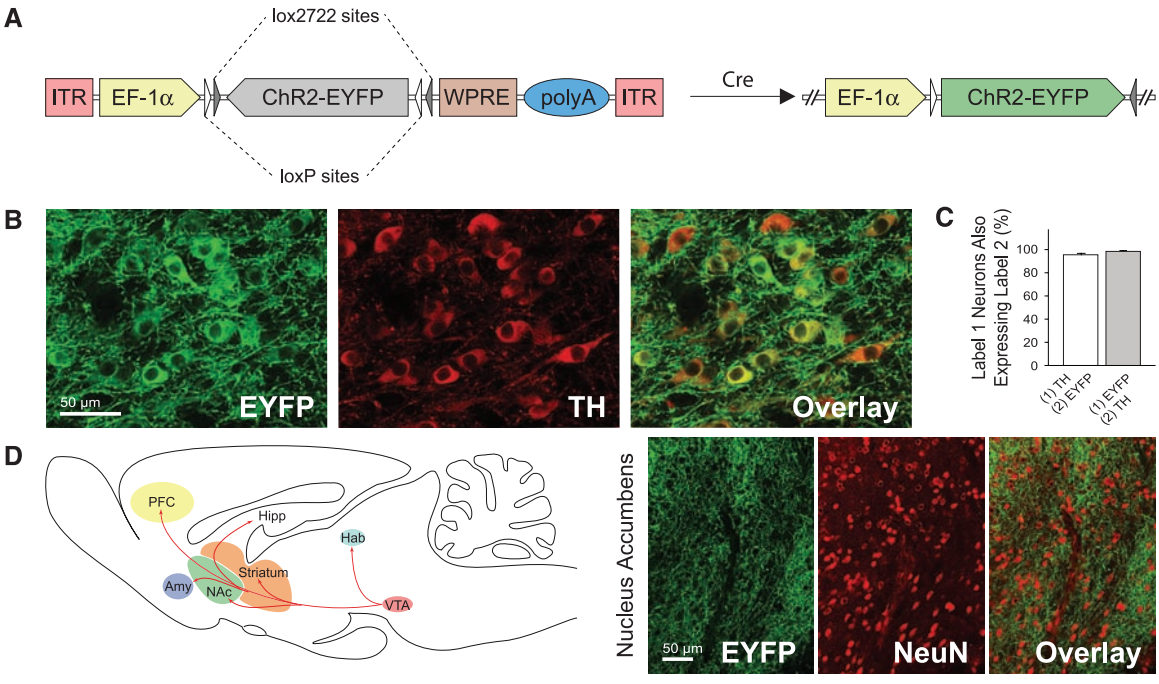

Fig. 1. Specific ChR2 expression in DA neurons. (**A**) Schematic of the Cre-dependent AAV; the gene of interest is doubly flanked by two sets of incompatible lox sites. Upon delivery into TH::IRES-Cre transgenics, ChR2-EYFP is inverted to enable transcription from the EF-1α promoter. (**B**) Confocal images showing cell-specific ChR2-EYFP expression (green) in TH neurons (red). (**C**) Statistics of expression in TH neurons (n = 491); error bars represent SEM throughout. (**D**) Labeled VTA DA neurons project to downstream brain regions; confocal images of ChR2-EYFP–positive axons (green) innervating target neurons in NAc (NeuN, red).

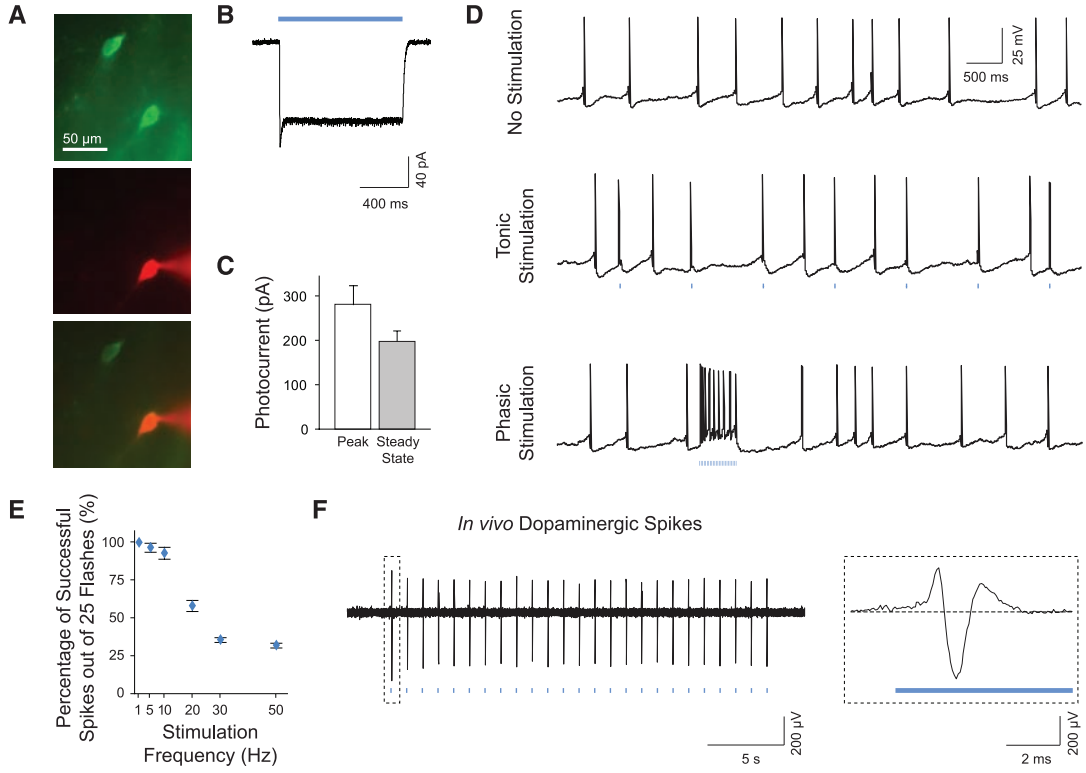

Fig. 2. Photoactivation of DA neurons in intact tissue. (**A**) Recording from transduced neurons in acute VTA slices. Recorded neurons are verified by intracellular dye loading (ChR2-EYFP, green; AlexaFluor 594, red). (**B**) Continuous blue light (473 nm) evokes inward photocurrents. (**C**) Summary of photocurrent properties (n = 10). (**D**) Whole-cell recording of DA neurons showing spontaneous activity and tonic and phasic firing evoked by 1-Hz and 50-Hz light flash trains, respectively (25 flashes, 15 ms per flash). (**E**) Light-evoked spike trains are reliable over a range of frequencies; percentage of action potentials evoked by 25 light flashes at indicated frequencies (1 to 50 Hz) is shown (n = 7). (**F**) In vivo optrode recording of VTA DA neurons in a transduced TH::IRES-Cre anesthetized mouse showing light-evoked DA spikes; see fig. S2. (Inset) Typical triphasic DA extracellular spike.

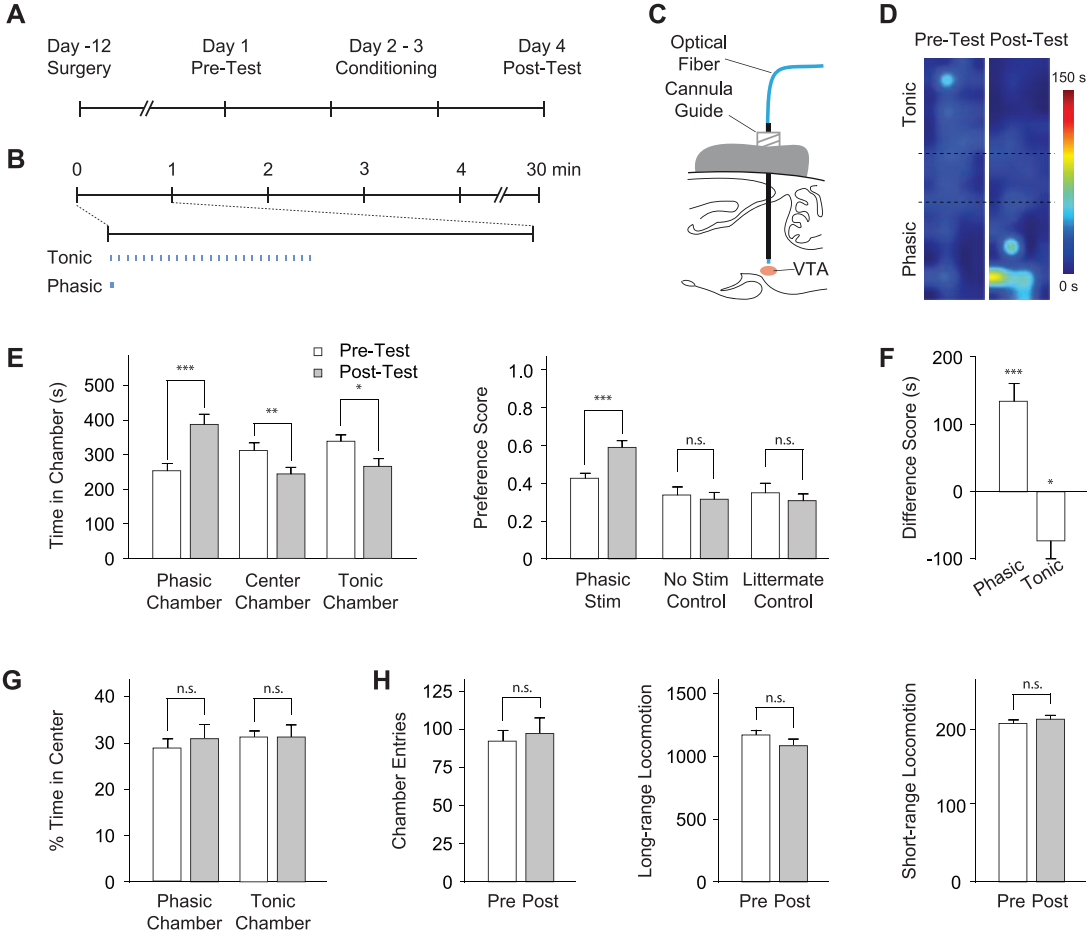

Fig. 3. Photoactivation of DA neurons induces place preference. (**A**) CPP timeline (see also fig. S3). (**B**) Light delivery parameters; 25 flashes at 1 or 50 Hz were delivered with a periodicity of 1 min. (**C**) Optical fiber is inserted through a cannula guide implanted over the VTA to photoactivate DA neurons. (**D**) Representative density maps showing conditioned preference; pseudocolor represents duration at each position. (**E**) Conditioning effect of DA neuron modulation. (Left) Comparison of time in each chamber during pretest (white) and posttest (gray). (Right) Comparison of preference scores for experimental (Phasic Stim, n = 13) and control cohorts (No Stim Control, n = 9; Littermate Control, n = 9). n.s. indicates not significant, $^{*}P < 0.05$, $^{**}P < 0.01$, and $^{***}P < 0.001$. (**F**) Difference scores (calculated as the difference between time spent during pre- and posttest in the specified chamber) for each chamber shows a statistically significant shift in place preference. (**G**) Analysis of anxiety (fractional time in center of a chamber; n = 13). (**H**) Chamber entries, long-range locomotion (different sequential beam breaks), and short-range locomotion (repeated break of the same beam) during pre- and posttest (n = 13).

preference for the chamber associated with phasic optical stimulation by several measures (Fig. 3, D to F; $P < 0.001$ by Student's t test; $n = 13$ mice), and both cohorts of mice exhibited this conditioned preference independent of chamber pairing (fig. S5).

We performed two classes of control experiments to validate the results. First, nontransgenic littermates ($n = 9$) were injected with Cre-dependent ChR2-EYFP AAV and subjected to the same stimulation paradigm as the experimental animals. Separately, TH::IRES-Cre transgenic mice ($n = 9$) were injected with Cre-dependent ChR2-EYFP AAV but received no optical stimulation during conditioning to further control for spontaneous preference shifts. Neither control group showed a significant CPP (Fig. 3E right, $P > 0.5$ by Student's t test). Furthermore, we did not find any significant changes in anxiety-related behaviors (Fig. 3G) or in locomotor activity (Fig. 3H) during preference tests and in open field tests (fig. S6).

Next, we tested whether the CPP effect observed was due to an appetitive effect from 50-Hz stimulation or to an aversive effect from 1-Hz stimulation. We compared the effect of each firing modality with no stimulation in two independent cohorts. Consistent with the previous CPP experiments (Fig. 3, E and F), the phasic cohort displayed significant place preference for the stimulation chamber after conditioning (Fig. 4, A and C), from 251 ± 28 s during pretest to 522 ± 63s during posttest ($n = 7$ mice; $P < 0.05$, Student's t test). However, the 1-Hz cohort ($n = 6$) showed no place aversion for the 1-Hz stimulation chamber (showing a trend toward place preference for 1 Hz instead; Fig. 4, B and C). We hypothesized that the CPP effect observed for the phasic cohort could be due to larger transient DA release triggered by the 50-Hz optical stimulation. We therefore used in vivo fast-scan cyclic voltammetry (FSCV) (*16*, *17*) to detect DA transients. Maintaining the optical fiber in the VTA, we implanted a carbon fiber electrode for measuring DA signals in the NAc, one of the major targets of VTA DA projections (Fig. 1D). Despite sharing the same total illumination duration and number of light flashes (25 15-ms light flashes at 1 Hz or 50 Hz), the 50-Hz light train elicited larger DA transients (Fig. 4, D and E). Indeed, the mean peak DA transient concentrations in the NAc were measured at 75.9 ± 24.5 nM and 1.3 ± 0.8 nM, respectively, for the 50-Hz and 1-Hz stimuli (Fig. 4E); the former is similar to the magnitude of natural reward-triggered dopamine transients (*16*), whereas DA accumulation during chronic 1-Hz stimulation remained much lower (fig. S7; this level of DA could still theoretically contribute to behavioral changes).

Rodents learn to associate the effects of stimuli with their environment and subsequently display a conditioned place preference for that environment (*18*). Previous studies have demonstrated the important role of DA in the processing of salient signals (*19*) and goal-directed behaviors (*20*). However, it has been unclear whether other circuits and neurotransmitter systems are required at the same time (*21*) and whether specific patterns of activity in distinct neuron types are sufficient to effect place preference. To enable direct testing of the role of phasic DA neuron firing on behavioral conditioning, we developed a versatile Cre-inducible gene expression system to decouple the strength of transgene expression from cell type–specific promoters (which are often too weak to drive functional expression of opsins). By using this system, we selectively modulated DA neuron activity with defined stimulation patterns in the CPP paradigm and found that phasic stimulation suf-

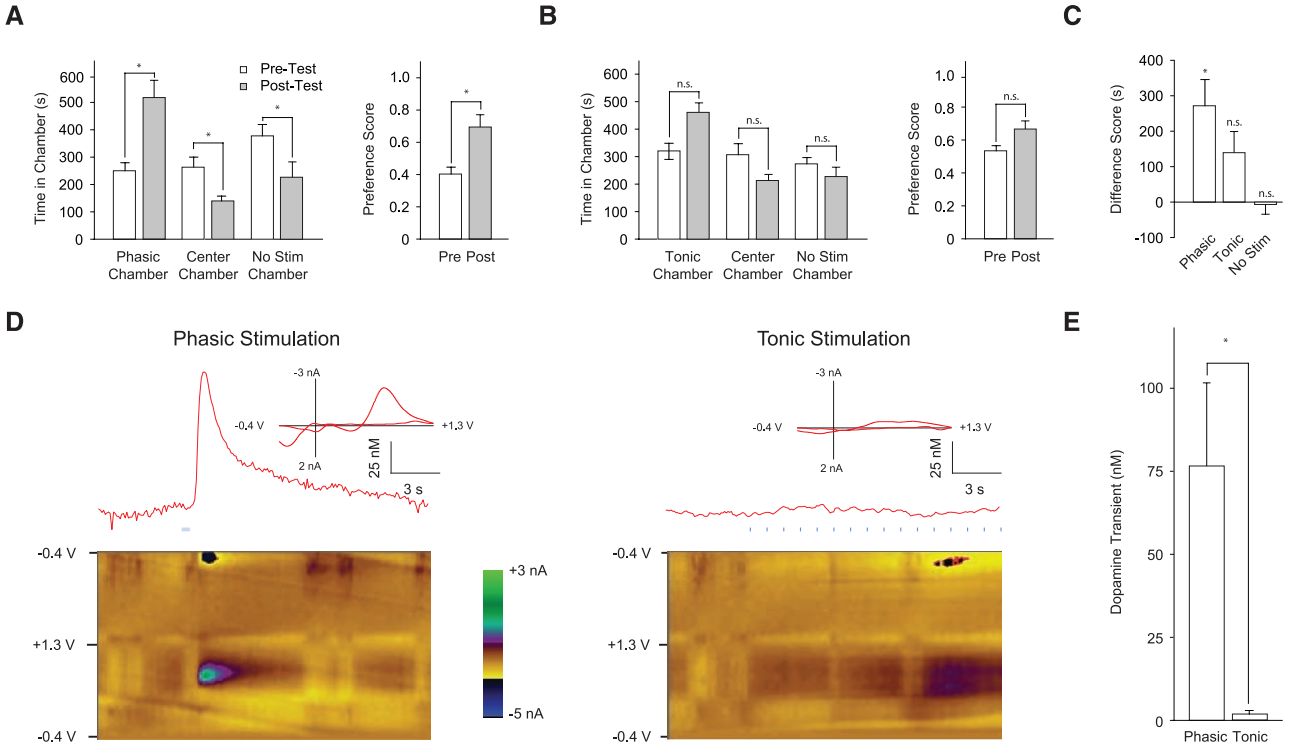

Fig. 4. Phasic DA neuron stimulation leads to transient DA release and place preference. (**A** and **B**) Effect of phasic (50 Hz) (A) and tonic (1 Hz) (B) stimulation on place preference. (Left) Time spent in each chamber during preference test. (Right) Comparison of preference scores; for A, $n = 7$, and for B, $n = 6$. *$P < 0.05$. (**C**) Relative effects of stimulation frequency examined by using the difference scores for phasic, tonic, and nonassociative control (same as No Stim in Fig. 3E) cohorts. (**D**) FSCV measurements of VTA stimulation–triggered transient DA release in NAc in anesthetized TH::IRES-Cre mice. (Top) Representative voltammetry traces during phasic (25 flashes per 50 Hz) and tonic (16 flashes per 1 Hz) stimulation of VTA. (Insets) Background-subtracted voltammogram taken from the peak of stimulation, indicating that signal measured is DA on the basis of comparison to voltammograms of DA obtained in vitro. (Bottom) All background-subtracted voltammograms recorded over the 20-s interval. y axis is applied potential (E_{apps} versus Ag/AgCl reference electrode); x axis is the time at which each voltammogram was recorded. Current changes at the electrode are encoded in color. DA can be seen during stimulation at the feature ~0.650 V (oxidation peak encoded as green) and between ~−0.20 V and ~−0.25 V at the end of the voltage scan. (**E**) Comparison of phasic and tonic light-evoked DA transients ($n = 3$).

ficed to establish place preference in the absence of other reward. These results establish a causal role in behavioral conditioning for defined spiking modes in a specific cell type; of course, even a single cell type can release multiple neurotransmitters and neuromodulators (for example, VTA DA neurons primarily release DA but can also release other neurotransmitters such as glutamate) and will exert effects through multiple distinct downstream cell types. Indeed, the optogenetic approach, integrated with electrophysiological, behavioral, and electrochemical readout methods, opens the door to exploring the causal, temporally precise, and behaviorally relevant interactions of DA neurons with other neuromodulatory circuits (*22*–*25*), including monoaminergic and opioid circuits important in neuropsychiatric illnesses (*26*–*28*). In the process of identifying candidate interacting neurotransmitter systems, downstream neural circuit effectors (*29*), and subcellular biochemical mechanisms on time scales appropriate to behavior and relevant circuit dynamics, it will be important to continue to leverage the specificity and temporal precision of optogenetic control (*30*).

References and Notes

1. R. A. Wise, *Nat. Rev. Neurosci.* **5**, 483 (2004).
2. B. J. Everitt, T. W. Robbins, *Nat. Neurosci.* **8**, 1481 (2005).
3. T. E. Robinson, K. C. Berridge, *Brain Res. Brain Res. Rev.* **18**, 247 (1993).
4. G. F. Koob, M. Le Moal, *Science* **278**, 52 (1997).
5. W. Schultz, *Annu. Rev. Neurosci.* **30**, 259 (2007).
6. M. A. Ungless, P. J. Magill, J. P. Bolam, *Science* **303**, 2040 (2004).
7. F. Zhang, Larry C. Katz Memorial Lecture presented at the Cold Spring Harbor Laboratory Meeting on Neuronal Circuits, Cold Spring Harbor, NY, 13 to 16 March 2008.
8. D. Atasoy, Y. Aponte, H. H. Su, S. M. Sternson, *J. Neurosci.* **28**, 7025 (2008).
9. E. S. Boyden, F. Zhang, E. Bamberg, G. Nagel, K. Deisseroth, *Nat. Neurosci.* **8**, 1263 (2005).
10. G. Nagel *et al*., *Proc. Natl. Acad. Sci. U.S.A.* **100**, 13940 (2003).
11. Materials and methods are available as supporting material on *Science* Online.
12. A. Bjorklund, S. B. Dunnett, *Trends Neurosci.* **30**, 194 (2007).
13. Q. S. Liu, L. Pu, M. M. Poo, *Nature* **437**, 1027 (2005).
14. S. Robinson, D. M. Smith, S. J. Mizumori, R. D. Palmiter, *Proc. Natl. Acad. Sci. U.S.A.* **101**, 13329 (2004).
15. A. R. Adamantidis, F. Zhang, A. M. Aravanis, K. Deisseroth, L. de Lecea, *Nature* **450**, 420 (2007).
16. P. E. Phillips, G. D. Stuber, M. L. Heien, R. M. Wightman, R. M. Carelli, *Nature* **422**, 614 (2003).
17. G. D. Stuber *et al*., *Science* **321**, 1690 (2008).
18. T. M. Tzschentke, *Addict. Biol.* **12**, 227 (2007).
19. C. M. Cannon, R. D. Palmiter, *J. Neurosci.* **23**, 10827 (2003).
20. A. A. Grace, S. B. Floresco, Y. Goto, D. J. Lodge, *Trends Neurosci.* **30**, 220 (2007).
21. T. S. Hnasko, B. N. Sotak, R. D. Palmiter, *J. Neurosci.* **27**, 12484 (2007).
22. P. W. Kalivas, *Am. J. Addict.* **16**, 71 (2007).
23. M. R. Picciotto, W. A. Corrigall, *J. Neurosci.* **22**, 3338 (2002).
24. J. A. Dani, D. Bertrand, *Annu. Rev. Pharmacol. Toxicol.* **47**, 699 (2007).
25. G. C. Harris, G. Aston-Jones, *Neuropsychopharmacology* **28**, 865 (2003).
26. E. J. Nestler, W. A. Carlezon Jr., *Biol. Psychiatry* **59**, 1151 (2006).
27. J. Williams, P. Dayan, *J. Child Adolesc. Psychopharmacol.* **15**, 160 (2005).
28. A. M. Graybiel, *Annu. Rev. Neurosci.* **31**, 359 (2008).
29. W. Shen, M. Flajolet, P. Greengard, D. J. Surmeier, *Science* **321**, 848 (2008).
30. F. Zhang *et al*., *Nature* **446**, 633 (2007).

31. We thank M. Wightman, P. Phillips, and the entire Deisseroth laboratory for their support. All reagents and protocols are freely distributed and supported by the authors (www.optogenetics.org); because these tools are not protected by patents, Stanford University has applied for a patent to ensure perpetual free distribution to the international academic nonprofit community. H.C.T. is supported by a Stanford Graduate Fellowship. F.Z. and G.D.S. are supported by NIH National Research Service award. A.R.A. is supported by the Fonds National de la Recherche Scientifique, NARSAD, and the Fondation Leon Fredericq. L.d.L. is supported by National Institute on Drug Abuse (NIDA), Defense Advanced Research Projects Agency, and NARSAD. K.D. is supported by NSF; National Institute of Mental Health; NIDA; and the McKnight, Coulter, Snyder, Albert Yu and Mary Bechmann, and Keck foundations.

Supporting Online Material

www.sciencemag.org/cgi/content/full/1168878/DC1
Materials and Methods
Figs. S1 to S7
References

24 November 2008; accepted 7 April 2009
Published online 23 April 2009;
10.1126/science.1168878
Include this information when citing this paper.

The Human K-Complex Represents an Isolated Cortical Down-State

Sydney S. Cash,[1]*† Eric Halgren,[2]* Nima Dehghani,[2] Andrea O. Rossetti,[5] Thomas Thesen,[3] ChunMao Wang,[3] Orrin Devinsky,[3] Ruben Kuzniecky,[3] Werner Doyle,[3] Joseph R. Madsen,[4] Edward Bromfield,[5] Loránd Erőss,[6] Péter Halász,[7,9] George Karmos,[8,9] Richárd Csercsa,[8] Lucia Wittner,[6,8] István Ulbert[6,8,9]*

The electroencephalogram (EEG) is a mainstay of clinical neurology and is tightly correlated with brain function, but the specific currents generating human EEG elements remain poorly specified because of a lack of microphysiological recordings. The largest event in healthy human EEGs is the K-complex (KC), which occurs in slow-wave sleep. Here, we show that KCs are generated in widespread cortical areas by outward dendritic currents in the middle and upper cortical layers, accompanied by decreased broadband EEG power and decreased neuronal firing, which demonstrate a steep decline in network activity. Thus, KCs are isolated "down-states," a fundamental cortico-thalamic processing mode already characterized in animals. This correspondence is compatible with proposed contributions of the KC to sleep preservation and memory consolidation.

Although the electroencephalogram (EEG) is known to directly and instantaneously reflect synaptic and active transmembrane neuronal currents, the specific channels, synapses, and circuits that generate particular EEG elements in humans remain poorly specified. Much of the EEG is composed of repeated wave forms with characteristic morphologies, durations, amplitudes, frequency content, evoking events, and background states (*1*). The largest of these EEG "graphoelements" is the KC, characterized by a short surface-positive transient followed by a slower, larger surface-negative complex with peaks at 350 and 550 ms, and then a final positivity peaking near 900 ms, followed sometimes by 10- to 14-Hz "spindles" (*2*–*4*). KCs occur in non–rapid-eye-movement (non-REM) sleep, especially stage 2. Deeper sleep (stages 3 to 4) is characterized by slow waves, demonstrated in extensive animal studies to consist of a "slow oscillation" between periods of intense firing by both excitatory and inhibitory cortical neurons (termed "up-states") and periods of neuronal silence ("down-states") (*5*–*9*). Using micro- and macro-electrode arrays placed in patients undergoing evaluation for epilepsy (*10*), we demonstrate that the microphysiological characteristics of human KCs appear identical to those of down-states recorded in the same patients.

Typical KCs were recorded in eight patients (*11*). KCs were either spontaneous or evoked by a weak auditory stimulus. Within a given patient, the basic KC wave forms were similar regardless of whether they were recorded at the scalp or intracranially (Fig. 1A). In all cases, the wave form was dominated by a large deflection occurring ~500 to 600 ms after the onset of a stimulus, or after the onset of the initial deflection for spontaneous KCs. Characteristic KC wave forms were recorded by subdural electrodes placed on all cortical lobes, demonstrating widespread

[1]Department of Neurology, Epilepsy Division, Massachusetts General Hospital, Harvard Medical School, Boston, MA 02114, USA. [2]Departments of Radiology, Neurosciences, and Psychiatry, University of California at San Diego, San Diego, CA 92093, USA. [3]Comprehensive Epilepsy Center, New York University School of Medicine, New York, NY 10016, USA. [4]The Children's Hospital, Boston, MA 02115, USA. [5]Brigham and Women's Hospital, Boston, MA 02115, USA. [6]National Institute of Neurosurgery, H-1145 Budapest, Hungary. [7]National Institute of Psychiatry and Neurology, Epilepsy Center, H-1145 Budapest, Hungary. [8]Institute for Psychology, Hungarian Academy of Sciences, H-1394 Budapest, Hungary. [9]Péter Pázmány Catholic University, Department of Information Technology, H-1083 Budapest, Hungary.

*These authors contributed equally to this work.
†To whom correspondence should be addressed. E-mail: scash@partners.org

generation (Fig. 1B). In all scalp and most intracranial sites, this deflection was surface-negative. Different KCs recorded in the same patient varied in their relative size and timing across cortical locations (Fig. 1C). That is, KCs were not completely synchronous across the cortical surface, nor were the direction or duration of the transcortical delays constant across different KCs.

Potential gradients across cortical layers during KCs were recorded during these same events by using linear arrays of microelectrodes in temporal, frontal, and parietal sites (Fig. 1A). In all cases, KCs seen on the scalp electrodes were also observed on microelectrodes of the array and vice versa. Spontaneous and evoked KCs were recorded in four patients. They showed similar wave-form characteristics and distribution (Figs. 1D and 2), with the maximal negative response present on the same recording channel. No significant differences were found in the peak amplitude or area under the curve during this peak between spontaneous and evoked KCs (*t* test and Kolmogorov-Smirnov test; powered ≥0.80 to detect a 20% difference at $P < 0.05$).

Current source density calculated from these data showed a consistent pattern for both spontaneously occurring and triggered KCs. During the surface-negative slow deflection, there was a current sink in the channels closest to the cortical surface, whereas a substantial source was present in middle channels ~450 to 600 μm below the sink. This pattern, observed in all subjects, likely corresponds to a passive sink centered in layer I and an active source centered in layer III (Figs. 2, A and B, and 3A1). Successful recordings of multiunit neuronal firing were obtained in four subjects, all of whom showed decreased firing during the surface-negative slow deflection of either spontaneous or evoked KCs (Figs. 2, A and B, and 3A2). The pattern of sinks and sources and the decreased neuronal firing changes described here indicate hyperpolarizing current flow in layer III during the large surface-negative deflection.

Analysis of the spectral content of both spontaneous and evoked events consistently demonstrated a broadband decrease in the activity during the surface-negative event in multiple cortical layers when we used microelectrodes and in multiple locations with subdural macroelectrodes (Fig. 3). This was particularly pronounced for higher-frequency (gamma) activity from 20 to 100 Hz; low-frequency components—representing the wave form itself—were often maintained. High frequencies could remain depressed past resolution of the negative deflection. In six subjects, higher-frequency power briefly increased at KC onset. However, in no case was the surface-negative slow event preceded by rhythmic modulations of current or gamma power.

This study provides strong evidence that KCs are induced cortical down-states. First, our recordings demonstrate that KCs are generated in widespread cortical locations. Previous extracranial EEG (*12*), magnetoencephalogram (MEG) (*13*), and intracranial EEG recordings (*14*, *15*) have not provided unambiguous localization of KC generators because of difficulties in localizing widely distributed sources. Local KC generation near the electrode contact is highly likely in our recordings from the cortical surface and is certain when steep gradients are recorded at 150-μm intervals with microelectrode arrays. Widespread intracortical generation of KCs is consistent with the generation of down-states in lower mammals, which arise in distributed cortico-cortical networks (*16*).

The current study also demonstrates that KCs in humans are associated with strong and consistent decreases in gamma and multiunit activity, similar to those observed in animals during the down-state and indicating widespread decreases in cortical activity (*5*, *6*, *8*, *9*, *17*). Direct confirmation of identical microphysiology was obtained in our subjects by comparing KC and slow-oscillation down-states recorded within the same sleep session and by the same microelectrode arrays (Fig. 2). Even at the 150-μm resolution of these recordings, the two conditions evoke identical laminar distributions of transmembrane currents (correlation coefficient at the peak of the deflection was 0.95 between spontaneous KC and slow waves and 0.96 between evoked KC and slow waves, with $P < 10^{-12}$ for both). The indices of network synaptic activity (gamma power) and of population firing (multiunit activity) were both decreased during the KC in all cortical layers, but especially in the supragranular layers, as is characteristic of the slow-oscillation down-state (Fig. 3). Finally, although various inhibitory processes in the cortex have a wide range of durations, from less than 20 ms to several seconds, the KC and slow-oscillation down-states both last ~400 ms.

Although the data thus strongly support the proposal of Amzica and Steriade (*7*) that the KC reflects a cortical down-state, it does not support their corollary proposal that the KC is always part of an underlying oscillation (*18*). Rather, our evidence indicates that, at both the intracortical and epicortical levels, isolated KCs are the rule rather than the exception during stage 2 sleep. This is consistent with numerous observations over the past 70 years (*2*–*4*). Also consistent with these previous studies, but in contrast with Amzica and Steriade (*7*), we found the major component of KCs to be surface-negative.

The down-state is characterized by hyperpolarizing potassium currents, as well as low synaptic activity (*6*). The lack of a local up-state preceding the KC may pose difficulties for the proposal that an activity-dependent accumulation of calcium or adenosine diphosphate (ADP) triggers a potassium current and, thus, the down-state (*19*–*21*). Our findings, as well as recent evidence that the onset of the down-state is more synchronous than that of the up-state (*16*), suggest the need for additional synchronizing mecha-

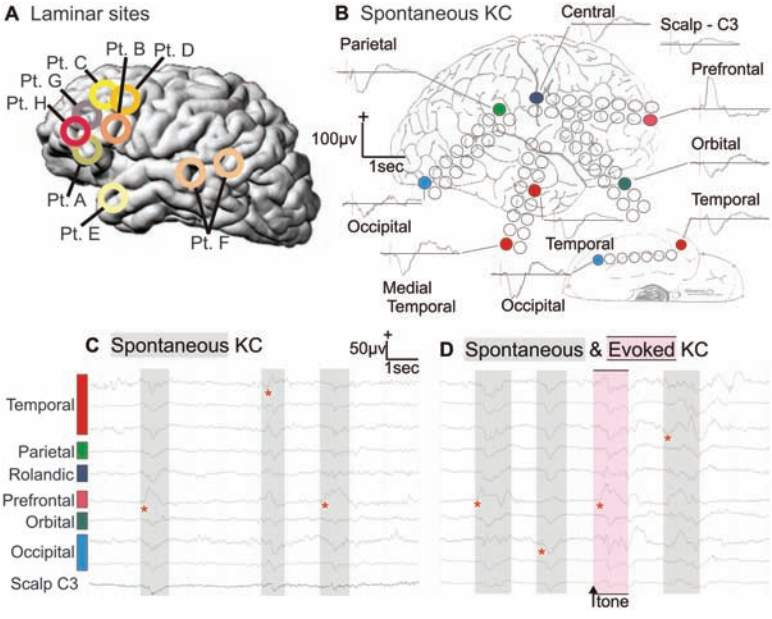

Fig. 1. Spontaneous and evoked KCs recorded simultaneously from the surface of all cortical lobes. (**A**) Approximate locations of microelectrode arrays in the eight patients (Pt.) studied. (**B**) Averaged spontaneous KCs recorded with grid electrodes in multiple cortical locations and from the scalp (subject E). Unaveraged spontaneous (**C** and **D**) and evoked (D) KCs from the same electrodes. Red asterisks show earliest deflection during the KCs and demonstrate the variability in onset and spread. Sleep stages and KCs were identified during natural sleep with standard criteria (*27*). KCs were evoked with occasional tones. Subdural electrode arrays were placed to confirm the hypothesized seizure focus and to locate epileptogenic tissue in relation to essential cortex, so as to direct surgical treatment.

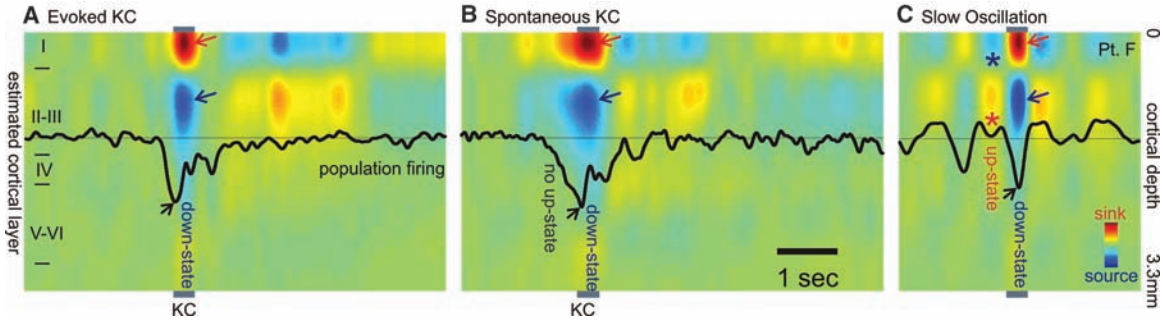

Fig. 2. Population transmembrane currents and neuronal firing in different cortical layers during single evoked (**A**) and spontaneous (**B**) KC in stage 2 sleep, and (**C**) during the slow oscillation in stage 3 to 4 sleep. Evoked and spontaneous KC and the slow-oscillation down-state are all characterized by outward currents (sources) in cortical layers II to III (blue arrows), paired with inward currents (sinks) near the cortical surface (red arrows), and decreased neuronal firing (black arrows). Unlike the KC, the slow-oscillation down-state is embedded in rhythmic alternation with up-states consisting of layer II/III sinks (*), layer I sources (*), and increased firing. Patient F.

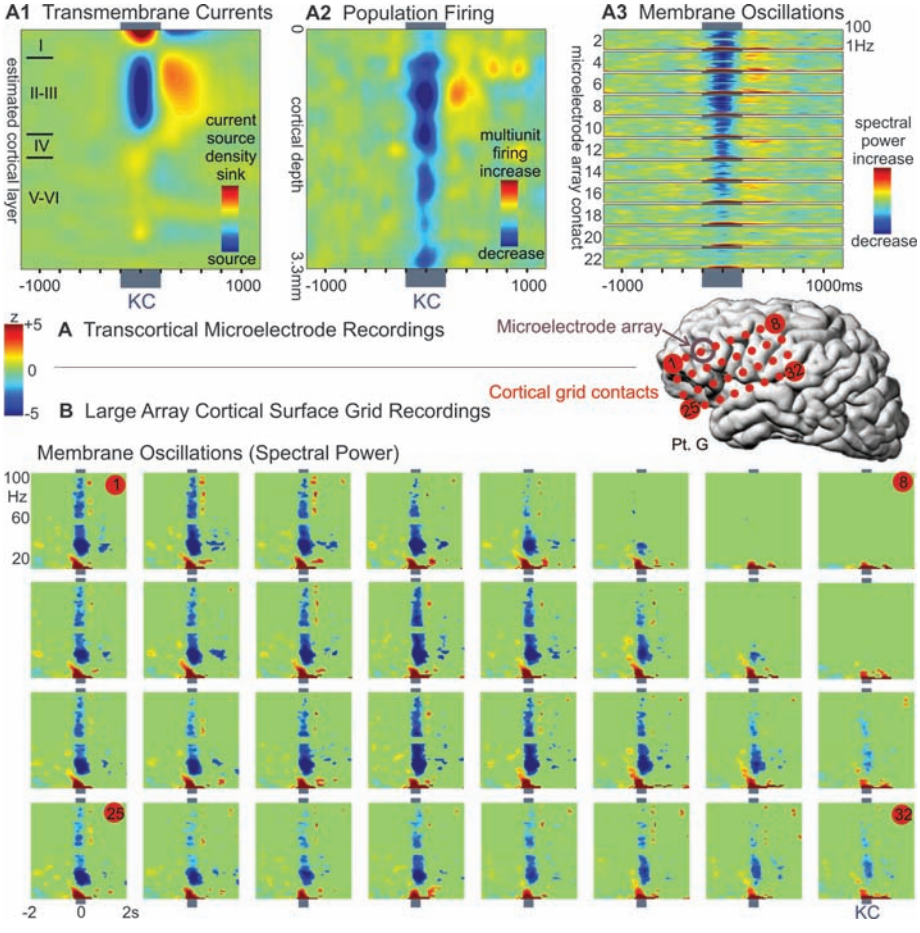

Fig. 3. Decrement in population firing and high-frequency membrane oscillations during KC. (**A**) Microelectrode array recordings of (A1) averaged spontaneous KCs show a layer III source, (A2) decreased neuronal firing, and (A3) membrane oscillations (higher-frequency spectral power), in all layers, especially upper layers. (**B**) Simultaneous recordings in the same patient from a large grid array of electrodes on the cortical surface also show a decrease in high-frequency spectral power during KC. Plots are set to the same threshold to show significant ($P < 0.01$) spectral power changes compared with a period of 1500 to 250 ms before the KC.

nisms, for instance, cortico-thalamo-cortical interactions, as have been shown for the sleep spindle (*22*). For example, in the tone-evoked KC, initial medial geniculate and auditory cortex activation could trigger a local down-state that spreads via thalamo-cortical and cortico-cortical connections. KCs would then occur spontaneously because of a similar mechanism, only with the sensory stimulus occult to the investigator (e.g., gastric), or because of a spontaneous burst of cortical activity. Thus, the KC down-state may follow an up-state, but only in the initiating zone. Our finding that successive KCs arise in variable cortical locations (Fig. 1D), which confirmed scalp recordings (*12*) and computational models (*19*), is consistent with this interpretation.

Sleep is thought to perform essential restorative and mnestic functions (*23*). Maintaining sleep is therefore crucial, but so is awakening in the face of danger. Our finding that the KC represents an isolated down-state supports the theory that it suppresses cortical activity and, thus, arousal in response to stimuli that are judged by the sleeping brain not to be dangerous (*3*, *4*). Increasing evidence supports a strong contribution to memory consolidation of stage 2 sleep, characterized by KC and spindles (*24*). The cortical down-state may provide a period when the near absence of neural activity induces a blanket suppression of synaptic strengths, balancing the synaptic enhancement occurring during waking and up-states and thus preserving the signal-to-noise ratio in network representations (*25*). In addition, during the recovery from the down-state, cortical firing "reboots" in a systematic order, which allows the potential for engrams encoded in dynamic assemblies of neuronal firing to be repeatedly practiced and thus consolidated (*26*). The current study ties a universal, normal, prominent, easily-observed EEG phenomenon to its underlying substrate of membrane currents and neuronal circuits through direct observation and homology with animal studies. This allows previous observations relating human sleep EEG to memory and sensory arousal to be interpreted within mechanistic neural models.

References and Notes

1. G. Buzsaki, *Rhythms of the Brain* (Oxford Univ. Press, Oxford, 2006).
2. A. L. Loomis, E. N. Harvey, G. Hobart, *J. Neurophysiol.* **13** (suppl.), 231 (1938).
3. I. M. Colrain, *Sleep* **28**, 255 (2005).
4. P. Halasz, *Sleep Med. Rev.* **9**, 391 (2005).
5. M. Steriade, F. Amzica, A. Nunez, *J. Neurophysiol.* **70**, 1385 (1993).
6. D. Contreras, I. Timofeev, M. Steriade, *J. Physiol.* **494**, 251 (1996).
7. F. Amzica, M. Steriade, *Neuroscience* **82**, 671 (1998).
8. M. V. Sanchez-Vives, D. A. McCormick, *Nat. Neurosci.* **3**, 1027 (2000).
9. I. Timofeev, F. Grenier, M. Steriade, *Proc. Natl. Acad. Sci. U.S.A.* **98**, 1924 (2001).

10. I. Ulbert, E. Halgren, G. Heit, G. Karmos, *J. Neurosci. Methods* **106**, 69 (2001).
11. Materials and methods are available as supporting material on *Science* Online.
12. M. Massimini, R. Huber, F. Ferrarelli, S. Hill, G. Tononi, *J. Neurosci.* **24**, 6862 (2004).
13. J. Numminen, J. P. Makela, R. Hari, *Electroencephalogr. Clin. Neurophysiol.* **99**, 544 (1996).
14. M. Velasco *et al.*, *Clin. Neurophysiol.* **113**, 25 (2002).
15. R. A. Wennberg, A. M. Lozano, *Clin. Neurophysiol.* **114**, 1403 (2003).
16. M. Volgushev, S. Chauvette, M. Mukovski, I. Timofeev, *J. Neurosci.* **26**, 5665 (2006).
17. M. Mukovski, S. Chauvette, I. Timofeev, M. Volgushev, *Cereb. Cortex* **17**, 400 (2007).
18. F. Amzica, M. Steriade, *Neurology* **49**, 952 (1997).
19. M. Bazhenov, I. Timofeev, M. Steriade, T. J. Sejnowski, *J. Neurosci.* **22**, 8691 (2002).
20. A. Compte, M. V. Sanchez-Vives, D. A. McCormick, X. J. Wang, *J. Neurophysiol.* **89**, 2707 (2003).
21. M. O. Cunningham *et al.*, *Proc. Natl. Acad. Sci. U.S.A.* **103**, 5597 (2006).
22. D. Contreras, A. Destexhe, T. J. Sejnowski, M. Steriade, *Science* **274**, 771 (1996).
23. J. A. Hobson, E. F. Pace-Schott, *Nat. Rev. Neurosci.* **3**, 679 (2002).
24. R. Stickgold, *Nature* **437**, 1272 (2005).
25. G. Tononi, C. Cirelli, *Sleep Med. Rev.* **10**, 49 (2006).
26. S. Ribeiro *et al.*, *PLoS Biol.* **2**, E24 (2004).
27. A. Rechtschaffen, A. Kales, *A Manual of Standardized Terminology, Techniques and Scoring System for Sleep Stages of Human Subjects*. (U.S. Government Printing Office, Washington, DC, 1968).
28. Supported by National Institute of Neurogical Disorders and Stroke (NIH) grants NS18741 and NS44623 to E.H. and Neuroprobes IST-027017, OTKA49122, ETT135/2006, János Szentágothai Knowledge Center RET 05/2004 grants to I.U. We thank L. Papp for technical support; and L. Grand, A. Magony, B. Dombovári, and D. Fabó for support in data analysis and recording. The authors dedicate this work to the memory of Edward Bromfield, who passed away on 10 May 2009.

Supporting Online Material
www.sciencemag.org/cgi/content/full/324/5930/1084/DC1
Materials and Methods
Fig. S1
Table S1
References

11 December 2008; accepted 20 March 2009
10.1126/science.1169626

Crystal Structure of the Nuclear Export Receptor CRM1 in Complex with Snurportin1 and RanGTP

Thomas Monecke,[1]* Thomas Güttler,[2]* Piotr Neumann,[1] Achim Dickmanns,[1] Dirk Görlich,[2]† Ralf Ficner[1]

CRM1 mediates nuclear export of numerous unrelated cargoes, which may carry a short leucine-rich nuclear export signal or export signatures that include folded domains. How CRM1 recognizes such a variety of cargoes has been unknown up to this point. Here we present the crystal structure of the SPN1·CRM1·RanGTP export complex at 2.5 angstrom resolution (where SPN1 is snurportin1 and RanGTP is guanosine 5′ triphosphate–bound Ran). SPN1 is a nuclear import adapter for cytoplasmically assembled, m_3G-capped spliceosomal U snRNPs (small nuclear ribonucleoproteins). The structure shows how CRM1 can specifically return the cargo-free form of SPN1 to the cytoplasm. The extensive contact area includes five hydrophobic residues at the SPN1 amino terminus that dock into a hydrophobic cleft of CRM1, as well as numerous hydrophilic contacts of CRM1 to m_3G cap-binding domain and carboxyl-terminal residues of SPN1. The structure suggests that RanGTP promotes cargo-binding to CRM1 solely through long-range conformational changes in the exportin.

Nuclear transport proceeds through nuclear pore complexes (NPCs) and supplies cell nuclei with proteins and the cytoplasm with nuclear products such as ribosomes and tRNAs. Most nuclear transport pathways are mediated by importin β–type nuclear transport receptors, which include nuclear export receptors (exportins), as well as importins (*1*, *2*). These receptors bind cargoes directly or through adapter molecules, shuttle constantly between the nucleus and cytoplasm, and use the chemical potential of the nucleocytoplasmic RanGTP-gradient to act as unidirectional cargo pumps (where GTP is guanosine 5′ triphosphate and RanGTP is GTP-bound Ran) (*3*).

Exportins recruit cargo at high RanGTP levels in the nucleus, traverse NPCs as ternary cargo·exportin·RanGTP complexes, and release their cargo upon GTP hydrolysis into the cytoplasm. CRM1 (exportin1/Xpo1p) (*4*, *5*) and CAS (Cse1p/exportin2) (*6*) are the prototypical exportins. Whereas CAS is specialized to retrieve the nuclear import adapter importin α back to the cytoplasm (*6*), CRM1 exports a very broad range of substrates from nuclei (*4*, *5*, *7*–*11*), including ribosomes and many regulatory proteins. It also depletes translation factors from nuclei and is essential for the replication of viruses such as HIV.

CRM1 has a dual function during biogenesis of spliceosomal U small nuclear ribonucleoproteins (snRNPs). It exports m^7G-capped U small nuclear RNAs to the cytoplasm (*4*, *12*), where they recruit Sm-core proteins and receive a 2,2,7-trimethyl (m_3G) cap structure. The import adapter snurportin 1 (SPN1) and importin β then transport the mature m_3G-capped U snRNPs into nuclei (*13*). To mediate another import cycle, SPN1 is returned to the cytoplasm by CRM1 (*14*).

Many CRM1 cargoes harbor a leucine-rich nuclear export signal (NES) that typically includes four characteristically spaced hydrophobic residues (*7*). Examples are the HIV-Rev protein (*15*) or the protein kinase A inhibitor (PKI) (*16*). In other cases, however, CRM1 recognizes not just a short peptide, but instead a large portion of the export cargo; here, SPN1 is the prototypical example (*14*). CRM1 binds SPN1 tighter than other export substrates, apparently because CRM1 must displace the imported U snRNP from SPN1 before export may occur.

The cytoplasmic dissociation of CRM1 from SPN1 is essential for multi-round import of U snRNPs. Hydrolysis of the Ran-bound GTP alone is insufficient to fully disrupt the interaction (Fig. 1, A to C) (*14*), but importin β can displace CRM1 from SPN1 (Fig. 1A). Thus, either the binding sites of SPN1 for CRM1 and importin β overlap, or importin β forces SPN1 into a conformation that is incompatible with CRM1 binding.

Two functional domains in SPN1 have been described: (i) the m_3G cap-binding domain ($SPN^{97–300}$) (*17*) and (ii) the N-terminal importin β–binding (IBB) domain ($SPN1^{40–65}$) (*14*, *18*, *19*), which confers binding to and import by importin β (*20*). A multiple alignment of SPN1 from various species revealed another conserved region that precedes the IBB domain and includes the hydrophobic residues Leu^4, Leu^8, Phe^{12}, and Val^{14}. Mutating any of those residues to serine or deleting Met^1 strongly impaired the interaction with CRM1, in particular at higher salt concentrations (Fig. 1B and fig. S1). Even though the SPN1 N terminus (with its conserved hydrophobic residues) resembles a classical NES, there are clear differences: foremost that CRM1 binds the isolated SPN1 N terminus ($SPN1^{1–21}$) considerably weaker than, for instance, the PKI-NES (Fig. 1C). In the context of full-length SPN1, however, this difference is more than compensated by the contribution of the m_3G cap-binding domain to the CRM1 interaction.

We then assembled, purified, and crystallized an export complex containing full-length human $SPN1^{1–360}$, full-length mouse $CRM1^{1–1071}$, and GTP-$RanQ69L^{1–180}$, a C-terminally truncated and GTPase-deficient form of human Ran (*21*).

[1]Abteilung für Molekulare Strukturbiologie, Institut für Mikrobiologie und Genetik, GZMB, Georg-August-Universität Göttingen, Justus-von-Liebig-Weg 11, 37077 Göttingen, Germany. [2]Abteilung Zelluläre Logistik, Max-Planck-Institut für Biophysikalische Chemie, Am Fassberg 11, 37077 Göttingen, Germany.

*These authors contributed equally to this work.
†To whom correspondence should be addressed. E-mail: goerlich@mpibpc.mpg.de

The resulting crystals contained two complexes per asymmetric unit. The structure was solved by molecular replacement with the use of known structures of GTP-bound $Ran^{7–176}$ (*22*), $SPN1^{97–300}$ (*17*), and a short human $CRM1^{707–1027}$ fragment (*23*). The final model, refined at a resolution of 2.5 Å, includes residues 12 to 1055 of CRM1 and $Ran^{9–179}$, as well as $SPN1^{1–360}$. $CRM1^{67–69}$ and four regions of SPN1 appear to be disordered (table S1) (*21*).

As expected from previous sequence analysis (*23*, *24*), CRM1 is built from so-called HEAT repeats (Fig. 2, fig. S2, and table S2), which include two consecutive helices (A and B) that pack in antiparallel orientation against each other and against the adjacent repeat (*25*). However, previous structure prediction (*23*) failed to predict the correct number and exact positions of the 21 repeats. This reflects the highly degenerate nature of some of the repeats, which even leads to an inverted topology of helices at the C terminus of CRM1 (fig. S2).

In contrast to importin β (*26*), transportin (*27*), and CAS/Cse1p (*22*, *28*), the overall CRM1 structure shows remarkably little superhelical twist (Fig. 2). However, it is bent to a distorted toroid structure, with HEAT 21 touching helices 2B and 5A, as well as the loop between HEATs 4 and 5 (Fig. 2 and fig. S2). Ran is enclosed into this toroid and stabilizes the ring closure by extensive contacts. In contrast to the IBB–importin β interaction (*18*, *19*, *26*), the cargo SPN1 is not enveloped by CRM1 but instead rests on the outside of the CRM1 toroid (Fig. 2). This different binding topology might reflect the fact that CRM1 carries cargoes, such as ribosomal subunits, that are too large to be engulfed by an exportin. In addition, the outside of the torus provides a larger surface area and possibly also a greater variety of binding sites for cargo recognition than does the inner face that already accommodates the Ran molecule.

The structure of m_3G cap-bound $SPN1^{97–300}$ was previously solved (*17*) and remained essentially unaltered in the SPN1·CRM1·RanGTP complex (root mean square deviation = 0.67 Å). However, several residues of SPN1 as well as of CRM1 HEATs 12 and 13 protrude into the m_3G cap-binding pocket (fig. S3). With the physiological import cargo of SPN1 (fully assembled U snRNPs), the clashes would be even more severe, because the RNA would run into the CRM1 molecule. Thus, SPN1 cannot simultaneously bind its import cargo and its export receptor, which agrees with previous data (*14*). This ensures that only cargo-free SPN1 is returned to the cytoplasm and allows SPN1 to mediate unidirectional transport of m_3G-capped U snRNPs into nuclei.

SPN1 binds CRM1 through an elaborate contact area (2330 $Å^2$), which includes three parts: (i) the N terminus ($SPN1^{1–35}$), (ii) the m_3G cap-binding domain ($SPN1^{97–300}$), and (iii) a C-terminal region, $SPN1^{349–360}$ (Fig. 3A). This is consistent with biochemical data that revealed strong contributions of $SPN1^{1–21}$ and the cap-binding domain to CRM1 binding (Fig. 1, B and C, and fig. S1) (*14*) and a weaker contribution of $SPN1^{286–360}$ (*14*).

All N-terminal residues that were found to be critical for CRM1-binding ($SPN1^{Met1, Leu4, Leu8, Phe12, Val14}$) (Fig. 1B and fig. S1) dock into a hydrophobic cleft that is formed by helices 11A and 12A and the intervening helical linker between 11B and 12A of CRM1 (Fig. 3B and fig. S4). The side chain of $CRM1^{Lys534}$, which is positioned by a salt bridge to $CRM1^{Glu575}$, closes the cleft and introduces a sharp kink into the SPN1 chain between $SPN1^{Val14}$ and $SPN1^{Ser15}$. There are several additional contacts in this area, such as electrostatic attraction between the negatively charged N-terminal helix of SPN1 and basic regions on the CRM1 surface, as well as hydrogen bonds

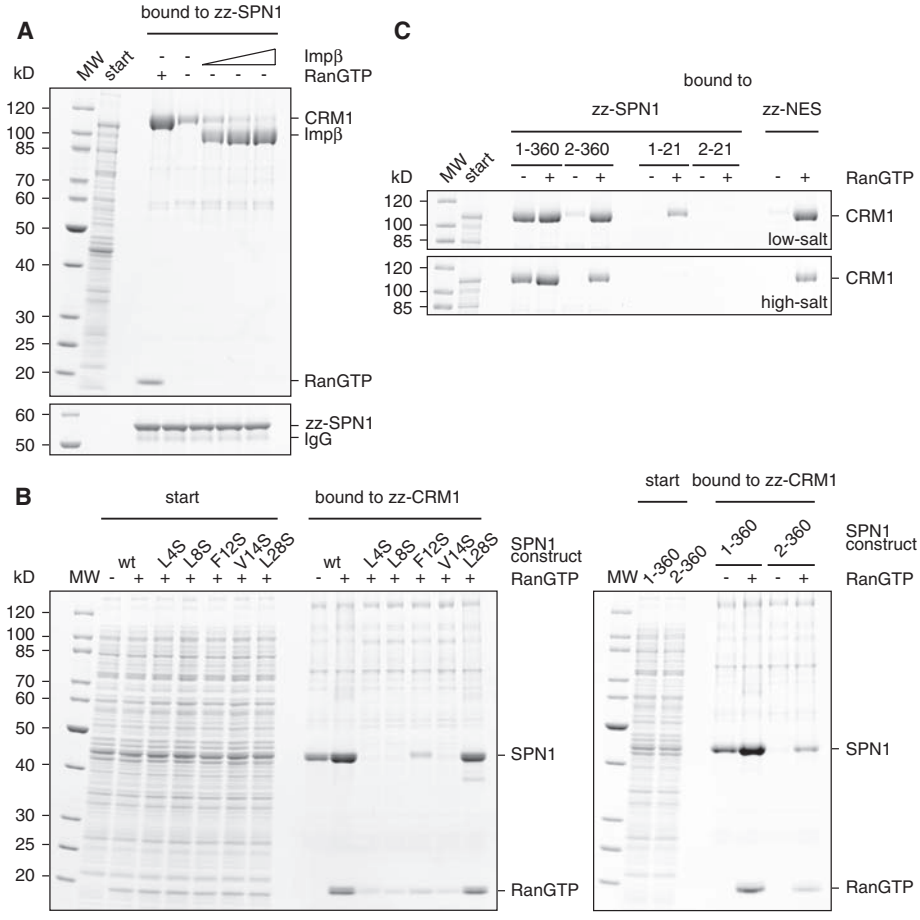

Fig. 1. (**A**) Effects of RanGTP and importin β on the SPN1·CRM1 interaction. 1 μM SPN1 was mixed with an *Escherichia coli* lysate containing 200 mM NaCl, 1 μM CRM1, and the indicated combinations of 3 μM RanGTP and 1, 2, or 3 μM importin β (Impβ) (*21*). Complexes were retrieved by immunoglobulin G (IgG)–Sepharose via the zz-tag of SPN1. SPN1-ligands were eluted with 1.5 M $MgCl_2$ (upper panel); the remaining baits (zz-SPN1; lower panel) were eluted with SDS. Analysis was by SDS–polyacrylamide gel electrophoresis/Coomassie staining. Note that RanGTP enhanced CRM1-binding to SPN1; however, this interaction was also detectable in the absence of Ran. This residual CRM1·SPN1 interaction could be suppressed by importin β that binds the IBB domain of SPN1. MW, molecular weight standard. (**B**) Met^1, Leu^4, Leu^8, Phe^{12}, and Val^{14} of SPN1 are all required for high-affinity binding to the CRM1·RanGTP complex. zz-tagged CRM1 immobilized on IgG-Sepharose was incubated with an *E. coli* lysate containing 200 mM NaCl and indicated combinations of 3 μM RanGTP and 1 μM untagged wild-type SPN1 or the specified mutants. CRM1-ligands were eluted with $MgCl_2$ and analyzed as described in (A). Note that mutating Leu^4, Leu^8, Phe^{12}, or Val^{14} to Ser (left) or deleting Met^1 (right) abolished or substantially impaired SPN1 binding to CRM1·RanGTP, whereas mutating Leu^{28} did not (left). (**C**) The N terminus of SPN1 contains export determinants that allow autonomous, RanGTP-stimulated binding to CRM1. Indicated zz-tagged SPN1 derivatives or the PKI-NES immobilized on IgG-Sepharose were incubated with an *E. coli* lysate containing 1 μM CRM1 and 3 μM RanGTP as specified. Bound ligands were eluted with $MgCl_2$ and analyzed as described in (A). At low NaCl concentration (50 mM, upper panel), $SPN1^{2–360}$ bound CRM1·RanGTP nearly as efficiently as full-length $SPN1^{1-360}$; however, a clear decrease in binding was observed without Ran. $SPN1^{1–21}$ recruited CRM1 in a strictly RanGTP-dependent manner. This CRM1 binding was lost when $SPN1^{Met1}$ was deleted. Even though $SPN1^{1–21}$ contains five hydrophobic residues, it bound CRM1 considerably weaker than the classical PKI-NES with only four hydrophobic residues. This difference was particularly apparent at 200 mM NaCl (lower panel).

between SPN1^{Ser15} and CRM1^{Glu575} and between SPN1^{Tyr35} and CRM1^{Glu529} (fig. S4). The CRM1 inhibitor leptomycin B (LMB) covalently modifies CRM1^{Cys528} (*29*). Cys^{528} is located within the hydrophobic cleft (Fig. 3B), which explains plausibly why LMB-modified CRM1 cannot bind export cargoes that rely on this cleft.

The N-terminal part of snurportin's export signature (with its five critical hydrophobic residues) resembles a classical NES and binds CRM1 in a conformation where residues Met^{1} to Ser^{11} form an α helix (Fig. 3A and fig. S4). The classical NES from the HIV Rev protein (*15*) must be recognized differently for three reasons: (i) The spacing of the hydrophobic residues is different, (ii) the intervening prolines would not allow such a helix to form, and (iii) this classical NES contains only four critical hydrophobic residues (*15*). Nevertheless, we cannot exclude the possibility that the same hydrophobic cleft also accommodates some or all of the key hydrophobic residues from classic NESs.

The interaction between the SPN1 m_3G cap-binding domain and CRM1 is dominated by polar contacts. SPN1$^{349–360}$, the third part of the export signature, binds to helices 14A, 15A, and 16A of CRM1 (Figs. 2 and 3A).

Importin β can displace CRM1 from the rather stable Ran-free SPN1·CRM1 complex (Fig. 1A) and therefore restore m_3G cap-binding of SPN1 in the cytoplasm (fig. S3) (*14*). This antagonism between CRM1 and importin β is not caused by an overlap of the respective binding sites; rather it appears to be caused by a combination of conformational changes in SPN1 and volume extrusion. The IBB domain binds importin β as a straight helix (*18*, *19*). However, within the CRM1 complex, the central part of this IBB helix is unwound, and the remaining helix-fragments are kinked by ≈80° (shown in green in Fig. 3A). This distortion of the IBB helix appears to be enforced by contacts of the 35 N-terminal residues of SPN1 with CRM1. Thus, straightening of the IBB helix by importin β is likely to break crucial contacts between CRM1 and SPN1.

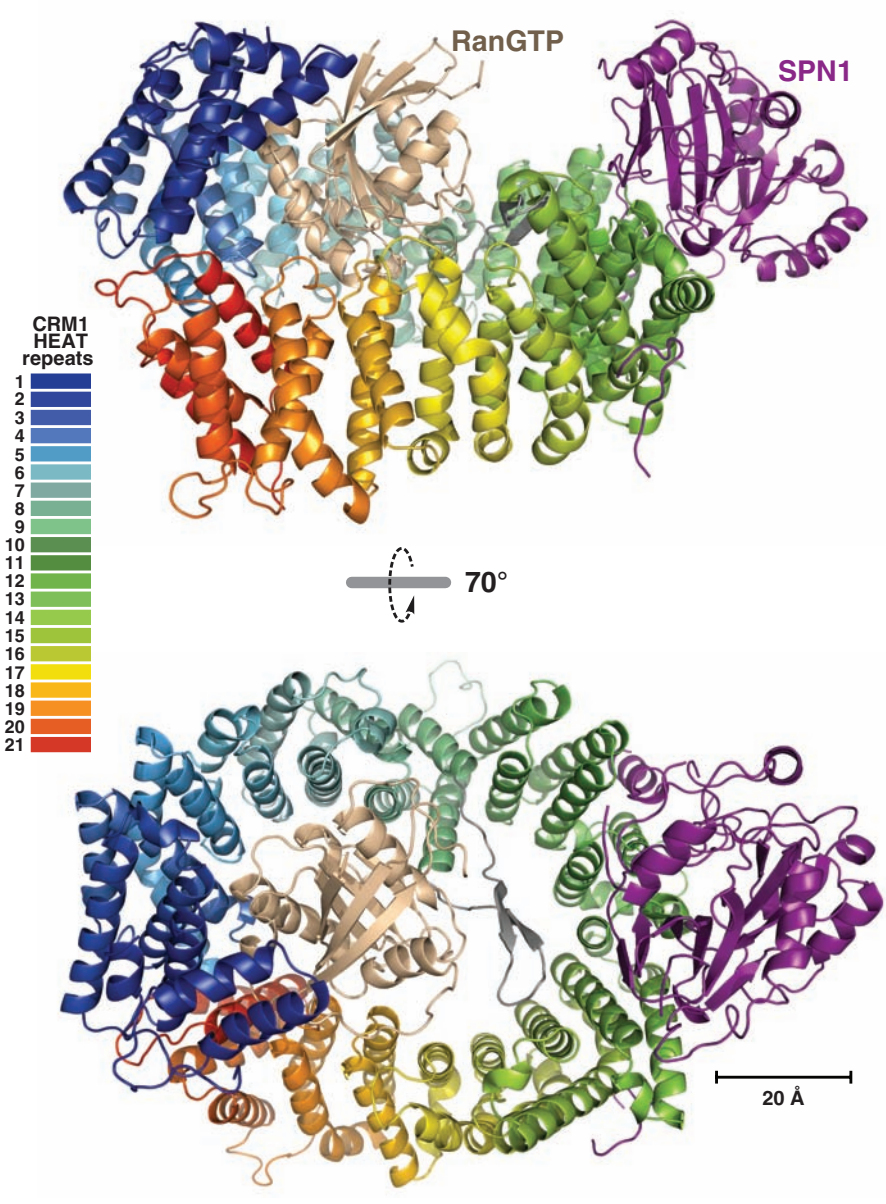

Fig. 2. Structure of the SPN1·CRM1·RanGTP nuclear export complex. Two views of the complex are depicted. Color-codes for Ran, SPN1, and the 21 consecutive HEAT repeats of CRM1 are indicated. Except for HEAT 21, A helices of the HEAT repeats are located at the outer surface of the CRM1 toroid and B helices at the inner surface (see also fig. S2). RanGTP is engulfed by the toroid-shaped structure of CRM1 and fixed by the so-called acidic loop (shown in the lower panel in gray), which is part of HEAT repeat 9. SPN1 is bound on the outer surface of CRM1, far away from the Ran molecule.

The structure of Ran in the SPN1·CRM1·RanGTP complex is virtually identical to that in other transport receptor·RanGTP complexes (*22*, *30*, *31*). Ran is almost completely engulfed by the CRM1 toroid and contacts four distinct areas of CRM1 (Figs. 2 and 4, A to C, and movie S1). The first area is located within the region that is most conserved between nuclear transport receptors (*24*, *32*). HEATs 1 to 3 bind switch II of Ran, whereas HEATs 4 and 5 pack against Ran helix 3 and the so-called "basic patch" (*30*), respectively (Fig. 4, B and C). The second Ran-binding region (HEATs 7 to 9) also contacts the basic patch and extends to β strand 6 of Ran. Analogous interactions occur in RanGTP complexes with CAS, transportin, and importin β (*22*, *30*, *31*). In contrast, the long "acidic loop" within HEAT 9 (region 3) binds Ran in an unprecedented manner. It forms a β hairpin, touches HEAT helices B12 to B15, and reaches through the entire central "hole" of the CRM1 toroid (Figs. 2 and 4, A and B, and figs. S2 and S5). The acidic loop locks RanGTP closely to the N- and C-terminal HEAT repeats and binds Ran^{37} from switch I, as well as Ran^{127,129,155} from the loops involved in guanine recognition. The fourth C-terminal Ran-binding region (HEATs 17 and 19) was not anticipated by sequence similarity or previous structures. It contacts both switch regions of Ran.

To function as an effective, unidirectional cargo-pump, CRM1 must strongly discriminate between GTP- and guanosine diphosphate (GDP)–bound Ran. CRM1 can sense the nucleotide state of Ran because it contacts switches I and II; i.e., the regions that differ most between GDP- and GTP-Ran (Fig. 4, B and C, and fig. S5). The structure of RanGDP (*33*, *34*) is incompatible with CRM1 binding, because switch I of RanGDP would clash with CRM1 HEAT 1 and switch II would collide with HEAT 19.

Ran switches the affinity of importin β–type transport receptors for their cargoes and thereby provides energy for the transport cycles. In the case of Cse1p, RanGTP increases the affinity of the exportin for its cargo importin α by directly interacting with both Cse1p and importin α (*22*). There are, however, no direct contacts between Ran and cargo in the SPN1·CRM1·RanGTP com-

plex (Fig. 2). The ≈1000-fold increase in the affinity of CRM1 for RanGTP by SPN1 and the equally large strengthening of the CRM1·SPN1 interaction by RanGTP (*14*) must therefore be caused solely by conformational changes in the CRM1 molecule.

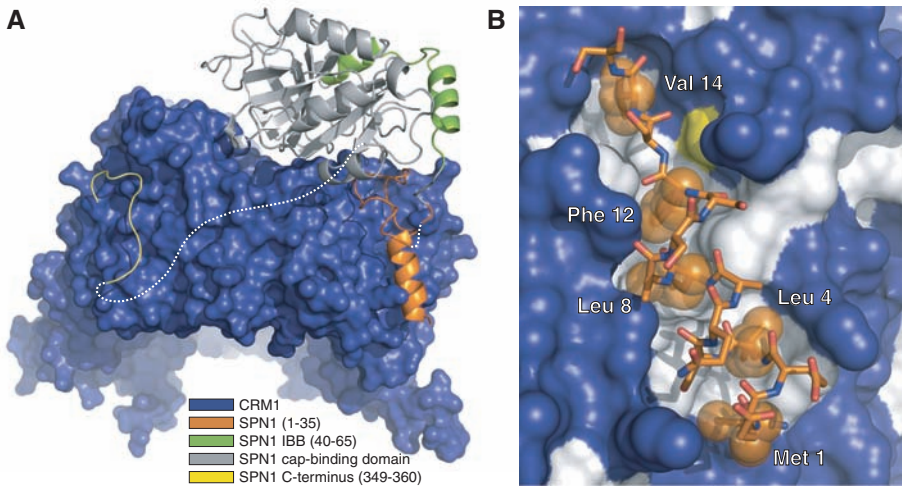

Fig. 3. The nuclear export signature of SPN1 involves a large interface formed by residues from all three domains of SPN1. (**A**) Three domains of SPN1 contact CRM1. These include N-terminal residues of SPN1 (orange), the cap-binding domain (gray), and the C-terminal residues (SPN1$^{349–360}$, yellow). The IBB domain of SPN1, which forms a straight helix within the importin β complex (*18*, *19*), is here partially unwound and bent (green). White dashed lines mark unresolved stretches. (**B**) The N-terminal hydrophobic residues of SPN1 (Met^{1}, Leu^{4}, Leu^{8}, Phe^{12}, and Val^{14}) dock into a hydrophobic cleft of CRM1. Carbons of SPN1 are shown as orange, oxygens as red, and nitrogens as blue sticks. The side chains of the hydrophobic residues are depicted as spheres. CRM1 is shown as a surface representation (blue indicates hydrophilic areas, white denotes hydrophobic areas). The yellow patch marks the sulfur of Cys^{528}, which is covalently modified by the CRM1-specific inhibitor LMB (*29*).

Both RanGTP and SPN1 obviously select the same conformation of CRM1 for high-affinity binding (here referred to as the nuclear conformation), whereas the free cytoplasmic conformation of CRM1 has only a low affinity for the two ligands (Fig. 1 and fig. S1). To explain this cooperativity, one must assume that the nuclear conformation is under considerable tension and that this tension is compensated for by the released binding energies of the Ran·CRM1 and SPN1·CRM1 interactions. In other words, Ran apparently promotes SPN1-binding by stabilizing the strained nuclear conformation of CRM1 and vice versa.

Ran and SPN1 are ≈55 Å apart in the export complex (Fig. 2). The conformational changes in CRM1 that coordinate their binding must therefore be transmitted over a considerable distance, probably through rigid body movements along the HEAT repeats. The splitting of the Ran-binding site on CRM1 into distinct regions is probably crucial for driving these movements, because even small changes in their distances will greatly affect the binding of Ran. Ran-binding regions 2 and 4, for example, are located on opposite sides of the CRM1 toroid (Fig. 4B), and it is quite possible that they are too far apart in the relaxed CRM1 conformation to contact Ran simultaneously (Fig. 4D). Hence, a low affinity for Ran would result. The transition to the nuclear conformation would bring these inter-

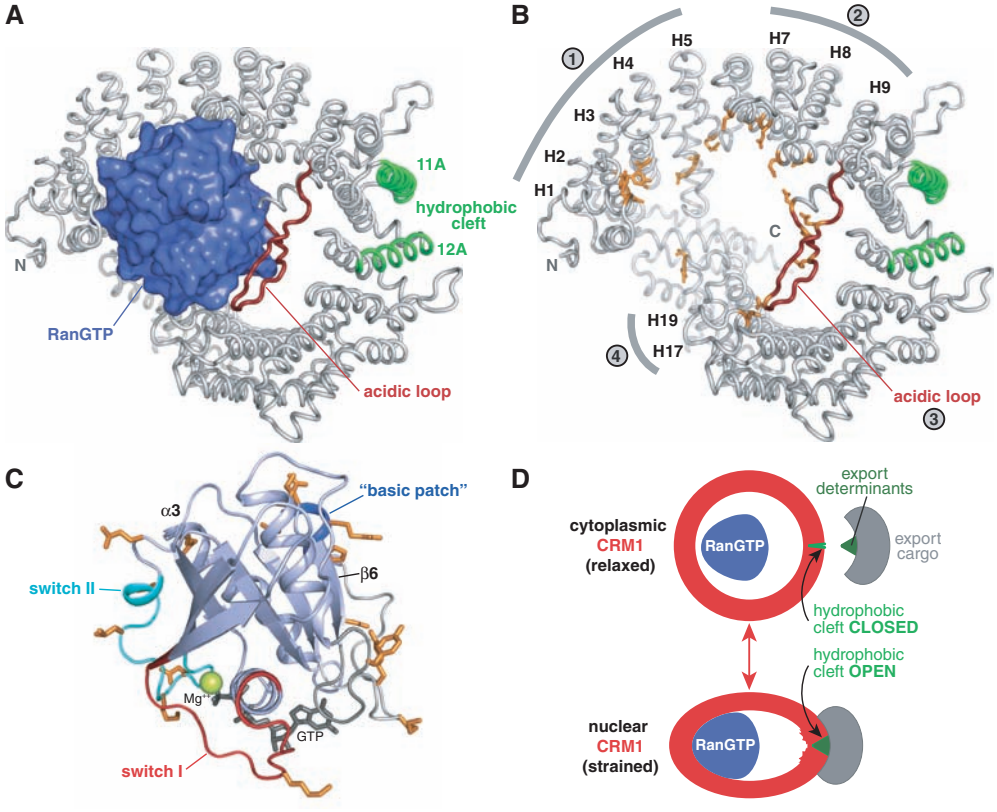

Fig. 4. Molecular details of the CRM1·RanGTP interaction (see also table S3). (**A**) CRM1 is shown as a gray backbone tube, and Ran is depicted as a surface representation. HEAT helices 11A and 12A, forming the cargo-binding hydrophobic cleft, are shown in green, and the acidic loop is shown in red. (**B**) RanGTP contact areas on CRM1. Orientation of CRM1 is as in (A), but Ran has been removed, and Ran-binding residues of CRM1 (distance < 3.6 Å) are shown as orange sticks. Note that the Ran-binding site includes four distinct areas (labeled 1 to 4). See also movie S1. (**C**) Contacts of RanGTP to CRM1. Ran is depicted as a ribbon diagram. Orientation is as in (A). CRM1-binding residues are shown in orange, switch I (Ran$^{30–47}$) is shown in red, and switch II (Ran$^{65–80}$) is depicted in blue. CRM1 contacts both switches. The basic patch (Ran$^{139–142}$, dark blue) shows extensive contacts to CRM1 regions 1 and 2 [see panel (B)]. Secondary structure elements are numbered as in (*33*). GTP is depicted as gray sticks; the Mg^{2+} ion is shown as a green sphere. (**D**) Model for conformational states of CRM1. CRM1 switches between a relaxed cytoplasmic (top) and a strained nuclear conformation (bottom). In the hypothetical cytoplasmic conformation, the contact sites for RanGTP inside the CRM1 toroid are too far apart to bind Ran with high affinity. Also, the hydrophobic cleft on the outer side of the toroid is closed. Rigid body movements allow transition to the nuclear conformation. Here, the Ran-binding sites are close enough to bind Ran simultaneously and thus with high affinity. The conformational change also alters the curvature of the toroid near the cargo-binding site, opens the hydrophobic cleft, and allows the export cargo to dock. For details, see main text.

faces closer together and allow high-affinity binding of Ran.

Conformational changes in CRM1, which favor the CRM1·Ran interaction, must also activate the cargo binding site(s). Thus, we suggest that the hydrophobic cleft is also controlled by these transitions. The cleft might be closed in the cytoplasmic, relaxed conformation of CRM1 (Fig. 4D). Putting the CRM1 toroid under tension to bind Ran with all interfaces should also change the curvature of the CRM1 molecule around the cargo-binding site. This might stretch the contacts between the outer A helices of HEATs 11 and 12 and consequently open the hydrophobic cleft. The observation that CRM1 binding of the isolated SPN1 N terminus and, thus, docking into the hydrophobic cleft is efficient only in the presence of RanGTP (Fig. 1C) strongly supports this model.

References and Notes

1. D. Görlich, U. Kutay, *Annu. Rev. Cell Dev. Biol.* **15**, 607 (1999).
2. A. Cook, F. Bono, M. Jinek, E. Conti, *Annu. Rev. Biochem.* **76**, 647 (2007).
3. D. Görlich, N. Pante, U. Kutay, U. Aebi, F. R. Bischoff, *EMBO J.* **15**, 5584 (1996).
4. M. Fornerod, M. Ohno, M. Yoshida, I. W. Mattaj, *Cell* **90**, 1051 (1997).
5. K. Stade, C. S. Ford, C. Guthrie, K. Weis, *Cell* **90**, 1041 (1997).
6. U. Kutay, F. R. Bischoff, S. Kostka, R. Kraft, D. Görlich, *Cell* **90**, 1061 (1997).
7. U. Kutay, S. Güttinger, *Trends Cell Biol.* **15**, 121 (2005).
8. O. Gadal *et al.*, *Mol. Cell. Biol.* **21**, 3405 (2001).
9. T. I. Moy, P. A. Silver, *J. Cell Sci.* **115**, 2985 (2002).
10. A. W. Johnson, E. Lund, J. Dahlberg, *Trends Biochem. Sci.* **27**, 580 (2002).
11. M. T. Bohnsack *et al.*, *EMBO J.* **21**, 6205 (2002).
12. M. Ohno, A. Segref, A. Bachi, M. Wilm, I. W. Mattaj, *Cell* **101**, 187 (2000).
13. J. Huber *et al.*, *EMBO J.* **17**, 4114 (1998).
14. E. Paraskeva *et al.*, *J. Cell Biol.* **145**, 255 (1999).
15. U. Fischer, J. Huber, W. C. Boelens, I. W. Mattaj, R. Lührmann, *Cell* **82**, 475 (1995).
16. W. Wen, J. Meinkoth, R. Tsien, S. Taylor, *Cell* **82**, 463 (1995).
17. A. Strasser, A. Dickmanns, R. Lührmann, R. Ficner, *EMBO J.* **24**, 2235 (2005).
18. D. Wohlwend, A. Strasser, A. Dickmanns, R. Ficner, *J. Mol. Biol.* **374**, 1129 (2007).
19. G. Mitrousis, A. S. Olia, N. Walker-Kopp, G. Cingolani, *J. Biol. Chem.* **283**, 7877 (2008).
20. D. Görlich, P. Henklein, R. Laskey, E. Hartmann, *EMBO J.* **15**, 1810 (1996).
21. Materials and methods are available as supporting material on *Science* Online.
22. Y. Matsuura, M. Stewart, *Nature* **432**, 872 (2004).
23. C. Petosa *et al.*, *Mol. Cell* **16**, 761 (2004).
24. D. Görlich *et al.*, *J. Cell Biol.* **138**, 65 (1997).
25. M. A. Andrade, C. Petosa, S. I. O'Donoghue, C. W. Müller, P. Bork, *J. Mol. Biol.* **309**, 1 (2001).
26. G. Cingolani, C. Petosa, K. Weis, C. W. Müller, *Nature* **399**, 221 (1999).
27. B. J. Lee *et al.*, *Cell* **126**, 543 (2006).
28. A. Cook *et al.*, *Mol. Cell* **18**, 355 (2005).
29. N. Kudo *et al.*, *Proc. Natl. Acad. Sci. U.S.A.* **96**, 9112 (1999).
30. I. R. Vetter, A. Arndt, U. Kutay, D. Görlich, A. Wittinghofer, *Cell* **97**, 635 (1999).
31. Y. M. Chook, G. Blobel, *Nature* **399**, 230 (1999).
32. M. Fornerod *et al.*, *EMBO J.* **16**, 807 (1997).
33. K. Scheffzek, C. Klebe, K. Fritz-Wolf, W. Kabsch, A. Wittinghofer, *Nature* **374**, 378 (1995).
34. M. Stewart, H. M. Kent, A. J. McCoy, *J. Mol. Biol.* **284**, 1517 (1998).

35. We thank the staff of synchrotron beamlines at BESSY (Berlin), the European Molecular Biology Laboratory/Deutsches Elektronen-Synchrotron (Hamburg), and the European Synchotron Radiation Facility (Grenoble) for assistance during data collection; D. Deichsel for excellent technical help; and S. Frey and S. Güttler for comments on the manuscript. We received funding from the Deutsche Forschungsgemeinschaft (grant SFB523 to R.F. and T.M.), the Max-Planck-Gesellschaft (to D.G. and T.G.), the Alfried Krupp-Foundation (to D.G. and T.G.), and the Boehringer Ingelheim Fonds (to T.G.). Coordinates and structure factors have been deposited in the Protein Data Bank with accession code 3GJX.

Supporting Online Material

www.sciencemag.org/cgi/content/full/1173388/DC1
Materials and Methods
Figs. S1 to S5
Tables S1 to S3
References
Movie S1

11 March 2009; accepted 9 April 2009
Published online 23 April 2009;
10.1126/science.1173388
Include this information when citing this paper.

New Products

Refrigerated Benchtop Bath

The FTS-Multi-Cool is a mechanically refrigerated benchtop bath that eliminates the costs and hazards associated with coolants such as liquid nitrogen and dry ice. Compact and self-contained, the Multi-Cool provides up to eight liters of working fluid at temperatures between -80°C and +100°C, with temperature control ±0.1°C. Fitted with an integral magnetic stirrer with variable speed control, the Multi-Cool offers temperature uniformity and stability, enabling superior results to be achieved in applications including Charpy impact testing, controlled temperature reactions, pour-point determinations, tissue freezing, and viscosity studies. An RS232 interface allows control and data collection from a remote location.

SP Industries
For information 845-687-5315
www.spindustries.com

Dynamic Array

The 48.48 Dynamic Array provides an efficient platform for single-cell gene expression quantification studies using off-the-shelf TaqMan polymerase chain reaction (PCR) assays and reagents. Fluidigm has introduced a new single-cell gene expression technique that, when used with the BioMark System, produces inexpensive, reproducible gene expression results from single-cell samples. The key to this advance is the matrix of channels, chambers, and valves in the 48.48 Dynamic Array that do the work of assembling assays. Scientists can use the product to enjoy the same quantitative PCR data quality and experimental flexibility that they are currently receiving from 384-well systems while increasing throughput 24 times. Users can test 48 genes against 48 samples in a single run.

Fluidigm Europe
For information +33-44-259-3861
www.fluidigm.com

Workflow Automation

Two new instruments can help laboratories automate their workflow. Rotor-Gene Q is a real-time polymerase chain reaction (PCR) cycler. QIAgility enables PCR setup in a wide range of formats. Rotor-Gene Q offers high-resolution melting and fast PCR on one instrument, suitable for many emerging applications. It features superior thermal and optical performance, unbreakable tubes, and flexible formats. Maintenance and calibration requirements are minimal. Versatile software enables real-time analysis. QIAgility's rapid, reliable PCR setup eliminates manual pipetting steps prone to human error. Operated via easy-to-use software, its products are ready for immediate use in downstream applications.

Qiagen
For information 001-240-686-7660
www.qiagen.com

Drug Candidate Software

FieldStere software enables medicinal chemists to enrich their short-list of drug candidates with structurally diverse compounds that share the same desired biological activities (bioisosteres). FieldStere allows the fine-tuning of the resulting bioisosteres to enhance potency and specificity while removing undesirable absorption, distribution, metabolism, excretion, and other properties. FieldStere builds on the proprietary Field technology, which describes chemical structures in terms of the surface properties of the whole molecule. These properties accurately predict how a compound will interact with other molecules. The Field technology has applications in lead optimization, candidate switching, compound evaluation, and investigation of new patent opportunities.

Cresset Biomolecular Discovery
For information +44-1707-356120
www.cresset-bmd.com

Protein Extraction Buffer

The new 2-D Protein Extraction Buffer line is a series of six buffers for efficient and reproducible extraction of high-quality protein lysates with high yield. The protein lysates are suitable for applications such as two-dimensional (2D) gel analysis and one-dimensional gel electrophoresis, or for rehydrating immobilized pH gradient strips prior to 2D electrophoresis. The new buffers are modifications of well-studied protein solubilizers, and are supplied as dry powders that are rehydrated with the diluent provided. The dry powder formulation eliminates problems associated with carbamylation, which can occur in solutions containing urea and may alter protein charge.

GE Healthcare
For information 262-501-0777
www.gelifesciences.com

Sealing Film

ThermalSeal RTS films for high-clarity sealing combine clear 50 µm polyolefin with a 50 µm encapsulated silicone adhesive layer. This unique construction provides for superior performance in real-time quantitative polymerase chain reaction, crystallization, and storage applications. The chemically inert silicone is nontacky for easy handling until pressed to a microplate, which releases adhesive in sealing areas only. The films are free of deoxyribonuclease and ribonuclease, are DMSO resistant, and exhibit minimal autofluorescence. They are sized to fit within the rim of any standard rim-raised plate. Their temperature range is -70°C to +100°C.

Excel Scientific
For information 760-246-4545
www.excelscientific.com

Electronically submit your new product description or product literature information! Go to **www.sciencemag.org/products/newproducts.dtl** for more information.

Newly offered instrumentation, apparatus, and laboratory materials of interest to researchers in all disciplines in academic, industrial, and governmental organizations are featured in this space. Emphasis is given to purpose, chief characteristics, and availabilty of products and materials. Endorsement by *Science* or AAAS of any products or materials mentioned is not implied. Additional information may be obtained from the manufacturer or supplier.

Seattle Children's
HOSPITAL · RESEARCH · FOUNDATION

Neurological Surgery
Associate Professor / Professor

The recently established Center for Neuroscience at the Seattle Children's Research Institute invites applications for a full-time faculty position, with the University of Washington School of Medicine Department of Neurological Surgery, at the rank of Associate Professor or full Professor, without tenure. Qualified applicants should be established investigators who are applying techniques of molecular, genetic or cellular biology to study mechanisms underlying hydrocephalus. The Center for Neuroscience at the Seattle Children's Research Institute's research vision is to restore children's health through a mechanistic understanding. The applicant's area of research interest should be complementary to the interests of current faculty working on various areas of neuroscience and bioengineering. Researchers interested in understanding CSF hydrodynamics, choroid plexus function, neuroendocrinology, brain metabolism, blood brain barrier function, brainstem neurobiology and proteomics research are particularly encouraged to apply. The successful candidate must have a M.D. and/or Ph.D. degree and have active nationally funded research grants. Level and salary will be based on applicant's qualifications and experience. Responsibilities of the position include development of an independent, extramurally funded research program, establishing a hydrocephalus section within the Center for Neuroscience and mentoring graduate and post-doctoral students and junior faculty investigators.

This position is open until filled. Address any inquiries to **Dr. Jan-Marino Ramirez, Center Director**, at **nino.ramirez@seattlechildrens.org**. Please send CV, a statement of current and future research interests and the names and contact information of three references to: **Wendy Kramer, Seattle Children's Research Institute, 1900 Ninth Avenue, M/S C9S-9, Seattle, WA 98101**.

For more information about Seattle Children's Research Institute, please visit:
http://research.seattlechildrens.org.

All University of Washington faculty engage in teaching, research, and service.
The University of Washington is an Equal Opportunity/Affirmative Action Employer.
Women and minorities are encouraged to apply.

UW Medicine
SCHOOL OF MEDICINE

MANA NIMS National Institute for Materials Science wpi

Principal Investigator

International Center for Materials Nanoarchitectonics
National Institute for Materials Science, JAPAN

The National Institute for Materials Science (NIMS) invites applications for principal investigators at the International Center for Materials Nanoarchitectonics (MANA), Tsukuba, Japan. Applications for experimental or theoretical work in the Nano-Bio or Nano-Green research fields are welcome. A few appointments will be considered. Information about MANA is available at **http://www.nims.go.jp/mana/**.

We are looking for outstanding scientists with internationally recognized experience and a strong record of research performance in Nanotechnology for biomedical or energy and environmental applications. The candidate must also be able to demonstrate his/her potential for attracting external research funding. Annual base salary ranges from 10 million JPY to 20 million JPY, depending on qualification and experience. We offer enough start-up funds, a high degree of work autonomy, and a highly international research environment with new state-of-the-art equipment and facilities.

Inquiries about employment conditions can be addressed to the **MANA Administrative Director Takahiro Fujita (FUJITA.Takahiro@nims.go.jp)**. Candidates should send a curriculum vitae, bibliography, statement of research interests and a list of references to **mana@nims.go.jp** by **July 31, 2009**. Only electronic submission will be accepted. MANA wishes to increase the share of female scientists and especially welcomes application from women.

सत्यमेव जयते

GOVERNMENT OF INDIA

MINISTRY OF SCIENCE & TECHNOLOGY
DEPARTMENT OF BIOTECHNOLOGY

NEW DELHI

INVITES

APPLICATIONS FOR THE POST OF DIRECTOR OF THE NATIONAL BRAIN RESEARCH CENTRE, MANESAR, HARYANA, INDIA

Applications are invited for the post of Director, National Brain Research Centre (NBRC), a deemed university for brain research. The Centre, located at Manesar, Haryana, 50 km south west of Delhi, is involved in high quality multidisciplinary research in Neuroscience. The major objectives of NBRC are to undertake basic research to understand brain function in health and disease. In addition to the intramural research activity at the main centre, NBRC also promotes networking of the existing research groups in neuroscience in the country.

The research interests at NBRC span from molecular to behavioural and computational neuroscience. The institute has state-of-the-art facilities such as DNA microarray, rodent and primate animal facility, imaging facility with a 3 Tesla MRI and EFG/ERP and promotes multidisciplinary and novel approaches to the understanding of the functioning of the human brain. The institute promotes translational research with a mission to 'discover rationale therapies and cures for brain disorders'. The institute has an excellent academic programme with rigorous course work for students pursuing Ph.D. and integrated Ph.D. It admits students with Bachelor's and Master's Degree in wide ranging fields from biology to engineering.

The Director is expected to provide dynamic leadership in academic, scientific and administrative matters relating to its various areas of interest in both extramural and intramural activities. The applicant must have a holistic vision of neuroscience and be capable of providing leadership in different areas that encompass neuroscience such as computational, cognitive, systems and molecular neuroscience.

The applicant should possess: Ph.D. or equivalent degree in related biomedical field. Outstanding scientific and academic credentials in neuroscience as evidenced through proven ability to carry out independent research and high quality publications and other recognitions. The eligible applicant must have at least 15 years of research experience. Leadership ability for running high quality institutions/centres/departments is considered as an asset for this position. Track record of research in neuroscience is essential requirement. The position offers enormous opportunities to promote neuroscience both nationally and internationally.

The applicant should not be exceeding 55 years of age but age relaxation will be allowed for exceptional cases. The appointment will be on contract basis for a period of five years which will be extendable for a further term, subject to the maximum age limit of 60 years. The post carries pre-revised pay scale of Rs.25,000 (Fixed) (revised to fixed pay of Rs.75,000 alongwith a Special Allowance of Rs.5,000 per month) and usual allowances as per Govt of India rules. The applications along with details, curriculum vitae indicating the date of birth, address for correspondence including telephone, fax and e-mail address, qualifications acquired, professional and research experience, present position and scale of pay with total emoluments, publication details and a 500 word write-up on the candidate's vision of NBRC for the next ten years may be sent to **Shri Virendra Kapoor**, Deputy Secretary, Department of Biotechnology, Block 2, CGO Complex, Lodi Road, New Delhi-110 003 superscribing the cover 'Application for the Post of Director, NBRC', so as to reach latest by **6thJuly, 2009.**

KATHOLIEKE UNIVERSITEIT LEUVEN

K.U.Leuven, Belgium's largest and oldest university (established 1425), is a leading European research institution. It offers, together with its associated teaching hospitals, a wide variety of academic programmes taught in Dutch and English that are nurtured by internationally acclaimed, high-quality interdisciplinary research.

More than six thousand researchers from over a hundred countries participate in investigatory and strategic frontier research, as well as research that is specifically targeted at current and foreseen national and global issues. As a consequence of this K.U.Leuven enjoys many close and intense research collaborations with external partners. As a comprehensive university, K.U.Leuven offers three-year Bachelor's and one- or two-year Master's programs in almost all disciplines. The Leuven doctoral schools organize and co-ordinate international Ph.D. tracks of nearly three thousand five hundred doctoral candidates.

Leuven is a hospitable, agreeable and multicultural town, with a vibrant student community. It is situated only a short train ride away from Brussels, Paris and London.

The **Science, Engineering and Technology** Group at K.U.Leuven invites applications for the following vacant academic positions at the level of **professor or associate professor** in:

Modelling of Stellar and Circumstellar Media
Electrical Engineering
Network Software and Middleware
Multiscale Physics of Biological Systems
Socio-Economic Aspects of Human-Environment Interactions
Polymer Synthesis
Mathematical Engineering
Architectural History and Conservation

In addition, a limited number of **research professorships** is open for excellent candidates with a high-quality research programme.

The Science, Engineering and Technology Group at K.U.Leuven invites applications for the following vacant **tenure track** positions in:

Nanoscale Fluxonics and Plasmonics
Traffic and Infrastructure
Genomic Data Analysis
Plant Health and Protection
Nanoparticle Design for Sustainable Chemistry and Chemical Technology
Material-biology Interface Science
Privacy Technologies
Software Engineering

Detailed descriptions of these profiles and information on how to apply can be found at **www.set.kuleuven.be/vacancies. The deadline for applications is 30 September 2009.**

The K.U.Leuven pursues a policy of Equal Opportunity and Diversity.

Postdoctoral Associate

Stony Brook University's Department of Physiology and Biophysics is seeking a postdoctoral associate for stem cell research.

The function and regulation of Wnt signaling will be explored at the cellular level by using embryonic stem cells as a model system. The candidate will apply molecular biological, biochemical, and microscopic techniques in the study of the project.

Required qualifications: Ph.D. or equivalent in biological sciences. Prior experience in cell signaling with up to two years of postdoctoral training is preferred.

For a full position description, application procedures, or to apply online, visit *www.stonybrook.edu/jobs* (Ref. #HS-R-5795-09-04-S).

To apply, submit a cover letter and résumé to: Dr. Hsien-yu Wang, Associate Professor of Research, Department of Physiology and Biophysics, Health Sciences Center BST T5-180, Stony Brook University Stony Brook, NY 11794-8661

Fax: (631) 444-3432

Equal Opportunity/Affirmative Action Employer. Women, people of color, individuals with disabilities, and veterans are encouraged to apply.

STONY BROOK

Department of Health and Human Services
National Institutes of Health
Office of the Director, NIH
Director, Office of Behavioral and Social Sciences Research

The National Institutes of Health (NIH) in Bethesda, Maryland, the world's largest medical research facility, is seeking applications from exceptional candidates for the challenging position of Director, Office of Behavioral and Social Sciences Research (OBSSR). The Director, who also functions as the NIH Associate Director for Behavioral and Social Sciences Research, serves as the NIH focal point for establishing agency-wide policies and goals in behavioral and social sciences research, coordinates the activities undertaken in the performance of this research, and provides advice and staff support to the NIH Director, Deputy Director, and Division of Program Coordination, Planning, and Strategic Initiatives within the Office of the Director. The OBSSR employs approximately 14 full time positions: 9 scientific staff, 2 program analysts, 1 communications specialist, and 2 support staff, and has an FY 2009 estimated budget of more than $27M. Salary is commensurate with experience, and a full package of Civil Service benefits is available including retirement, health and life insurance, long-term care insurance, leave, and savings plan (401k equivalent). A detailed vacancy announcement that includes mandatory qualifications requirements and application procedures may be obtained at NIH's Executive Jobs Site: **http://www.jobs.nih.gov/vacancies/executive.htm or by contacting Regina Reiter at (301) 402-1130**. CV, bibliography, and a statement addressing the qualifications requirements must be received by close of business **AUGUST 31, 2009**.

With nationwide responsibility for improving the health and well being of all Americans, the Department of Health and Human Services (HHS) oversees the biomedical research programs of the NIH.

Department of Health and Human Services
National Institutes of Health
National Cancer Institute

Tenure-Track Investigator in Cancer Biology and Inflammation
Cancer and Inflammation Program, Center for Cancer Research

The National Cancer Institute (NCI) Intramural Center for Cancer Research (CCR) has a Principal Investigator position opening at the Cancer and Inflammation Program (Giorgio Trinchieri, M.D., Director) at NCI-Frederick. The Cancer and Inflammation Program (**CIP, http://ccr.cancer.gov/labs/lab.asp?labid=790**) was established three years ago and currently consists of fifteen principal investigators studying the role of inflammation and innate/adaptive resistance in controlling or promoting carcinogenesis, immunosurveillance and immunoediting, tumor progression, growth, and dissemination. An individual is sought with research interests in these areas. Expertise in peptide or lipid biochemistry or an interest in advanced flow cytometry technologies would also be attractive.

The Laboratory of Experimental Immunology and the Laboratory of Molecular Immunoregulation constitute the Cancer and Inflammation Program (CIP), which is the major immunologic component of the CCR's inflammation and cancer initiative, spanning the NCI's two major campuses in Frederick and Bethesda. This initiative seeks to partner NCI's expertise in inflammation and immunology with its cutting edge cancer etiology and carcinogenesis program. Applicants should have a Ph.D. and/or M.D. degree, a strong publication record, and a demonstrated potential for imaginative research. Salary will be commensurate with experience. Applicant will independently direct a research group of postdoctoral fellows and technicians funded by the NCI intramural program and will be provided sufficient space, equipment and supply budget. The applicant's research activity will be expected to be cooperative and well integrated in the Program's scientific focus of advancing the understanding of the inflammatory mechanisms involved in cancer initiation, promotion, progression, and dissemination with the ultimate goal to identify new therapeutic targets for cancer prevention and therapy. Several state of the art technical facilities in Frederick and in Bethesda, MD, will be accessible to the selected candidate including a fully staffed flow cytometry facility (**http://web.ncifcrf.gov/research/flow-cyto-lab.asp**). A one- or two-page statement of research interests and goals should be submitted in addition to three letters of recommendation and a curriculum vitae to: **Ms. Lisa Virts, Administrative Officer, NCI-Frederick, PO Box B, Bldg. 578, Frederick, Maryland 21702-1201, Tel. 301-846-5079, FAX 301-846-6053, E-mail: virtsl@mail.nih.gov**.

Applications must be postmarked by **July 22nd, 2009**.

THE NIH IS DEDICATED TO BUILDING A DIVERSE COMMUNITY IN ITS TRAINING AND EMPLOYMENT PROGRAMS

Boehringer Ingelheim

caesar
center of advanced european studies and research

MAX-PLANCK-GESELLSCHAFT

Boehringer Ingelheim, caesar and the Max Planck Society announce an

Independent Junior Research Group

in the area of "Autophagy in Neurodegenerative Diseases"

The lysosome as a protein-degrading intracellular organelle has been investigated extensively for more than half a century. More recently, upstream events delivering proteins via macroautophagy, microautophagy and chaperone-mediated autophagy to lysosomal degradation have been characterized on the molecular level. However, several key questions remain poorly understood: the contribution of autophagy to the maintenance of cellular integrity of post-mitotic cells; the mechanisms by which misfolded proteins affect autophagy; removal mechanisms for soluble and insoluble aggregates; pathways for the regulation of autophagy in neurodegenerative disease; the cause of the progressive decline in activity of the proteolytic systems during aging; potential long-term consequences of autophagy up-regulation; the identification of molecular targets for pharmacological induction of autophagy.

The Junior Research Group will be established at the center of advanced european studies and research in Bonn (caesar; www.caesar.de), an interdisciplinary research center associated with the Max Planck Society.

Funding of the Research Group covers a set-up package, the position of the group leader, a technician, one PhD and one post-doctoral fellowship, secretarial support, plus consumables, and is (initially) for 5 years. The successful candidate should have experience in one of the above mentioned research areas. Applications should include a CV, a list of publications, a one-page summary of scientific achievements, a two-page research plan and two letters of recommendation. Successful candidates will be invited to a symposium in August/September 2009 in Bonn.

Boehringer Ingelheim is a family-owned, research-driven global pharmaceutical company, founded in 1885 and committed to the goal of serving humankind through research into diseases and the development of new drugs and therapies. Boehringer Ingelheim operates with 41,300 employees in 47 countries across the globe. **caesar** (center of advanced european studies and research, located in Bonn, Germany) is conducting research in the field of neurosciences focussing on sensory systems, neurophotonics and neurodegenerative diseases. State-of-the-art techniques for imaging, molecular biology as well as chemical and material sciences open excellent opportunities in basic and applied research. caesar is associated with the Max Planck Society. The **Max Planck Society for the Advancement of Science** is an independent, non-profit research organization that primarily promotes and supports basic research. The society currently operates 80 institutes and research facilities with more than 23,400 employees, including 4,400 scientists.

Boehringer Ingelheim, caesar and the Max Planck Society are committed to equal opportunities and to employing disabled persons.

Please send your application **no later than June 15, 2009** to: **Prof. Dr. U. B. Kaupp, Forschungszentrum caesar, Ludwig-Erhard-Allee 2, D - 53175 Bonn.**

For further information please contact
- general: Dr. J. Reifarth, phone: +49 (0)228 9656 107 or juergen.reifarth@caesar.de
- science: Prof. Dr. U. B. Kaupp, phone: +49 (0)228 9656 100 or u.b.kaupp@caesar.de

---

BROWN
Alpert Medical School

CHAIR
Department of Molecular Microbiology and Immunology

The Warren Alpert Medical School and the Division of Biology and Medicine of Brown University invite applications for the position of Professor and Chair of the Department of Molecular Microbiology and Immunology. This position is to lead an interdisciplinary group of faculty and build a research program in host-pathogen interactions and pathogenesis of disease. The Department contributes to the teaching of undergraduate, graduate, and medical students.

Brown University is expanding opportunities for research and educational activities that bridge basic scientists and clinical translational researchers at its affiliated hospitals. The next Chair will provide leadership in expanding the research activities of the department and in recruiting and mentoring new faculty. Excellent core research facilities, interdisciplinary graduate programs with external funding, and newly renovated research space are available to foster expansion of the department.

The new Chair should have a record of scholarship and externally funded research that is recognized internationally, and demonstrated leadership and administrative skills. Applicants should submit their application electronically to: **Professor Agnes Kane, Chair, MMI Chair Search Committee, Agnes_Kane@brown.edu (mail to: Jane_Sanchez@brown.edu), Brown University, Division of Biology and Medicine, Box G-E5, Providence, Rhode Island 02912.** Applicants should include a letter describing their vision as the new Chair and future career plans, a curriculum vitae, and five names of potential external referees with contact information. Review of applications will begin immediately and will continue until the position is filled. A complete description of the department and faculty can be found at the department's website: **http://bms.brown.edu/mmi/**.

Brown University is an EEO/AA Employer and invites applications from women, minorities, and protected persons.

BIG DREAMS. BOLD FUTURE.

CENTER DIRECTOR

The Florida Center of Excellence for Biomolecular Identification and Targeted Therapeutics (FCoE-BITT) at the University of South Florida (USF) invites applications for the position of Center Director. FCoE-BITT is a comprehensive center funded by the State of Florida and USF with a research portfolio involving scientists and engineers who are investigating important models that are significant for understanding human health and show promise for translation into diagnostics, therapeutics, or detection technologies.

FCoE-BITT seeks a person with a Ph.D., or equivalent degree, in a relevant field who is a nationally recognized leader in research and experienced in administration (Associate/Full Professor rank) to provide vision for all aspects of the Center, including research, finance, administration and education. The Director will supervise current resident members of the FCoE-BITT Center and oversee the recruitment of new members. The Director is also responsible for Center communication with the USF campus, and building partnerships with industry, government agencies and community organizations.

Resident members of FCoE-BITT are housed along with new core facilities for structural biology, proteomics, and cell biology in an interdisciplinary research facility opened in 2007. The Center is affiliated with over 100 faculty laboratories in the Colleges of Arts and Sciences, Engineering, Medicine and Public Health, creating an opportunity for extensive interdisciplinary collaborations.

Please send electronic versions of a cover letter briefly describing your administrative experience and philosophy, a current CV, a short statement of research interests and funded projects, and arrange for at least three letters of recommendation to be sent electronically to **Ms. Alma Julia (ajulia@bitt.usf.edu), FCoE-BITT Administrative Specialist, University of South Florida, 3720 Spectrum Boulevard, Suite 324,Tampa, FL 33612.** Review begins June 5, 2009 and continues until the position is filled. More information can be found at **http://www.bitt.usf.edu**.

For disability accommodations, contact Ms Alma Julia at (8I3) 974-0274 a minimum of five working days in advance. According to Florida law, search records, including applications and search committee meetings, are open to the public.

USF is an Equal Opportunity/Equal Access University.

USF UNIVERSITY OF SOUTH FLORIDA

• TAMPA • ST. PETERSBURG • SARASOTA - MANATEE • POLYTECHNIC

Roche

Scientific Expert Diabetic Nephropathy

Who we are

At Roche, 80'000 people across 150 countries are pushing back the frontiers of healthcare. Working together, we've become one of the world's leading research-focused healthcare groups. Our success is built on innovation, curiosity and diversity, and on seeing each other's differences as an advantage. To innovate healthcare, Roche has ambitious plans to keep learning and growing – and is seeking people who have the same goals for themselves.

The headquarters in Basel is one of Roche's largest sites. It is home to the Corporate Executive Committee, the Pharmaceuticals and Diagnostics Divisions and the global business functions. Roche Basel also covers the entire business chain from research, development and production through to marketing. Over 8'000 people from more than 60 countries work at the site.

The Position

Within Roche Pharmaceuticals Research the department Metabolic Diseases is responsible for the pre-clinical research and the discovery of new medicine in the field of vascular and metabolic diseases. The department is globally organized. The position is based in Basel, Switzerland.
As a study director you will join a pharmacology research unit and work in our AAALAC-accredited facility. The unit you will be working in is responsible for profiling all our potential clinical candidates in animal models. In addi-tion we support the mole-cules in clinical development by appropriate pre-clinical in vivo studies. As of today, our strength are in the field of diabetes, obesity, dyslipidemia and atherothrombosis.
Key responsibilities: In your role as a study director you will be responsible to design and run in vivo studies internally or coordinate them with CRO's. You will work in multidisciplinary project teams and contribute to their progress by providing the in vivo pharmacological data. Further, it will be your task to strengthen our unit by building up in house expertise in kidney diseases, such as diabetic nephropathy or acute kidney failures.

Who you are

You're someone who wants to influence your own development. You're looking for a company where you have the opportunity to pursue your inte-rests across functions and geographies, and where a job title is not considered the final definition of who you are, but the starting point.

The successful candidate should have a Ph.D. in pharmacology or related areas and 5+ years of in vivo experience in the field of kidney diseases, in particular in diabetic nephropathy. The ideal candidate brings along also experience in drug development in the pharmaceutical industry. She or he is a team player, self driven and demonstrates leadership, coordination and commu-nication skills. The candidate should be fluent in English (oral and written) and should have a working knowledge in German or willingness to learn.

Job ID No.: 12254
Contact HR: M. Ceroni, +41 61 687 34 58
Contact Line: M. Boehringer, +41 61 688 85 07

The next step is yours. To apply online today or learn about other exciting positions, please visit http://careers.roche.com

FULL PROFESSOR POSITIONS
Capital Normal University, Beijing, China

Established in 1954, Capital Normal University (CNU) is a key university in Beijing supported by the Beijing Government. CNU is a comprehensive ("211 project") university that focuses on teacher training and encompasses liberal arts, sciences, engineering, management, law and education. Currently we have 10,475 undergraduate and 5,275 graduate students. We are expanding to be an international research institute dedicated to inspiring a new age of scientific achievement. Therefore, we are seeking outstanding applicants for the position of Professor both nationwide and worldwide.

I. Fields (Full-time professor)

1. College of Life Sciences:
Basic research or application oriented basic areas in biochemistry, genetics, ecology, and cellular and developmental biology

2. College of Resource Environment and Tourism:
Physical geography

3. Physics:
Condensed physics, optical engineering, electrical engineering, biophysics and astrophysics, terahertz spectroscopy and imaging, nondestructive testing with terahertz and infra-red thermal wave technology, interaction between terahertz and materials, ultrafast phenomena, photonic band gap structure, and X-CT imaging

4. Chemistry
Analytical chemistry, organic chemistry, and physical chemistry

II. Candidate Qualifications:

- a PhD degree and postdoctoral experiences in relevant scientific areas
- a strong record of research accomplishments, as documented by first-author or communication-author publications in internationally leading journals
- demonstrated capacity in coordinating and leading a team

III. Benefit package

The overall start-up package, including salary, start-up funds, housing, and family settlement in Beijing, is very competitive. It will be based on the applicants' qualifications and will be negotiated.

IV. Contact Information:

Review of applications will begin immediately and please arrange to send all the following materials to the following two addresses by **July 30th, 2009**: curriculum vitae (including awards and funding history), a statement of research plans, reprints of 5 representative papers in recent five years and three letters of recommendation.

1. Mr. Wenxin Chen, Mr. Gaofeng Ji
Tel: 86-10-68902989
Fax: 86-10-68981338
Email: cnu_rsc@mail.cnu.edu.cn
Department of Human Resources
105 Xi San Huan Road (N), Capital Normal University, Beijing 100048, P. R. China

2. Each corresponding Department:

College of Life Sciences
Dr. Yikun He, Xiaofang Zhang Tel: 86-10-68902037
Email: yhe@mail.cnu.edu.cn, yikunhe2009@gmail.com, zhangxf320@163.com

College of Resource Environment and Tourism
Dr. Xiaojuan Li Tel: 86-10-68923030
Email: keeperzhufy@126.com

Department of Physics
Dr. Cunlin Zhang Tel: 86-10-68902914
Email: cunlin_zhang@mail.cnu.edu.cn

Department of Chemistry
Dr. Zhuoyong Zhang Tel: 86-10-68902424
Email: cnuchemistry@sohu.com

Center for Immunology and Microbial Disease
Albany Medical College
Faculty Position

The Center for Immunology and Microbial Disease at Albany Medical College invites applications for a tenure-track faculty position from individuals who have a doctoral degree, postdoctoral experience, and demonstrated research productivity. Those with an interest in host-pathogen interactions are particularly encouraged to apply. The successful candidate will be expected to establish an independent, extramurally funded research program and participate in the teaching of medical and graduate students. The basic science departments at Albany Medical College are organized as interdisciplinary research centers and the Center for Immunology and Microbial Disease has a focus on microbial pathogenesis and immune defense, particularly as related to biothreat agents and emerging infections. Faculty at the Albany Medical College receive competitive salaries, attractive start-up packages, and access to the Center's ABSL-3/BSL-3, Microbiology and Immunology Core Labs. In addition, we have established a close relationship with the New York State Department of Health Wadsworth Laboratories, providing a diverse environment that is rich in infectious disease expertise. Albany Medical College is located in a mid-sized city within the upstate New York Capital Region, and has easy access to Boston, New York City, and the Adirondack Mountains.

Applicants should send their curriculum vitae, a statement of research plans, and three letters of reference to: **Dennis W. Metzger, Ph.D., Professor, Theobald Smith Alumni Chair and Director, Center for Immunology and Microbial Disease, Albany Medical College, 47 New Scotland Avenue, MC-151, Albany, NY 12208.**

For further information about the Center, visit **www.amc.edu/Academic/Research/imd.htm**.

An Equal Opportunity/Affirmative Action Employer.
Women and minorities are encouraged to apply.

INSTITUT DE PHYSIQUE DU GLOBE DE PARIS
Earth - Planets - Environnement - Natural Hazards

DIRECTOR

The Institut de Physique du Globe de Paris (IPGP) is seeking applications for the position of Director of IPGP, which will begin October 1, 2010.

The IPGP is the largest institute of Earth Sciences in France and also one of the largest in Europe. The Institute conducts research and education in geology, geophysics, geochemistry and the environmental sciences. It is in charge of monitoring the three active French volcanoes (Guadeloupe, Martinique, La Réunion) through its volcanic and seismologic observatories. It is also in charge of the magnetic observatory of Chambon-la-Foret (international INTERMAGNET network) and the global seismological network GEOSCOPE. IPGP currently employs about 300 permanent researchers and staff. There are in addition some 200 MSc and PhD students, post-docs and visitors.
The Director will be responsible for supervising the Institute's research and teaching activities, including general administrative tasks, and conducting negotiations with national and European funding agencies. The Director is also the chair of the Institute's scientific Council, whereas the IPGP Board is chaired by a scientist from outside IPGP.
Candidates are expected to be highly accomplished scientists. They will be evaluated on the basis of their academic record in research and teaching, their experience in management, and their vision for the future of IPGP. Interested candidates should submit a two-page vision statement, their Curriculum Vitae and names of three individuals who are willing to be contacted references.

Applications must be received by June 15, 2009.

Application materials should be sent to:
Lydia Zerbib - IPGP General Secretary, Institut de Physique du Globe
4 Place Jussieu, 75252 Paris Cedex 5, France
E-mail: zerbib@ipgp.fr - www.ipgp.fr

HEALTH SCIENCES CENTER | TEXAS TECH UNIVERSITY

Professor of Comparative Medicine – Infectious Disease

Texas Tech University and the Texas Tech University Health Sciences Center have collaborated to form a new Institute of Comparative Medicine with an initial focus on Infectious Disease. This new Institute will support the One Health national initiative to study and provide solutions to animal and human health concerns. The Institute will recruit a number of new faculty, assign and remodel new space suited to this line of research, and provide meaningful start-up funds in areas of Infectious Disease including, but not limited to:

- Emergence of drug-resistant bacterial infection and immunity
- Viral immunity
- Basic Immunology

Some areas of research interest include studies involving biofilms, antibiotic resistant bacteria, hanta virus and/or influenza, and enteric, respiratory and wound infections. Collaboration with existing and newly hired comparative medicine faculty members and interaction in a team environment is expected. Funds are available to remodel and equip shell space in our Experimental Sciences Building. State-of-the-art biocontainment animal facilities are on site. Opportunities are present to collaborate on human clinical studies in the Texas Tech System. New faculty will be expected to have competitive grant funding and a record of research productivity. Graduate advising and teaching is expected in areas of interest to the faculty. Service to the institutions and the profession are important aspects of successful faculty. Primary appointment will be in any academic department at either institution. Level of academic appointment is open to all ranks.

Applicants must submit a letter of interest expressing their vision for research contributions and graduate education goals, a complete resume/CV, the names of five references who may be contacted to provide a professional assessment of research and graduate education capabilities, and start-up requirements to: **Institute of Comparative and Experimental Medicine, Texas Tech University, Experimental Sciences Building, Box 43132, Lubbock, TX 79409-3132; icem@ttu.edu**. These positions shall remain open until the positions are filled. See www.icem.ttu.edu for more information.

Texas Tech University System is an Equal Opportunity Institution.

KU THE KIDNEY INSTITUTE

Fellowship Position

An immediate opening for a 2-yr Fellowship Position for MD, MD/PhD, or PhD is available in the Kidney Institute at the University of Kansas Medical Center. The position is funded by an NIH T32 training grant and the project investigates FGF23 regulation and function.

US citizen or permanent resident and ability to start in July 2009 are prerequisites.

Applicants should email curriculum vitae (PDF file) to:

Ms. Zora Asefi
at
zasefi@kumc.edu

FACULTY POSITION IN REPRODUCTIVE OR DEVELOPMENTAL BIOLOGY

Women's Health and Infant Development Research Center

Eastern Virginia Medical School

The newly established Women's Health and Infant Development Research Center at Eastern Virginia Medical School (EVMS) is seeking investigators to fill tenure-track faculty positions in the areas of reproductive/perinatal endocrinology and fetal/neonatal development. EVMS is making a major commitment to strengthen, expand and integrate the academic enterprise in basic and clinical research. The Women's Health and Infant Development Research Center spans across and is comprised of investigators from several departments and the new recruits will hold a primary academic appointment within the Department of Physiological Sciences, Pediatrics or Ob/Gyn. The candidates are expected to have a Ph.D., and/or M.D., postdoctoral training in reproductive or developmental biology, a strong background in molecular biology, U.S. citizenship, and conduct an active externally funded research program. Considerable opportunity exists at EVMS for collaboration in various aspects of reproduction, developmental and pediatric research. Applicants should submit a letter of interest, an NIH biosketch and full CV to: Eastern Virginia Medical School, Women's Health and Infant Development Research Center, Attention: **Sandra Huband**, email: **Hubandsb@EVMS.edu**.

EVMS is an Equal Opportunity/Affirmative Action and Drug Free Workplace Employer and encourages applications of women and minorities.

Dean, Graduate School of Biomedical Sciences

The Medical College of Wisconsin invites applications for the position of **Dean of the Graduate School of Biomedical Sciences (www.mcw.edu/graduateschool)**. The College seeks a strong and dynamic leader with a distinguished record of research, teaching and service, including experience with the challenges and opportunities unique to graduate education in a medical school environment. The successful candidate will provide vision and leadership for a graduate school encompassing more than 200 faculty and enrolling more than 300 students seeking PhD, MPH, MS and MA degrees. The Dean, who reports directly to the President of the College, will have primary responsibility for the Graduate School's existing academic programs and for building new programs of national and international distinction. The Dean serves as the advocate for graduate education both within the College and with external constituencies, oversees the administration of the Graduate School, and also oversees the Office of Postdoctoral Education and the Summer Program for Undergraduate Research.

The successful candidate must hold a doctoral degree, possess academic credentials for a tenured appointment at the rank of Professor, and have experience as a graduate mentor and as a leader in graduate education. We anticipate that the Dean will maintain an active research program (50% time); a program development package and research space commensurate with that effort will be provided.

The Medical College of Wisconsin (**www.mcw.edu**), the largest private research institution in Wisconsin, has a state-of-the-art research infrastructure, strong academic departments, and innovative interdisciplinary centers. The Medical College is part of an academic medical center that includes nationally distinguished children's and adult hospitals and the Blood Research Institute. The location of the College campus on the outskirts of Milwaukee provides access to a diverse urban environment and a multitude of cultural and recreational opportunities.

The position is available July 1, 2009; the Search Committee will begin reviewing candidates immediately and will continue until the position is filled. Applicants should provide a curriculum vitae, statement of interest, and the names and contact information of three references to: Paula Traktman, PhD; Chair, Graduate School Dean Search Committee, ptrakt@mcw.edu.

MCW encourages applications from women and minority candidates. EOE/M/F/D/V

TENURE-TRACK CLINICAL PHARMACOLOGY FACULTY POSITION AT JOHNS HOPKINS

The Division of Clinical Pharmacology at The Johns Hopkins University School of Medicine invites applications for a **tenure-track Assistant Professorship**. Targeted research is drug metabolism, and this may include drug-drug interactions, pharmacogenetics, or drug transporters, for example. Applicants must have an MD, be licensed to practice in the US, have training and experience in molecular laboratory research, and be interested in conducting both translational and hands-on clinical research. We seek individuals with a record of accomplishment in research and high potential for creative scholarship. An interest in teaching is important. The School of Medicine and University as a whole provide a stimulating and supportive environment to carry out research in the biomedical sciences, and a start up package is available.

A letter of inquiry, CV, summary of a research proposal (1-4 pages), up to two reprints, and three reference letters should be sent by interested applicants to:

Dr. Theresa A. Shapiro
Chair, Faculty Search Committee
The Johns Hopkins University School of Medicine
303 Hunterian Building
725 North Wolfe Street
Baltimore, MD 21205-2186
tshapiro@jhmi.edu
http://www.jhuclinicalpharmacology.org/

The Johns Hopkins University is an Equal Opportunity Employer and does not discriminate on the basis of race, color, gender, religion, age, sexual orientation, national or ethnic origin, disability, marital status, veteran status, or any other occupationally irrelevant criteria. The University promotes affirmative action for minorities, women, disabled persons, and veterans. Minorities and women are encouraged to apply.

TENURE-TRACK FACULTY LAB DIRECTOR POSITION AT JOHNS HOPKINS

The Division of Clinical Pharmacology, jointly under the Departments of Medicine and of Pharmacology and Molecular Sciences, at The Johns Hopkins University School of Medicine, invites applications for a **tenure-track faculty position**. We seek individuals with experience and interest in analytical chemistry and pharmacokinetics, to direct the Clinical Pharmacology Analytical Laboratory. This facility supports dozens of ongoing clinical trials in the Division and throughout the School of Medicine, processing and analyzing thousands of samples per year. Numerous validated assays are in use and new ones are routinely added; most use mass spectrometry. Existing laboratory personnel include two PhDs and three technicians. The laboratory director collaborates closely with other faculty to design and analyze clinical studies. The position offers ample opportunity to pursue independent research.

Applicants should have an MD, MD/PhD, or PhD degree. An interest in teaching is important. The School of Medicine and University as a whole provide a stimulating and supportive environment to carry out research in the biomedical sciences. Strong research programs exist in pharmacology, chemical biology, toxicology, and chemistry. A letter of inquiry, CV, and names of three references should be sent to : **Dr. Craig Hendrix, Chair, Faculty Search Committee, The Johns Hopkins University School of Medicine, 600 N. Wolfe Street, Harvey 502, Baltimore, MD 21287; chendrix@jhmi.edu; http://www.jhuclinicalpharmacology.org/.**

The Johns Hopkins University is an Equal Opportunity Employer and does not discriminate on the basis of race, color, gender, religion, age, sexual orientation, national or ethnic origin, disability, marital status, veteran status, or any other occupationally irrelevant criteria. The University promotes affirmative action for minorities, women, disabled persons, and veterans. Minorities and women are encouraged to apply.

POSITIONS OPEN

California Pacific Medical Center
A Sutter Health Affiliate

SCIENTIFIC DIRECTOR
California Pacific Medical Center
Research Institute

The position provides scientific, strategic, and operational leadership and reports directly to the CEO of the California Pacific Medical Center (the largest nonprofit medical center in San Francisco and a member of Sutter Health). Preferred candidates are accomplished scientists with a record of extramural funding and administrative experience. CPMCRI has a diverse group of scientists, including laboratory-based investigators, clinical researchers, and epidemiologists. **Website: http://www.cpmc.org/professionals/research/programs/.** Funding totaled $26 million in 2008. Applicants should submit a letter of interest and curriculum vitae by July 15, 2009, to: **Lynne Day, Director Research Operations, e-mail: dayl@cpmcri.org.**

For more than 130 years, Lilly has been dedicated to meeting the health care needs of people in the United States and around the world. We address these needs primarily by developing innovative medicines—investing a higher percentage of our sales in research and development than any other major pharmaceutical company. If you are interested in being considered for employment with a "best in class" pharmaceutical company, please review the following opportunity: **Job I.D. Number 50351130.** Lilly seeks a **MEDICAL DIRECTOR** in Indianapolis, Indiana, for its Immunomodulation Team to provide medical leadership for the accelerated and integrated development of monoclonal antibodies for autoimmune disorders. Specific duties include: leading strategy and tactics to sustain full development and optimization of new medications, including exploration of additional indications, focusing on adult and pediatric indications; managing teams that are currently designing and implementing 10 phase 1 and phase 2 clinical trials in rheumatoid arthritis, psoriasis, multiple sclerosis, and multiple myeloma; and interacting with FDA, EAME, Japanese PMDA, and Chinese SFDA for all regulatory issues relative to the antibodies developed. Candidate must have Ph.D. in biology, molecular and developmental biology, or related field and relevant experience and an M.D. Salary: $226,000 per year. Please submit resume to **website: http://www.lilly.com/careers** and cite the relevant job title and job I.D. number in your submission. *Lilly is an Equal Opportunity Employer that values the strength diversity brings to the workplace.*

Eight **POSTDOCTORAL POSITIONS** for research focused on optimization of vaccines and mechanistic studies on immune regulation at the University of Georgia. Immediate openings on NIH-funded projects: (1) examines the effect of immune suppressive pathogens on efficacy of vaccines for HIV-1; (2) optimizing efficacy of zoonotic vaccines; (3) determine how immune modulatory agents alternatively activate antigen-presenting cells. Looking for individuals with expertise in plasmid design, production, and purification, cell signaling, protein-protein interactions, fluorescence activated cell sorting analysis, and production of plasmids for transfection of mammalian cells. Send curriculum vitae, including names of three references, to: **Dr. Donald Harn, Department of Infectious Diseases, College of Veterinary Medicine, University of Georgia, Athens, GA 30602. Or to e-mail: dharn@uga.edu.** Applications received before June 6, 2009, are assured full consideration. *The University of Georgia is an Equal Opportunity/Affirmative Action Employer.*

POSITIONS OPEN

VANDERBILT Institute of Chemical Biology

ASSISTANT DIRECTOR
Vanderbilt Institute of Chemical Biology,
High-throughput Screen Center

The Vanderbilt Institute of Chemical Biology is offering a position for Assistant Director of the Institute's high throughput screening (HTS) facility. This facility is a state-of-the-art screening facility focusing on using fully automated and workstation-based screening approaches to enable Vanderbilt investigators to develop and utilize HTS-compatible assays and small-molecule screening approaches. The successful candidate will be responsible for managing a team of HTS biologists to develop and implement screens for a wide variety of biological targets and systems. A broad range of knowledge in building, implementing, and interpreting HTS is required. A strong background in HTS related to oncology targets and systems is preferred. The successful candidate will work as part of a multidisciplinary team of scientists including medicinal chemists, physicians-scientists, pharmacologists, chemiinformaticists, engineers, and others to discover and characterize small molecules in support of basic and translational research. The position requires a Ph.D. in cell biology, biochemistry, pharmacology, chemistry, or related discipline plus a minimum of four years experience with HTS in an academic or industrial setting. Strong written and oral communication skills and demonstrated excellence in leading and participating in multidisciplinary teams are also required. Salary is dependent on experience. Please send applications and curriculum vitae to: **Dave Weaver, e-mail: david.weaver@vanderbilt.edu.**

Vanderbilt University is an Equal Opportunity Employer.

RESEARCH ASSOCIATE
Influenza Research
The Pathogen Evolution Group
LoT applies* Salary: Grade 7
Salary Range: £27,183 to £35,469 per annum

We invite applications for a postdoctoral Research Associate to work in the Department of Zoology on the development of new analytical techniques for quantifying the evolutionary selection pressures on influenza viruses. We aim to better understand their evolutionary dynamics and to inform control strategies. The project, which is funded by NIH Director's Pioneer Award, is to start as soon as possible. The candidate should have a Ph.D. in computational biology, computer science, virology, epidemiology, a related subject or equivalent and should have excellent programming skills in C++, Python, Java, or Lisp and ideally other languages.

*The appointment will be for a period of up two years in the first instance.

Informal enquiries may be made to **Professor Derek Smith at e-mail: am688@cam.ac.uk.** To apply see: **website: http://www.zoo.cam.ac.uk/zooone/administration/vacancy.html.** Closing date: Friday 5 June 2009. Interviews as soon as possible thereafter.

FACULTY - PHARMACEUTICAL SCIENCES

The Department of Pharmaceutical Sciences, School of Pharmacy and Health Professions, University of Maryland Eastern Shore, Princess Anne, Maryland, seeks applicants for 12-month, tenure-track Faculty positions in the pharmaceutical sciences. Ph.D. or equivalent degree in a pharmaceutical or biomedical science required; teaching and/or postdoctoral experience preferred. The candidate will be expected to develop and teach in integrated, basic science course modules in a three-year Pharm.D. curriculum. For application procedures and further information on qualifications and responsibilities, see our **website: http://www.umes.edu/hr.** *UMES is an Equal Employment Opportunity/Affirmative Action Employer.*

POSITIONS OPEN

POSTDOCTORAL POSITIONS in
Center for Neurodegenerative and
Vascular Brain Disorders at
University of Rochester,
School of Medicine and Dentistry

The **Zlokovic** laboratory, at the forefront of translational research using cutting-edge technologies in Alzheimer's disease (AD) and stroke, has vacancies for two enthusiastic and energetic Postdoctoral Fellows.

(1) To work on the molecular mechanisms for the control of cerebral blood flow and amyloid deposits in AD using techniques such as 2-photon microscopy, laser speckle, laser Doppler, and autoradiography.

Qualifications and experience: Ph.D. in molecular biology/physiology or equivalent biological areas in Alzheimer's disease. Experiences with in vivo studies and ability to work as a team are essential.

(2) The second postdoctoral fellow will work on the role of copper and cholesterol in the clearance of Aβ from brain in AD.

Qualifications and experience: Ph.D. in molecular biology/physiology or equivalent biological areas in AD. Experiences in cell culture and in vivo studies and ability to work as a team are essential. Experience with metal ions and protein trafficking, using confocal and/or 2-photon microscopy, would be helpful.

Interested candidates please forward your resume to **Mohammad Ali** at **e-mail: mohammad_ali@urmc.rochester.edu.**

POSTDOCTORAL POSITION to study structure and function of the bacterial cytoskeleton during the cell cycle and other cellular processes, using molecular biological, cell biological, and biochemical techniques, including the unique imaging resources of the Center for Cell Analysis and Modeling. Experience in protein or membrane biochemistry will be an asset but is not a requirement. NIH support, 2004-2014. Relevant papers: *Mol. Microbiol.* **72:**170, 2009; *Proc. Natl. Acad. Sci.* **104:**17795, 2007; *J. Biol. Chem.* **283:**13850, 2008. Respond to: **Professor L. Rothfield, Department of Molecular, Microbial and Structural Biology, University of Connecticut Health Center, Farmington, CT 06032, U.S.A. E-mail: lroth@neuron.uchc.edu.** *University of Connecticut Health Center is an Equal Employment Opportunity Employer.*

MARKETPLACE

5 Scientific Conferences 1 Location

Join us on August 3-6, 2009 in Boston, Massachusetts to learn practical strategies to help you accelerate small molecules, antibody therapeutics and oligonucleotide therapeutics from early discovery to the clinic.

Register today to attend the one conference that best meets your needs, or get the most out of your budget and **purchase an All-Access Conference Pass** for admission to all five conferences.

Best Value:
All Access Conference Pass

The Next Wave of Antibody Therapeutics

August 3-5, 2009

With a Focus On:

- Antibody-Drug Conjugates
- Improving Potency and Efficacy
- Combinations of Antibody Drugs
- Bi/Multi-Specific Antibody Drugs
- Pharmacodynamic Biomarkers of Antibodies

www.drugdisc.com/antibody

Oligonucleotide Therapeutics: From Concept to Implementation

August 3-5, 2009

With a Focus On:

- Leveraging on the RNA Promise
- Novel Delivery Systems
- Efficacy, Toxicity and Specificity Challenges
- PreClinical to Clinical Development
- siRNA miRNA Antisense and Aptamers

www.drugdisc.com/oligo

New Frontiers in Cancer Drug Development

August 4-6, 2009

With a Focus On:

- Exploiting Cancer Stem Cells
- Combining Molecular Targeted Therapies
- Epigenetics and Emerging Targets
- Companion Diagnostics and Biomarkers
- Regulatory Pathways and Perspectives

www.drugdisc.com/cancer

Targets in Context – Linking Targets to Diseases

August 4-6, 2009

With a Focus On:

- Omics Approaches to Target Finding
- RNAi for Target Validation
- In Vivo and Computational Approaches
- High Content High Throughput Approaches
- Clinical Validation of Targets

www.drugdisc.com/targets

Drug Safety Strategies to De-Risk Compounds

August 4-6, 2009

With a Focus On:

- Predicting Hepatoxicity and Cardiotoxicity
- Translating Preclinical Models to Humans
- Drug-Induced Mitochondrial Toxicity
- Decision-Making from Preclinical Data
- Safety Biomarker Regulatory Pathways

www.drugdisc.com/drugsafety

Part of
Drug Discovery & Development Week

August 3-6, 2009
World Trade Center Boston
Boston, MA USA

Want more information?
Complete agendas are available online.

Register Today!

ibc Life Sciences
an informa business

Use Priority Code: ID9201TSA

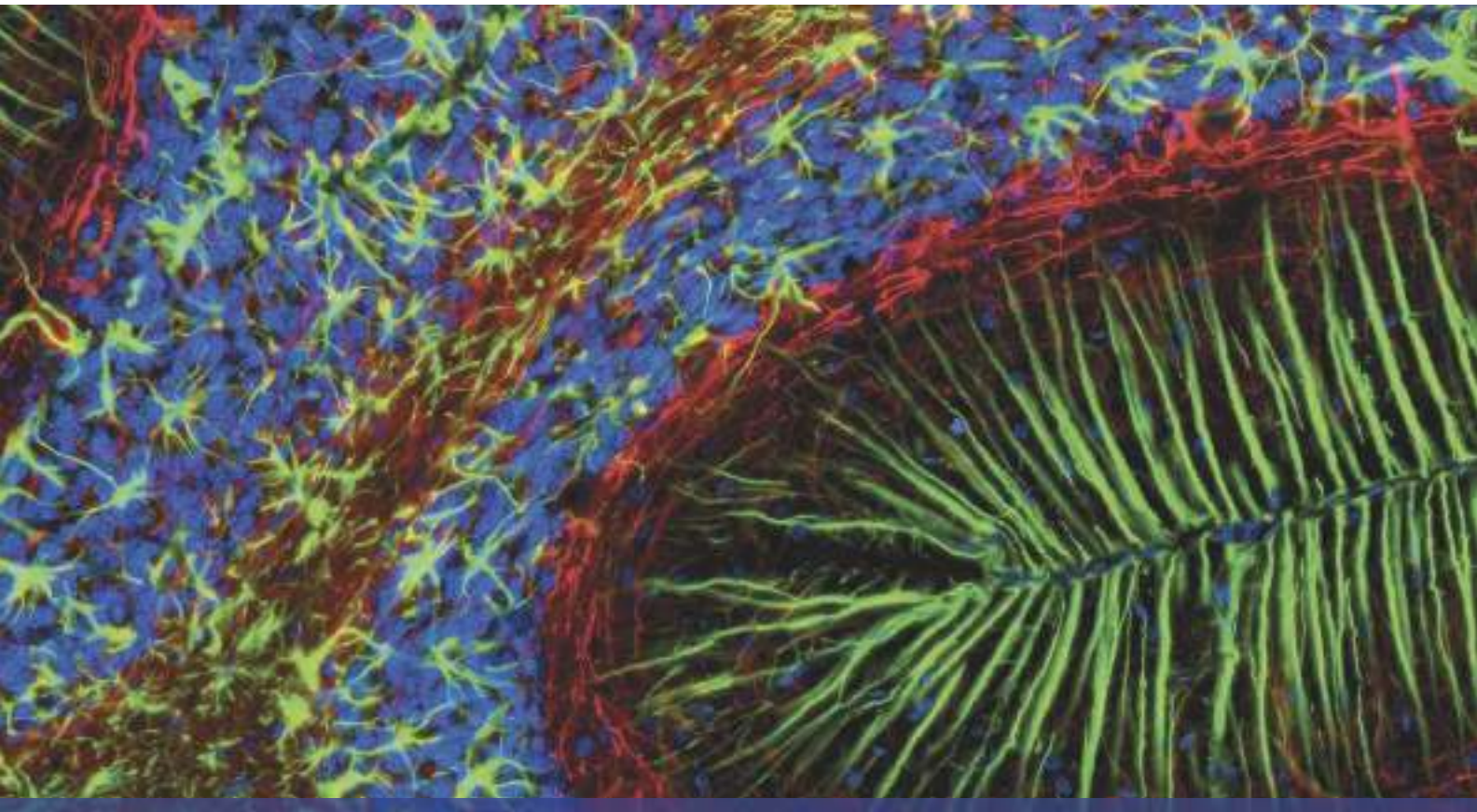

Alexa Fluor® Conjugated Antibodies

from Cell Signaling Technology®

▲ *Confocal immunofluorescent analysis of rat brain using* ***GFAP (GA5) Mouse mAb (Alexa Fluor® 488 Conjugate) #3655*** *(green) and Neurofilament-L (DA2) Mouse mAb #2835 (red). Blue pseudocolor = DRAQ5® #4084 (fluorescent DNA dye).*

Unparalleled product quality, validation and technical support.

:: The highest quality antibodies provide you with the brightest signal and the lowest background.

:: Extensive validation by our in-house conjugation group means optimization is not left up to you, the user.

:: Technical support provided by our conjugation group translates into a thorough, fast and accurate response.

:: High quality custom conjugations of our off-the-shelf antibodies also available contact drugdiscovery@cellsignal.com.

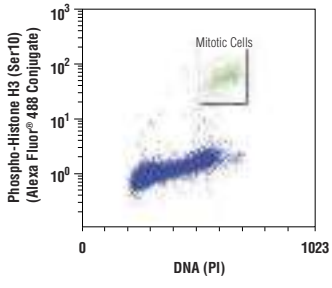

◀ *Flow cytometric analysis of Jurkat cells using* ***Phospho-Histone H3 (Ser10) (D2C8) Rabbit mAb (Alexa Fluor® 488 Conjugate) #3465*** *compared to propidium iodide (DNA content). The box indicates phospho-histone H3 positive cells.*

Flow cytometric analysis of Jurkat cells, untreated (blue) or IFN-α-treated (green), using ***Phospho-S6 Ribosomal Protein (Ser235/236) (D57.2.2E) Rabbit mAb (Alexa Fluor® 488 Conjugate) #4803****, compared to* ***Rabbit (DA1E) mAb IgG Isotype Control (Alexa Fluor® 488 Conjugate) #2975*** *(red).* ▶

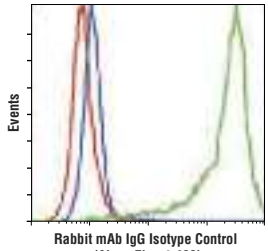

for quality products you can trust...

www.cellsignal.com

Cell Signaling TECHNOLOGY®